REAL SPACE ANALYSIS OF LASER INDUCED FREEZING

BY

KHALID LOUDIYI

Bachelor of Science
Southwest Missouri State University
Springfield, Missouri
1980

Master of Science
Oklahoma State University
Stillwater, Oklahoma
1983

Submitted to the Faculty of the
Graduate College of the
Oklahoma State University
in partial fulfillment for
the requirements
of the Degree of
DOCTOR OF PHILOSOPHY
December 1989

REAL SPACE ANALYSIS OF LASER INDUCED FREEZING

Thesis Approved:

Thesis Advisor

Dean of the Graduate College

ACKNOWLEDGEMENT

The author wishes to express sincere appreciation and deep gratitude to his major advisor, Dr. B. J. Ackerson, for the interest, assistance and invaluable guidance throughout the course of this work. Additional thanks is extended to Dr. H. L. Scott, G. S. Dixon, Dr. R. C. Powell and Dr. R. K. Yarlagadda for serving in my committe and all the exchange of information they have provided. Special thanks is expressed to Dr. E. E. Lafon, Dr. A. Chowdhury, Dr. H. AlMoghrabi, Mr. S. Paulin and Miss T. Morris for their comments and discussions. I am deeply appriciative to the Physics Department, expecially Dr. L. Halliburton for letting me use their facilities to write this thesis.

For you, dear parents, brothers and sisters and all my friends I would like to give my honest gratitude for all the moral and emotional support you have provided during the frustrating periods of my graduate career.

TABLE OF CONTENTS

LIST OF TABLES

LIST OF FIGURES

Figure Page

Figure Page

Figure Page

Figure Page

Figure Page

CHAPTER I

INTRODUCTION

Scope of Study

Colloidal suspensions are novel systems for the study of many physical phenomena related to, amongst others, statistical mechanics, electrostatics, hydrodynamics, and crystallography. The submicron size of these particles in suspensions makes them ideal for the study of microscopic problems on a macroscopic scale. Amongst some of the studies where these suspensions serve as experimental models are the nature of phase transitions in two and three dimensional systems (1, 2, 3), layering transitions (4, 5), crystallization processes (7), elastic properties (8), deformations under the influence of externally applied fields (9, 10, 11, 12), and the nature of interaction between particles (13, 14, 15, 16).

The purpose of this thesis is to study the effect of an externally applied potential on the local order of charged colloidal particle suspensions comprised of submicron polystyrene spheres suspended in water that is highly deionized. The externally applied field is in the form of a periodic potential well produced from the crossing of two coherent laser beams and controlled through the beam input power and crossing angle. The real space ordering of the suspensions when the field is applied is analyzed through pair correlation functions produced from measurements of the microsphere positions.

The results of a Monte Carlo (MC) simulation for a model two dimensional system of point particles interacting via a screened Coulomb potential are also studied here. It is found that, by changing the salt concentration or the density of excess ions, the model system goes through a phase transition. Different equilibrium states (solid and liquid) of this simulation were chosen and subjected to an exter- nal sinusoidal potential which corresponds to experimental radiation pressure field. The ordering transition of the point particles in this external field is monitored by changing the amplitude and period of the potential.

The MC simulation results were consistent with the experimental observations. In both cases, the application of the external radiation field caused the particles to aline along the potential's minima. The degree of this localization was found to be dependent on the external field's amplitude. Along with the particle electrostatic interaction, this localization was found to cause the system to organize in different structures depending on the period of the externally applied field.

Particle alignment in the high intensity regions of the stationary sinusoidal fringe pattern, produced from the crossing of two mutually coherent laser beams, form diffraction gratings. The scattering from these gratings is used to study the growth and decay of these density modes. In this thesis the dependence of the interacting (charged) systems main density mode on the lasers input power is investigated and compared with data obtained from the MC simulation. These were found to be different from the results reported by Chowdhury (10).

General Background

The existence of monodisperse colloidal particles that can organize in long crystalline structures has fascinated and captured the interest of many scientists throughout the years. Iler(8) was the first to show that opal-like crystallization of silica particles could be monitored in a laboratory setup.

Since colloids have been recognized as a suspension of solid particles in a host fluid, a great deal of work has been done on the use of theories involving the interparticle forces to study the nature of interaction between the particles. The most famous theory is known as the DLVO (Derjaguin, Landau, Verwey and Overbeek) theory (17), which assumes additivity of the screened Coulomb electrostatic repulsion (V_r) and Van der Waals attraction forces (V_a) which are given by the following equations for the case of spherical particles (17):

$$V_a = A\{ 4a^2/(r^2-a^2) + 4a^2/r^2 + 2\ln[(r^2-a^2)/r^2]\}$$

$$V_r = Z^2e^2e^{-kr}/cr \qquad k^2 = 4\pi ne^2/\epsilon k_BT \qquad (1\text{-}1)$$

where A is the Hamaker constant (10^{-13} for polystyrene in water), r is the separation of the centers,'a' is the sphere radius, Z is the charge per sphere, 'ϵ' the dielectric constant of the solvent, k the inverse screening length, and n the total number of particles and ions in solution (including negative and positive monovalent ions). Although both forces are important for understanding coagulation, only long range electrostatic forces are important for this study because of large particle separations and the Van der Waals forces are short ranged.

The screened Coulomb potential (V_r) is also known as the Debye-Huckel (DH) or Yukawa potential (equation (1-1)) and it is the form

used in this thesis work for the MC simulations of the interacting colloidal particles. This potential is the solution to the Poisson-Boltzman (PB) equation in the linear approximation, and it gives a good qualitative picture of the electrostatic forces (7).

The effective charge on the polystyrene colloidal particles is found by considering the charge neutrality of the system, and taking the Weigner-Seitz cell surrounding each particle as providing for the charge neutrality around that point. Using this concept, Alexander et al (7) have shown that solutions to the DH and PB distribution can be used to calculate the surface potential for the spheres and the value of their effective charges. Such techniques will be discussed in detail in Chapter V where the effective charge for the 1.07um polystyrene spheres is calculated.

The repulsive nature of the Coulombic interaction between similarly charged microspheres as presented by DLVO theory has been questioned by Ise and co-workers (14, 13). These workers have argued the there exists an attractive force between highly charged macroionic solutions at large distances and repulsions at small separations, thus leading to the existence of a secondary minimum from only electrostatic considerations. This is believed by Ise to cause for the observed ordering of the highly charged latex particles having higher than expected density in the crystalline state. However, we will use only the DLVO form in analyzing our results or in MC Simulations.

The question concerning long range order (LRO) in two-dimensional systems has attracted the attention of many scientists (18, 19, 20). It was believed that the long wavelength phonons prevented the 2-D solid from fully attaining a crystalline structure. However in 1973

Kosterlitz and Thouless (18) put forth their famous idea of phase transitions accompanied by a change of "topological order" rather than the conventional LRO. About five years after KT advanced their theory, Halperin, Nelson and Young (19, 20) introduced an orientational order parameter to the problem not considered by KT, thus leading to the famous KTNHY continuous melting theory. This theory predicts that melting may occur by way of two transitions, the first associated with loss of long range positional order and resistance to shear, and the second with loss of orientational ordering, and that these transitions can be continuous. The hexatic phase (a fluid with no translational order but with some orientational order) is predicted, through this theory, to exist between the two transitions. The limitation in scale of the 2-D studies carried in this thesis does not allow us to say much our the nature of the observed transitions.

Structural and phase transition simulations for charged colloidal suspensions are given in a number of papers (3, 21, 22, 23, 24). Amongst these W. Van Megen et al. (3) used a MC method to determine the struc- ture of a very dilute colloid in 3-D. These workers calculated the radial distribution functions and converted them to structure factors; which they subsequently compared with corresponding quantities determined form laser light scattering experiments and have found that their model presented a reasonable description for the systems of colloidal particles. R. Kalia et al. (22), have used a molecular dynamics (MD) simulation for two-dimensional systems of point particles interacting with Yukawa potential and have observed first order solid-liquid transitions. Our MC simulation of a similar system seems to predict a first order phase transition too. M. P.

Allen et al. (21) reported an MC study of the two-dimensional melting mechanism for 2500 particles interacting by repulsive inverse sixth power potential. Their thermodynamic results, taken alone, were quite consistent with a first-order melting mechanism and although some of their results were consistent with the two stage melting process (KTNHY theory), these were not enough to verify the existence of a hexatic phase.

The same controversy concerning the nature of transition for two dimensional colloidal systems was investigated experimentally by Van Winkle et al (1) and Y. Tang et al (23). Van Winkle and Murray (1), have observed a two-stage melting transition with the intermediate phase having the signature of a hexatic. Y. Tang et al. (23), on the other hand, have observed a first order transition in their analysis of a freely expanding colloidal monolayer lattice. The work used in this thesis could be related to the nature of phase transition for two dimensional systems, but this question will not be considered here.

The structural transition of thin layers of colloidal crystal has been found to follow triangular to square packing for wedged gap cells (4, 6). The transition format as the gap confining the layers increased was found to follow the form: 1T, 2S, 2T, 3S, 3T, where T represents a triangular lattice, S a square lattice and the numbers represent the layers. Such layering transitions were also observed in the experimental samples used in this work.

When colloidal suspensions are subjected to external fields the local order can be changed, this concept has been used in various studies for different fields (10, 12, 25, 26). Since Ashkin reported on the trapping, levitation and acceleration of dielectric suspensions

with a strongly focused laser beam (27, 28, 29, 30), the application of radiation pressure as a way to manipulate micrometer sized dielectric particles has led to new discoveries, such as the "laser induced freezing" considered in this work. The radiation pressure forces act both parallel and perpendicular to the direction of propagation of the incident beam (10, 31). The transverse force is employed in four-wave mixing experiments to draw spheres, with an index of refraction greater than the host fluid, to the high intensity regions thus creating density modes. The scattering from these modes was studied experimentally by Chowdhury (10) who has found that the first order diffracted intensity maximum signal increased as approximately the cube of the incident beam intensity for the case of noninteracting colloidal particles in self scattering experiments. The experimental results for the noninteracting particles studied by Chowdhury et al (11) were found to be consistent with Rogovin theory (32, 33) on the alignment of dielectric spheres in the Four Wave Mixing, FWM, geometries.

The decay of the main density modes created by the crossing of two laser beams was investigated by Chowdhury in his thesis work (10) and has found that the measured self diffusion coefficients were smaller than free diffusion constant (Theoretical diffusion coefficient value for an infinitely dilute sample with no boundary). The inconsistency in this measurements were attributed to either the con- centration or boundary effects.

This 'Forced Rayleigh scattering' (FRS) has been used by many workers in measuring the self diffusion constant of charged and noncharged doped or nondoped particles (34, 35, 36). B. Dozier et al.

(37) have used charged polystyrene colloids and measured the self diffusion as a function of the strength of interaction between the particles. They have found that the diffusion constant decreased monotonically from the Stokes value as the repulsive interaction is increased, until the interactions are sufficiently strong to form a colloidal crystal.

The investigation of structure in interacting colloidal fluid states was investigated by use of cross-correlation intensity fluctuation spectroscopy, CCIFS, (38, 39, 40). B. J. Ackerson et al. (38) have used the CCIFS to indicate a local hexagonal structure in the fluid phase, they have also found that their experimental observations were in agreement with a model calculation in which they have treated the two dimensional fluid phase as a randomly oriented hexagonal solid with large lattice vibrations.

The Hamiltonian of an array of atoms interacting with a periodic potential with period 'b' and connected with harmonic springs can be written as (41):

$$H = \sum_n \{1/2b^2(x_{n+1}-x_n-a_0) + V[1-\cos(2\ x_n/b)]\} \qquad (1\text{-}2)$$

where x_n is the nth atom position, b is the period of the periodic potential, V is the amplitude of this potential and a_0 is the lattice constant. In the absence of the periodic potential, V, or if the external potential is weak, the observed structure will in general be in the incommensurate phase (IC). This means that the harmonic term would favor a lattice constant a_0 which is incommensurable with 'b' as shown in Figure 1(a). In such a case the diffracted Bragg spots would be at positions $Q=2\pi N/a_0$, where N is an integer. None of these will coincide with the Bragg spots of the periodic potential

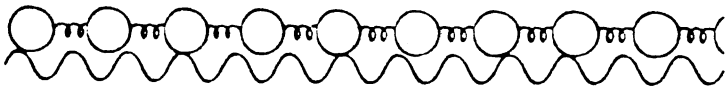

a) Incommensurate Structure

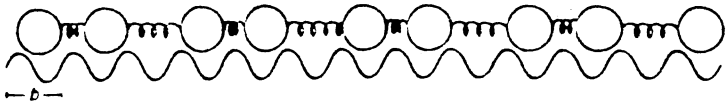

b) Commensurate Structure

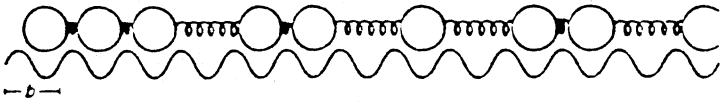

c) Chaotic Sturcture

Figure 1. One Dimensional Demonstration of Incommensurate (a), Commensurate (b) and Chaotic (c) Structures. The Springs Represent Interaction Between Atoms and the Wavy Line the Periodic Potential.

at positions G=2PiM/b, where M is an integer. If the external potential is made strong enough, it may be favourable for the lattice to relax into the external periodic potential where the average lattice spacing, a, is a simple rational fraction of the potential's period, b. This is known as the commensurate structure, and it is shown in Figure 1(b), where a situation with 2a=3b is taken as an example. In such case the differaction pattern of the substrate and absorbed layer has an infinite number of coinciding Bragg spots (41).

If the potential is not strong enough to force the chain into commensurability, the atoms will move toward the potential's minima and the average period may approach a simple commensurate value but remain incommensurate. The C and IC structures do not exhaust the stable configuration. There are additional choatic structures which cannot be described as above (Figure 1c). In this phase the diffraction pattern is not made up of well-defined Bragg spots.

Thesis Overview

The main goal of this thesis is to carry a real space analysis of the "laser induced freezing" phenomenon. The general theoretical background needed in describing this work is considered in Chapter II of this thesis. In this chapter concepts such as: light forces on colloidal particles, description of the stationary sinusoidal fringe pattern, potential for finite size particles, steady state characteristics and two dimensional pair correlation functions are discussed. The succeeding chapter (Chapter III) is devoted to the different experimental procedures and techniques used to force the interacting colloidal suspensions into ordered states. The viewing, imaging and

detection of the colloidal particles is also considered in Chapter III.

Chapter VI is devoted completely to the real space analysis of the charged colloidals suspensions. The observed structuring in a wedged cell geometry is discussed at the beginning of this chapter, succeeded by the real space analysis of the crossed beams experiments, and some scattered intensity measurements are given at this end of Chapter IV.

A simulation of the laser induced freezing is given in Chapter V. The theory needed for the Monte Carlo simulation is presented at the beginning of this chapter. Then, the phase transition results for a system of particles interacting via a screened Coulomb potential is analyzed. At the end of Chapter V, the effect of an externally applied periodic potential on different equilibrium phases is studied as a function of the potential's amplitude. The comparison between the results obtained experimentally with those observed in the simulation is carried in Chapter VI.

The conclusions and future suggestions are given in Chapter VII. Appendices at the end of this work are where the different programs used in this study are presented.

CHAPTER II

THEORETICAL BACKGROUND

Introduction

The work that will be presented in the succeeding chapters will deal with various experimental techniques, computer simulations as well as the analysis of the results. The understanding of these topics will require some theoretical background, which will be the subject of the present chapter.

The areas that will be discussed here will include the effect of light forces on colloidal particles, the interference pattern produced form the crossing of two mutually coherent laser beams, the potential for finite size particles, the steady state characteristics of colloidal suspensions in periodic potential fields, a comparison between cross correlation intensity fluctuation spectroscopy and laser trapping of colloidal suspensions, and the functional relation between the scattered intensity an the two-dimensional pair correlation function.

Optical Light Forces on Colloidal Particles

Colloidal particles experience a variety of motions besides the Brownian motion(27, 40). For example a charged particle will move due to electorphoresis in an electric field and magnetophoresis in a magnetic field. Particles will also fall under the influence of the gravitational field. Movement will also occur when there is a

temperature gradient (thermophoresis). Finally, other colloidal particle motion may even be caused by light.

The forces of light responsible for the particles movement are of two types, photophoresis and radiation pressure. In photophoresis there is a differential absorption between the particle and surrounding solvent. As a result temperature differences develop and drive convection of the solvent which then moves the particles. The direction of motion may be towards or away from the light source depending on the absorption coefficients, thermal conductivities, etc. (9). Radiation pressure is a result of the elastic scattering of the radiation in the suspension. The change in momentum of the incident radiation, when it changes direction in the scattering process, results in a momentum transfer to the particle-solvent system in order to conserve total momentum. Thus, radiation pressure causes suspended particles to move in the direction of propagation of the incident beam because scattering reduces the forward momentum of the radiation.

Such principles have been used to optically accelerate, slow, stably trap and manipulate micrometer-sized dielectric particles and atoms. In 1970's, A. Ashkin(27, 30), has reported the first observation of using radiation pressure from a cw visible laser light to accelerate transparent latex spheres. Ashkin et al.(29) have reported that the continuous wave power required to levitate uniform solid or liquid dielectric spheres in the size range .5um to 100um varies from microwatts to several watts.

If we consider a dilute medium containing dielectric spheres, then in the presence of a radiation field, the spheres become polarized. In the cgs units, this polarization is given by,

$$\underline{P} = 3(\epsilon - 1)\underline{E}/(4 \quad (\epsilon + 2) \tag{2-1}$$

where ϵ is the relative dielectric constant of the sphere to the medium, and $\underline{E}$ is the electric field. Here it is assumed the sphere radius is small compared to any spatial variation in the radiation pressure field.

The resulting dipole moment of such polarized spheres is given by

$$p = CE_0 \tag{2-2}$$

$$C = n_s^2(n^2-1)/(n^2+2) \tag{2-3}$$

where a is the radius of the sphere, $n=n_a/n_s$, n_a is the refractive index of the sphere, and n_s is the refractive index of the surrounding. The force exerted on these polarized spheres is simply the Lorentz force ,

$$\underline{F} = (\underline{P}.\text{Grad})\underline{E} + 1/c[\partial \underline{P}/\partial t \text{ X } \underline{B}] \tag{2-4}$$

In the above equation $\underline{B}$ is used for the magnetic field induction and $\underline{F}$ is the force on the sphere. Using equation (2-2) and the first term on the right hand side of equation (2-4), we get:

$$(\underline{P}.\text{Grad})\underline{E} = C(\underline{E}.\text{Grad})\underline{E}$$

$$= C[1/2 \text{ Grad}(E^2) - \underline{E} \text{ Curl}(\underline{E})] \tag{2-5}$$

Substituting the above equation in expression (2-5), the force on the sphere is found to be of the form,

$$\underline{F} = C[1/2 \text{ Grad}(\underline{E}^2) + 1/c\,\partial(\underline{E}\text{X}\underline{B})/\partial t] \tag{2-6}$$

For dielectric spheres with an index of refraction greater than that of the surrounding solvent, C becomes positive leading the first term on the right hand side of the above equation to move particles to the high intensity regions of the radiation field. Conversely, if $n<1$, the particles will move out of the beam. The poynting vector term in the above equation is responsible for moving the particles in

the direction of the beam's propagation.

Crossed Beams Mathematical Description

If we consider two laser beams whose Gaussian profiled electric fields at point $\underline{r}$ (Figure 2) are given by,

$$\underline{E}_1 = E_{01}\exp\{i(\underline{k}_1.\underline{r}-w_1t+P_1)-(\underline{k}_1x\underline{r})^2/(k_2R)^2\} \quad (4\text{-}7)$$

$$\underline{E}_2 = E_{02}\exp\{i(\underline{k}_2.\underline{r}-w_2t+P_2)-(\underline{k}_2x\underline{r})^2/(k_2R)^2\} \quad (4\text{-}8)$$

where the parameters used in the above equations are defined as:

R is the width of the laser beam,

k_1 and k_2 are the beams wave vectors,

E_{01} and E_{02} are amplitudes of the beams electric fields,

w_1 and w_2 are the beams oscillation frequencies,

P_1 and P_2 are phase angles for the two laser beams,

θ is crossing angle.

The total electric field produced from the crossing of the two laser beams is,

$$\underline{E}= \underline{E}_1 + \underline{E}_2 \quad (2\text{-}9)$$

Letting $E_{10}=E_{20}=E_0$, $P_1=P_2=0$ (since a phase factor only shifts the field pattern with respect to the origin) and $w_1=w_2$, then after carrying the cross product the resultant intensity pattern is found to be:

$$I \quad \underline{E}^*.\underline{E} = E_0^2\{\exp[-(2r^2\sin^2(\theta+P))/R^2]+[\exp(-(2r^2\sin^2(\theta-P))/R^2]+ 2[\exp(-r^2[\sin^2(\theta+P)+\sin^2(\theta-P)]/R^2)x\cos(\underline{k}_1-\underline{k}_2).\underline{r}]\} \quad (2\text{-}10)$$

Letting $\underline{k}=\underline{k}_1-\underline{k}_2$ expression (2.10) can be rewritten as,

$$\underline{E}^*.\underline{E} = 2E_0^2\exp(-2r^2\cos^2(\theta)/R^2][1 + \cos\{2kr\sin(\theta/2)\}]. \quad (2\text{-}11)$$

The last cosine term in the above equation produces an intensity

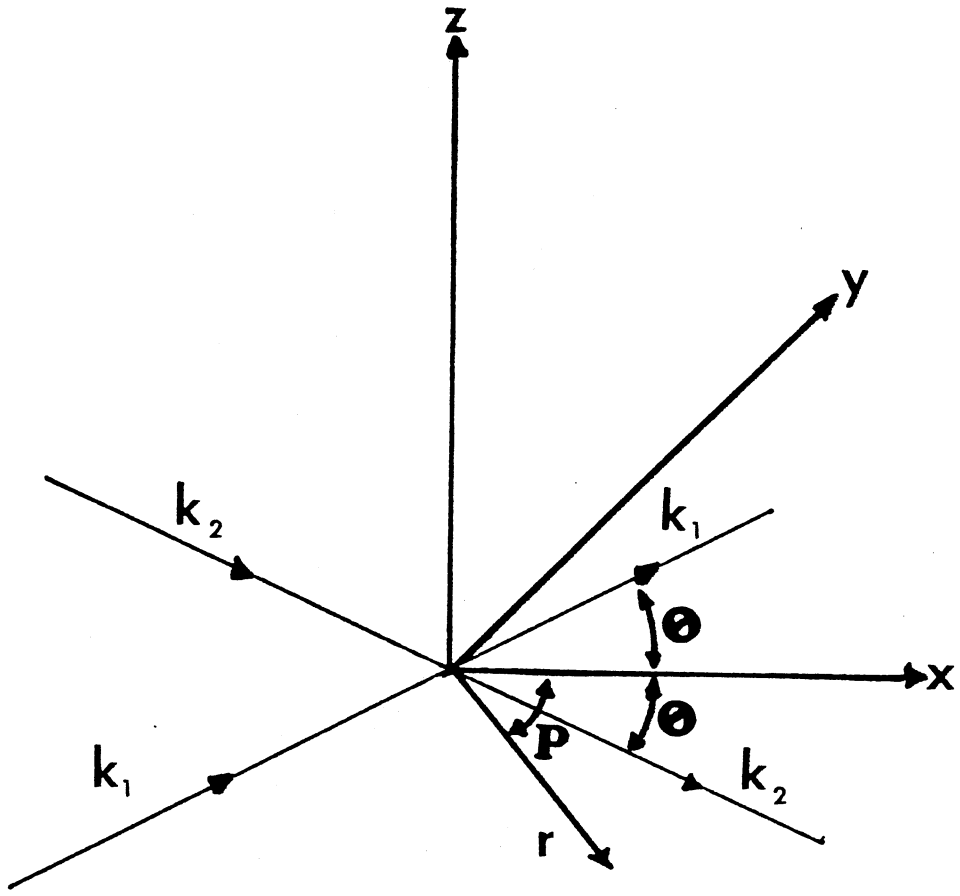

Figure 2. Graphical Representation of the Crossed Beam Geometry

maximum when $\cos[2kr\sin(\theta)]=1$, that is

$$2kr\sin(\theta/2) = 2n \quad ,n=0,1,2,..... \tag{2-12}$$

Choosing 'r=d', where 'd' is the fringe separation and substituting for $k=2\pi/\lambda$, where λ is the wavelength of the incident laser's beam, the fringe spacing can be found as,

$$d = \lambda/2\sin(\theta/2). \tag{2-13}$$

Hence the fringe spacing can be determined from knowing the laser's wavelength and the angle at which the two beams intersect. The intensity minima occur when $\cos(2kr\sin(\theta))=-1$.

The Potential For Finite Size Particles.

The force on a sphere found by equation (2-7) is true for particles whose spatial dimension is small compared to the variation in the field gradient. For particles whose diameter is in the same order as the field gradient variation, the lateral force on the parctiles is considered as being the negative gradient of the potential U, where $U=-\text{Grad}(E^2)/2$. Thus a sphere of radius 'a' can be taken as a collection of point particles subjected to the potential given above, where E^2 is found from equation (2-11). The total potential for the particle is then found by integrating this spatially varying potential over the volume of the particle. Using this argument, Chowdhury (10) has found that,

$$U_t = A/V\int_V \cos(\underline{q}.\underline{v})\,d\underline{v} \tag{4-14}$$

where, $q=2\pi/d$ and has the direction of the potential's periodicity, r is the sphere's displacement from the origin, $\underline{v}$ is the displacement to a volume element from the origin, r'is the displacement to the volume element form the sphere's center (Figure 3) V is the sphere's volume,

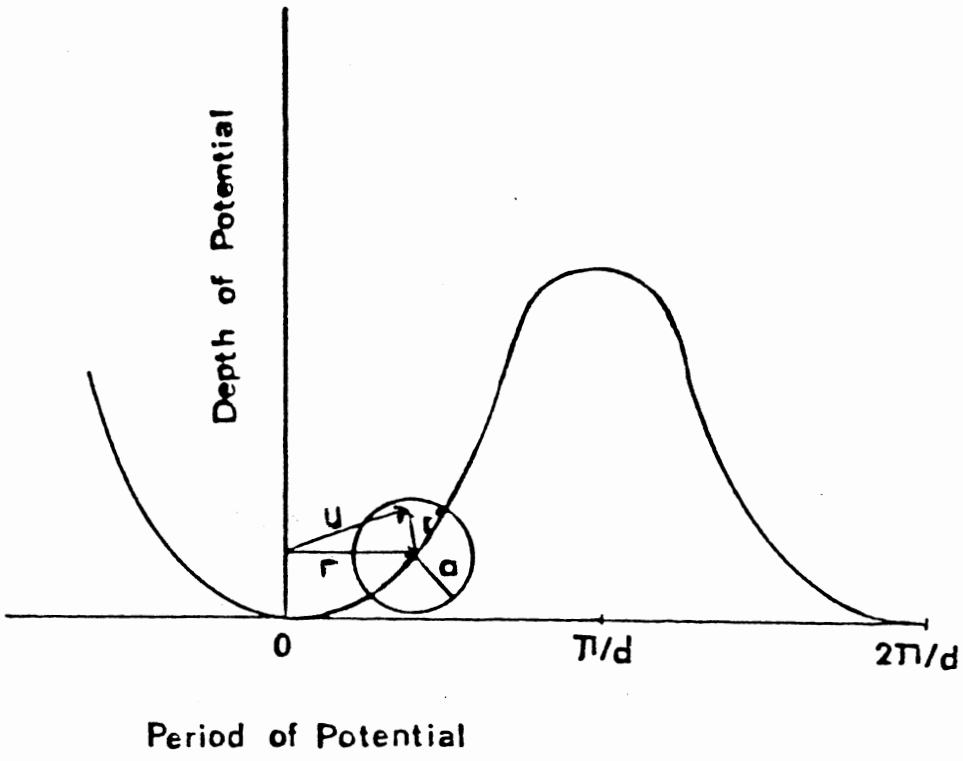

Figure 3. Dielectric Sphere of Radius a in a Periodic Intensity Potential.

and A is a constant. If we let the sphere be at a distance '$\underline{r}$' from the center of the intensity maxima in such a way that '$\underline{r}$' is parallel to '$\underline{q}$', as shown in Figure 3, then the following result is found,

$$U_t = 2A/V\int_c^r r'^2 dr' \int_o^{\pi} \sin(0)[1+\cos(qr+qr'\cos(0)]d0$$

$$= B[3\{\cos(qr)/qa\}j_1(qa)] \qquad (2\text{-}15)$$

$$B = 4n_s^2 Ia^3(n^2-1)/[k_B TcR^2(n^2+1)] \qquad (2\text{-}16)$$

where n_s is the refractive index of the host fluid, n is the ratio of the refractive index of the sphere to the host fluid, I is the input intensity of one of the laser beams in Watts/sec, R is a measure of the radius of the incident beam, c is the velocity of light in free space, k_B is Boltzman constant, T is the absolute temperature, $\underline{q}=\underline{k}_1-\underline{k}_2$ is the wave vector and $j_1(qa)$ is the first order spherical Bessel function.

In the case where b=0 (the particle placed at the origin) and assuming a point charge we see that U_t=2B, which is a maximum. The other case of interest is when a/d----->oo , that is when the sphere's radius is much larger than the fringe spacing, the average potential decreases to zero. Finally, as a/d increases the average potential oscillates and decreases to a constant, leading to a zero net force on the spherical particles(10).

In some of the experiments performed for this thesis work, single and multiple spheres were captured and held in a single beam. Locked in stable rigid array, each particle was trapped at a local intensity maxima where drastic rearrangements occur only when one of the lower particles is displaced from its local trap. The radiation pressure forces were also used in a cross beam experiment to align polystyrene spheres suspended in water in a series of layers parallel to the

intensity fringes and in case of interacting particles in solid like structures.

Steady State Characteristics

Colloidal suspensions subjected to forces described by Equation (2-15) are immersed in an electrostrictive potential given by,

$$U = -1/2\,\mathrm{Grad}(E^2)$$
$$= U_0 \cos(qz). \qquad (2\text{-}17)$$

These particles will tend to move to those regions where U is smallest. Thus the particle density, n(r), will be modulated by this potential. Using the Planck-Nerst equation to characterize the microparticle density, we write

$$n(r,t)/\,t = D\,\mathrm{div}[\mathrm{Grad}(n(r,t))-Fn(r,t)/k_BT] \qquad (2\text{-}18)$$

where F=-Grad(U(r)), is the force on the sphere and D is the diffusion coefficient. For dilute suspensions D is given by the Stokes' theorem for spherical particles, of radius a,

$$D = k_BT/6\pi\eta a \qquad (2\text{-}19)$$

where η is the liquid's viscosity. For steady state $n/\,t=0$, and the density distribution equation reduces to,

$$\mathrm{div}[\mathrm{Grad}(n(r))-n(r)F/k_BT]=0 \qquad (2\text{-}20)$$

The Boltzman distribution is a solution to the steady state equation, this distribution is given by,

$$n(r,0) = A\exp[-U(r)/k_BT] \qquad (2\text{-}21)$$

The normalizing constant, A, can be obtained by the normalization condition over a fringe period (10),

$$\int n(r,0)dr = 1 \qquad (2\text{-}22)$$

The normalized probability for finding a sphere at 'r' is given by,

$$n(r,0) = k \sin(0)/I_0(p) \exp\{p \cos[2kr\sin(0)]\} \qquad (2\text{-}23)$$

$p=CE_0^2/k_BT$, C is given by equation (2-4) and I_0 is the zeroth order modified Bessel's function. Plots of n(r) versus r for different value of C are shown in Figure 4. By increasing the applied electric field n(r,t) becomes sharply peaked and for sufficiently large incident intensity this function (n(r)) is expected to behave as periodic distribution of delta functions.

Theoretical Consideration for CCIFS and LT

This section will deal with comparing the similarities and differences of two light scattering techniques, the cross correlation intensity fluctuation spectroscopy (CCIFS) and laser trapping (LT), used in the study of colloidal suspensions.

The laser trapping (LT) experiment makes use of light induced forces to produce density modes of colloidal particles (43). The scattered intensity distribution from these modes as given by Ackerson et al.(43) may be represented as:

$$\langle I(\underline{k})\rangle = \frac{e(\underline{r}_i)e(\underline{r}_j)\exp(i\underline{k}.(\underline{r}_i-\underline{r}_j)-(V+U)/k_BT)d\{\underline{r}\}}{\exp(-(V+U)/k_BT)d\{\underline{r}\}} \qquad (2\text{-}28)$$

where the authors used the first Born approximation to represent the scattered intensity with $e(\underline{r})$ determining the size of the scattering volume. The particles interact with a potential V and are in an external potential U, which in the case of potential well created by the radiation pressure is given by:

$$U(\underline{r}) = A \cos(\underline{q}.\underline{r}) = A \cos(qx) \qquad (2\text{-}29)$$

The expression in equation (2-28) assumes that only the scattering from a single probe beam from the sample is detected. Substituting

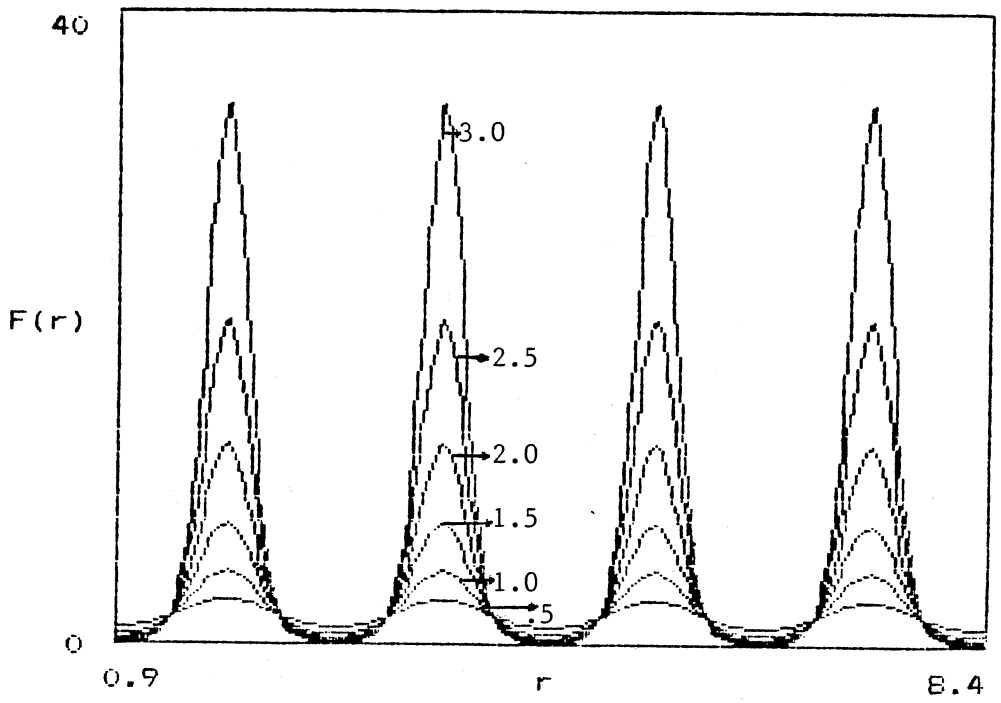

a) Density Versus Position for d=1.85um.

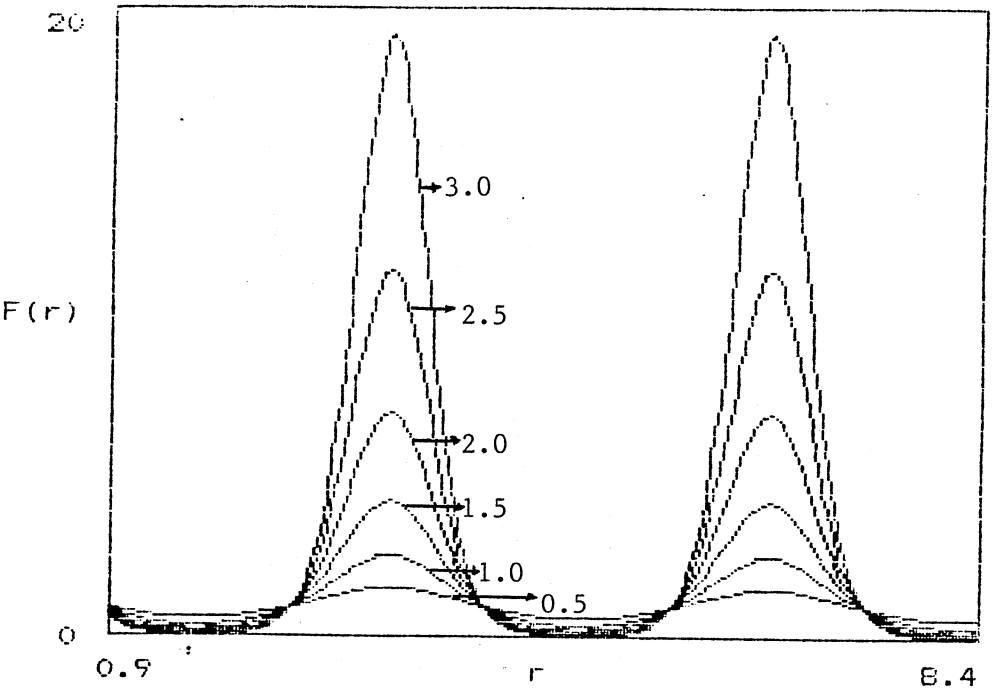

b) Density Versus Position for d=3.3um.

Figure 4. Density Distribution of Noninteracting Particles in Periodic Potential Wells with P=.5, 1.0, 1.5, 2.0 and 3.0.

equation (2-29) into equation (2-28) and expanding the numerator in terms of A/k_BT, the relative strength of the externally applied field to the thermal energy, the following relation is obtained (43),

$$<I(\underline{k})> = S(\underline{k}) + (A/k_BT)^2[S_2(\underline{k})S_2(\underline{q})\delta_{\underline{k},\underline{q}} + S_4(\underline{k},\underline{q}])(2\text{-}30) \quad (2\text{-}30)$$

where S_2 is an apertured static structure factor and S_4 function is an apertured multiparticle structure function which depends on one, two, three and four particle correlation functions.

Cross correlation intensity fluctuation spectroscopy (CCIFS) is a light scattering technique for studying the interparticle order in colloidal suspension (10). The technique uses two separate detectors to collect the scattered light and the resulting signals are cross correlated. In these experiments the orientation of the local structure in the scattering volume is determined with one of the detectors, while the other is used to scan the scattering pattern.

The distribution of the scattered intensity can be expressed in terms of one, two ,three or four particles correlation functions. The CCIF is given by (11),

$$C(\underline{q},\underline{k},t) = <I(\underline{k},t+T)I(\underline{q},T)>/(<I(\underline{k},T)><I(\underline{q},T)>) \quad (2\text{-}31)$$

where at wave vector $\underline{k}$ the instantaneous scattered intensity is $I(\underline{k},t+T)$ and at a later time, t, the intensity reading at wave vector $\underline{q}$. The k (or q)-space's position magnitude is given by

$$k = 4(\pi)n(\sin(\Theta/2))/\lambda \quad (2\text{-}32)$$

In the above equation n is the refractive index of the solvent, λ is the vacuum wavelength and Θ is the scattering angle. Using the first Born approximation to represent the scattered intensity from the scattering volume defined as $e(\underline{r})$, an expression for the CCIFS (equation (2-31)) over an equilibrium distribution of particles

mutually interacting via the potential V is found by Ackerson et al. (38) to be of the following form:

$$C(\underline{k},\underline{q},0) = \frac{\int\{\sum_{ij}\sum_{lm} e(\underline{r}_i)e(\underline{r}_j)e(\underline{r}_l)e(\underline{r}_m) \exp[i\underline{k}.(\underline{r}_i-\underline{r}_j) + i\underline{q}.(\underline{r}_l-\underline{r}_m)-V/k_BT]d\{\underline{r}\}/Z\}}{\int\sum_{ij}\{e(\underline{r}_i)e(\underline{r}_j)\exp[i\underline{k}.(\underline{r}_i-\underline{r}_j)-V/k_BT]d\{\underline{r}\}/Z \sum_{lm} e(\underline{r}_l)e(\underline{r}_m)\exp(i\underline{q}.(\underline{r}_l-\underline{r}_m)-V/k_BT)d\{\underline{r}\}/Z\}} \quad (2\text{-}34)$$

The partition function is given by,

$$Z = \int \exp(-V/k_BT)d\{r\}. \quad (2\text{-}35)$$

The expression given in equation (2-34) has been found in terms of multiparticle distribution functions (38) as:

$$C(\underline{k},\underline{q},0) = \frac{S_2(\underline{k})S_2(\underline{q})[1+ \underline{k},+\underline{q}]+S_4(\underline{k},\underline{q})}{S_2(\underline{k})S_2(\underline{q})} \quad (2\text{-}36)$$

where S_2 and S_4 are the same equilibrium functions presented in equation (2-30). The nongaussian term, S_4, includes four particle correlation functions and it becomes small for large scattering volumes as compared to the Gaussian contribution (the first term in equation (2-36)). Thus limitation of the CCIFS to small scattering volumes increases the relative importance of the nongaussian term (43).

The similarities between the CCIFS and LT techniques are well demonstrated in equations (2-30) and (2-36). Both techniques are sensitive to the presence of correlation in the density modes of fluid systems (43). In the laser induced freezing one density mode is stimulated by application of an external field and the other density modes, coupled to this one, result from the interparticle interaction

and are they are all monitored by scattering. The parallelism between the two is given in Figure 5, where the CCIFS data is presented in Figure 5a (43) and the LT intensity distribution is presented in Figure 5b. The large autocorrelaltion signal in CCIFS at o=0 degrees corresponds to the strong scattering form the directly stimulated mode in LT. Similarly, the weaker signals at o=60 and 120 degrees corresponds to the off axis scattering by the slaved modes. The advantage of LT is that the calculated scattering is not modulated by the aperture functions. The disadvantage of this LT is that extreme care must be taken in order to collect the data.

Scattering and Two Dimensional Pair Correlation Function

The study of the different diffracted intensity maxima produced from the laser induced freezing of interacting colloidal suspensions was carried by Chowdhury (10) as part of his thesis work. In this thesis work the real space analysis of the laser induced freezing is accomplished with the use of correlation functions, specifically the two dimensional pair correlation function. Thus the aim in this section is to find the theoretical connection between the scattering intensity function, the 2D correlation function, and the conditional probability function. This latter function, $P(\underline{r}1-\underline{r}2/\underline{r}2)$, is defined as the probability of finding a particle at position $\underline{r}1$ given a particle at $\underline{r}2$. The two dimensional pair correlation function ($g(\underline{r})$), in the other hand, is a measure of the translational as well as the orientational correlation between particles.

The scattered intensity of particles positioned at $\{\underline{r}_i$, i=1 to

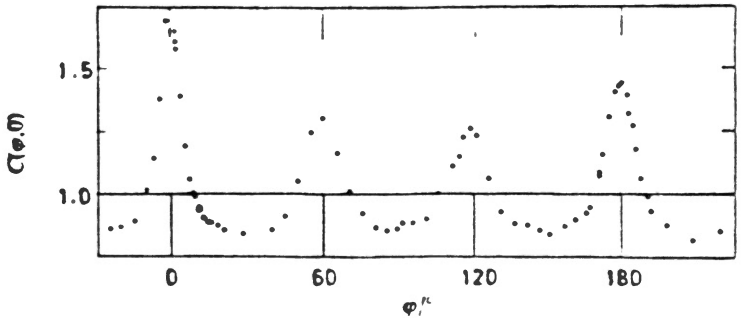

a) Normalized Zero Time Intensity Cross-Correlation Function $C(\varphi,0)$ Obtained form Two-Dimensional Colloidal Liquid.

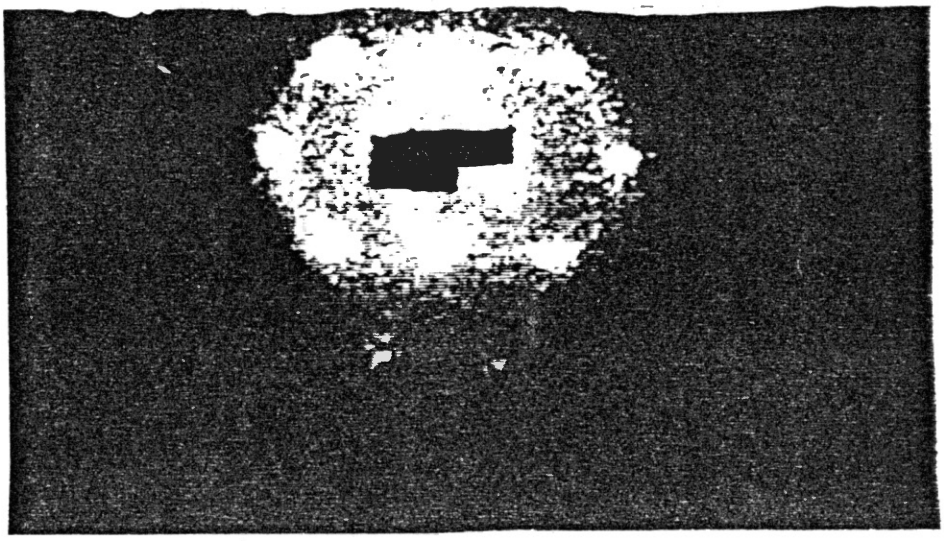

b) Self Scattered Light by Two Laser Beams Crossed in a Two-Dimensional Sample.

Figure 5. Zero Time Intensity Cross-Correlation Function (a) and the Self Scattering from Laser Trapping of Colloidal Monolayer at Commensurate Crossing Angle (b).

N} in the first Born approximation is given by:

$$I(\underline{k}) = \langle \sum_i \sum_j \int \exp\{i\underline{k}.(\underline{r}_i - \underline{r}_j)\} P(\underline{r}_i, \underline{r}_j)(1 - \delta_{ij}) d\underline{r}_i d\underline{r}_j + \sum_i \int P(\underline{r}_i) d\underline{r}_i \rangle$$
$$= N(N-1) \int \exp\{i\underline{k}.(\underline{r}1 - \underline{r}2) P(\underline{r}1, \underline{r}2) d\underline{r}1 d\underline{r}2 + N \qquad (4\text{-}29)$$

The two particle probability may be written in terms of a conditional probability as,

$$P(\underline{r}1, \underline{r}2) = P(\underline{r}1/\underline{r}2) P(\underline{r}2)$$
$$= P(\underline{r}1 - \underline{r}2/\underline{r}2) P(\underline{r}2) \qquad (4\text{-}30)$$

where $\underline{r}1 - \underline{r}2 = \underline{R}$ represent the pattern relative to $\underline{r}2$ depending on the position $\underline{r}2$ of the reference particle in the fringes. Using the above equation, the scattered intensity can be written as:

$$I(\underline{k}) = N + N(n-1) \int d\underline{r}1 \int d\underline{r}2 \exp\{(i\underline{k}.\underline{R}) P(\underline{R}/\underline{r}2)) P(\underline{r}2)$$
$$= N + N(N-1) \int d\underline{R}\, h(\underline{R}) \exp(i\underline{k}.\underline{R}) \qquad (4\text{-}31)$$

where $h(\underline{R}) = \int d\underline{r}2\, P(\underline{R}/\underline{r}2) P(\underline{r}2)$. For normal fluids $P(\underline{r}2)$ is equal to the average density of the system (d_0) and it is constant, thus referring to equation (4-30) we get,

$$P(\underline{R}/\underline{r}2) = P(\underline{R}) = g(\underline{R}) d_0. \qquad (4\text{-}32)$$

So $h(\underline{R}) = g(\underline{R}) d_0^2$ in this case is the standard fluid two dimensional pair correlation function. However the more general function $h(\underline{r})$ is the calculated function in our analysis and is referred to as the two dimensional pair correlation function, and as seen above it is directly related to a fourier inversion of $I(\underline{k})$.

The standard relationships between $P(\underline{r}1, \underline{r}2)$, $g(\underline{r}1, \underline{r}2)$ and $P(\underline{r}1/\underline{r}2)$ are given by,

$$P(\underline{r}1, \underline{r}2) = P(\underline{r}1/\underline{r}2) P(\underline{r}2) = P(\underline{r}1 - \underline{r}2/\underline{r}2) P(\underline{r}2)$$
$$= g(\underline{r}1, \underline{r}2) P(\underline{r}1) P(\underline{r}2)$$
$$= g(\underline{r}1 - \underline{r}2)/\underline{r}2) P(\underline{r}1) P(\underline{r}2) \qquad (4\text{-}33)$$

Considering $h(\underline{r})$ again, we obtain:

$$h(\underline{R}) = \int d\underline{r}2\ g(\underline{R}/\underline{r}2)\ P(\underline{r}2)\ P(\underline{r}1)$$
$$= \int d\underline{r}2\ g(\underline{R}/\underline{r}2)\ P(\underline{r}2)\ P(\underline{R}+\underline{r}2)$$
$$= \int d\underline{r}2\ g(\underline{R}/\underline{r}2)\ D(\underline{r}2)\ D(\underline{R}+\underline{r}2) \qquad (4\text{-}34)$$

where $D(\underline{r})$ is the density at $\underline{r}$. At large $\underline{R}$ we might expect $g(\underline{R}/\underline{r}2)$ to approach one, such that,

$$h_{oo}(\underline{R}) = \int d\underline{r}2\ D(\underline{r}2)\ D(\underline{R}+\underline{r}2) \qquad (4\text{-}35)$$

which is the form used to describe solids in mean field theory. A normalized $h(\underline{R})$ is given by $H(\underline{R})$ ($H(\underline{R})=h(\underline{R})/h_{oo}(\underline{R})$) which approaches one at large $\underline{R}$ values. It appears that we cannot get $g(\underline{r}1,\underline{r}2)$ or $P(\underline{r}1,\underline{r}2)$ or $P(\underline{r}1/\underline{r}2)$ directly without noting where the reference particle ($\underline{r}2$) is with respect to the fringes and then constructing $P(\underline{r}1-\underline{r}2/\underline{r}2)$. What we have is a reduced or effective $g(\underline{R})$ which gives the scattered intensity when Fourier transformed to k-space. Because of the translational properties of $I(\underline{k})$, i.e. only depending on (r_i-r_j), there is no explicit dependence on absolute particle position with respect to the fringes.

In terms of $H(\underline{R})$ the crux of the argument is what is the difference between

$$H(\underline{R}) = \int d\underline{r}2\ g(\underline{R}/\underline{r}2)\ D(\underline{r}2)\ D(\underline{R}+\underline{r}2) \qquad (4\text{-}36)$$

and

$$H'(\underline{R}) = \int d\underline{r}2\ D(\underline{r}2)\ D(\underline{R}+\underline{r}2) \qquad (4\text{-}37)$$

that determines whether $g(\underline{R}/\underline{r}2)$ has significant structure, $g(\underline{R}/\underline{r}2)=1$. In general,

$$D(\underline{r}) = < \delta(\underline{r}-\underline{r}_i) > \qquad (4\text{-}38)$$

which is constant for any homogeneous fluid structure in the absence of an external field, but $D(\underline{r})$ may have some structure when the fluid is in an external field.

Thus a liquid in no external field gives

$$H(\underline{R}) = g(\underline{R})\ d_0^2 \tag{4-39}$$

$$H'(\underline{R}) = d_0^2 \tag{4-40}$$

In the case of noninteracting particles in an external field, $g(\underline{R})=1$, giving:

$$H(\underline{R}) = \int d\underline{r}2\ (1)\ D(\underline{r}2)\ D(\underline{R}+\underline{r}2)$$

$$= g(\underline{R})\ H'(\underline{R}) \tag{4-41}$$

If we neglect particle position dependence in the external field, then $g(\underline{R}/\underline{r}2) \text{ ----> } g(\underline{R})$ and we have generally that:

$$H(\underline{R}) = g(\underline{R})\ H'(\underline{R}) \tag{4-42}$$

But this need not be true generally.

CHAPTER III

EXPERIMENTAL PROCEDURE

Introduction

This section describes the experimental methods used in preparing the colloidal samples employed in this study. The experimental set ups for the crossed beam analysis are presented and discussed. The sample cell designs and their specific use is shown and explained. The cleaning procedures for the colloidal particles and the cells are also presented in this chapter.

Cross Beam Expemental Set Up

The cross beam experimental set up is shown in Figure 6. The 488nm argon-ion laser beam is split into two beams. The beam splitter used for this purpose was set so that the transmitted to the reflected beams were 90 degrees apart. This produced a 2/3 intensity ratio between the two beams. This ratio is set to one by attenuating the beam with the higher intensity. The power of one of these final beams is what is referred to in this work whenever an intensity or laser's power is mentioned . These beams traverse the same optical path length, and upon their reflection by the prism they propagate parallel to each with the same polarization . The prism is mounted on a unidimensional translating plate allowing for controlling the separation between the two reflected beams from 0 to 3.0cm. This in turns allows

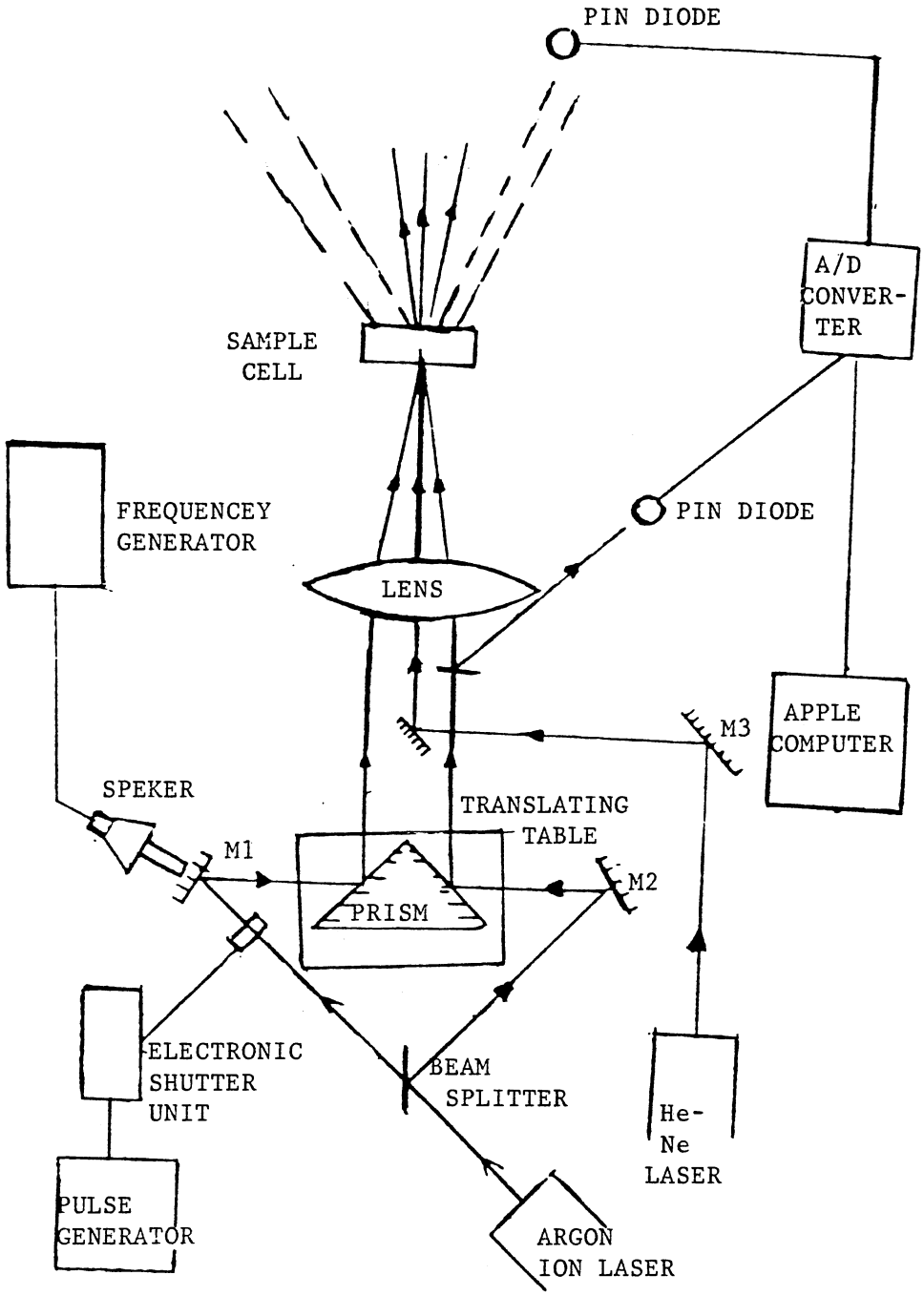

Figure 6. Crossed Beam Experimental Set-Up.

for regulating their crossing angle (from five to 15.5 degrees) after they traverse the converging lens. The translating plate is spring loaded to help the beams stay coplanar and thus cross at a single spot. The monitoring of the crossing regions is accomplished by probing the area with a microscope and projecting the intensity pattern on a screen.

The He-Ne laser, wavelength of 628nm, serves as a probe (or read) beam for the gratings produced by the mixing of the two Argon-Ion write beams. The alignment of this laser's beam with the crossing area of the write beams is accomplished with a couple spring loaded reflecting mirrors (M3 and M4). The direction of propagation for the probe beam is taken in the same half space as the two write beams. The scattered light is detected with a pin-diode whose digitized output is stored in and or printed by the Apple IIe computer.

The electronic shutter shown in Figure 6 is used to block one of the write beams, in the self scattering time dependent experiments, or the main argon ion beam for the nondegenerate probing experiments. This shutter is driven by a pulse generator, allowing for controlling the time of exposure to the radiation forces.

Some of the experiments I have carried in the course of this thesis work, dealt with having a vibrating sinusoidal intensity fringe pattern or just translating a single laser beam back and forth. This was done by placing a speaker behind one of the reflecting mirrors (mirror 1 or 2) and resting its driving arm on the backplane of the mirror. Driving the speaker with a frequency generator allows for the desired translation of beam, which causes a path difference and thus a phase difference leading to vibrating fringes.

Sample Viewing And Imaging

The direct viewing of the colloidal systems used for the structure analysis is accomplished with an Olympus BH2 microscope. The 100x, numerical aperture 1.25, oil immersion objective with depth of focus of .68um, and working distance of .17mm is used for direct observation of the formed structures. This microscope uses Koehler illumination. The viewing of the reflected images was observed either through the microscope eyepiece or through a side port with an MTI 67 series camera system. This camera system consists of camera head, cable assembly and control unit. It provides for complete auto or manual operation of the viewed images from a front panel.

For the crossed beam experiments the colloidal system is viewed by probing the sample cell with a 100x oil immersion lens with the same specifications as described above (Figure 7). The images produced from this are magnified even further by placing a second objective at 25cm distance from the first. This 20x objective has a .04 numerical aperature, depth of focus of 7.6um, and working distance of 9.15mm. This lab made micorscope is illuminated with the 488nm laser light. The magnified images are viewed on a transparent screen placed at about 1m distance from the second objective. The real space images are than recorded by placing a camera at 1m distance behind the transparent screen. In some cases neutral density filters were needed to reduce the intensity of the images reaching the camera.

Sample Cell Design

The cell used for the time dependent studies of the samples where only the scattered intensity data was measured consisted of: three

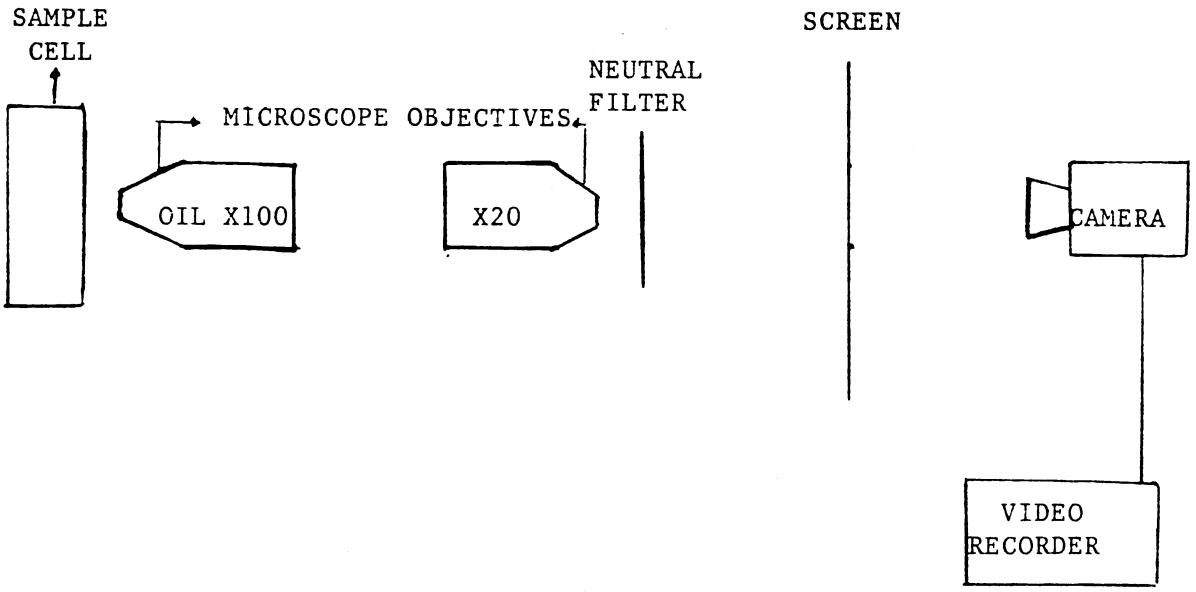

Figure 7. Experimental Set Up for Real Space

quartz plates, a viton rubber O-ring and a housing device. The 1.0cm diameter and .3cm thickness flat is glued to the 2.5cmx.4cm flat, the combination of these constitutes the lower boudary of the cell. This lower cell boundary is then housed in an aluminum holder unit; with the viton rubber O-ring (.4cm thickness) placed on the top of the larger plate. The other 2.5cmx.4cm flat is set on the top of the O-ring and is labeled as the top boundary for the cell. The whole set is kept together by screwing the other aluminum cell-holder unit to the bottom one as demonstrated in Figure 8. Tightening the screws seals the cell and controls the gap between bottom and top plates. This design proved to be well sealed against evaporation and unwanted ouside contaminents.

Modifications of the above cell design proved to be a necessity for the recognition of the spheres, in the real space analysis of the interacting colloidal suspensions. A diagram of such cell is shown in Figure 9. The top plate for in this case consists of a polystyrene ring (outer and inner diameters of 2.5cm and 1.2cm and thickness of .4cm), covering the top ring is a circular cover slide 18mmx.2mm. This cover is glued to the polystyrene plate with high torr epoxy, where all the excess glue is removed very carefully and a wide range of cleaning procedures are followed to get any glue residue from the inner cover slide's surface. This top plate is the one referred to in this thesis whenever the front cell wall is mentioned. Added to the bottom plate discussed above is a 1.0cmx.3cm saphire flat in order to reduce the local heating. This plate is glued to the quartz flat of the same dimensions. Again all the glued edges excess epoxy is carefully removed. In these cells the volume between the O-ring and the

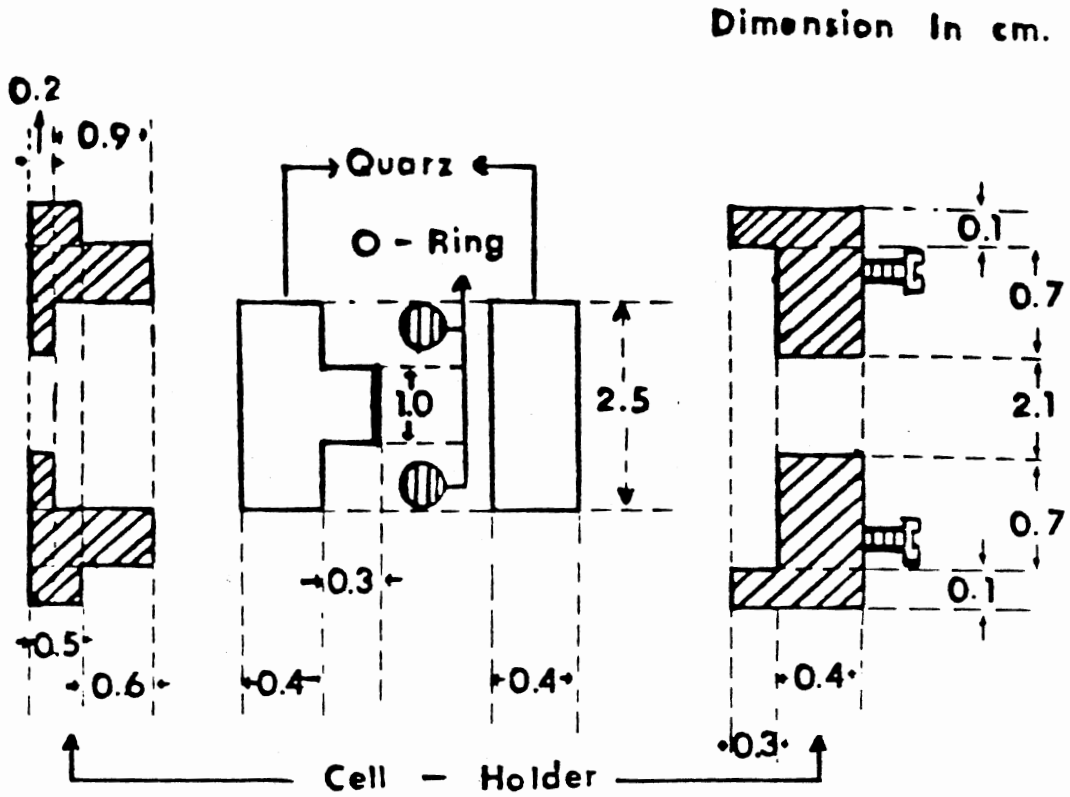

Cell Design

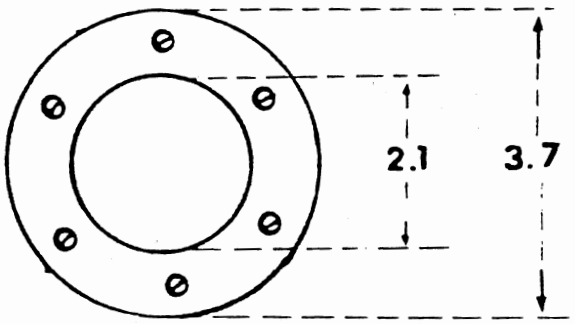

Front View

Figure 8. Side and Front View of Sample Cell Design.

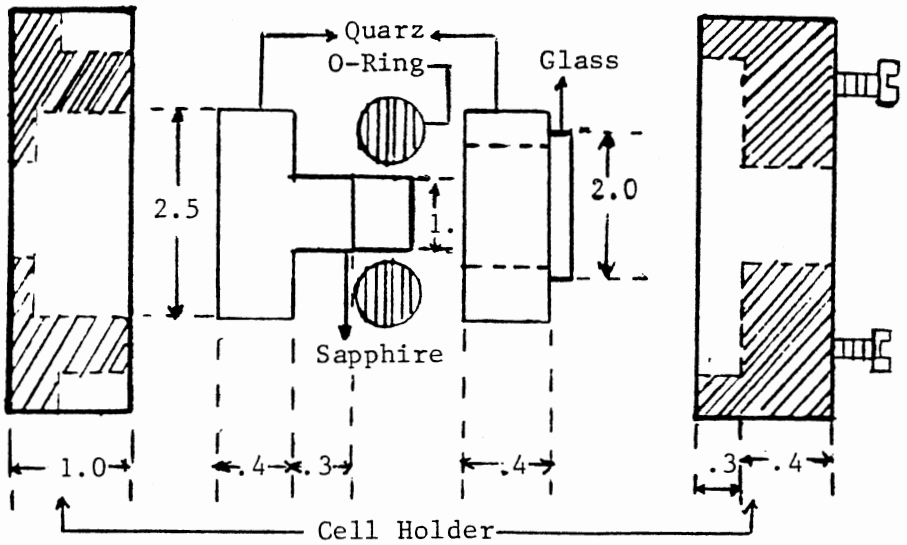

a) Side View

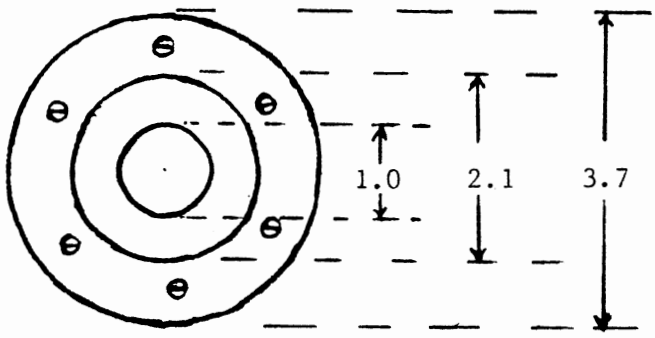

b) Front View

Figure 9. Side (a) and Front (b) View of the Sample Cell Used in Real Space Analysis.

periphery of the smaller flats is partially filled with the ion exchange beads mixture.

Cell Cleaning

For the interacting samples it is very important to have the cell cleaned of all impurities. This is accomplished by extensive cleaning of the top and bottom plates, O-rings, sample loading syringes, resin bead mixture and anything that comes in contact with the colloidal suspensions or the inner cell's surface. In this study, the first cleaning step is the removal of all excess glue or epoxy from all flats. The plates that make it through this step are then placed in a polyethylene mesh with the O-ring and the syringes and are subjected to the following cleaning process:

1) Stirring in a solution of micro detergent and deionized water at moderate temperature, below boiling water temperature.

2) rinsing each part separately with deionized water, and sonicating in a sonic bath for a period of about 5 minutes on the average. The transmitting fluid in the sonication process is a mixture of micro and deionized water.

3) Rinsing each element in deionized water at elevated temperature while stirring.

4) A final rinsing with highly deionized water (18megaohm resistance) is performed and each cleaned part is blown dry with freon.

This cleaning procedure gave the best and longest lasting results for making the particles interact over large length range via Coulombic repulsion forces. Samples left inside the cell for extended periods of time showed cuagulation problems. This is believed to be

caused by the leaching of stray ions from the cell.

The Paricle Cleaning Procedure

To improve the particle-particle coulombic interaction and reduce the number of particles sticking togother, the water-soluble species and inorganic salts are removed from the colloidal suspensions through the following process:

1) The particles are diluted in a liquid and centrifuged at 200rpm for a different time periods depending on the suspension liquid used.
2) The supernatant liquid above the solid is then siphoned.
3) A small volume of liquid is added to the settled particles, and the mixture is sonicated as long as it takes to shake the particles loose and have them suspend in the liquid.

These 3 steps are repeated for ten times. In the first and last two runs, highly deionized water is used as the diluting liquid and the centrifuging time was about thirty minutes period. In the other runs high grade methanol is used for diluting the suspensions and the centrifuging period is cut to ten minutes. The time required to shake the spheres loose depended on the suspension liquid and it took much less time when methanol was used as compared to water.

Before injecting the colloidal suspensions the cell gap is adjusted to 20um and then the 18megaohm deionized water is injected into the cell. The contents of the cell (water plus resin bead exchanger) are tumbled at low rotation rate for a period of 24 hours. The reason behind this is to reduce the number of stray ions that might be present in the cell before the injection of particles takes place. After this process, the water is extracted from the cell whith a clean

syringe. The microspheres are then injected at the cell with the desired concentration. The resin beads and the colloidal suspensions are then mixed at low rotation rates for a period of 2-3 hours. After this process the gap cell is again adjusted to values between 10-40um, giving a wedged shaped gap and having single to multi layered regions. This cleaning process proved to give the best results for the interaction between the spheres for long periods of time extending from one week to three weeks.

Image Processing

For the real space experiments all the experimental information is recorded on video tape for future analysis. This data is fed to the an Imaging Technology video deigitizer interfaced to a Scientific Micro Systems microcomputer system (Figure 10). The Imaging Technology system consists of one AP-512 Analog Processor and one FB-512 Frame Buffer in a monochrome (black/white) configuration(IP). The two modules are connected via the video bus and controlled via the Q-bus. This basic configuration digitizes, stores, and displays a single frame of video information. The SMS microcomputer system performs all image processing functions. The digitizing process consist of transforming an individual picture into a two dimensional integer array of numbers from 0 to 256 with dimensions of 512x480. This array is stored in the FB 256 K-byte RAM allowing for accessing each pixel and performing image transformations through mathematical functions designed for special purposes. Amongst these the following subroutines were used in the enhancement of the images and the detection of the microspheres:

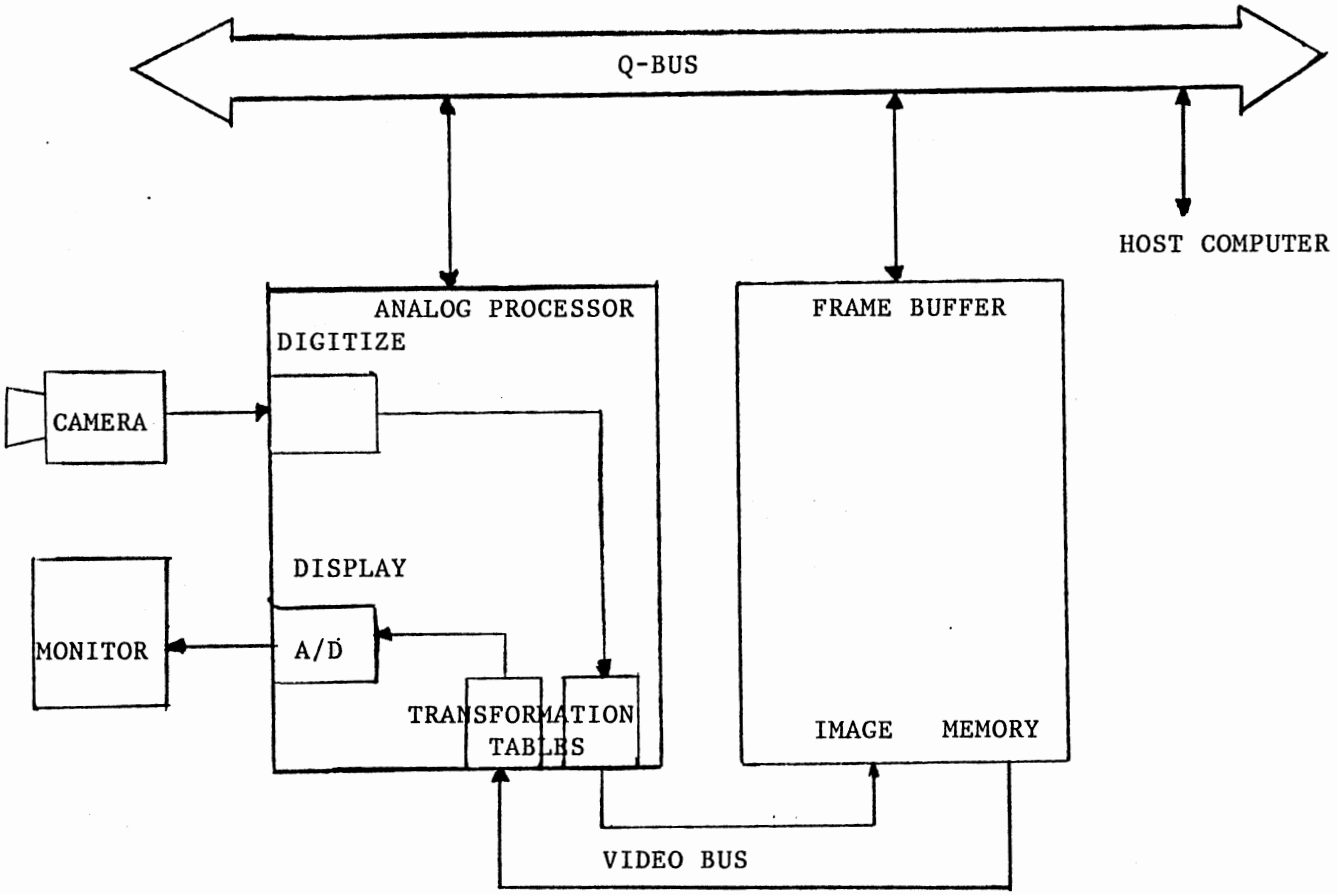

Figure 10. Block Diagram of the Imaging Technology Basic Monochrome Imaging System.

a. Image equalization using the a smoothing function between two given intensities I1 and I2 (I1<I2), the functional form used in this analysis was of the form (44):

$$\begin{aligned} f(I) &= 255*(I-I1)/(I2-I1) && \text{for } I2<I<I1 \\ &=0 && \text{for } I<I1 \\ &=255 && \text{for } I>I2 \end{aligned} \qquad (3\text{-}1)$$

This intensity equalization gave sharper images but did not help much in the detection subroutines which will be discussed later.

b. Edge detection using the Sobel operator and the Robert gradient techniques. The Robert gradient can be presented by the 2x2 template (44)

f(x,y)	f(x,y+1)
f(x,y+1)	f(x+1,y+1)

(3-2)

where f(x,y) is the intensity function at the given x-y position and G(f(x,y)) is the gradient of f at coordinates (x,y). In terms of an equation a typical approximation is given by the relation

$$G(f(x,y)) = \{[f(x,y)-f(x+1,y+1)]^2+[f(x+1,y)-f(x,y+1)]^2\}^{1/2} \qquad (3\text{-}3)$$

or using absolute values (symbol for absolute value is given by []),

$$G(f(x,y)) = [f(x,y)-f(x+1,y+1)] + [f(x+1,y)-f(x,y+1)] \qquad (3\text{-}4)$$

The Sobel operator on the other hand is a 3x3 template (44) ginven by the following experssion:

a	b	c
d	e	f
g	h	i

(3-5)

where a, b, c, d, e, f, g, h, and i are pixels' intensities values. Defining G_x and G_y as

$$G_x = (g+2h+i) - (a+2b+c)$$

$$G_y = (c+2f+i) - (a+2d+g) \qquad (2\text{-}6)$$

The gradient at e is then defined as,

$$G = [G_x^2 + G_y^2]^{1/2}$$

$$= [G_x] + [G_y] \qquad (3\text{-}7)$$

In equation (3-4) and (3-7), the [] stands for the absolute value of the given quantity, and this approximation is made to save on the speed of computation while analyzing the data. Both the Robert and Sobel gradients were found to give relatively large values for prominent edges in an image and small values in regions that are fairly smooth, being zero in regions that have a constant gray level. The Sobel operator being a 3x3 template gave sharper rings around the spheres and sphere like high intensity regions than its counter 2x2 template.

c. Image restortion oriented toward reconstructing an image that has been degraded by using some a priori knowledge of the degradation process. In terms of a mathermatical equation we have,

$$g(x,y) = Hf(x,y) + n(x,y) \tag{3-8}$$

where g(x,y) is the degraded image, H is the degradation operator, n(x,y) is an additive noise, and f(x,y) is the input image that is sought. This image is obtained by using the relation

$$\begin{aligned} f(x,y) &= f^{-1}[F(u,v)] \\ &= f^{-1}[G(u,v)/H(u,v)] \end{aligned} \tag{3-9}$$

for x,y= 0,1,2,.....N-1, G(u,v) is the FFT of g(x,y) and n(xy) is assumed to be zero. This procedure is implemented by means of an FFT algorithm. Different filters were used for the process of restoration (Butterworth high pass filter, Wiener filter, point spread function) but the time required for the analysis made the process unworthy.

d. Detection and recognition of the spheres was the main aim behind the analysis of the interacting samples. This process was first tried by generating a J x K template, which corresponds to one of the spheres and matching it with the given image, this resulted in some spheres being ignored while fictious regions where picked as being a paricle. This process of choosing a template could be thought of as a correlation, where by definition the correlation between two functions is given by,

$$R(m,n) = \sum_{x,y} f(x,y)w(x+m,y+n) \tag{3-10}$$

or

$$R(u,v) = F(u,v)W^{*}(u,v) \tag{3-11}$$

where F(u,v) is the 2D transform of the given 512x480 digital image f(x,y), $W^{*}(u,v)$ is the complex conjugate of the 2D transform of the JxK (J<512 and K<480) window function w(x,y). Note that m=0,1,..,511, and n=0,1,...,469 and the summation is taken over the region where

w(x,y) is defined. This correlation function was tried and the same problems observed with the templates were encountered with this function, namely the recognition of fictitious regions as spheres while ignoring positions where the particles are located. The time required to process a single image with the detection subroutines discussed so far was of the order of five minutes when the VAX and Contol Imaging system (property of Electrical & Computer Engineering Department) were used. The limitations of the SMS RAM memory (.5M bytes) and its slow computation time as compared to the VAX were the main determining factors in replacing the subroutines discussed above with the intensity slicing and edge detection subroutines.

The intensity slicing subroutine used the concept of subdividing the image into different windows, in each window the intensities that fall between a maximum and minimun value are collected and then made into clusters. Within a certain radius from each cluster's center an edge detection subroutine is suplemented. If the edges are detected along the x and y directions then the cluster's center is taken as a prospective position for a sphere's center. This detection program took from 1-2minutes for the recognition of the centers and was the most efficient way for detecting the microspheres, althought it did require input information about the cutoff intensities the maximun radii, the separation between particles and an interactive part helping in the accepting the first particle in each fringe.

The problems encountered in the detection of the spheres were a result of the background intensity of the stationary sinusiodal fringe pattern which at certain regions creates sphere like structures.

Accuracy In Positions

To estimate the distortion of the experimental optics and that due to the video camera, two set of analysis were performed. In the first of these, the distortion due to the objectives, was found by taking images of the standing fringe pattern alone; and of grooved gratings with their periodicity along the x and y directions. By fitting a linear fit through the low intensity regions of the fringe pattern (or gratings), it was found that the average separation between these lines stayed the same with a maximum deviation of two pixels along the x-direction and one pixel in the y-direction. The distortion due to the camera and video system is found by taking photographs of polar graph paper and finding the distances to different radii. The measured radii from the center of the polar plot for an average of 6 frames is given in Table I. The maximum destortion observed from the data given in this table is two pixels. For both cases the maximum distortion occurs at the edges of the digitized frames and it gives an error in locating a particle of 2 pixels. Most of the analized data was taken at the center far from this distortion region, thus no correction was needed for our analysis.

Table I

DATA FOR DISTORTION INTRODUCED BY VIDEOTAPING SYSTEM

Ring #	r1(pixels)	r2(pixels)	r2-r1
1	7	7	
2	30	30	
3	61	62	1
4	115	116	-1
5	155	154	-1
6	195	197	2
7	235	234	2

CHAPTER IV

INTERACTING PARTICLE STUDIES

Introduction

In this study the term 'Interacting Particles' is used to describe colloidal suspensions of polystyrene sulphonate latex spheres in water that is relatively free of electrolytes. Upon immersion in water the cationic counter-ions from the surface sulfate groups will diffuse away from the particle's surface causing the spheres to be uniformly charged. The stripped counterions can be exchanged with ions supplied by ion exchage resin and the resulting mixture of counterions and any added electrolyte serves to screen the charged spheres and modify significantly the coulomb repulsion between them.

When these colloidal suspensions are confined between two smooth repelling flats the particles order as in a solid in some regions and as a liquid in others. This makes these samples ideal for phase transition and structural transition studies.

The response of these self-organizing systems to externally applied field is studied in this work. Radiation pressure was used as one of these external fields to manipulate the interparticle order in these suspensions.

In this chapter, the analyses on the interacting particles samples will be divided into three sections. The first section will deal with the structural transition in a wedged sample cell. The second section

will be devoted to the real space analysis of the ordering induced by the externally applied radiation pressure field. In the third section an analysis of the scattering patterns as a function of input power and crossing angle is studied.

Equilibrium Structures Without External Fields

It is already established that a system of colloidal spheres submerged in aqueous suspensions can exhibit transitions from an ordered (solid) to a disordered state (liquid). Colloidal crystal, liquid and gas like states have been observed in different studies. In a colloidal crystal, for example, the suspended particles are positioned at regularly spaced intervals. The observed order is typically that of a body centered cubic crystal or face centered cubic crystals in dilute and concentrated charge stabilized suspensions, respectively (9). Two dimensional systems have been examined by trapping a single layer of particles between optical flats(3, 4, 5) or the water-air interface (45). Here states having HCP closest packed crystalline and liquid like order have been observed despite the apparent lack of long range order in two dimensional systems.

In this study the colloidal suspensions were trapped between two smooth repelling plates, as described in the experimental set-up chapter. The distance between the two plates is adjustable, allowing for a wedge shaped gap and for the trapping of a single to multi colloidal layers. The colloidal spheres are repelled from the glass surfaces for two reasons: glass plates become highly charged when they are brought in contact with water, this leads to a plate surface

charge density of $2.5 \times 10^{14} cm^{-2}$(1&2), which is comparable to that on the polystyrene surface. Another reason for this repulsion is caused by the dielectric constant contrast between the water-glass interface (c=80 of water and 5 for glass), which introduces repulsive image charges of the spheres.

Although extensive care was used in the cleaning of the samples and the cells, it was observed that all the experimental samples used in this study had a leaching problem. Ions from the cell's walls and foreign substances leak inside the sample and cause coagulation problems with the extended immersion time giving dumbbells and larger aggregates, about 5%.

By direct observation of 1.07um diameter interacting particles samples, different 3-D and 2-D phases were seen. Digitized images, 512 by 480 pixels, of some of these phases are shown in Figures 11 through 16. A region near the apex of a wedged cell is shown in Figure 11. This demonstrates the transition form a three dimensional solid structure to a two dimensional liquid phase. In the lower right corner a liquid state is observed where the particles appear to have no orientational nor translational order. This region is at the apex of the wedge. Right above this liquid phase a two dimensional (monolayer) hexagonal closed packed phase starts to form. At the center of this figure a transition from two dimensional HCP structure to three dimensional square structure is shown. This region is considered as the 'hopping' region, where hopping corresponds to intense particle motion normal to plane of gap. Finally, at the upper left corner of this figure a three dimensional square phase is established.

Figures 12 and 13 show two-dimensional HCP crystalline structure.

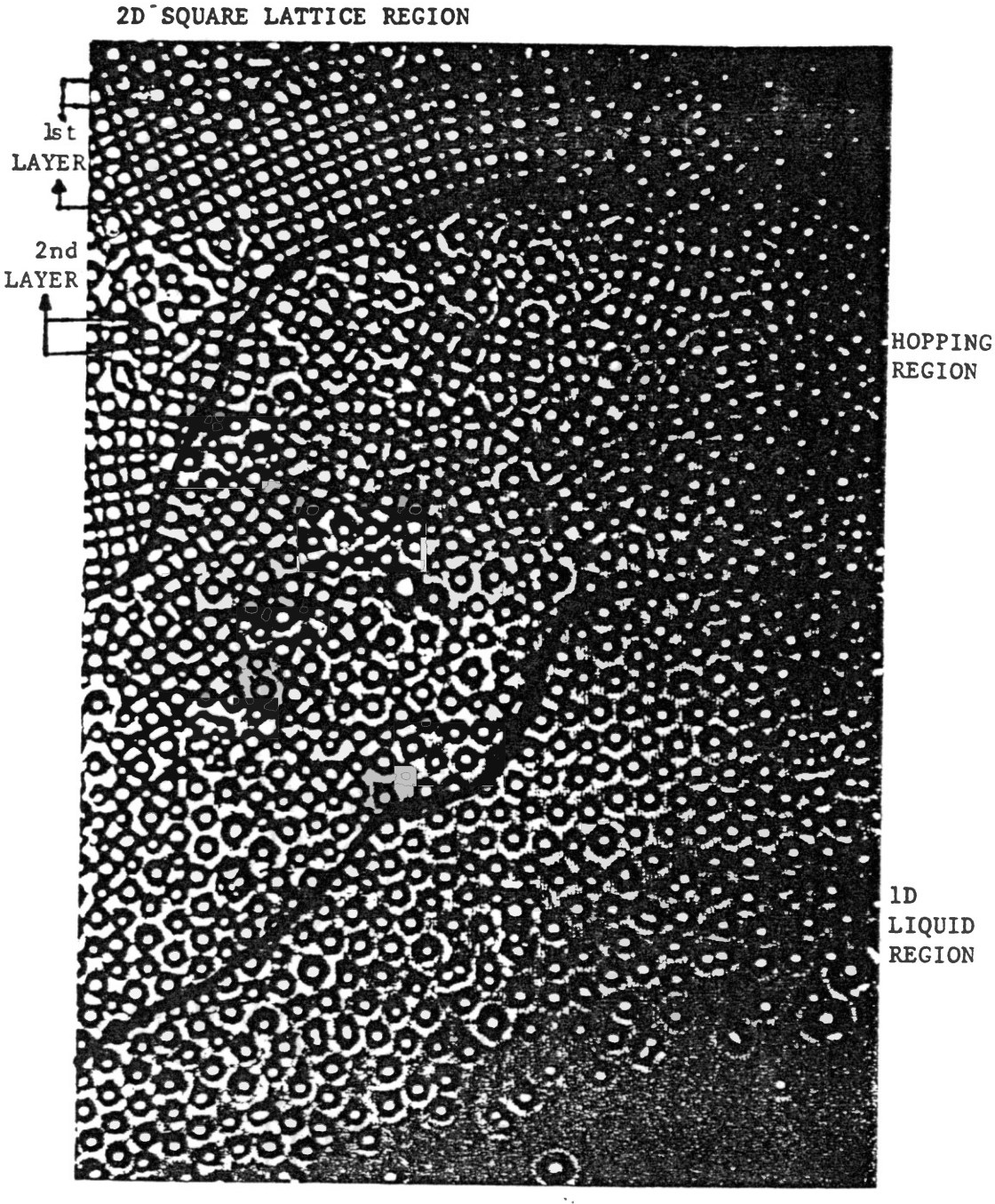

Figure 11. Transition Region From Monolayer Liquid Phase to Multilayer Solid Phase For 1.07um Interacting Polystyrene Spheres Suspended in Highly Deionized Water.

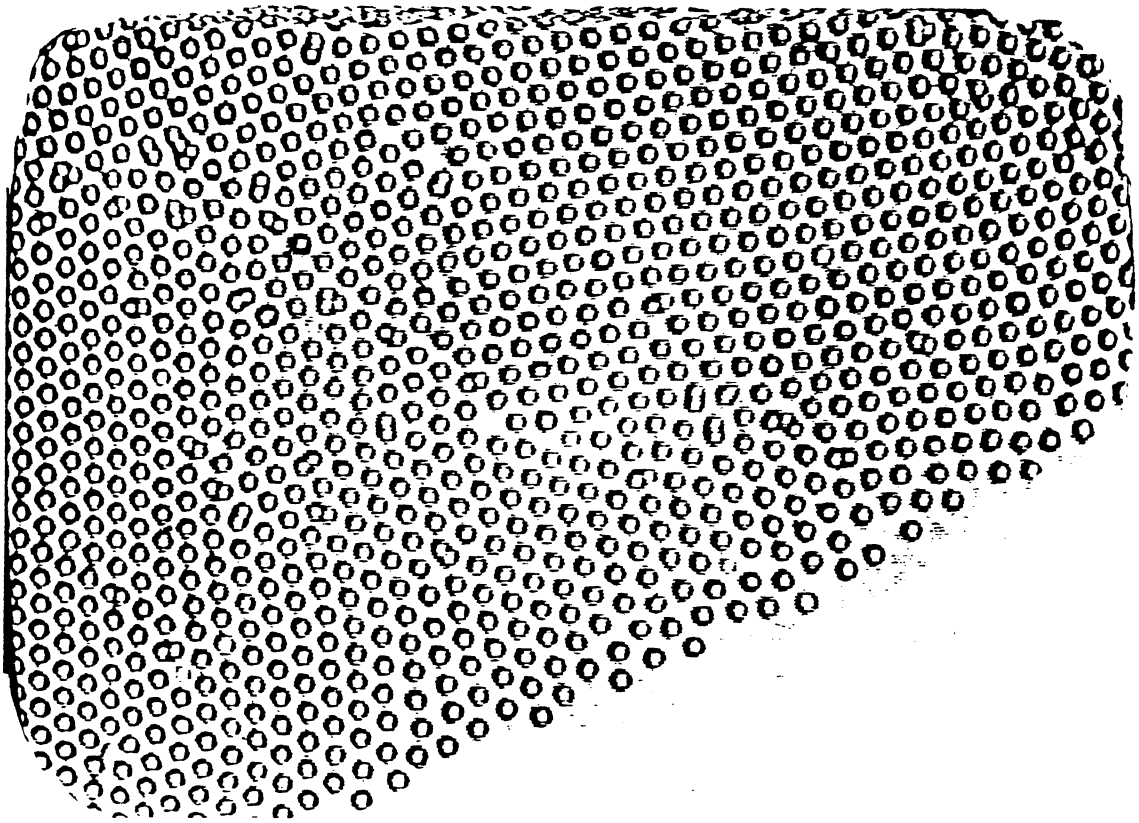

Figure 12. Crystalline Structure Near the Apex of a Cell of 1.07um Charged Polystyrene Spheres Suspended in Highly Deionized Water.

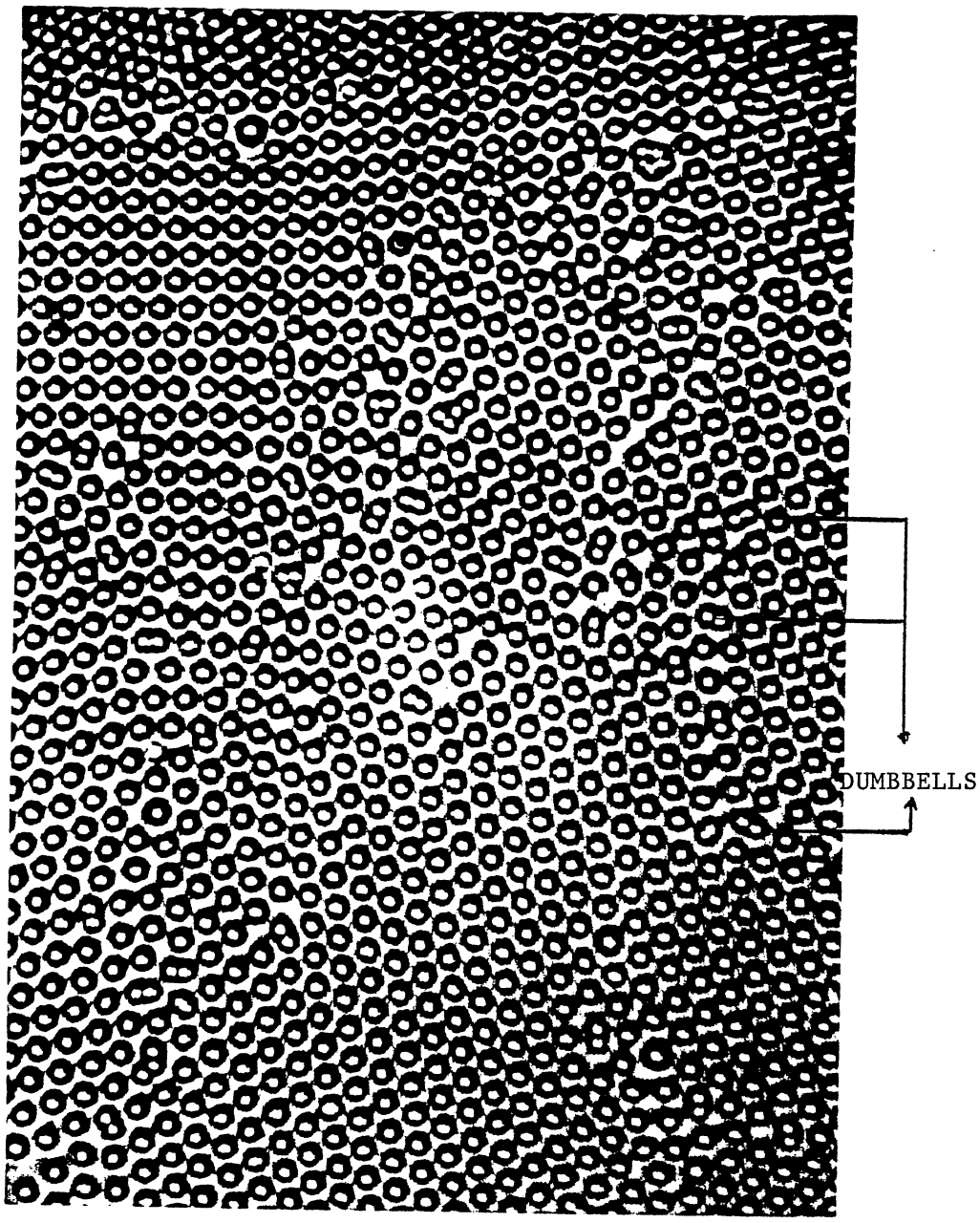

Figure 13. Crystalline Monolayer at 2mm Distance From the Region Shown in Figure 12.

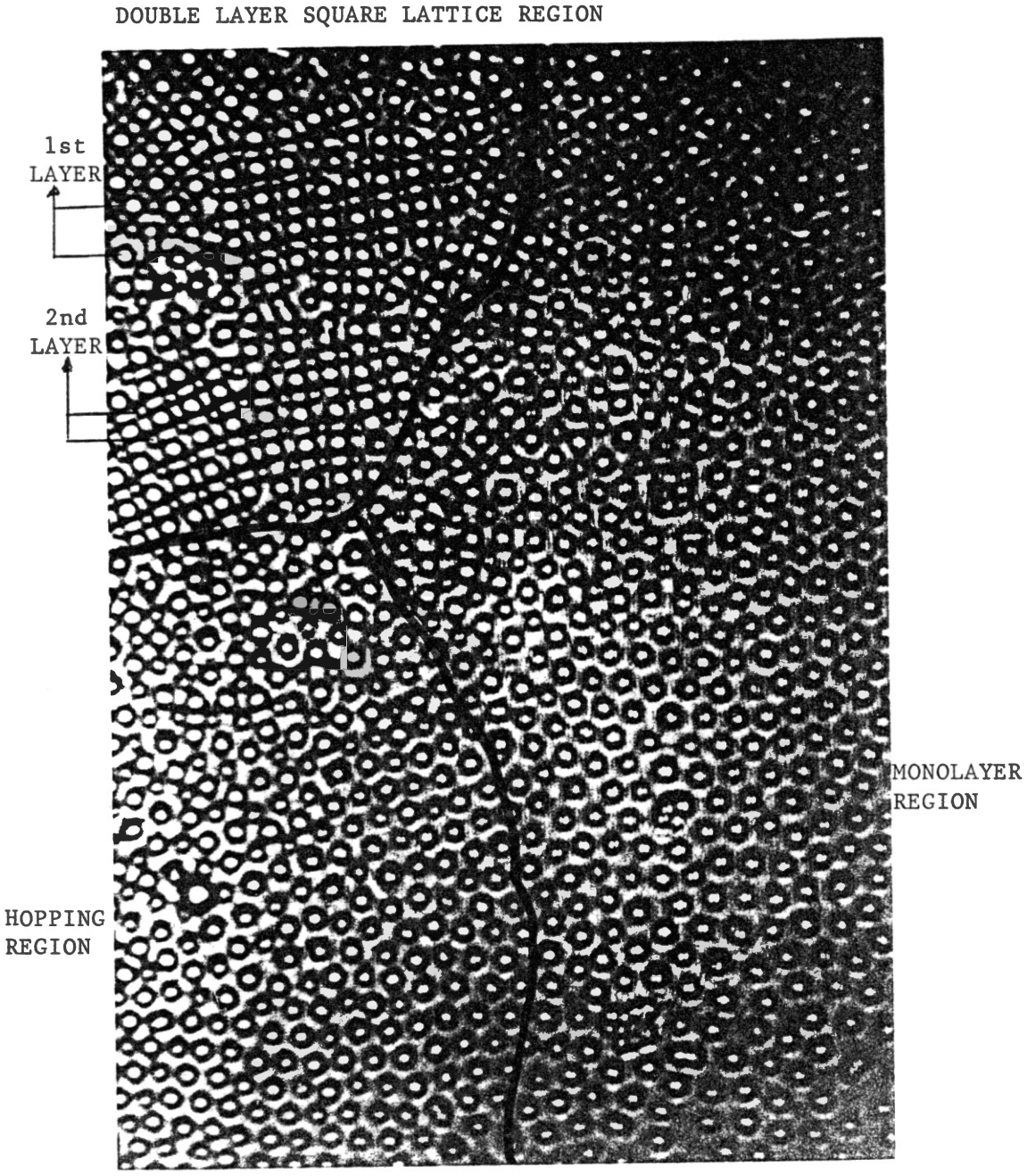

Figure 14. Transformation From a Monolayer Region to a Multilayer Square Lattice Region.

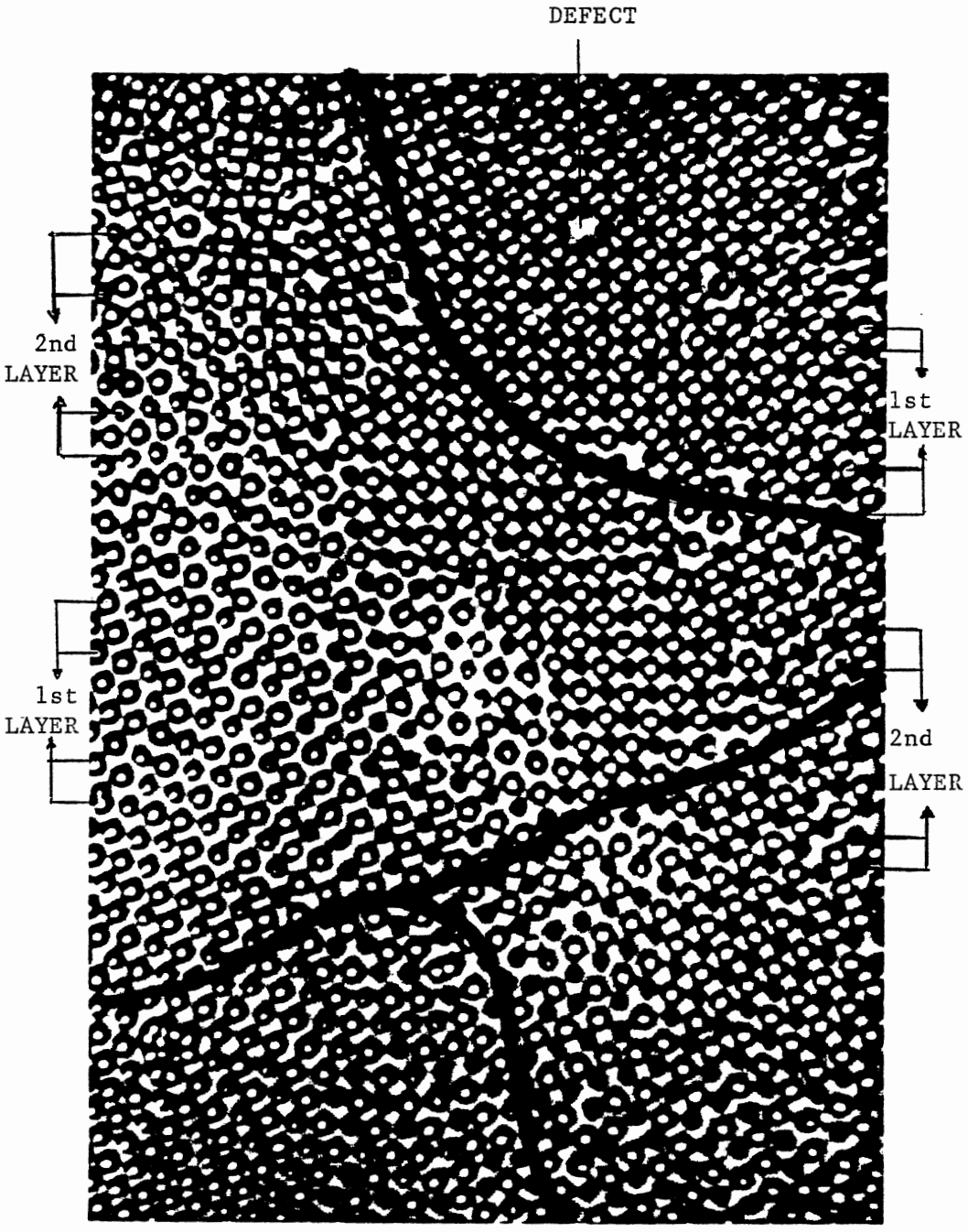

Figure 15. Multilayer Square Lattice Packing with Different Lattice Constants.

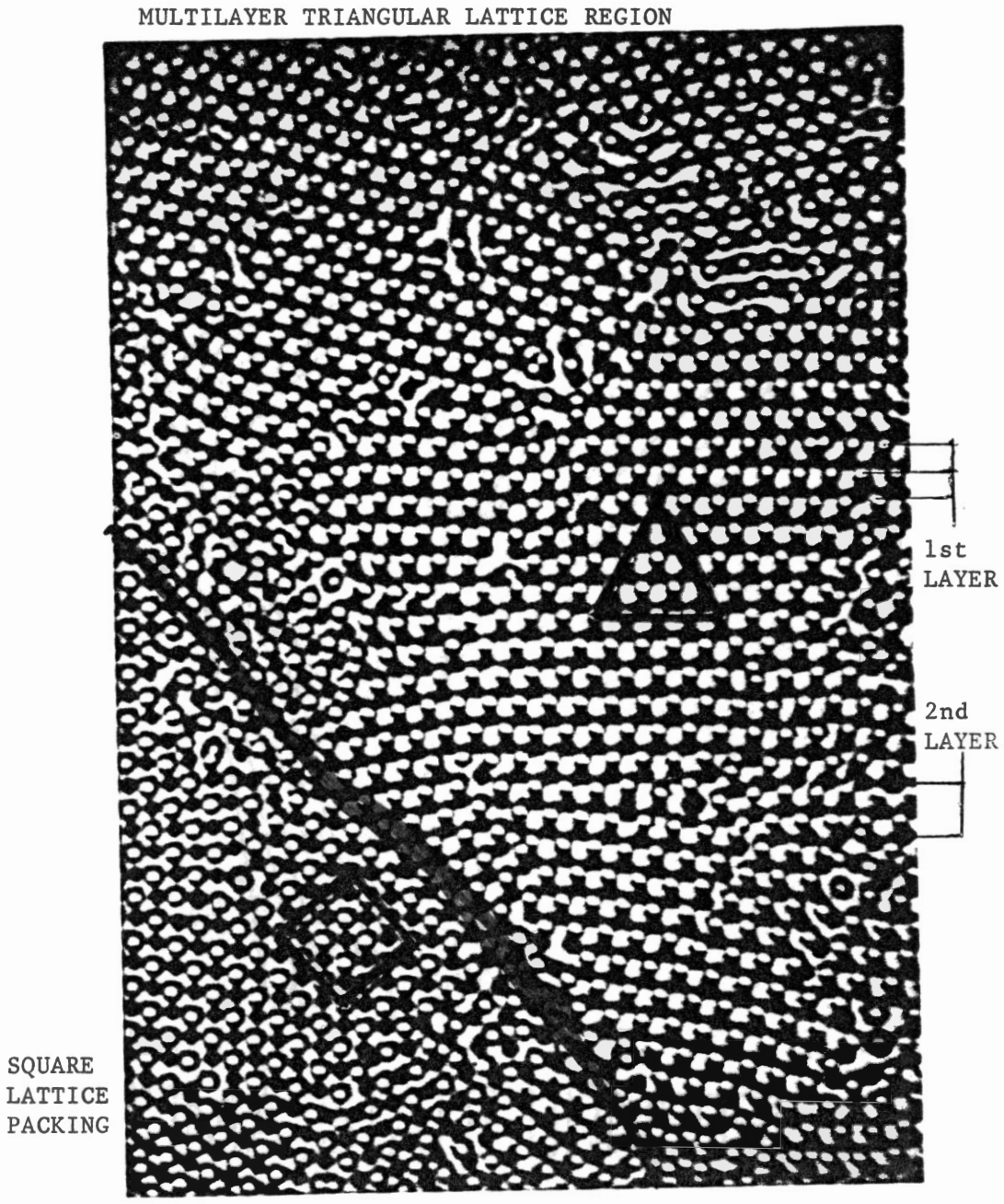

Figure 16. Transition for a Double Layer Region From Square Lattice Packing to Triangular Lattice.

In Figure 12 the particles shown are just above the apex of wedged region in the sample cell. Below this apex no particles were observed since the gap is small enough that the particle-wall interactions cause all the microspheres to be expelled to the 3D reservoir or the upper region of the sample. In this triangular lattice the average interparticle separation is of the order of twice a particle's diameter. Translating the sample about 2mm distance the same 2D crystalline structure appeared to persist as shown by Figure 13. The interparticle separation in this monolayer frame is 2.0um, of the same order as a particle's diameter. To be noticed in this figure is the existence of dumbbells and collection of three,four or five particles. These aggregates tend to reorient the axis of the crystalline structures, produce defects and are isolated primarily at grain boundaries.

As the cell gap is increased a transition to a double layered region starts to be occur (Figures 14 and 15). The first of these figures (Figure 14) demonstrates the deformation of the HCP monolayer structure as the plates' separation is increased, leading to a hopping region and eventually a double layer square lattice. The hopping region occurs in the lower right and to the right of the shown area of Figure 14. In this case the plate separation is slightly larger than the stable monolayer regime and slightly lower than the required gap for a stable two layers regime. For a gap large enough to support a stable two layer regime, it is observed that the particle density and the lattice constant for the square packing varied from one region to the other (Figure 15). This change is believed to be a result of small variations in the gap width introducing a distortion in the lattices. The left side of Figure 15, shows a deformed square

lattice whose lattice constant is different than that measured for the square lattice found on the right side of the same figure.

The transition from a two layer square to a triangular lattice was also observed in these samples, as shown by Figure 16. The lower left corner shows a square lattice, as we move to the right the gap increases allowing for a stable two layer triangular lattice.

The general structure of one to three layers of crystallized spheres in these experimental samples is similar to what has been observed by Pansu et al. (5, 41) and in another study by Van Winkle and Muray (4). These authors have observed a structural sequence of 1T - 2S- 2T - 3S - 3T phases, where T stands for the triangular lattice and S represents the square lattice and N is the layers' number. In this study we were able to reproduce results observed in references 1 , 4 and 5, despite the dumbbells.

Correlation Functions

1-D Pair Correlation Function (g(r))

The translational pair correlation function is constructed by taking the center particle in each digitized frame, its six nearest neighbors and the four particles located at the four corners of each digitized frame as separate reference particles. For each of these references, the number of particles within a ring of width dr about r is counted and divided by the area enclosed by the ring. This technique gives an equivalent of averaging over 220 frames with an averaging time of 20 to 60 seconds. This allows for the construction of the radial distribution function, and provides direct structural information which can be compared with theory.

Mathematically the one dimensional pair correlation function, g(r), is defined as:

$$g(r) = d(r)/d_0 \qquad (4\text{-}1)$$

were d_0 is the bulk density of the liquid expressed as the number of particles per unit area and d(r) is the local density of spheres at a distance r from the reference particle. Using the above description for d(r), equation (4-1) can be rewritten as:

$$g(r) = n/[\pi d_0(r_j^2 - r_i^2)] \qquad (4\text{-}2)$$

where r_j is the outer diameter of the ring and r_i is its inner diameter. The existence of a maximum at a distance r indicates an increase in local density around r. The sharper and higher this maximum, the more probable the arrangement at that point.

2-D Pair Correlation function (g(r))

The conditional probability of finding a particle at a position $\underline{r}_2$, given that a particle is located at $\underline{r}_1$ is constructed graphically by taking the position of the center-most microsphere in each frame as the origin, or as the vector $\underline{r}_1$, and plotting the x and y positions of the rest of the polyballs with respect to this origin, that is $\underline{r}_2 - \underline{r}_1$ where $\underline{r}_2$ represents the remaining sphere positions in the digitized frames. The averaging is accomplished by repeating this process for several frames. However, we also increase the number of frames used in the averaging for this function by taking the six nearest spheres to the origin and using each one of these as a new origin. Once the position of these new origins is determined the same procedure outlined above is followed, thus allowing for an averaging over the equivalent of 140 frames when averaging 20 frames

in all. These conditional probability plots or $g(\underline{r})$ evidence both orientational and translational correlation information. The programs used for the analysis are given in Appendix A.

All of the samples used for this study had a considerable number of multiple particles sticking to each other, these dumbbells created a problem in taking clean data. This same observation is noticed by other workers who examine the nature of layering transitions and the 2D melting processes in systems composed of colloidal suspensions (4, 5, 41). To avoid the complexities introduced by a large number of dumbbells, we select only the monolayered regions with less than 5% doublets for analysis.

Two Dimensional Systems With And Without External Radiation Field

This section will describe the details for the data collection procedure and results of the static experiments on the interacting colloidal particle samples. By crossing two mutually coherent laser beams in the sample, a periodic intensity potential well is produced. A force exerted by the potential draws the micron sized polystyrene spheres to the most intense regions since their index of refraction is larger than that of the solvent. This forces the particles to aline in a periodic arrangement. The final structures are controlled by the potential's period and the laser's input power. The radiation pressure forces tend to also push the particles in the direction of the beam's propagation towards the front cell's plate (top plate in Figure 9), and in the case of multilayered regions this causes the particles to compete for lining up in the layer closest to the cell's

confining plate.

In this study the region used for the analysis were either fluid monolayers of constant particle density or partial double layered fluid regions were the particles density changed as the radiation pressure force was applied. A standard digitized frame of the monolayer and multilayer amorphous regions used for this work are shown in Figures 17 and 18 respectively.

Equilibrium Without External Field

Equilibrium is observed with single beam illumination of the sample. This is just a uniform field which pushes particles near a plate with or without the transverse effects. Illuminating the sample cell with a single argon-ion beam (488nm wavelength) and probing the sample with a microscope the real space images observed for a monolayer amorphous phase is demonstrated by the snap-shot in Figure 17a. The particles in this region appear to have a random orientation with an average separation of 2.27um as found by direct measurement from the digitized image (implying a density of $1.9 \times 10^{12} m^{-2}$). The single beam scattering pattern from this region is presented in Figure 17b. The diffuse intensity ring concentric with the incident beam is referred to as the Debye-Sherrer ring and is characteristic of a liquid-like or amorphous structure. The k-space radius of this ring $k_{DS}=2\pi/a$ gives another measure for the average particle separation which was determined to be 2.18um.

The pair correlation function g(r) for this amorphous phase is shown in Figure 19a. This function shows a sharp maximum at a distance r=2.14um, an indication that there is structural arrangement

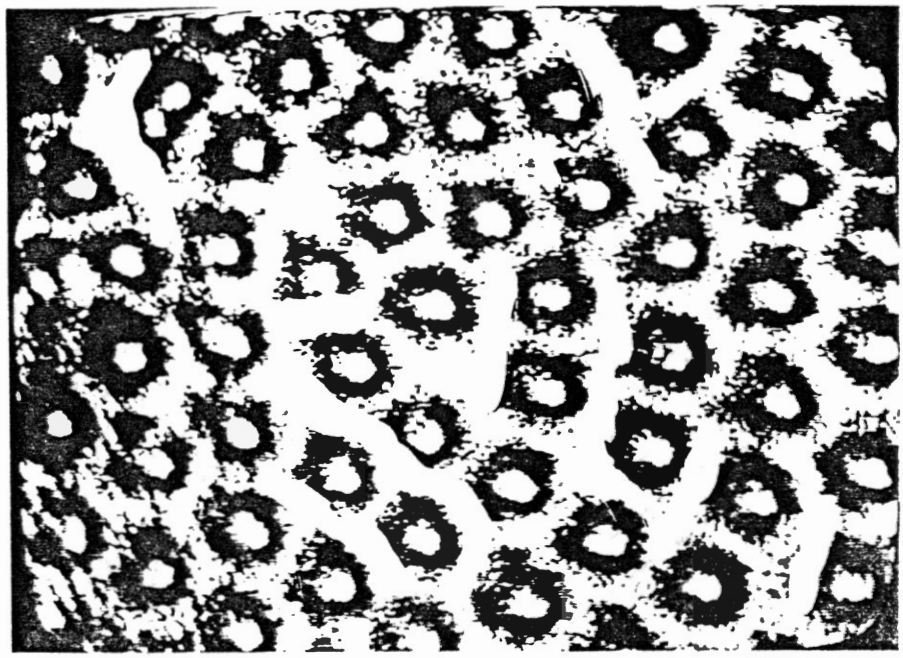

a) Real Space Snap-Shot

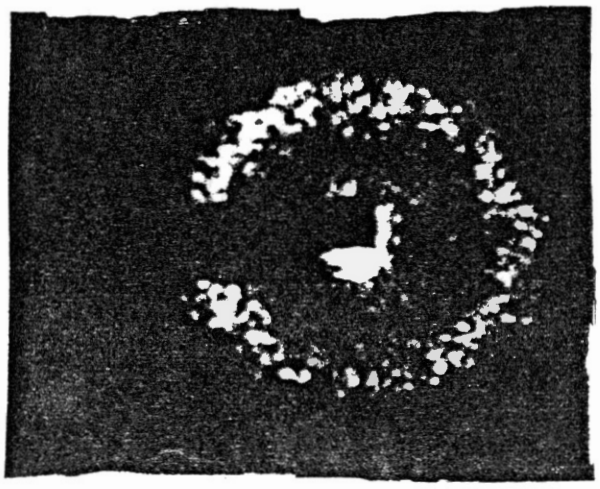

b) Self Scattering Pattern

Figure 17. Monolayer Amorphous Region With an Average Particle Separation of 2.2um as Measured From the Real Space Snap-Shot (a) and the Radius of the Debye-Sherrer Ring (b).

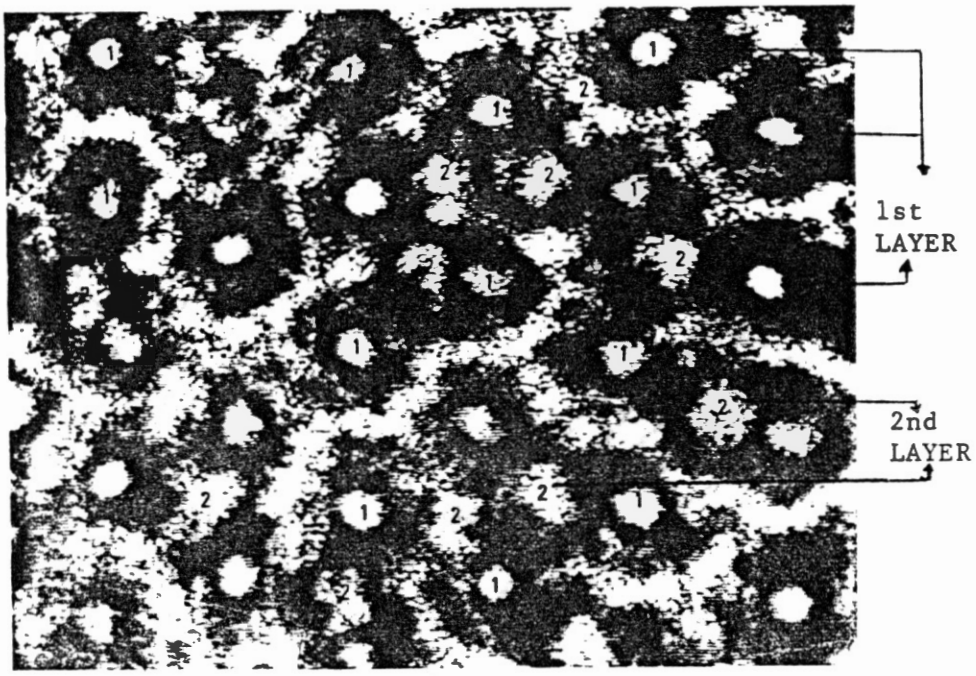

a) Real Space Snap-Shot.

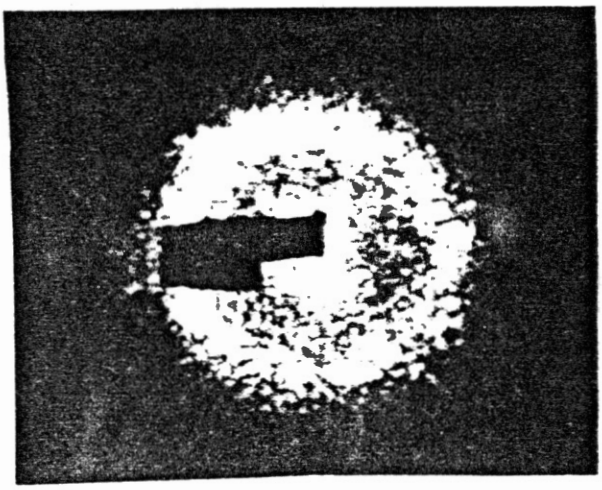

b) Self Scattering Pattern

Figure 18. Amorphous Multilayer Region of Interacting Polystyrene Spheres (1.07um Diameter) Suspended in Highly deionized Water.

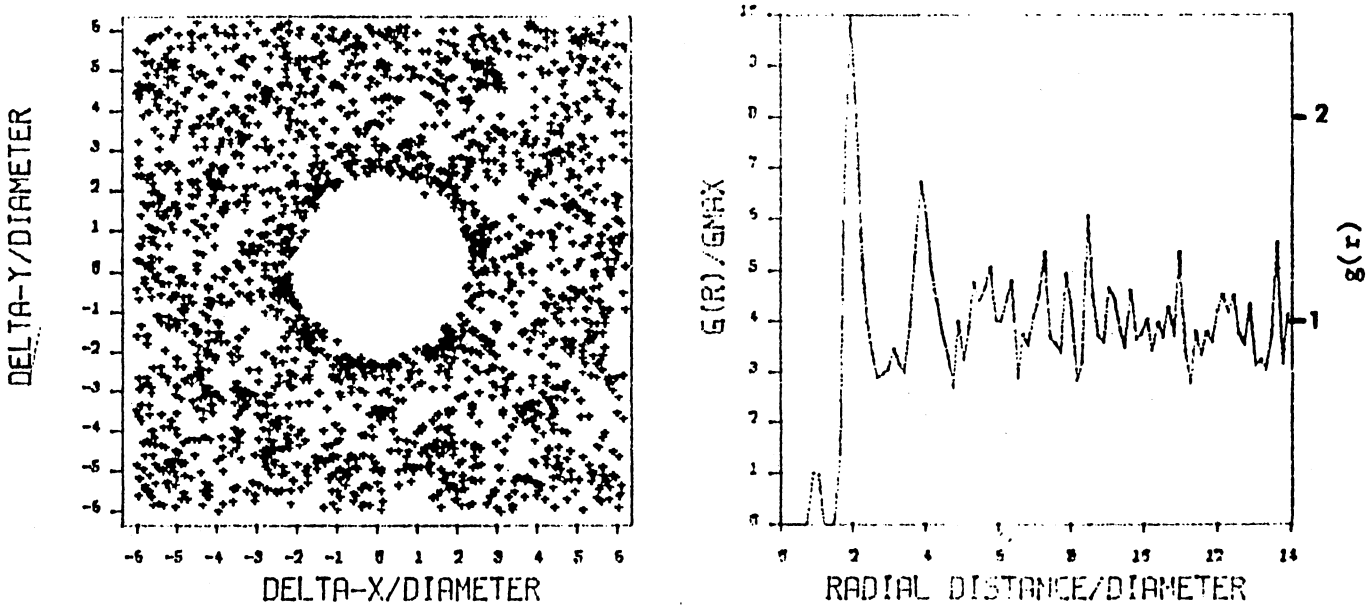

b) 2D Pair Correlation Function

a) 1D Pair Correlation Function

Figure 19. One Dimensional (1D) and Two Dimensional (2D) Pair Correlation Functions For the Monolayer Liquid Phase Shown in Figure 17.

at this position. The other peaks fluctuate around the value of one, where the fluctuation is due to statistical errors. This function shows the typical liquid-like behavior. The 2D pair correlation function (Figure 19b) shows that the probability is largest at the nearest neighbor distance (r=2.14um), is independent of the direction of r and decreases to the average particle density at large r values. The observed orientation is due to not averaging over a long enough time.

External Field Applied

The crossing of the to laser beams creates an external field which causes the system to reorganize in ordered structures. The experimentally finite extent of the crossed beams eventually creates a nonlinear distribution of the particles in the symmetry breaking fringes. This nonlinear effect is avoided by imaging region near the center of the crossing area, thus allowing for a fairly uniform distribution of the microspheres. The formed structures were observed to have order up to thirty fringe periods. The extent of this order depended on the area occupied by the fringes and the amplitude of the applied field. This long range order is not considered in this study for distance larger than ten fringes on the average. The short range order is considered in this analysis due to the uniform intensity distribution around these regions, and for analysis convenience.

Commensurate Structure

When the fringe spacing causes the interacting spheres to line up in their undestorted closest packed structure consistent with the

sample density (Figure 20a), the system is said to be commensurate with the externally applied potential. This occurs when d=acos(30), where d represents the fringes spacing and a is the average separation between the particle in the amorphous phase. The transverse component of the radiation field causes the spheres to line up along the high intensity region of the fringe patterns. The coupling of this alinement whith the strong electrostatic interaction between the particles, causes a uniform separation between adjacent particles in a row and successive ordering between adjacent rows. The final result is the "freezing" of the amorphous two dimensional system to a two dimensional ordered structure, where the one dimensional external field directly breaks the symmetry of the amorphous (or crystalline state).

When the amorphous equilibrium region (Figure 17) was exposed to the radiation forces produced from the crossing of the two argon ion laser beams, at an angle of d=1.96um (14.3 degrees), the particles aligned not only along the fringes but also in the other directions (Figure 20a), creating diffraction a two dimensional grating. The self scattering pattern produced from these gratings is given in Figure 20b. The horizontal row of intensity maxima passing through the two incident beam positions is produced by particle alignment with the intensity fringes. The other intensity maxima, at about 30, 90 and 120 degrees from the axis passing through the main beams (x-axis), are produced by secondary alignment of microspheres due to interparticle interactions. If one of the two write beams is blocked this pattern relaxes back to that of Figure 17.

The pair correlation functions for these commensurate monolayer structures are shown in Figures 21 through 23, where the laser's input

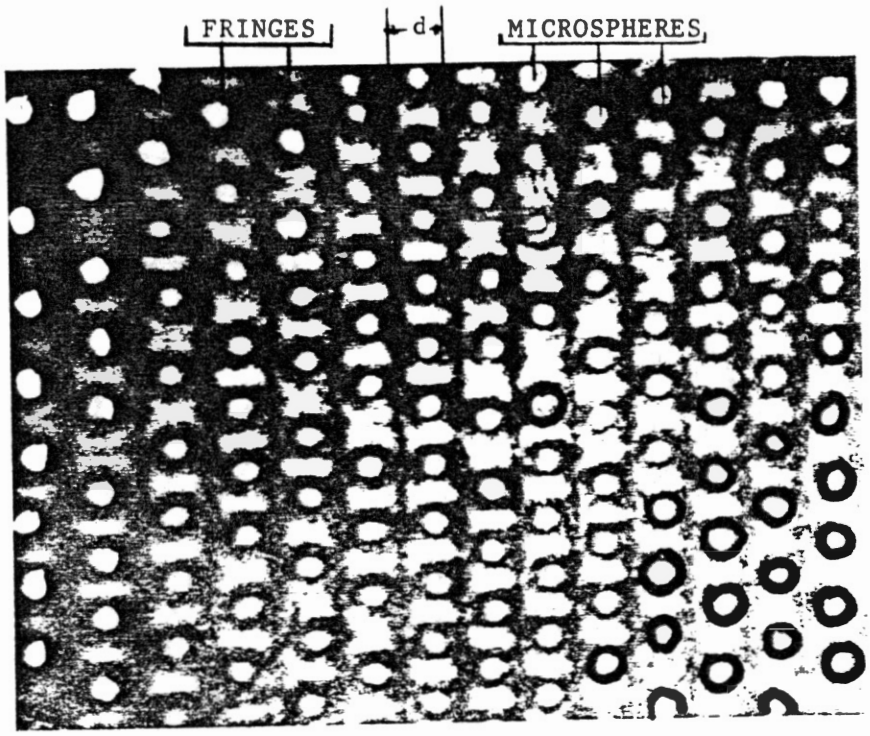

a) Real Space Snap-Shot of Particles Alinement Along the High Intensity Regions.

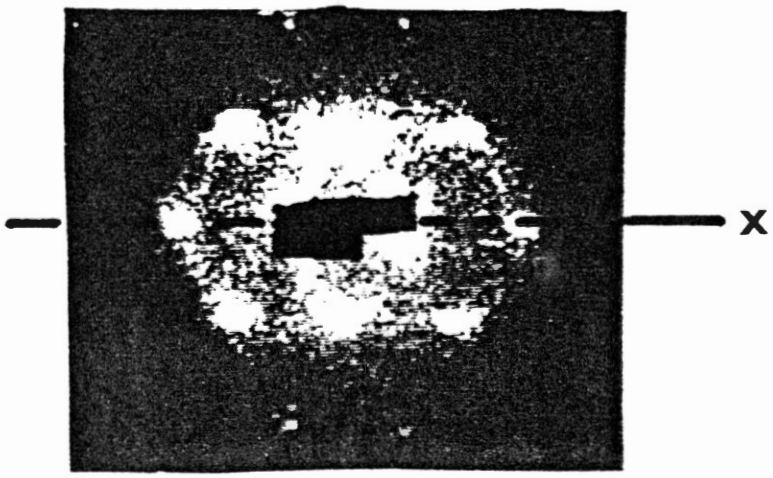

b) Self Scattering Pattern.

Figure 20. Alinement of the 1.07um Interacting Polystyrene Spheres in the High Intensity Regions of the Stationary Fringe Pattern at Commensurate Period

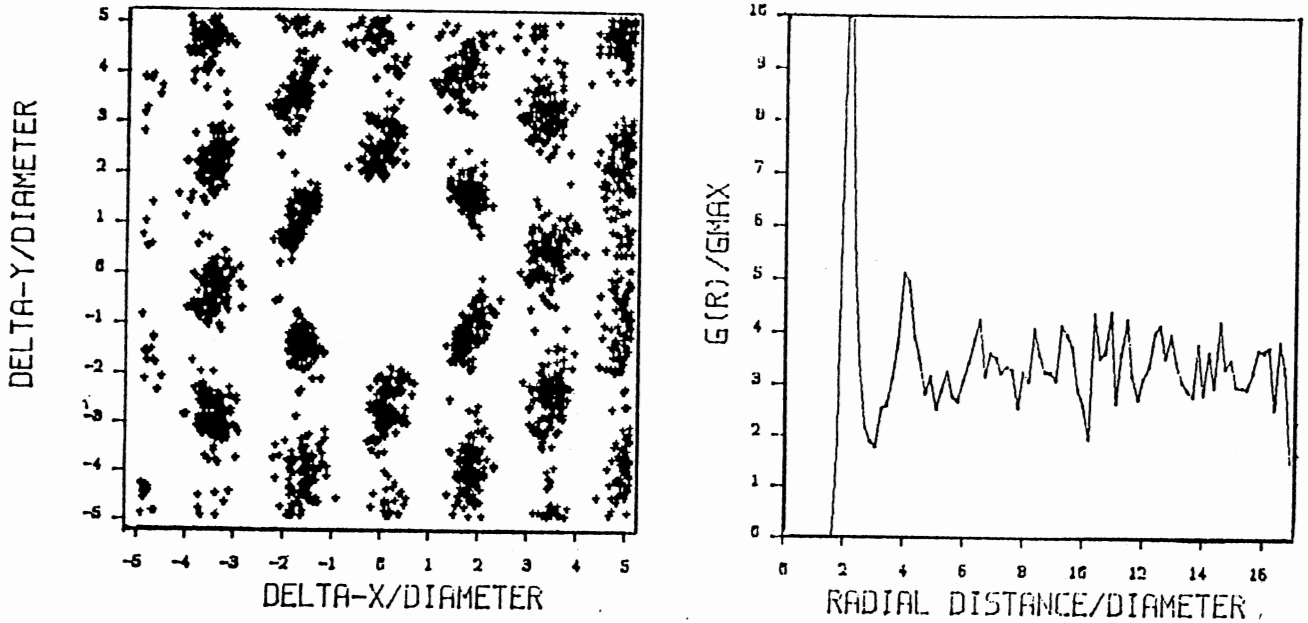

b) 2D Pàir Correlation Funcition

a) 1D Pair Correlation Funtion

Figure 21. Pair Correlation Function (a) $\grave{g}(r)$ and b) $g(\underline{r})$) for Monolayer at Commensurate Period (d=1.85um) and Input Power (P) of 42mW.

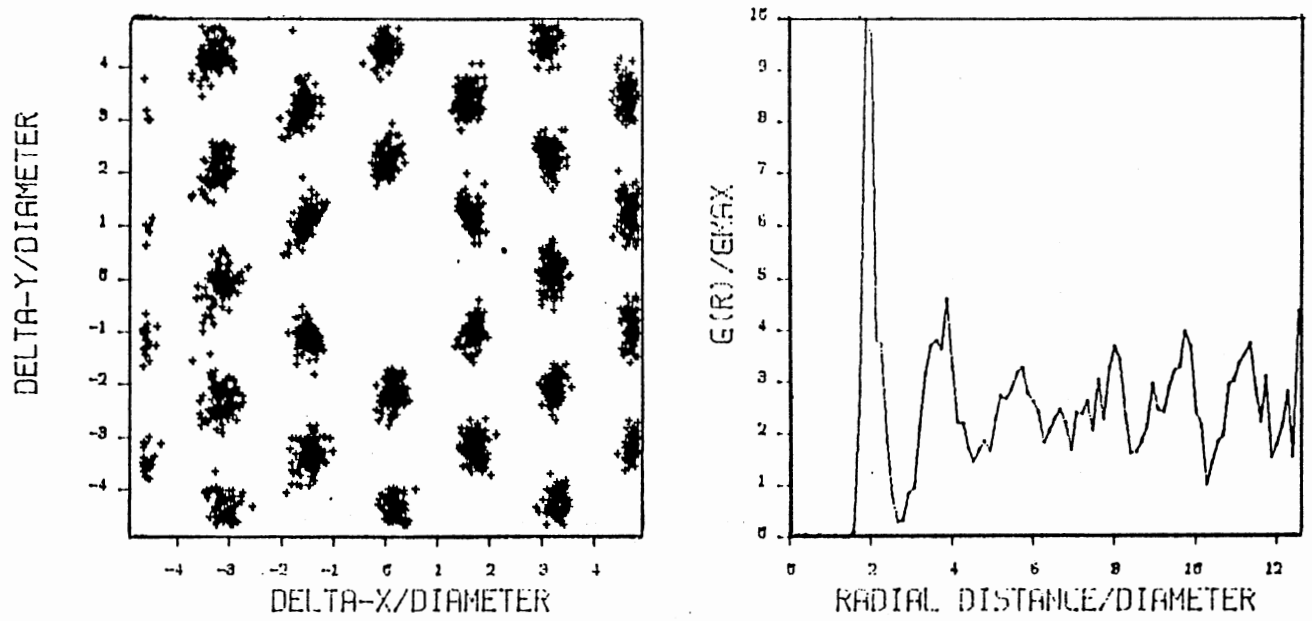

b) 2D Pair Correlation Function

a) 1D Pair Correlation Function

Figure 22. Pair Correlation Functions [a) g(r) and b)g(r)] for a Monolayer at Commensurate Period (d=1.85um) and Input Power of 86mW.

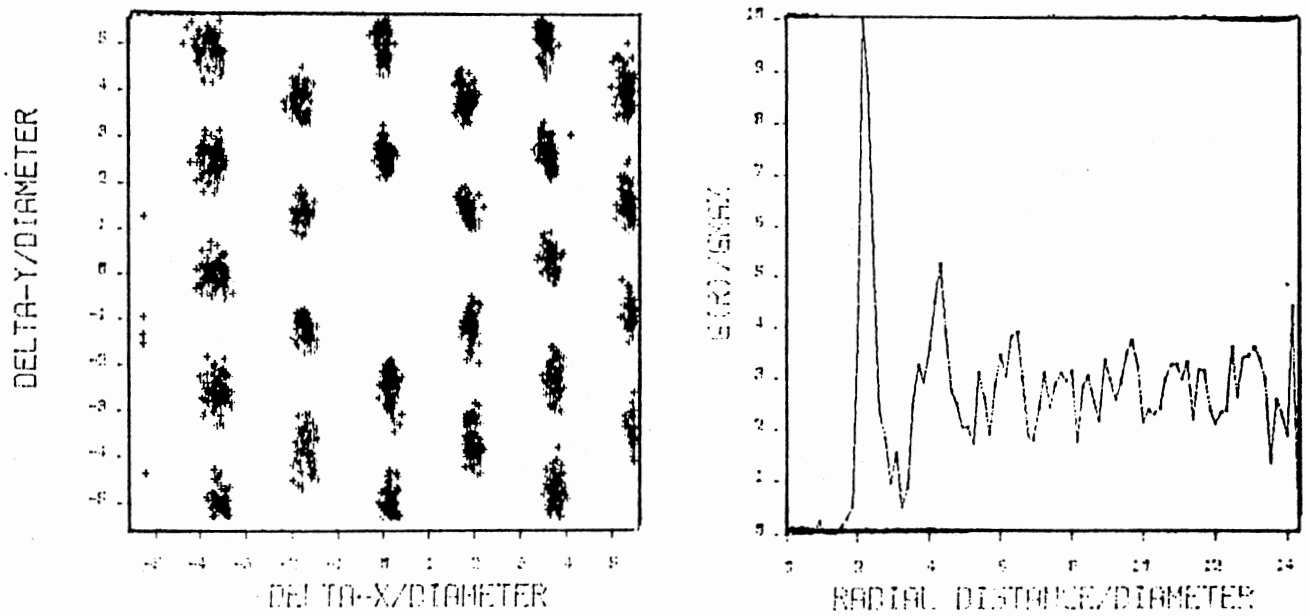

b) 2D Pair Correaltion Function

a) 1D Pair Correlation Function

Figure 23. Pair Correlation Functions [a) g(r) and b)g(r)] for a Monolayer at Commensurate fringe Period (d=1.85um) and Laser's Input Power of 111mW.

power increased from 42mW to 110mW for this particular analysis. At all these powers it is observed that the particle density stayed within a maximum of 3 percent from the average value of .190/(um)^2. At the lowest input power g(r) (Figure 21) shows a maximum at about 1.86um, an indication that there's local order between the microspheres at this separation. A broader and smaller peak is observed at about 4.28um radial distance. At higher r values, g(r) fluctuates around unity, with not well defined peaks to suggest the loss of correlation at these distances. As the input power increased the trough after the first maxima approached zero, an indication of greater correlation between the spheres. The second and third maxima are more pronounced for the input power of 86mW (Figure 22a) than what is observed for the 42mW case. At large r values, even at the higher input powers, we see a loss of correlation presented by fluctuations in g(r) around the value of one. In all of these figures, the higher and sharper the observed maxima are the larger the particles' density in the shell centered around that region.

The 2D correlation functions (Figures 21b-23b) shows the induced translational as well as orientation order as the amplitude of the externally applied potential is changed. The degree of correlation between the microspheres is measured by analyzing the distribution of the 2D function along each fringe period (Figures 24-26). These graphs are constructed by taking three rectangular boxes along the x-direction of the 2-D correlation functions. The x-coordinates of these rectangles were from -d/2 to d/2, d/2 to 3d/2 and 3d/2 to 5d/2 where d represents a fringe period. The y-coodinates were taken as those shown in the g(r) graphs. The density distribution along the y-

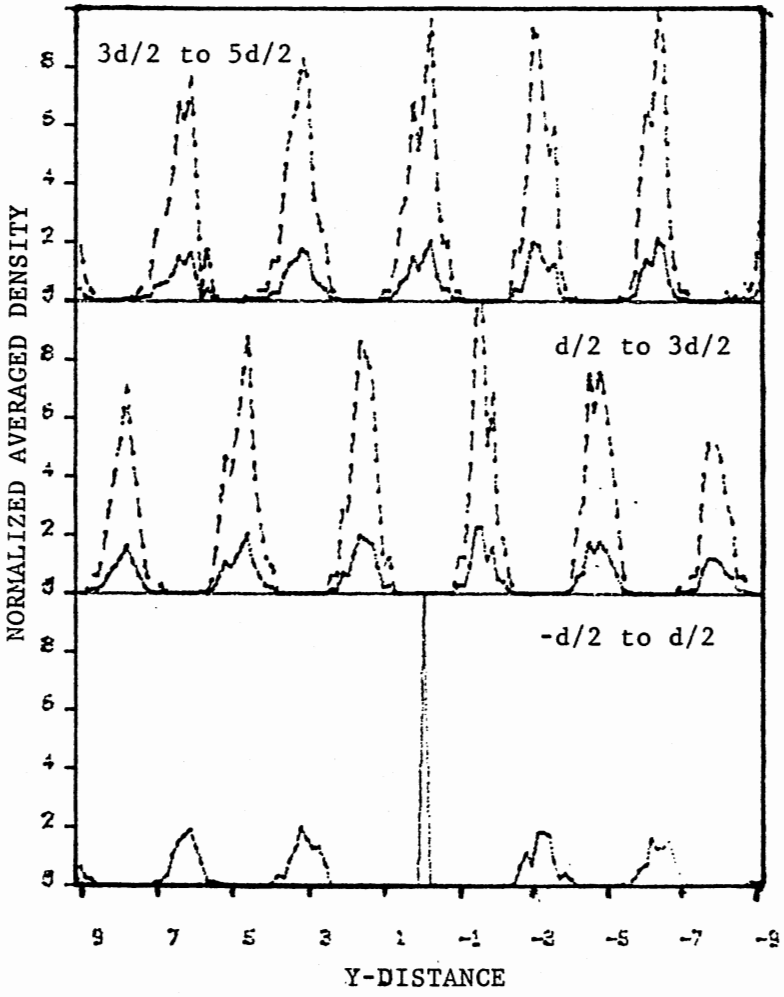

Figure 24. Normalized Average Density Distribution for the 2D Correlation Function Shown in Figure 21. The Solid Curves are Normalized to the Same Scale and Dashed Curves are Normalized with Respect to the Maximum Peak in the Given Box.

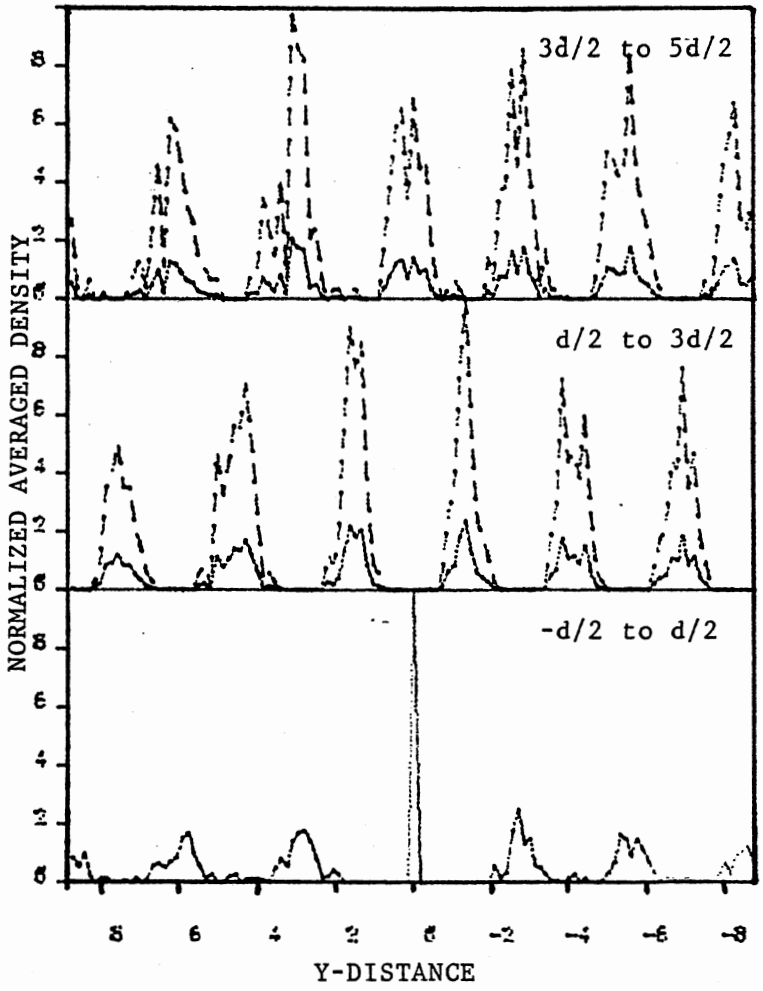

Figure 25. Normalized Average Density Distribution For the 2D Correlation Function Shown in Figure 22b.

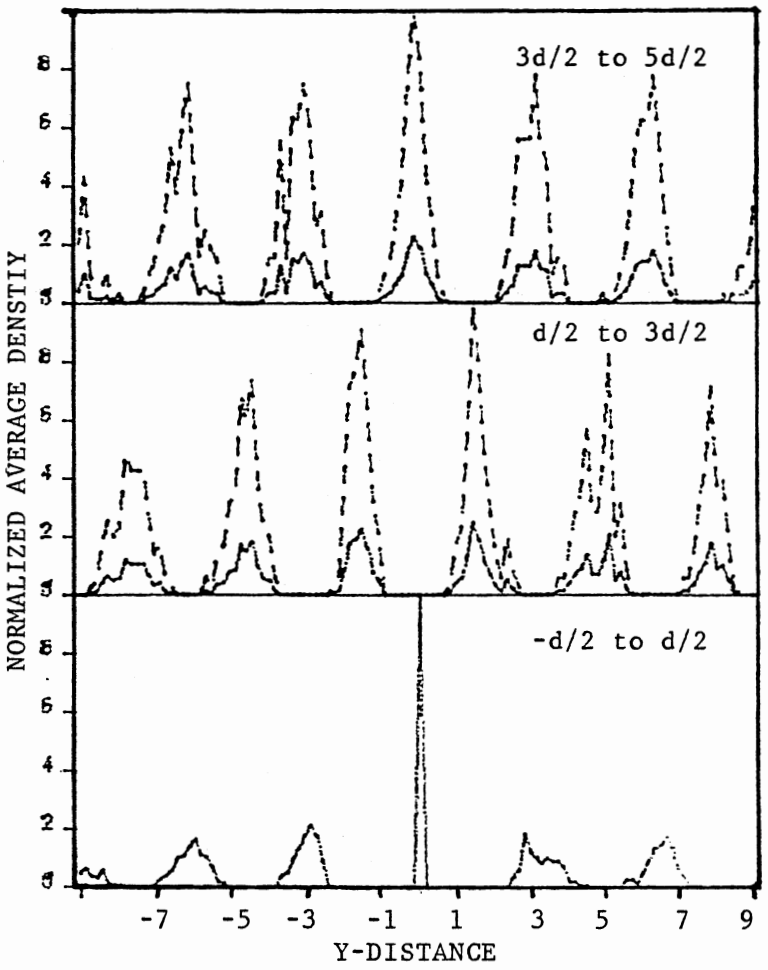

Figure 26 . Normalized Average Denstiy Distribution for the 2D Correlation Funciton Shown in Figure 23.

axis in each box is found and plotted. The bottom plot represents the first box (-d/2 to d/2 region), the following plots is for the second box (d/2 to 3d/2) and the lost plot for the third box (3d/2 to 5d/2). The solid curves in these plots show the density distribution to the same scale and the dashed curves are normalized by the maximum peak in that box (these are presented for clarity). These figures (24 to 26) show that as the input power is increased the the particles become more localized within the fringes and around some well defined mean position relative to the reference particle. The loss of correlation at large distances is demonstrated by the increase in the standard deviation of the particles' localization in the fringes (Table II), this found by finding the mean x-position of the microspheres in a particular fringe period than calculating the deviation around this mean. Another measure of the loss of correlation is also achieved by analyzing the height and the full width at half maximum (FWHM) of the peaks of the average density distribution plots. Thus at commensurate crossing angle, the induced order seems to be a function of the applied field's power.

A demonstration of the particles' distribution in the high intensity regions of the periodic potential is given in Figures 27a. By counting the number of particles within each well, the density along each fringe is obtained (Figures 27b). The period used for these density plots are measured directly from the digitized images. The fluctuation in this density is due to uneven counting of particles in the rectangular boxes used for the area of analysis (the edges of the box determine which particles to be included in the analysis), statistical fluctuations and defects.

TABLE II

ANALYSIS OF 2-D PAIR CORRELATION
FUNCTIONS FOR d=1.85um

Input Power (mW)	Fringe Positions (d/2)		$Mean_x/a$	Std_x/a
42	-1	1	0	.29
	1	3	1.8	.36
	3	5	3.5	.41
86	-1	1	0	.165
	1	3	1.75	.181
	3	5	3.55	.190
111	-1	1	0	.139
	1	3	1.73	.164
	3	5	3.5	.192

$Mean_x$ = mean x position of the particles in the given fringe period

Std_x = standard deviation around the mean x position of each fringe

a = diameter of a single particle

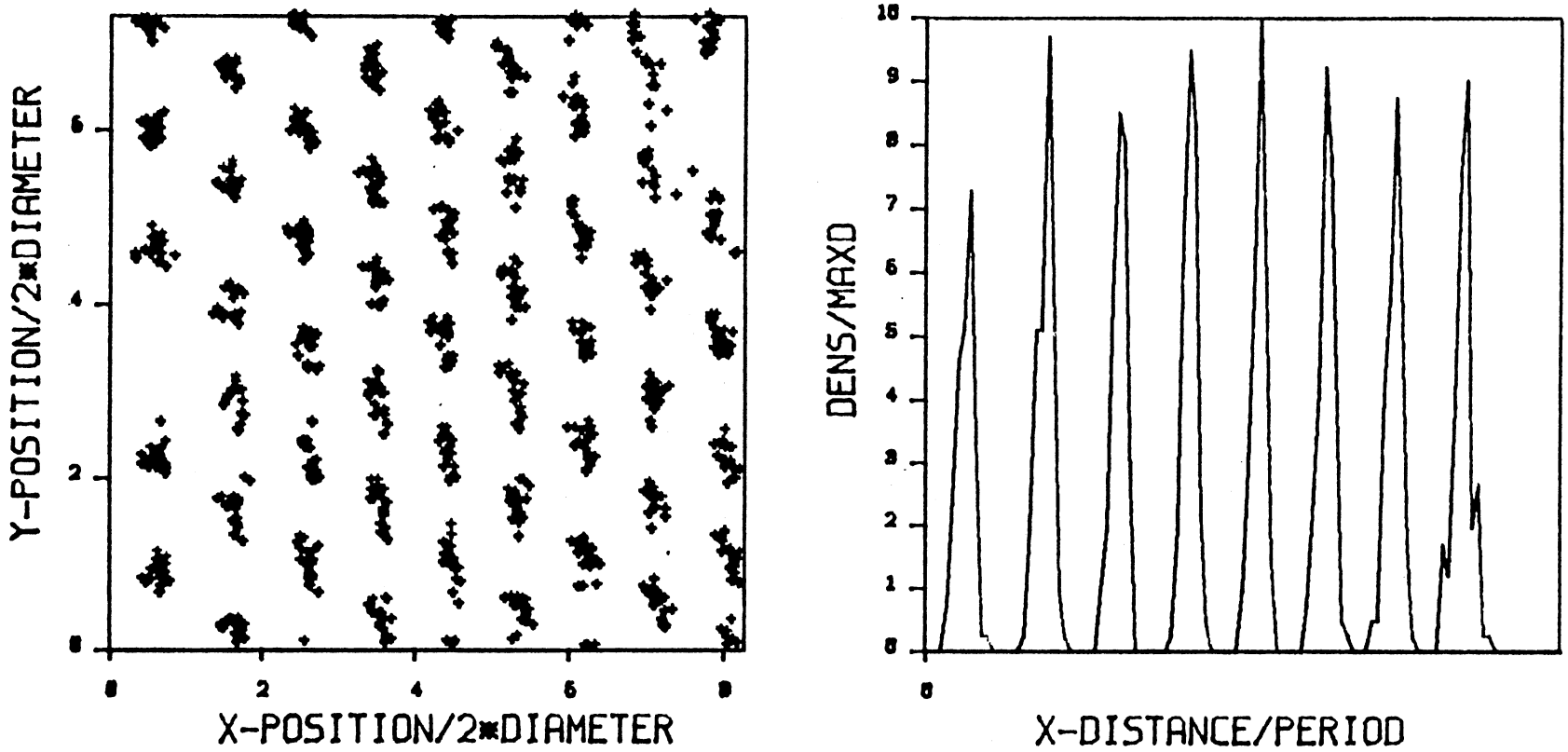

a) x-y Position Files

b) Density Distribution

Figure 27. Position Files for 20 Snap Shots of the Particles Positions at Fringe Period of 1.85um and Input Power of 86mW (a). The Density Distribution along the Fringes is Given in Part (b).

All of the above graphs show that at the commensurate crossing anlge the amorphous monolayers organized in hexagonal closed packed structures as the radiation field was applied. The growth of these structures is observed to be dependent on the radiation field's strength.

Noncommensurate Results

As the crossing angle was increased to 13.34 degrees (inside the sample cell), the formed fringe pattern had a period, d=2.1um, which is incommensurate with the equilibrium phase (Figure 28). At this crossing angle, the radiation fields force the microspheres to align in the fashion shown in Figure 29a. The produced self scattering pattern from this alignment is given in Figure 29b. This pattern shows that the Bragg spots produced from the main density modes' scattering move inside the Debye-Sherrer ring, and that the scattering from the enslaved density modes is weak compared to that observed for the commensurate case, an indication of loss of correlation between adjacent rows at this crossing angle.

The distribution of the microspheres in the periodic wells is plotted in Figures 30a for an input power of 42mW. An increase in the input power localizes the spheres to the minima of the applied potential. The density distribution along these potential minima is demonstrated in Figures 30b. These figures are obtained by averaging over 20 frames for each input power considered.

Using the positions files the pair correlation functions are constructed (Figures 31 to 33). At the minimum applied power (42mW, Figure 31a), the pair correlation function, g(r), exhibits a maximum

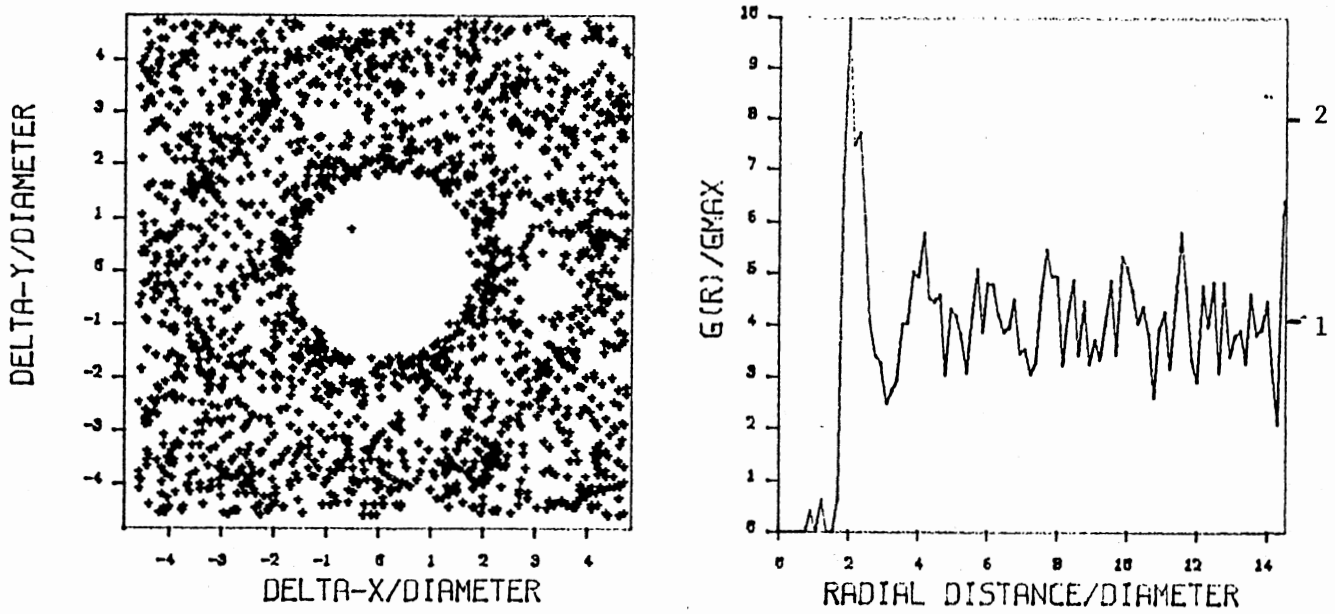

b) 2D Pair Correlation Function a) 1D Pair Correlation Function

Figure 28. Pair Correlation Functions for the Amorphous Monolayer Phase used in the Analysis at Fringe Period of 2.2um.

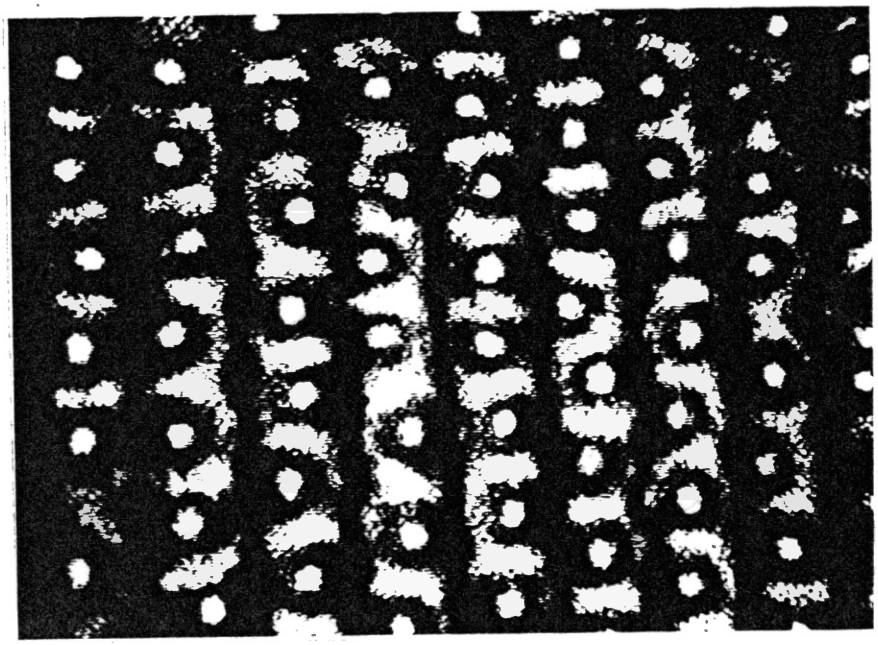

a) Microspheres Alinement Along the High Intensity Regions of the Fringe Pattern.

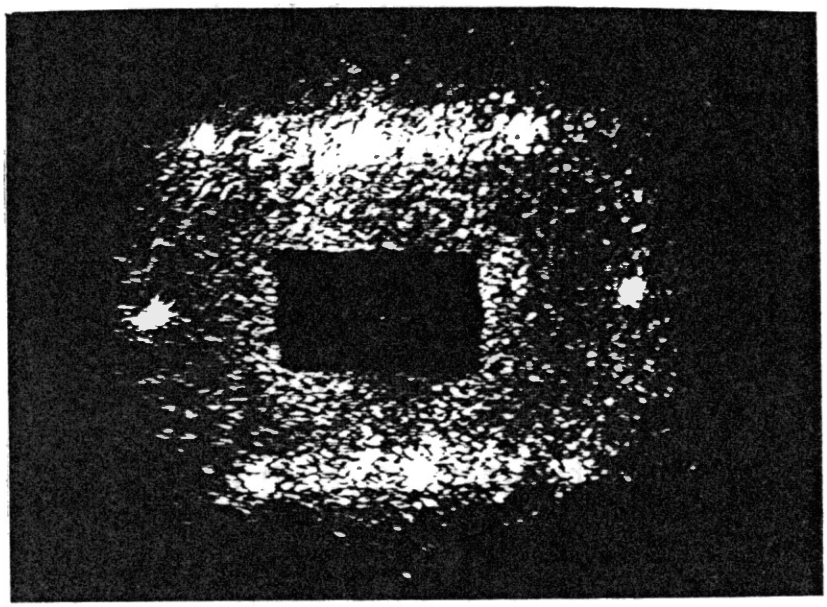

b) Self Scattering Pattern of Structure Shown Above.

Figure 29. Particles Alinement at Fringe Period of 2.2um (a) and the Produced Self Scattering Pattern (b).

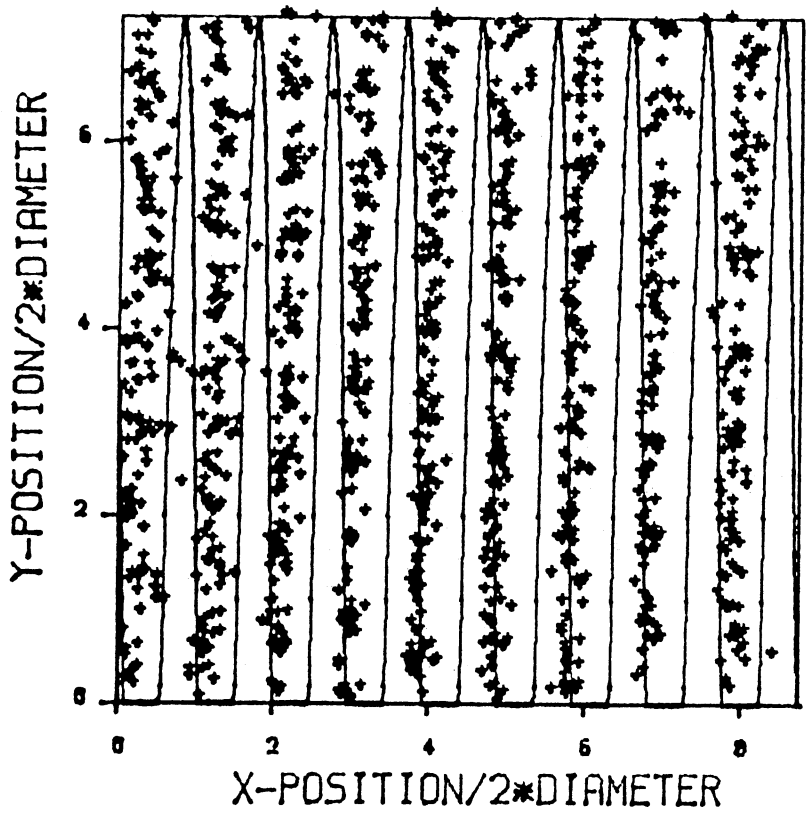

a) X-Y Positions for 20 Files.

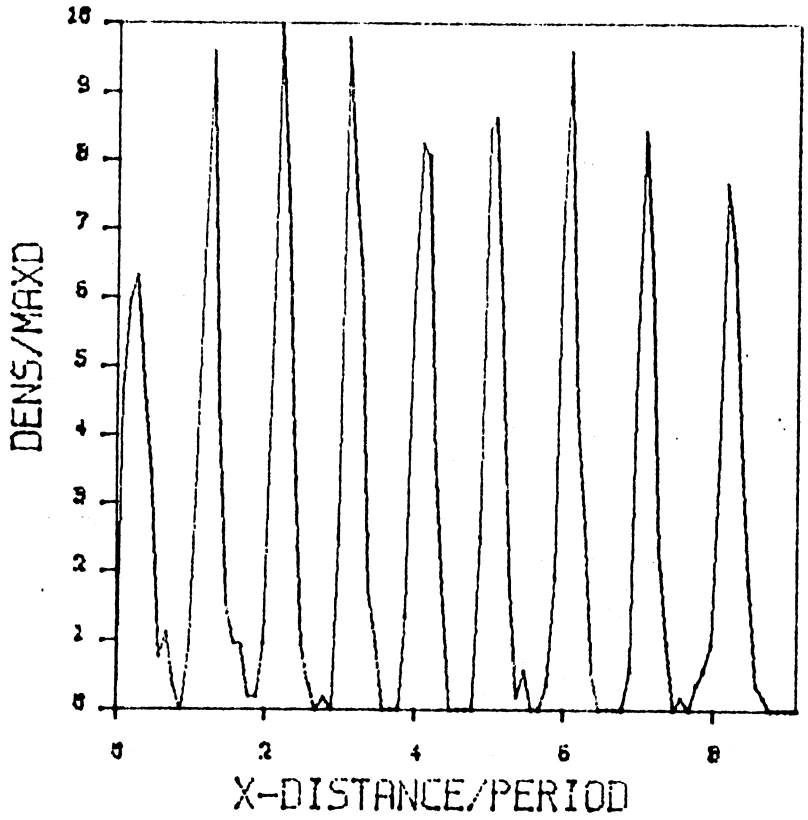

b) Density Distribution along the Fringes.

Figure 30. Position Files for 20 Snap Shots of a Monolayer at Fringe Period of 2.2um and Laser Input Power of 42mW (a) and the Density Distribution of the Particles along the Fringes (b). The Solid Curve in Part (a) of this Figure Represents the Standing Sinusoidal Intensity Fringe Pattern.

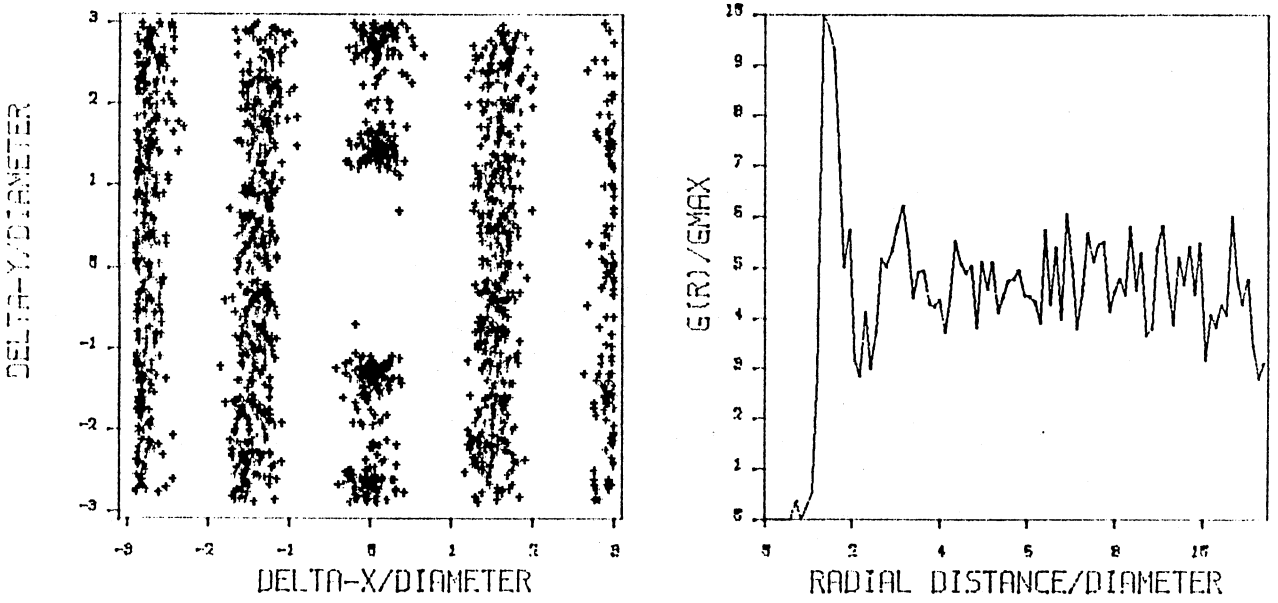

b) 2D Pair Correlation Function a) 1D Pair Correlation Function

Figure 31. Pair Correlation Functions [a) g(r) and b) g(r)] for a Monolayer at Non Commensurate Fringe Period of 2.2um and Laser Input Power of 42mW.

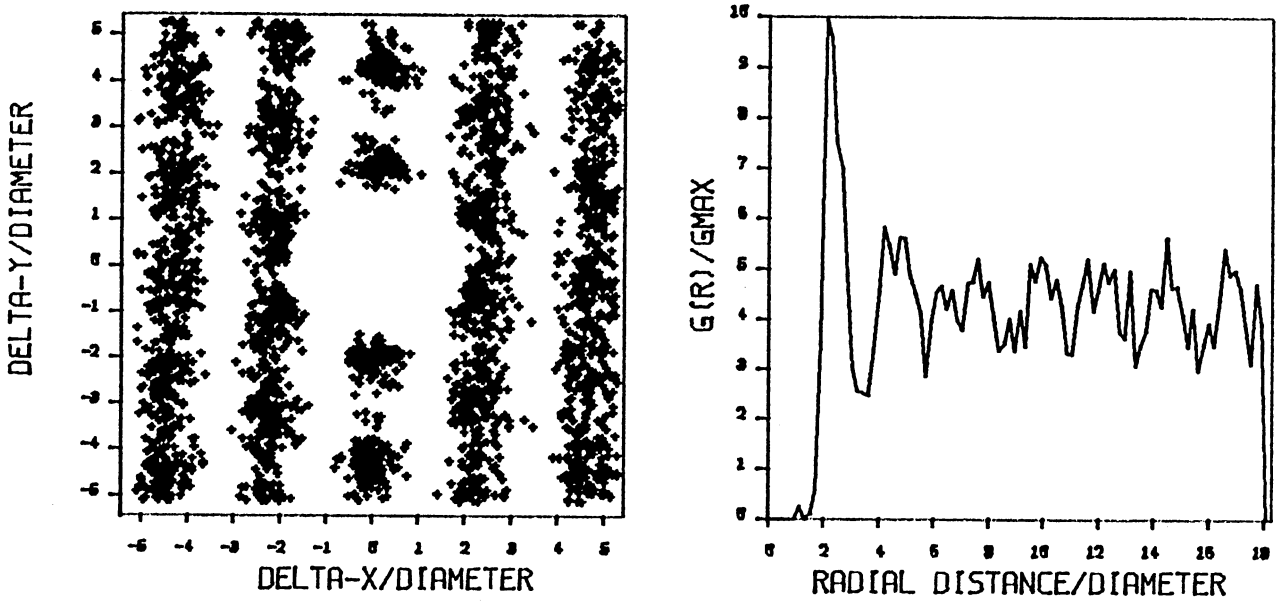

b) 2D Pair Correlation Function

a) 1D Pair Correlation Function

Figure 32. Pair Correlation Functions [a) g(r) and b) g(r)] for a Monolayer at Fringe Period of 2.2um and Laser Input Power of 65mW.

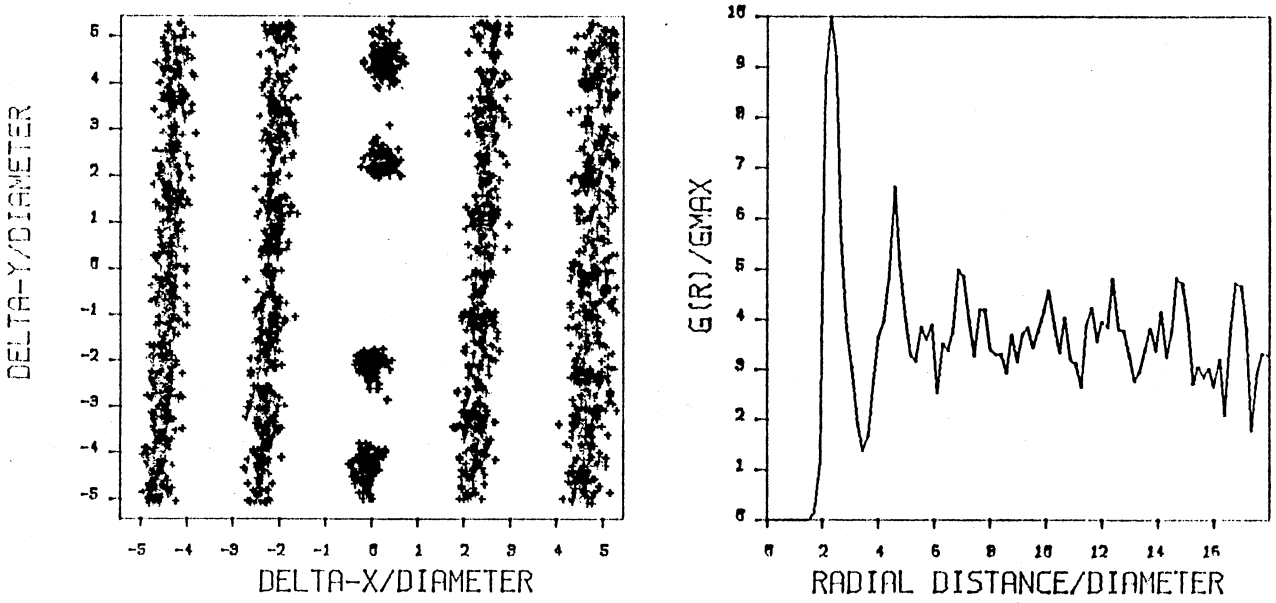

b) 2D Piar Correlation Function

a) 1D Pair Correlation Function

Figure 33. Pair Correlation Functions [a) g(r) and b) g(r) for a Monolayer at Fringe Period of 2.2um and Laser Input Power of 165mW.

at a radial distance of 2.2um; the existence of other maxima at 3.8um and about 6um are not so well defined. The 2D correlation function at this power (Figure 32b) displays the existence of some oriental as well as translational order. However, at the higher input powers (64 and 165mW) the existence of any induced order, beside the alignment along the high intensity regions, is not well defined through the correlation functions. An analysis of the distribution of the density along the fringes is constructed and given in Figures 34 to 36. The existence of some localization around particular positions is best seen at input powers of 42mW and 165mW (Figures 34 and 36). At the other powers it is hard to distinguishe the positions where the density is maximum.

The effect of the applied field's power on localizing the spheres in the high intensity regions is measured through the deviation around a mean position along the direction of the selected fringe periods, such data is presented in Table III. In this table it is observed that the calculated standard deviation, of the mean x-position in each fringe period, decreased as the input power increased. The loss of correlation at large distances is indicated by the systematic increase in the deviation as the successive fringes are considered in Table III. The highest interdependence at this crossing angle occurs for particles that are within the same fringe position, as demonstrated by the curves shown in the lower boxes of Figures 34 to 36.

As the crossing angle was made even smaller (8.8 degrees), the obtained of fringe period 3.3um was larger than the average particle separation in the equilibrium phase (Figure 37) by a factor of about 1.5. As the stationary sinusoidal intensity fringe pattern is applied

TABLE III

ANALYSIS OF 2-D PAIR CORRELATION FUNCTIONS FOR d=2.2um

Input Power (mW)	Fringe Positions (d/2)		$Mean_x/a$	Std_x/a
42	-1	1	0	.266
42	1	3	1.8	.283
	3	5	3.77	.298
65	-1	1	0	.223
	1	3	1.9	.241
	3	5	3.85	.252
165	-1	1	0	.226
	1	3	1.81	.231
	3	5	3.77	.257

$Mean_x$ = mean x position of the particles in the given fringe period

Std_x = standard deviation around the x position of each fringe.

a = diameter of a single particle.

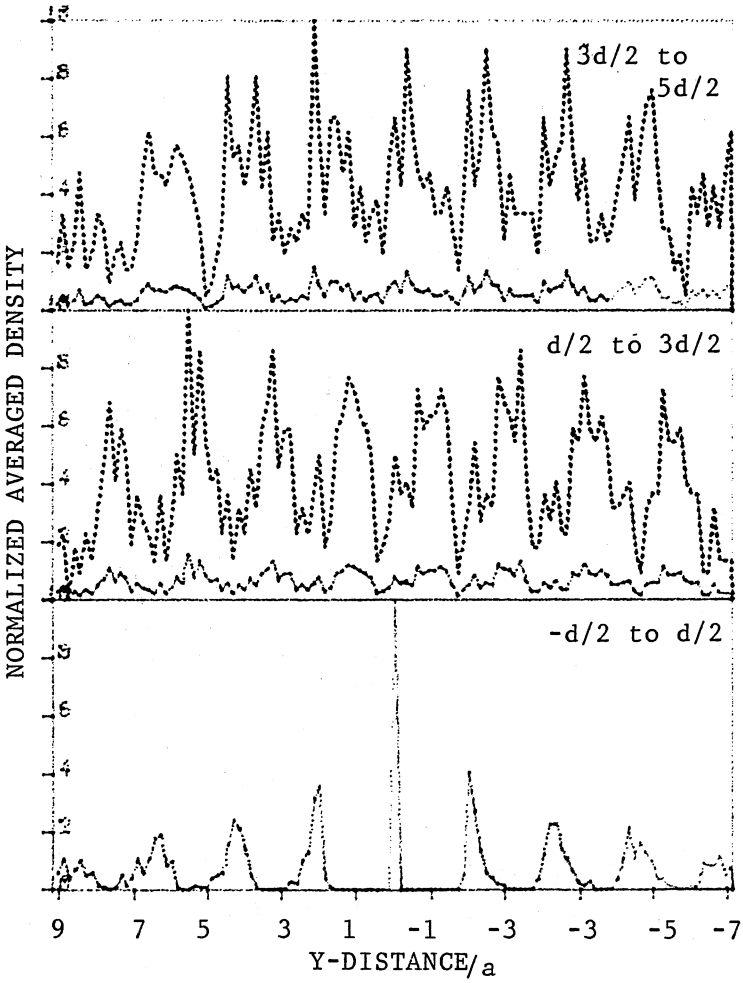

Figure 34. Normalized Average Density Distribution Along the Fringes of the 2D Correlation Function Shown in Figure 31.

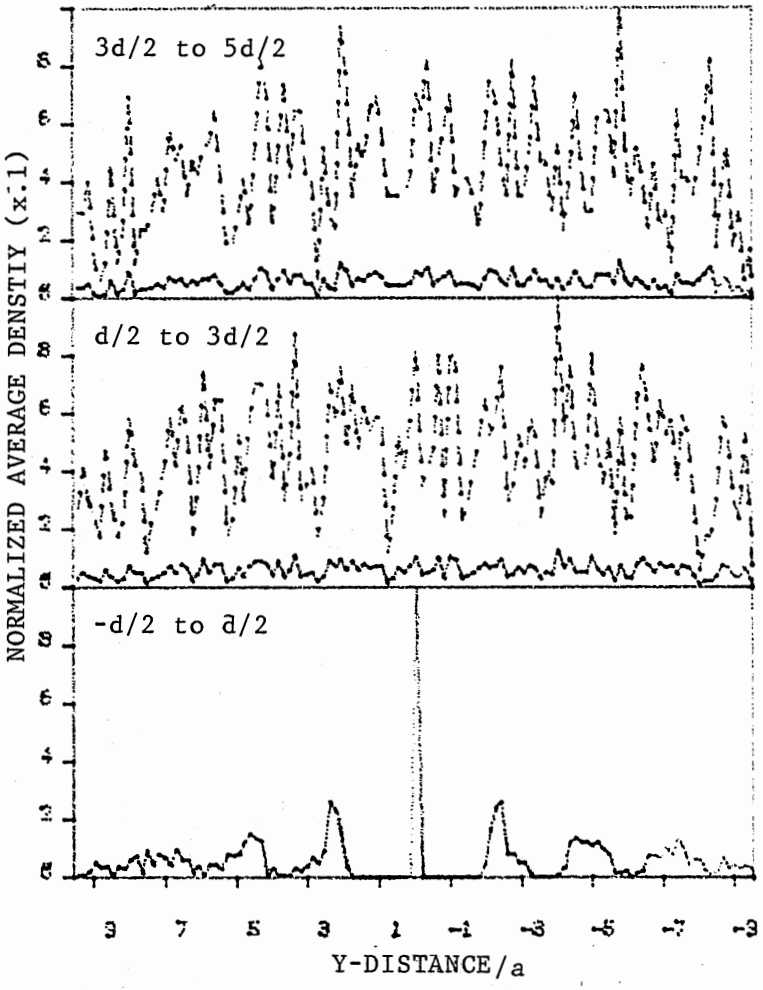

Figure 35. Normalized Average Density Distribution Along the Fringes of the 2D Correlation Function in Figure 32b.

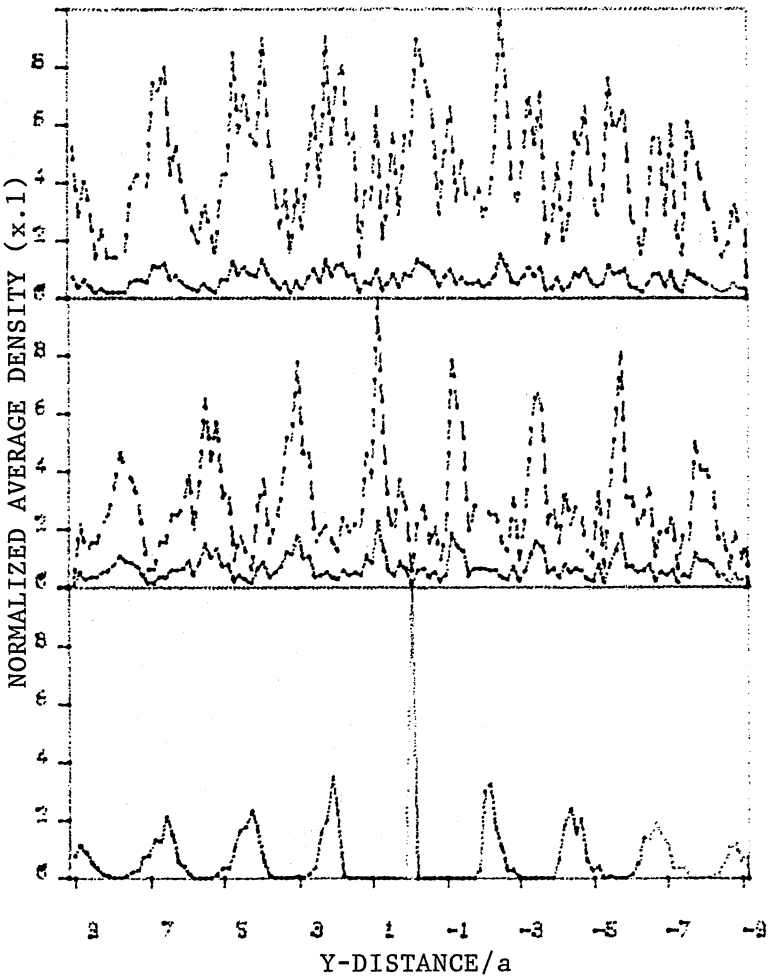

Figure 36. Normalized Average Density Distribution Along the Fringes of the 2D Correlation Function in Figure 33b.

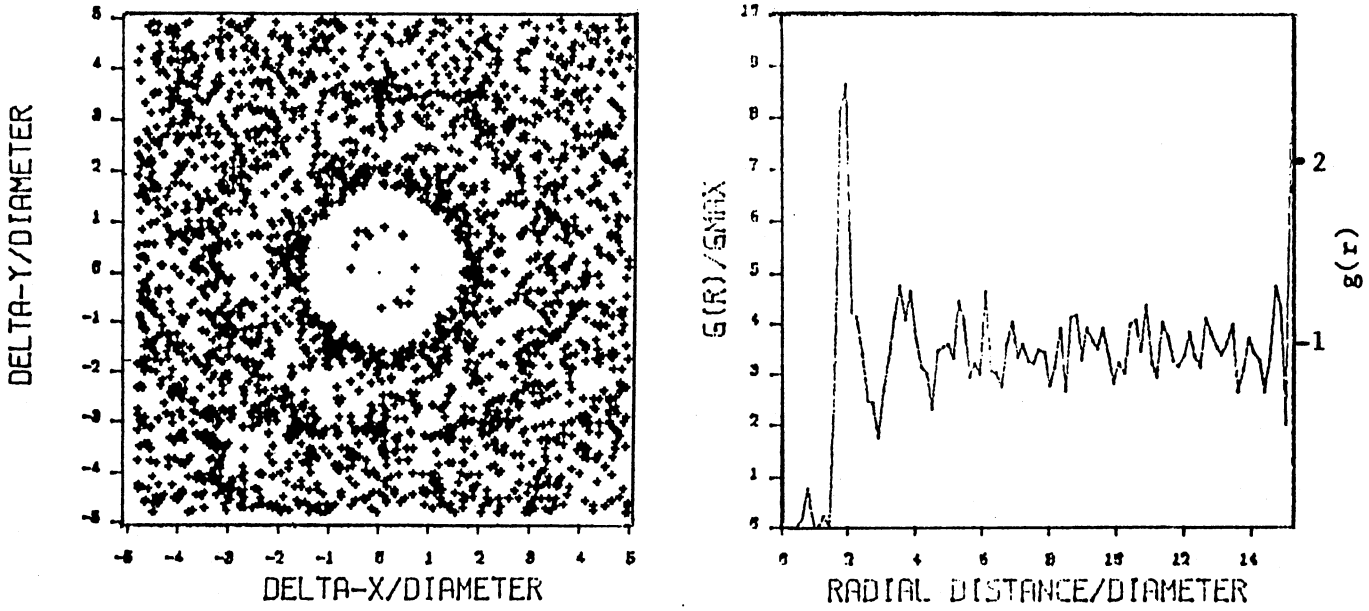

b) 2D Pair Correlation Function a) 1D Pair Correlation Function

Figure 37. Pair Correlation Functions For an Amorphous Monolayer Region used for the Crossed Beam Analysis at Fringe Period of 3.3um.

the response of the interacting spheres to this external field is demonstrated in Figure 38a. The self scattering produced from this is given in Figure 38b. These two figures show that at this fringe separation , the interation between the microspheres causes them to line up at high as well as the low intensity regions. This actually leads to a loss of correlation between the adjacent rows at low input powers. This behavior is demonstrated by plotting the positions files of 20 real space snap-shots, and the distribution of the particles' density along the potential's periods (Figures 39 and 40). At the low input powers (42mW) the density of the particles along the high intensity regions appears to be the same as in the low intensity regions (Figure 39b). As the laser's power was increased to 161mW, the density function showed well defined peaks (Figure 40b), an indication of the localization of the spheres along the applied potential's minima.

The corresponding pair correlation functions are given in Figures 41 through 43. In all of these figures is hard to distinguish the existence of well defined order at the applied powers. Analysis of the density distribution (Figures 44 to 46) at 42, 86 and 161mW input powers manifest the dependence of the local freezing at large fringe periods on the applied external field's strength. The localization of the spheres along the intensity maxima is shown by a decrease in the standard deviation around the mean of the particles' positions in each fringe (Table IV) as the input power increased.

The results obtained from this two-dimensional analysis are summarized in Table V. To be noticed is that the density at all crossing angles and at all input powers stayed constant within

TABLE IV

ANALYSIS OF 2-D PAIR CORRELATION
FUNCTIONS FOR d=3.3um

Input Power (mW)	Fringe Positions (d/2)		$Mean_x/a$	Std_x/a
42	-1	1	0	.925
42	1	3	2.96	.858
42	-1	-3	-2.96	.854
86	-1	1	0	.979
86	1	3	3.15	.935
86	3	5	-3.19	.919
161	-1	1	0	.851
161	1	3	2.90	.782
161	3	5	-2.95	.779

$Mean_x$ = mean x-position of the particles in the given fringe period

Std_x = standard deviation around the x-position of each fringe.

a = diameter of single particle.

TABLE V

SUMMARY OF THE TWO DIMENSIONAL ANALYSIS

	Commensurate Monolayer		Non Commensurate Monolayer		Non Commensurate Monolayer	
d(um)	1.85		2.1		3.31	
a(um)	2.19		2.08		2.11	
Power (mW)	Density ($x10^{11}/m^2$) Single Beam	Double Beam	Single Beam	Double Beam	Single Beam	Double Beam
22			1.95	1.95	1.96	1.96
42	1.93	1.93	1.95	1.95	1.96	1.96
65	1.91	1.91	1.95	1.95	1.98	1.98
86	1.90	1.90	1.95	1.95	1.96	1.96
111	1.90	1.90	1.96	1.96	1.96	1.96
135	1.91	1.91	1.95	1.95	1.96	1.97
161	1.91	1.91	1.95	1.95	1.97	1.97
182			1.95	1.95	1.96	1.96

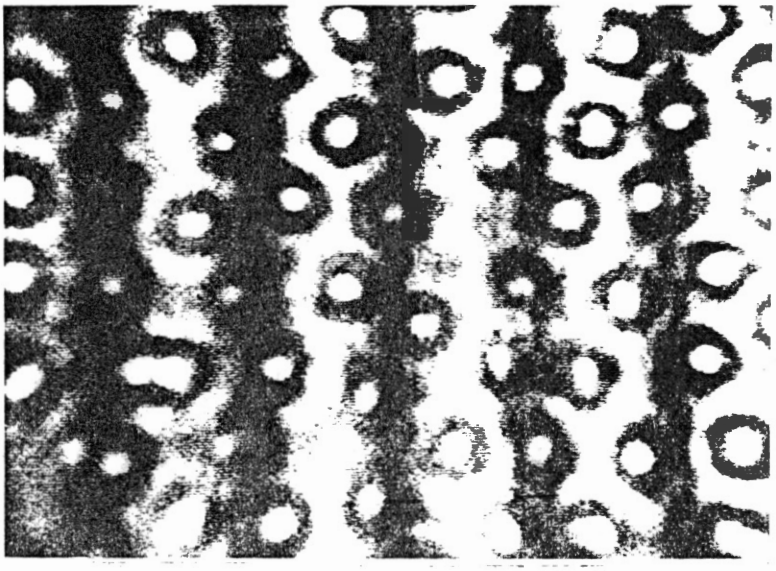

a) Alinement of the 1.07um microspheres Along the High Intensity Regions of the Fringe Pattern at Fringe Period of 3.3um.

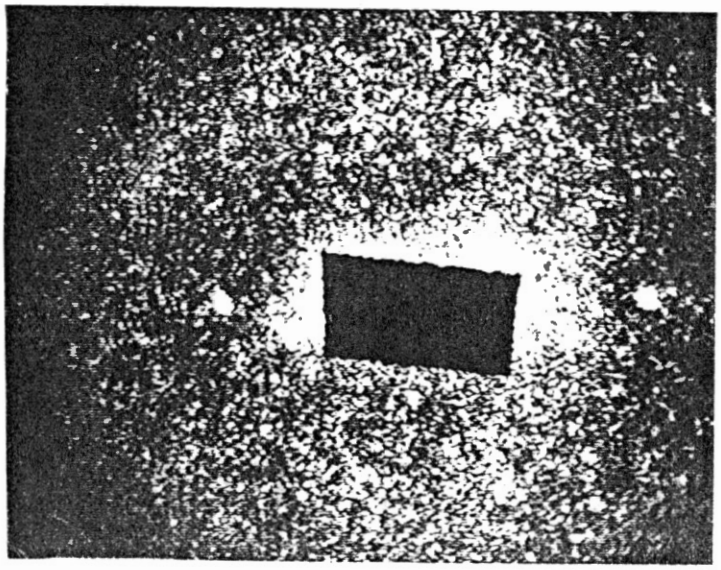

b) Self Scattering Pattern From the Structure Shown Above.

Figure 38. Particles Alinement at Fringe Period of 3.3um (a) and the Produced Self Scattering Pattern.

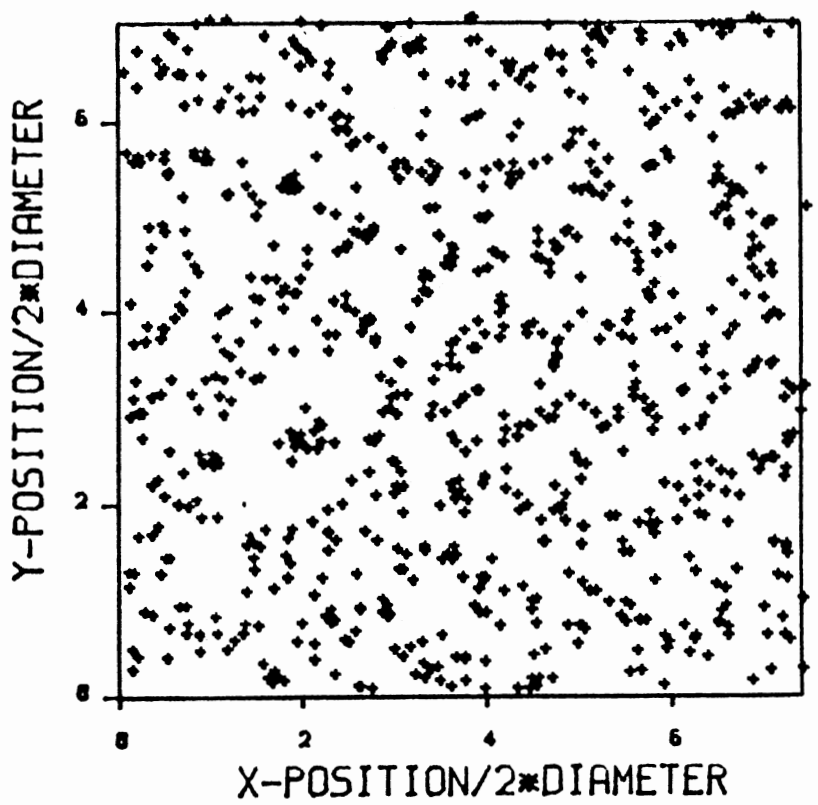

a) x-y Position Files.

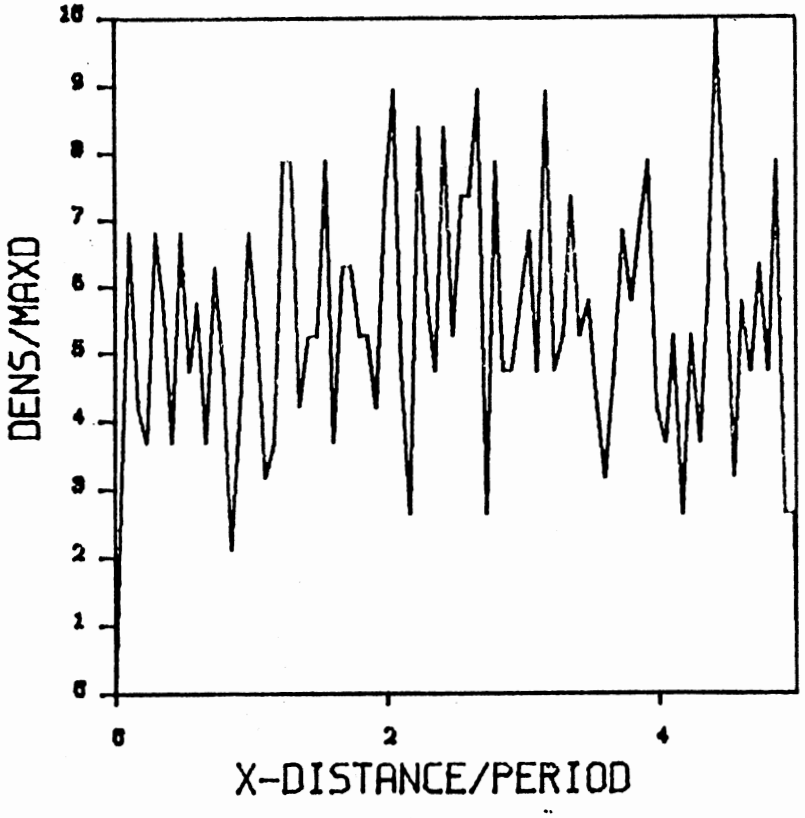

b) Density Distribution.

Figure 39. Position Files for 20 Snap Shots of a Monolayer at Fringe Period of 3.3um and Input Power of 42mW (a), and the Density Distribution of the Particles along the Fringes (b).

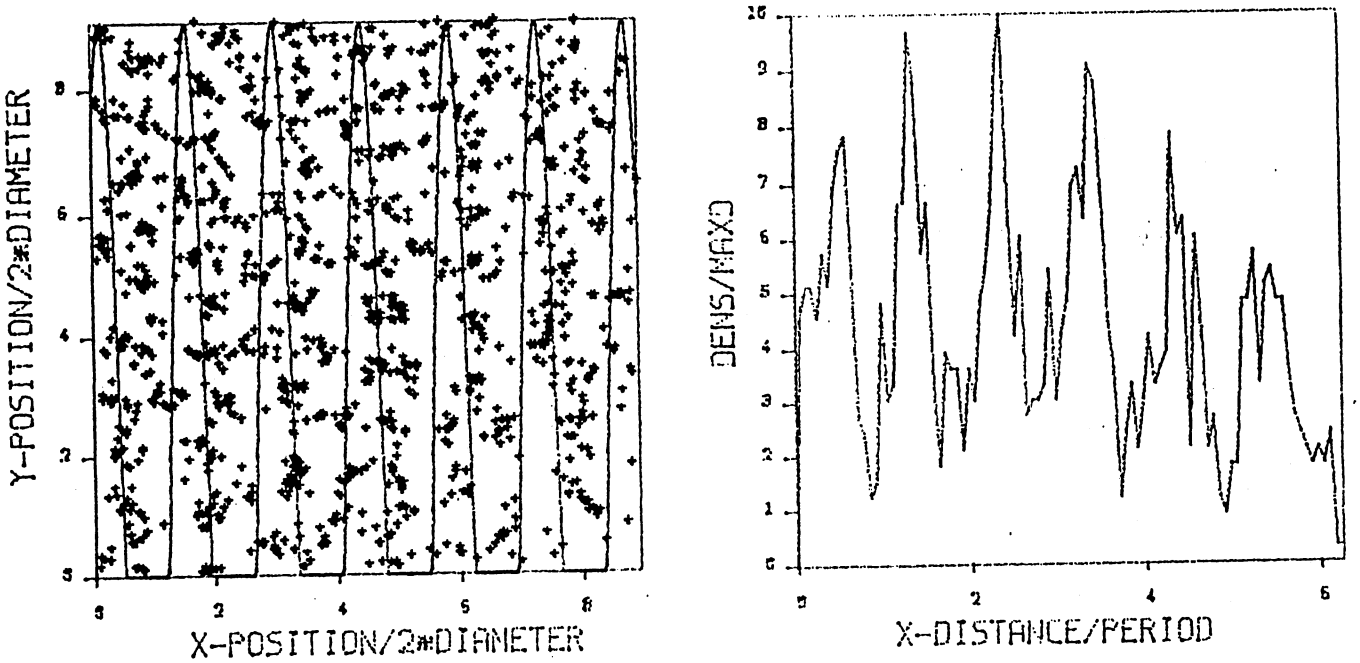

a) X-Y Positions for 20 Files.

b) Density along the Fringes.

Figure 40. Position Files for 20 Snap Shots of a Monolayer at Fringe Period of 3.3um and Laser Input Power of 161mW (a), and the Density Distribution of the Particles along the Fringes (b). The Solid Curve in Part (a) of this Figure Rpresents the Standing Sinusoidal Intensity Fringe Pattern.

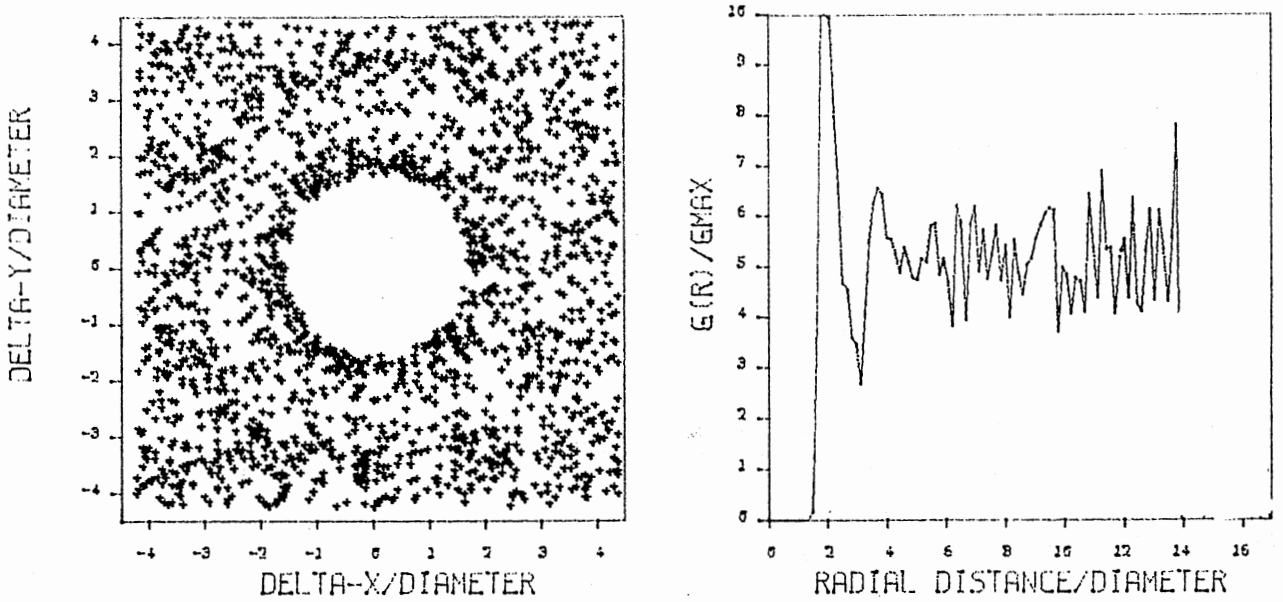

b) 2D Pair Correlation Function a) 1D Pair Correlation Function

Figure 41. Pair Correlation Functions [a) g(r) and b) g(r)] for a Monolayer at Fringe Period of 3.3um and Laser Input Power of 42mW.

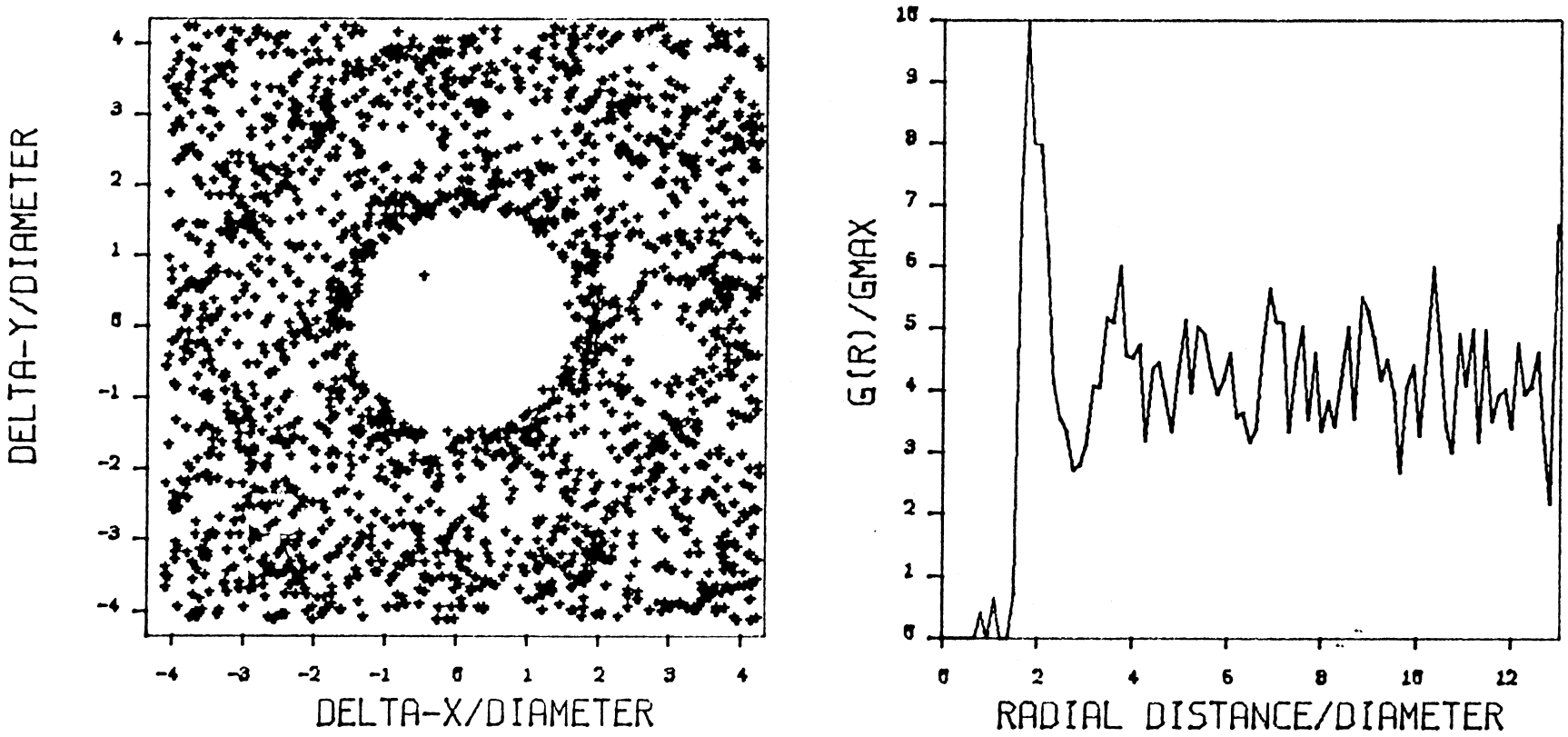

b) 2D Pair Correlation Function.

a) 1D Pair Correlation Function.

Figure 42. Pair Correlation Functions (a. g(r) and b) g(r)) for a Monolayer at Fringe Period of 3.3um and Laser Input Power of 86mW.

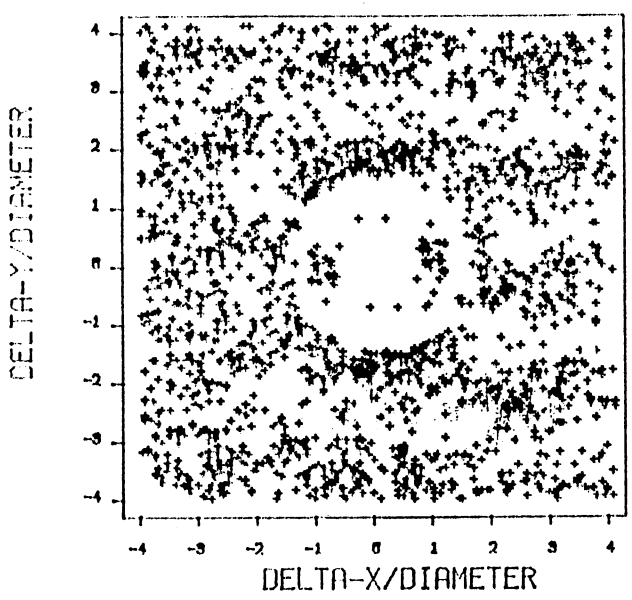

b) 2D Pair Correlation Function

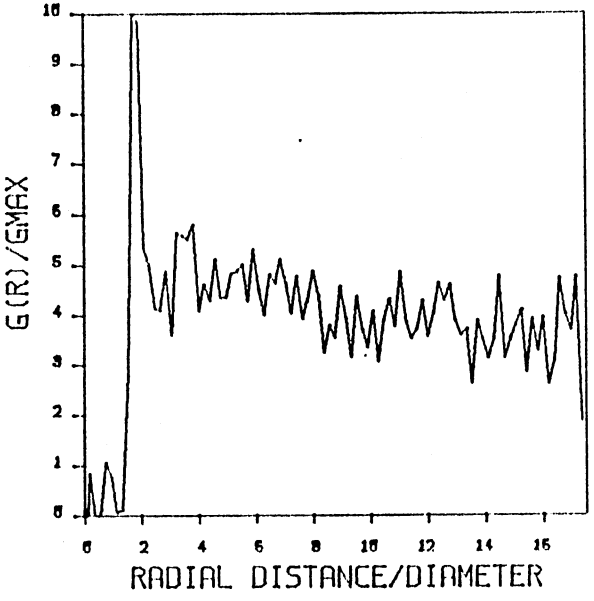

a) 1D Pair Correlation Function

Figure 43. Pair Correlation Function [a) g(r) and b) g(r)] for a Monolayer at Fringe Periodof 3.3um and Laser Input Power of 165mW.

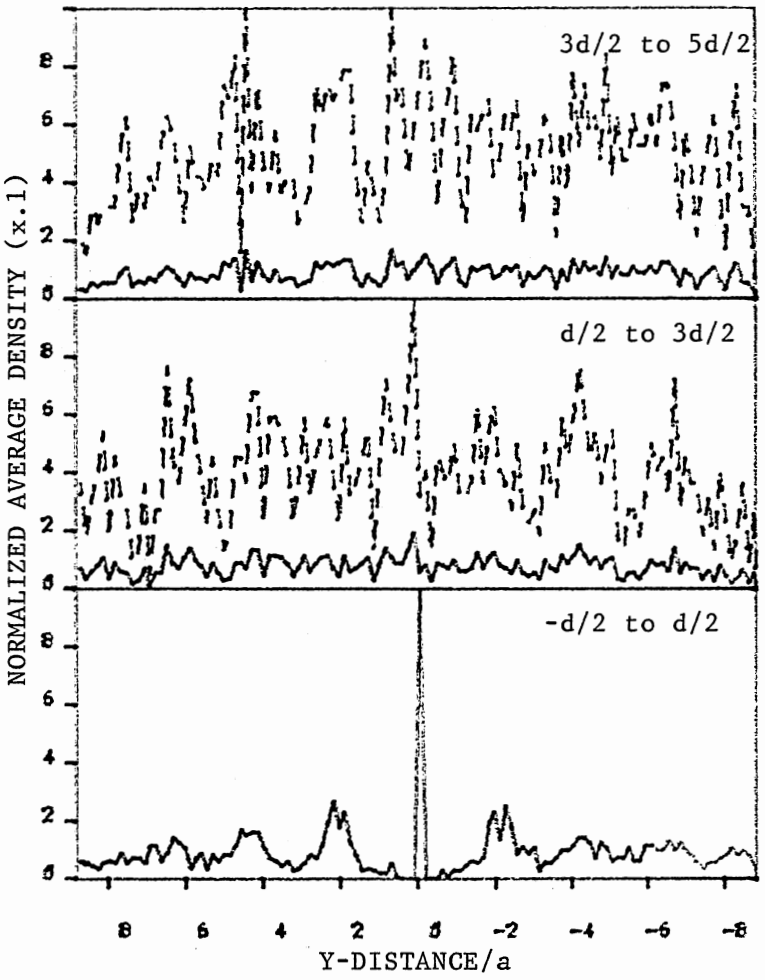

Figure 44. Normalized Average Density Distribution Along the Fringes of the 2D Correlation Function in Figure 41b.

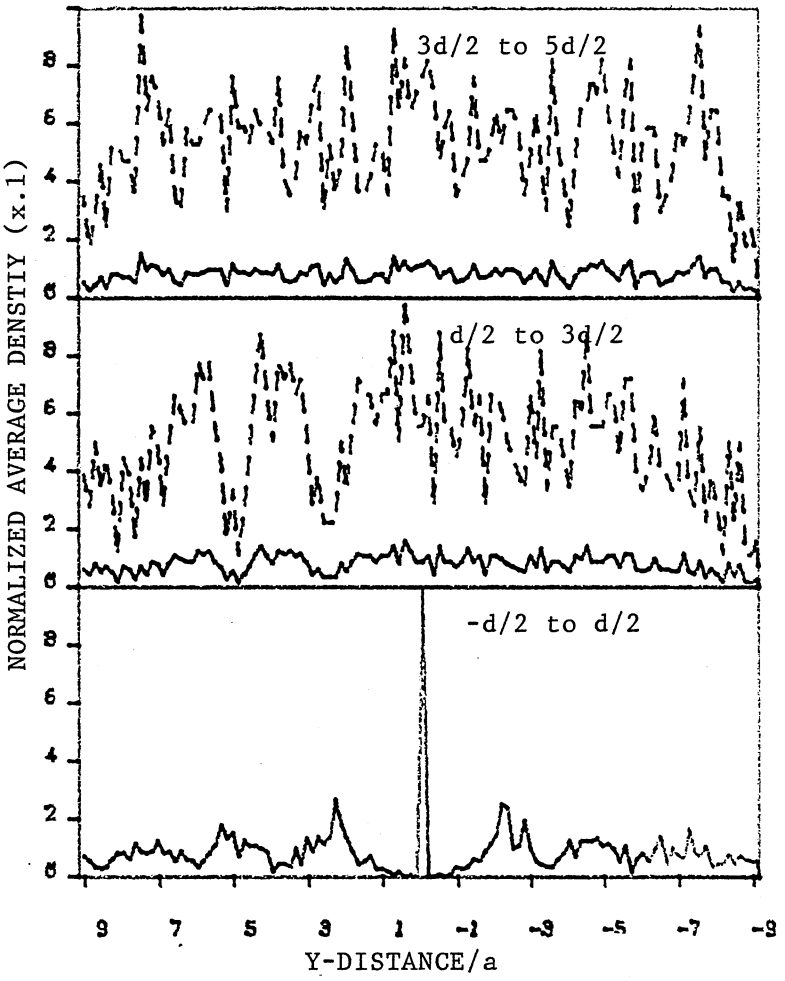

Figure 45. Normalized Average Denstiy Distribution Along the Fringes of the 2D Correlation Function Shown in Figure 42b.

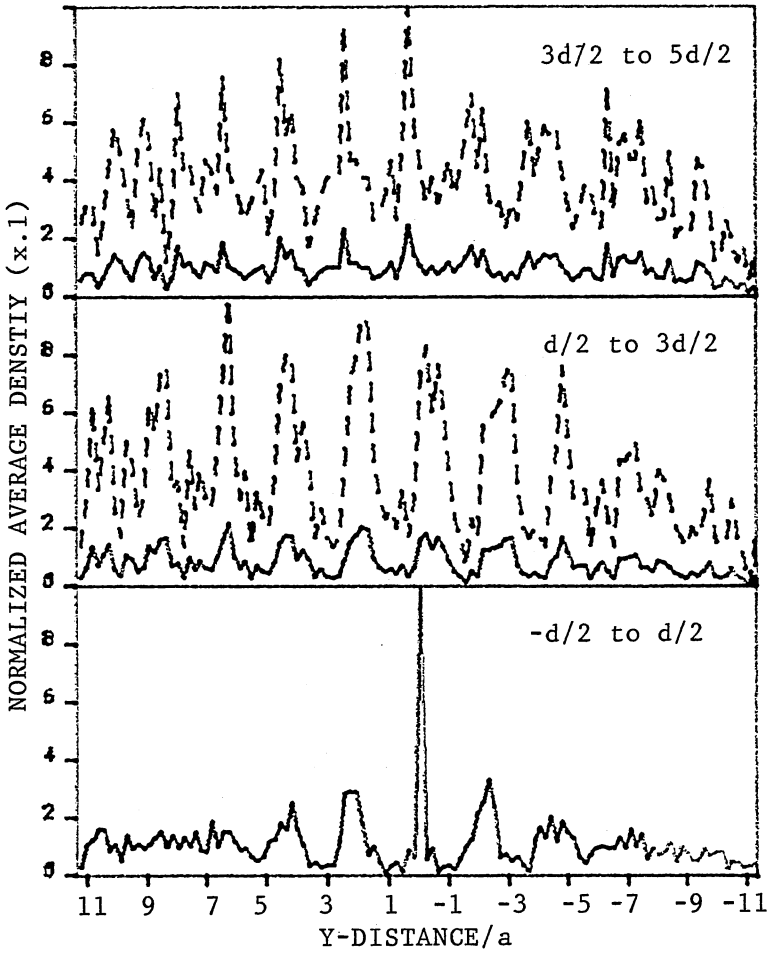

Figure 46. Normalized Average Density Distribution Along the Fringes of the 2D Correlation Function Shown in Figure 43b.

experimental error of 5%. In all of the above analysis, when one of the write beams was blocked the system relaxes back to an amorphous phase with the same density as we started with.

Three-Dimensional Analysis

Cell gap regions containing more than a single layer amorphous equilibrium phase were subjected to the radiation forces created from the crossing of the two mutually coherent laser beams. In all these cases it is observed that the longitudinal component of the radiation field pushes the suspended polystyrene spheres downstream in the direction of the beam propagation. Once these spheres near the cell boundary wall (front glass plate), they are repelled by the similarly charged wall. This forces the spheres to form a first layer near the bounding plate of the sample cell. The particles lining up behind this layer start competing with the spheres that present in it, for a least energetic state. This process eventually causes the micro-spheres in the first layer to expend outward leaving space for some of those in the second layer to end up in the same layer. The fact that the beam's intensity profile has a Gaussian distribution means that the particles near the beam's center experience a larger force than those located at its edges. This in turn causes the regions away from the center of the crossed beams to be multilayered when those near the center may be forced to line up in a monolayer. The transformation to a monolayer and the area occupied by this single layer depend on the laser input power, start up phase and radiation exposure time.

A pictorial demonstration of the evolution of a forced monolayer is given by Figure 47. The first snap-shot of this figure was taken

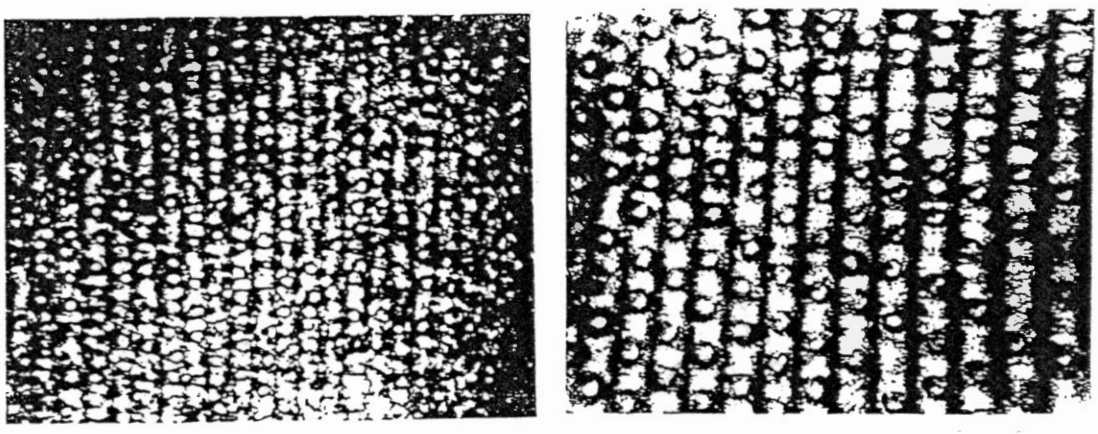

a) Multilayer at P=22mW

b) Multilayer at P=65mW

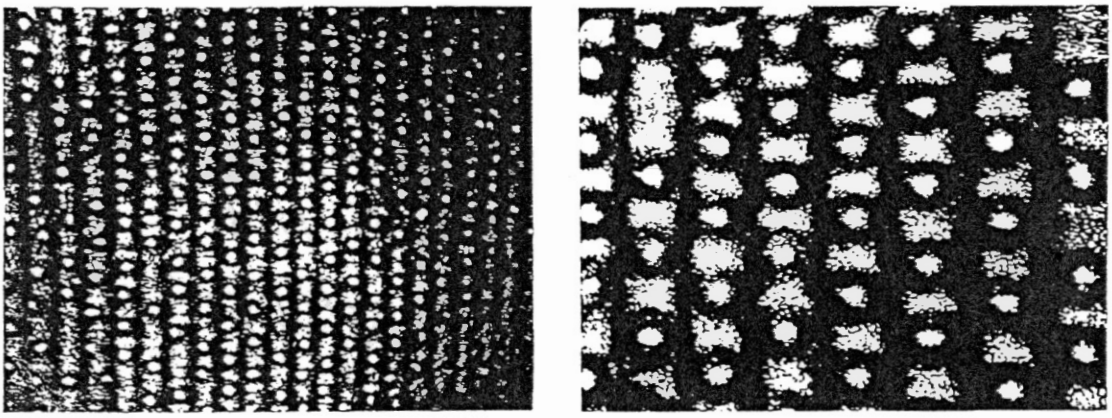

c) Monolayer at P=161mW

d) Monolayer at P=182mW

Figure 47. Transformation From a Multilayer Region (a) to a Monolayer region (d) for the Crossed Beams Case (d=1.85um) as a Function of the Laser Input Power.

when a multilayer region was first exposed to the crossing of two laser beams. Careful examination of this region reveals the existence of a second layer beside the focused layer. The competition to line up near the glass plate is demonstrated in Figure 47b and the final molayer is given in parts c and d of the same figure. The same results are also obtained by increasing the radiation field strength as demonstrated by Figure 48. In this case a multilayer region was exposed to a single beam illumination (Figure 48a)and as the laser's power was increased the forced monolayer region was produced (Figure 48b). In this case (single beam illumination) the input power required to cause the monolayer transformation was about twice as much as that observed for the crossed beams case. Even so, particles from the bakcstream are observed to hop in the monolayer region.

The following discussion will be devoted to the effect of the externally applied potential on the local order of these multilayer equilibrium regions.

Commensurate Structure

When the equilibrium phase shown in Figure 47a was exposed to the potential wells, produced from crossing the laser's beams at an angle of 15.1 degrees (d=1.85um), the system lined up in a hexagonal closed packed structure (HCP) similar to commensurate monolayer case. At this commensurate crossing angle low input powers (<60mW) particles line up in the high intensity regions as expected. However, the strength of their thermal energy at these low powers prevents them from being well localized in the intensity wells, such that they hop from one intensity maxima to another. The particles were also

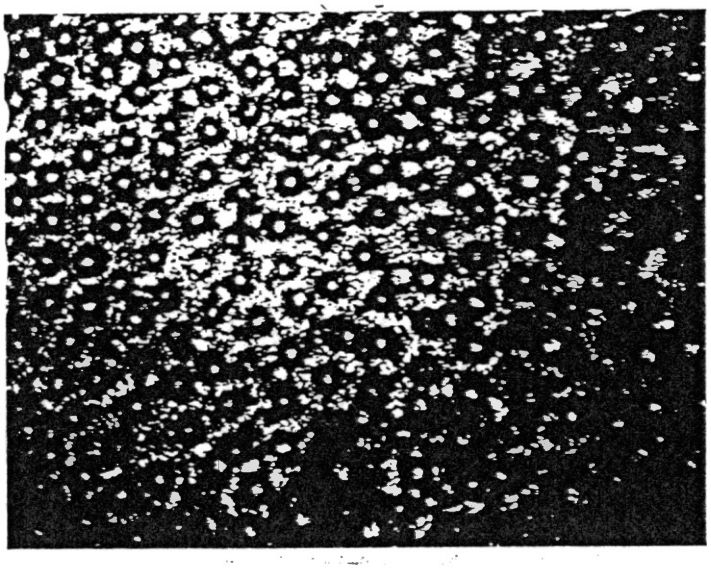

a) Multilayer at P= 42mW

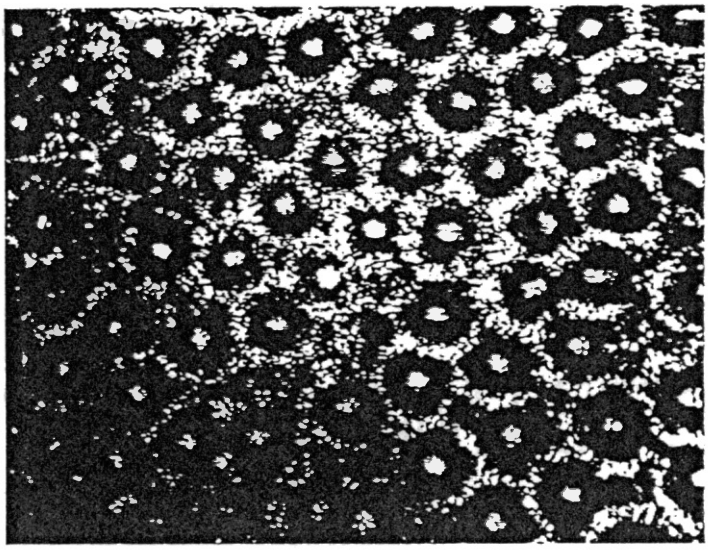

b) Monolayer at P=135mW.

Figure 48. Transformation from a Multilayer at Single Beam Illumination (a) to a Monolayer (b) as the Power of the Single Beam is Increased.

observed to have a random hoping from one layer to the next layer in the same or the adjacent intensity wells (Figure 47b). As the laser's power increased above 111mW, the radiation force restricts the particles' movement along the high intensity regions, thus making them stabilize within the potential wells as well as in a monolayered system.

The analysis for the regions discussed above is considered for powers ranging from 86mW to 161mW. Lower input powers are not considered due to the persistence of the second layer in this sample. At 86mW input power the forced monolayer developed at the center of the sinusiodal standing wave intensity pattern. The 2D equilibrium phase of this forced amorphous monolayer (Figure 49) had a density of $18x10^{10}/m^2$ with the average particle separation of about 2.1um. A plot of the position files when the two beams where crossed at this power is given in Figure 50a. It is apparent from this figure that the microspheres are well localized within the fringes and that there is correlation between adjacent wells. The correlation functions at this power (Figure 51) show well defined order. The pair correlation function (g(r)) has well defined peaks at radial distances of 2a, 3.5a and 4.1a (Figure 51a). The 2D function (Figure 51b) shows that the short ranged induced monolayer has a HCP structure with the lattice constant of 2.1um. The density of the system at this power increased by 12% from the equilibrium phase. This density change makes it hard to establish if the freezing is due to the externally applied potential or if its a result of the increase in density. The analysis of the 2D function is given by the distribution graph shown in Figure 52 where the induced order seems to extend for distances up to 28a,

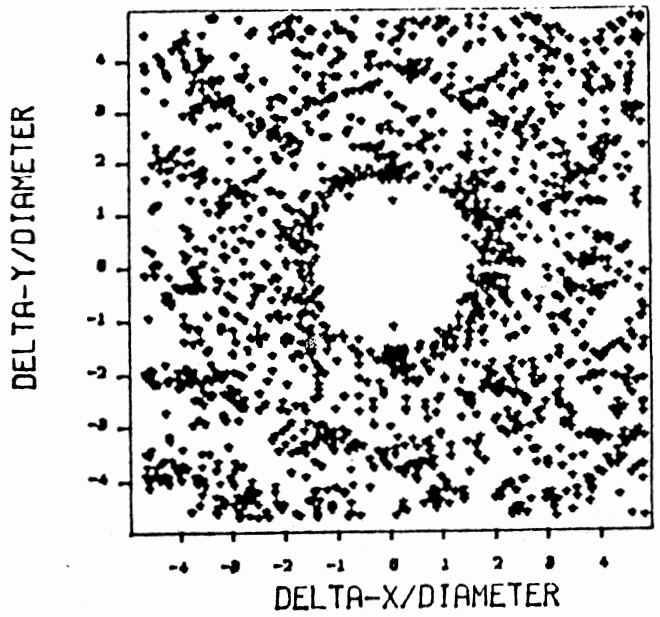

b) 2D Pair Correlation Function

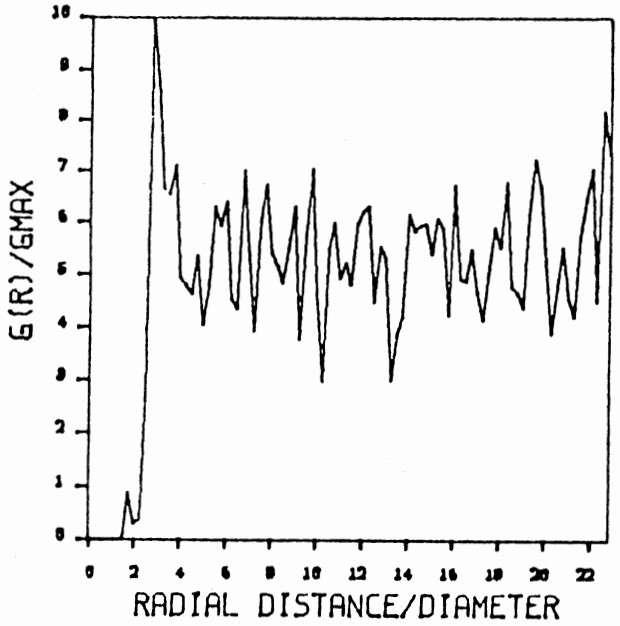

a) 1D Pair Correlation Function

Figure 49. Pair Correlation Functions for a Forced Monolayer at Input Power of 86mW. This Amorphous Phase is used for Analysis at Fringe Period of 1.85um.

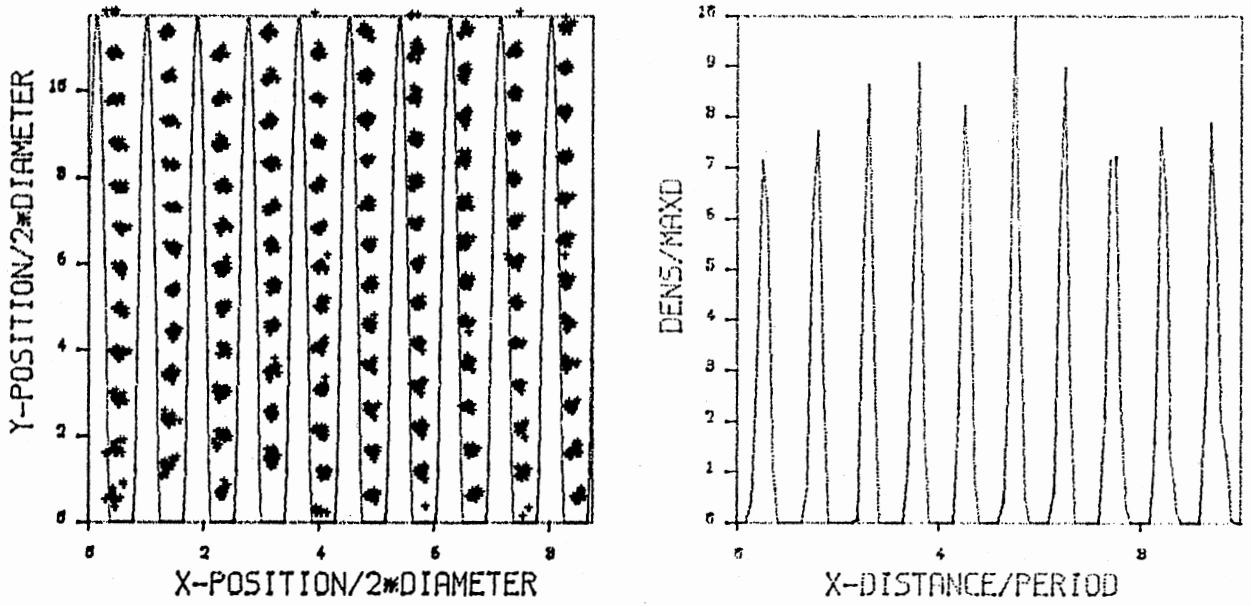

a) x-y Postions for 20 Files

b) Density Along the Fringes

Figure 50. Position Files for 20 Snap Shots of Forced Monolayer at Fringe Period of 1.85um and Laser Input Power of 86mW (a), and the Density Distribution of the Particles along the Fringes(b). The Solid curve in Part (a) of this Figure Represent the Standing Sinusoidal Intensity Fringe Pattern.

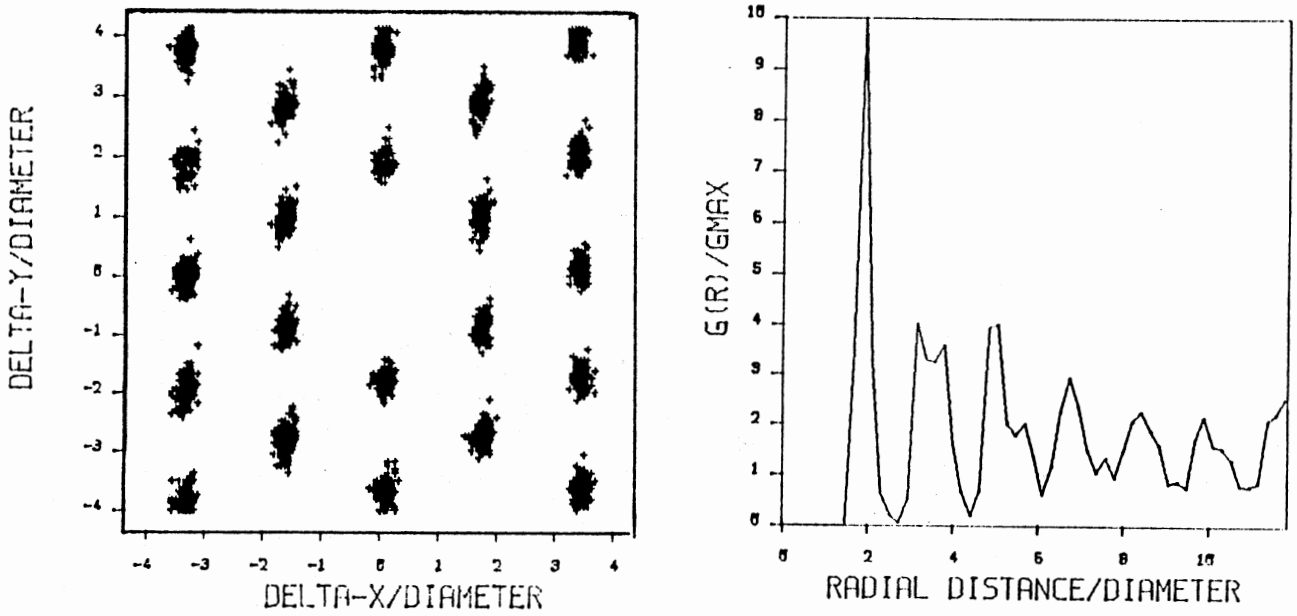

b) 2D Pair Correlation Function a) 1D Pair Correlation Function

Figure 51. Pair Correlation Functions [a) g(r) and b) g(r)] for a Forced Monolayer at Commensurate Fringe Period of 1.85um and Laser Power of 86mW

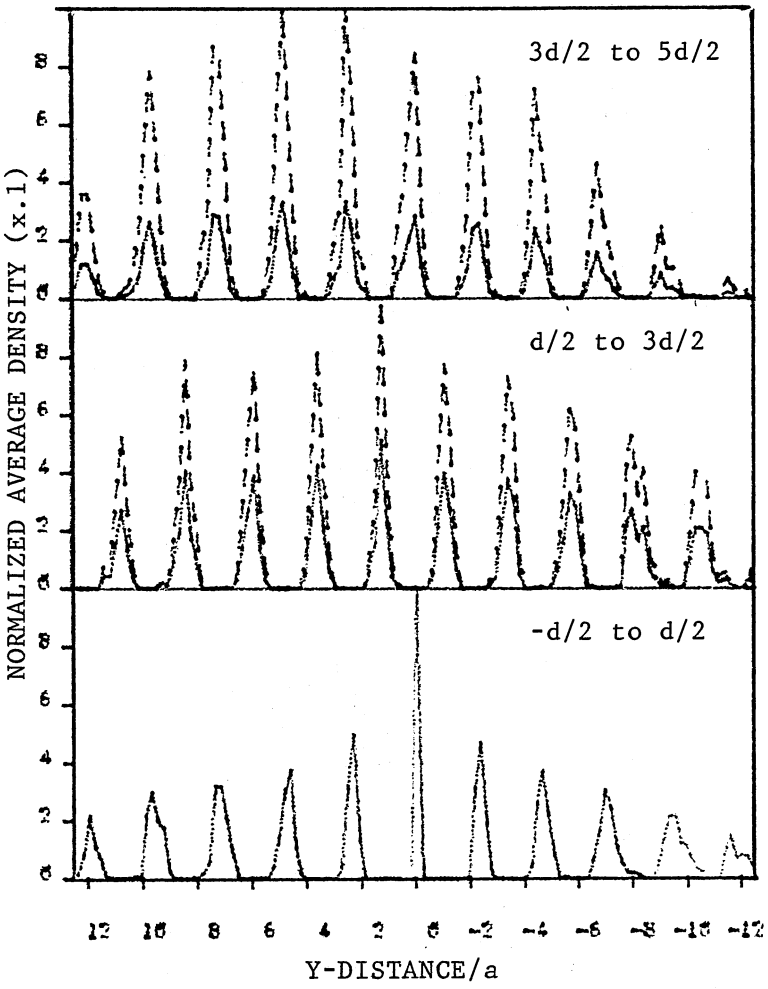

Figure 52. Normalized Average Density Distribution Along the Fringes of the 2D Correlation Function Shown in Figure 51b.

where a is the diameter of a sphere. This figure does also show a decrease in the correlation at large distances as evidenced by the increase in the FWHM of the peaks.

As the input power was increased to 135mW, the particles order becomes more pronounced. This is confirmed through the correlation functions plots (Figure 53) and the density distribution function along the fringes of the 2D correlation function (Figure 54).

As the external field's strength is even made higher (161mW), The the 2D correlation function (Figure 55b) shows a string like behavior where the probability distribution of the spheres along one of the fringes is equally likely. The analysis of the density distribution along the fringes of the 2D function reveals the existence of some correlation at the nearest neighbors distance, especially along the same fringe period. This behavior is not well understood, it is possible that at this power we start overheating the radiation region leading to a convection. The density distribution along the fringes of the 2D correlation function is given in Figure 56.

In the above analysis it was observed that blocking one of the write beams causes the system to relax back to a monolayer amorphous phase. However, when both of the write beams were blocked the system went to the multilayer liquid phase. In the forced monolayer analysis the density of the analyzed regions changed by as much as 20% when input power is was 86 and 135mW.

Noncommensurate Results

When multilayer regions were exposed to the periodic radiation fields, with periods were larger than that used for the commensurate

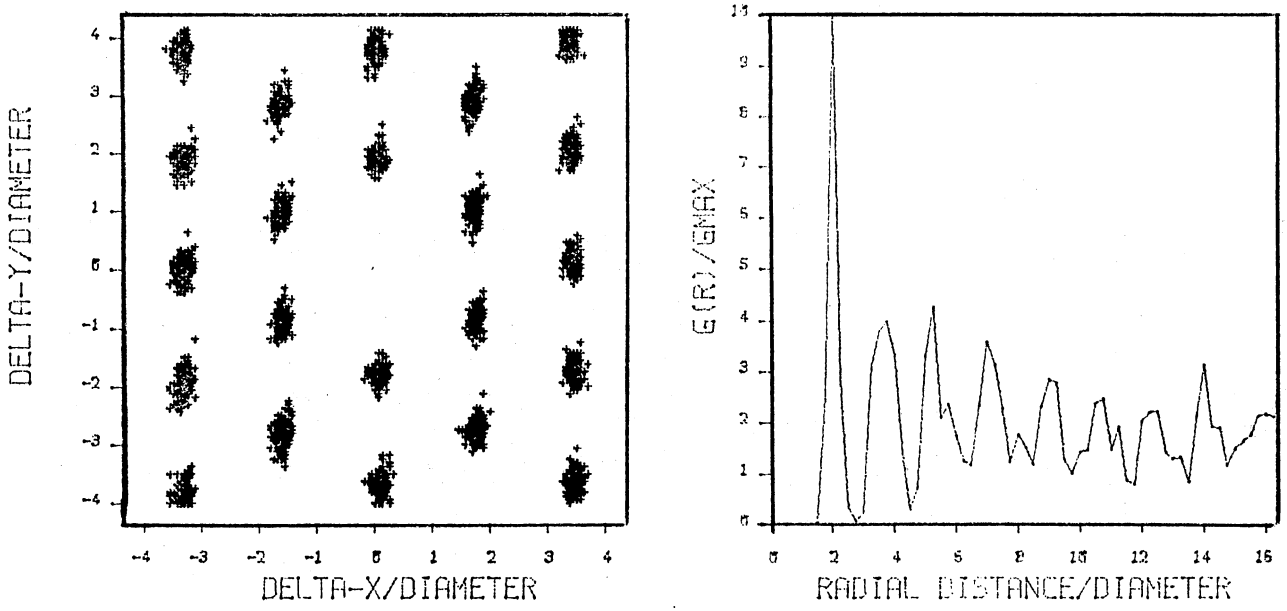

b) 2D Pair Correlation Function a) 1D Pair Correlation Function

Figure 53. Pair Correlation Functions [a) g(r) and b) g($\underline{r}$)] of a Forced Monolayer at Commensurate Period of 1.85um and Laser Power of 135mW.

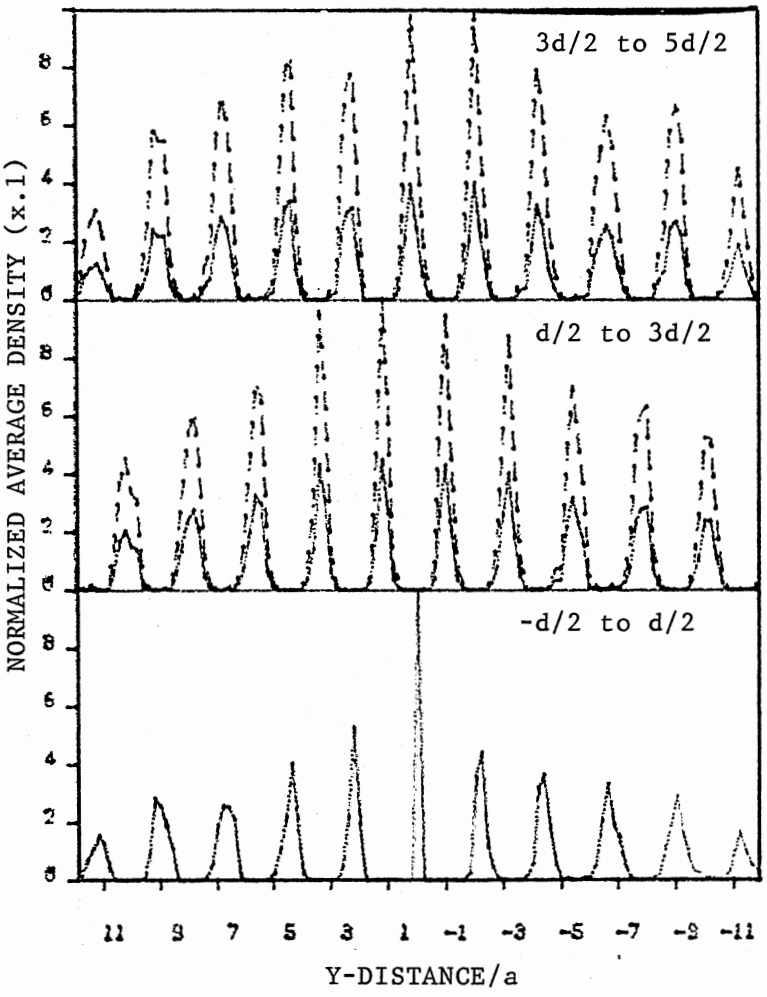

Figure 54. Normalized Average Density Distribution Along the Fringes of the 2D Correlation Function Shown in Figure 52

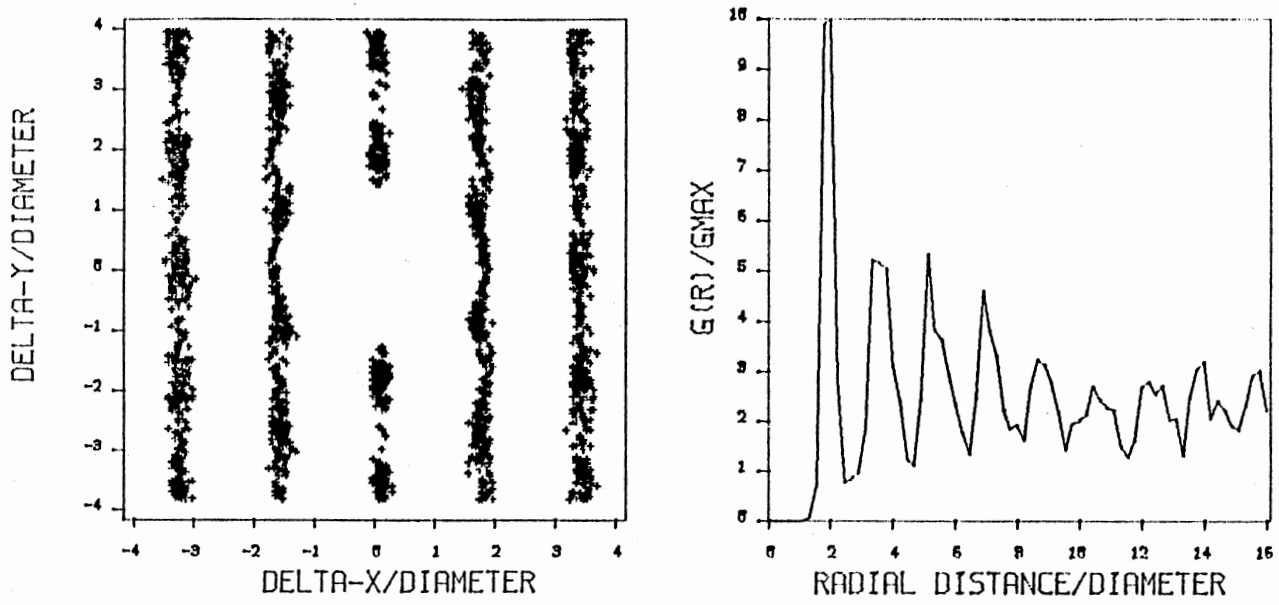

b) 2D Pair Correlation Function a) 1D Pair Correlation Function

Figure 55. Pair Correlation Functions [a) g(r) and b) g(r)] for a Forced Monolayer at Commensurate Fringe Period of 1.85um and Laser Power of 161mW.

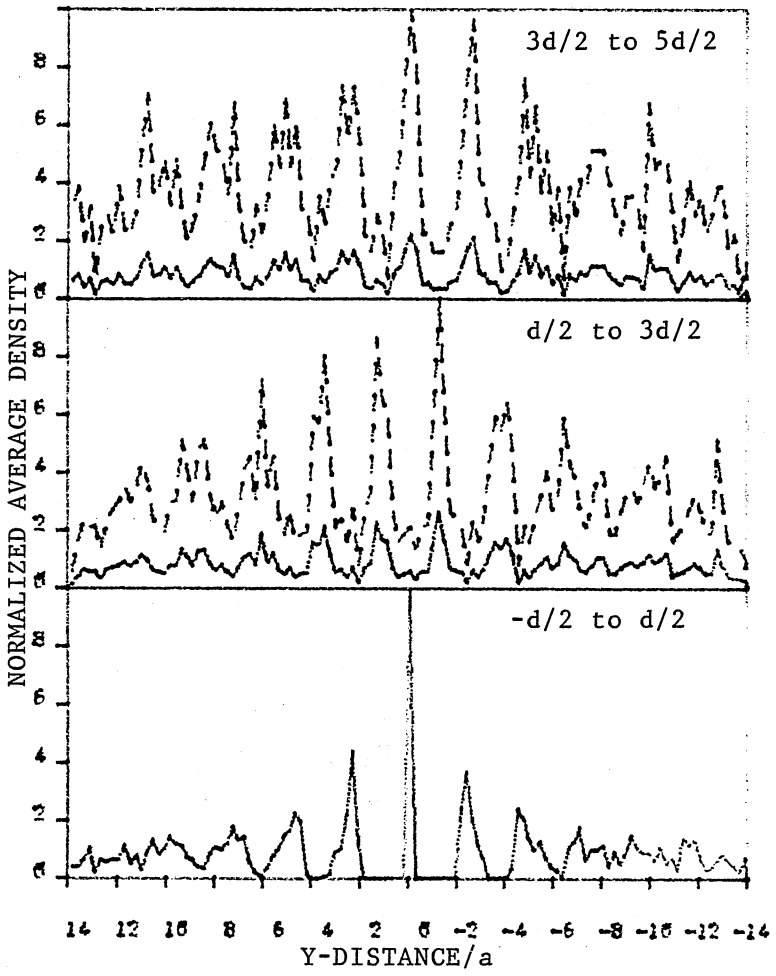

Figure 56. Normalized Average Density Distribution Along the Fringes of the 2D Pair Correlation Function Shown in Figure 55.

case, it is observed that there existed a transformation to a monolayered system. This forced transition seems to be dependent on the fields strength, the radiation exposure time and position of the particles in the field's Gaussian distribution, as was observed in the commensurate case.

For the crossing angle of 12.13 degrees, or the equivalent fringe period of 2.3um, the multilayered amorphous phase began to compete to form molayered regions at input powers as low as 22mW (Figure 57). The depletion of the forced monolayer for the sample used in this analysis (which is different than the previous sample used in the commensurate analysis) was reached at 161mW. The distribution of the particles' positions and their density distribution in the fringes, for the given period of 2.3um and input power of 86mW, are given in Figure 58. The pair correlation functions for this beam separation at input powers of 86, 111 and 182mW are given in Figures 59 to 61.

At 86mW input power, starting with a three dimensional region of the sample cell, it is observed that the radiation pressure forces cause the system to form a monolayered amorphous phase with some of the spheres hopping back and forth from this monolayer. As the beams are crossed at this power the organization of the system is shown through the pair correlation functions given in Figure 59. The 2D function demonstrates a distorted HCP Structure, where the average separation between neighboring centers of each cluster along the fringes (y-direction in Figure 59) is smaller than those between adjacent fringes by a factor of .887. The change of density from the amorphous phase to the crystalline phase in this case is 23% (Table VI).

TABLE VI

ANALYSIS OF 2-D PAIR CORRELATION FUNCTIONS FOR MULTILAYER REGIONS

Fringe Period (10^{-6}m)	Power (mW)	Positions (d/2)		Mean x/a	standard deviation STD/a
1.85	86	-1	1	0	.092
1.85	86	1	3	1.62	.121
1.85	86	3	5	3.35	.126
1.85	161	-1	1	0	.099
1.85	161	1	3	1.72	.111
1.85	161	3	5	3.85	.119
2.34	86	-1	1	0	.235
2.34	86	1	3	1.72	.271
2.34	86	3	5	2.93	.358
2.34	111	-1	1	0	.222
2.34	111	1	3	1.95	.269
2.34	111	3	5	3.05	.290
2.34	182	-1	1	0	.185
2.34	182	1	3	2.08	.191
2.34	182	3	5	4.22	.199
3.34	86	-1	1	0	.728
3.34	86	1	3	3.23	.782
3.34	86	3	5	6.30	.761
3.34	111	-1	1	0	.696
3.34	111	1	3	3.1	.682
3.34	111	3	5	6.4	.777
3.34	182	-1	1	0	.439
3.34	182	1	3	3.10	.511

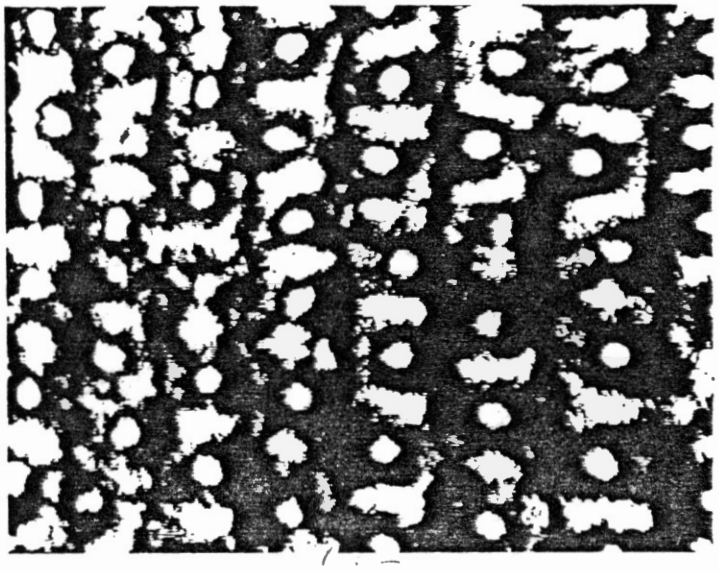

a) Multilayer Alinement of Microspheres at Noncommensurate Fringe Period of 2.3um and Laser Power of 22mW.

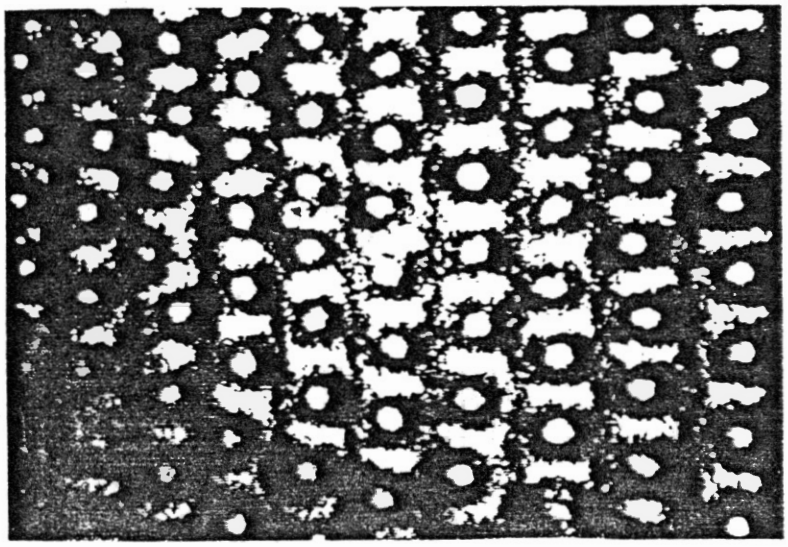

b) Forced Monolayer at Fringe Period of

Figure 57. Alinement of 1.07um Microspheres in the High Intensity Regions of Standing Fringe Pattern with Fringe Period of 2.3um and at Input Power of 22mW (a) and 65mW (b).

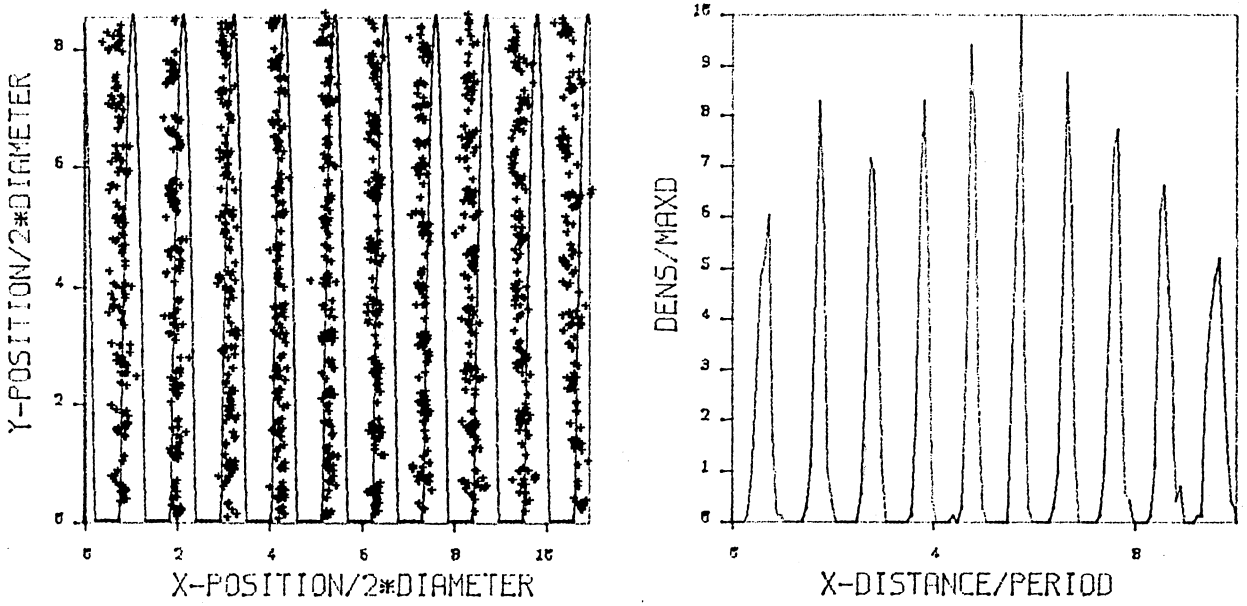

a) x-y Positions for 20 Files

b) Density Distribution

Figure 58. Position Files for 20 Snap Shots of Forced Monolayer at Fringe Period of 2.3um and Laser Input Power of 86mW (a), and the Density Distribution of the Microspheres along the Fringes (b). The Solid Curve in Part (a) of this Figure Represents the Standing Sinusoidal Intensity Fringe Pattern.

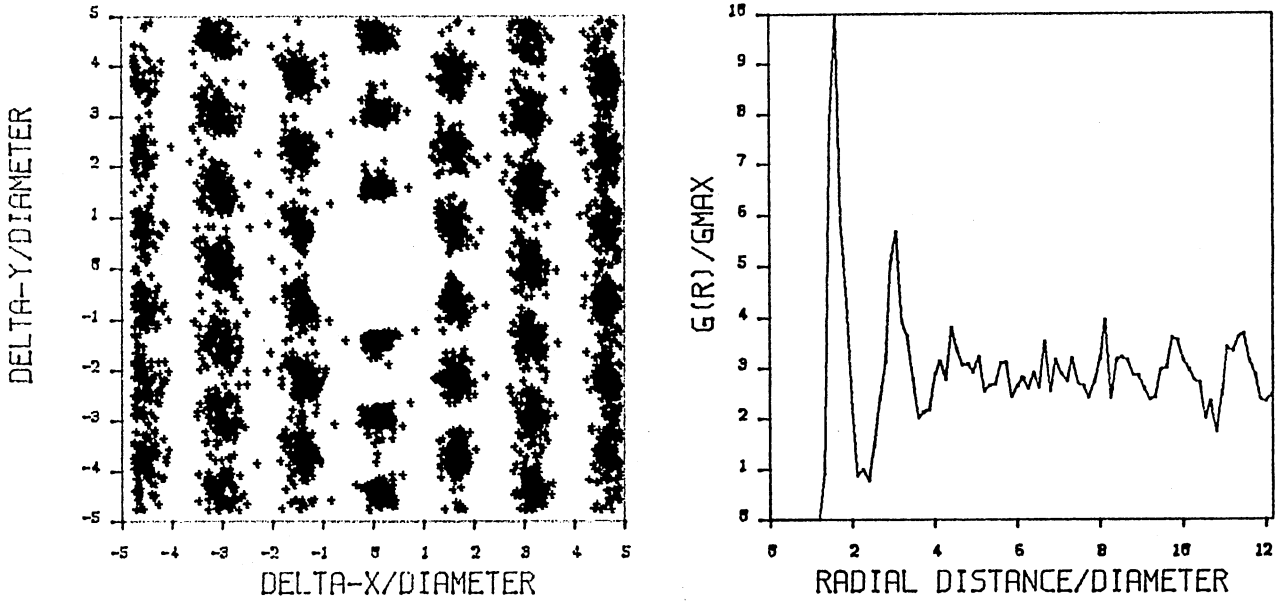

b) 2D Pair Correlation Function

a) 1D Pair Correlation Function

Figure 59. Pair Correlation Functions [a) g(r) and b) g(r)] for a Forced Monolayer at Incommensurate Fringe Period of 2.3um and Laser Power of 86mW.

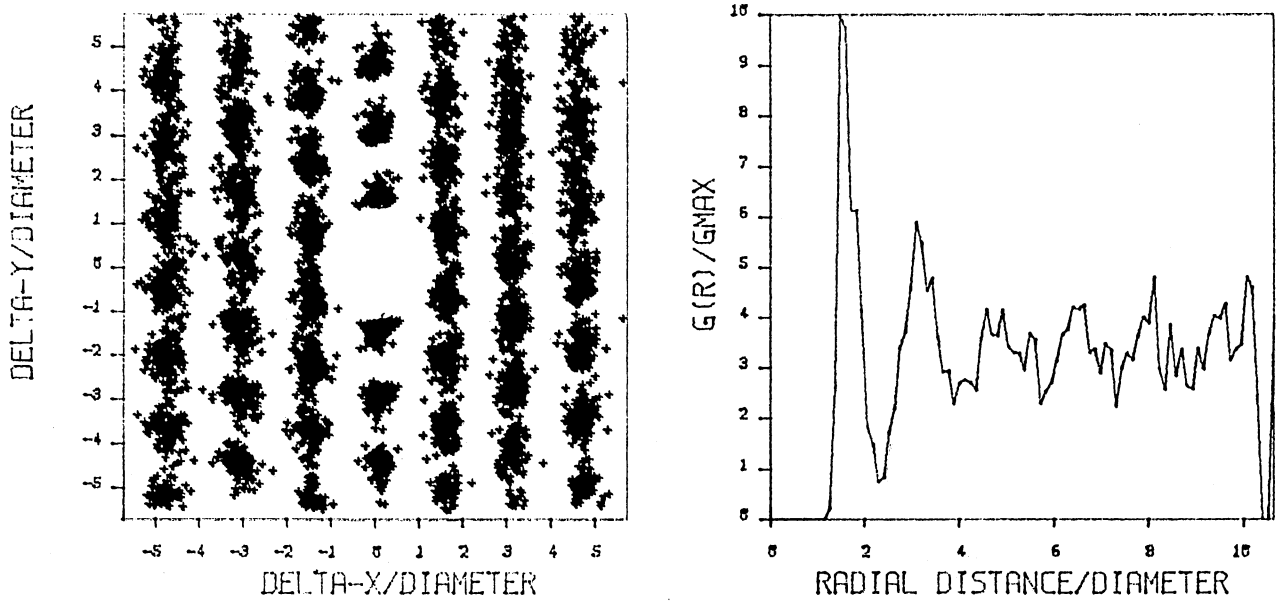

b) 2D Pair Correlation Function a) 1D Pair Correlation Function

Figure 60. Pair Correlation Functions [a) g(r) and b) g(r)] for a Forced Monolayer at Incommensurate Fringe Period of 2.3um and Laser Power of 111mW.

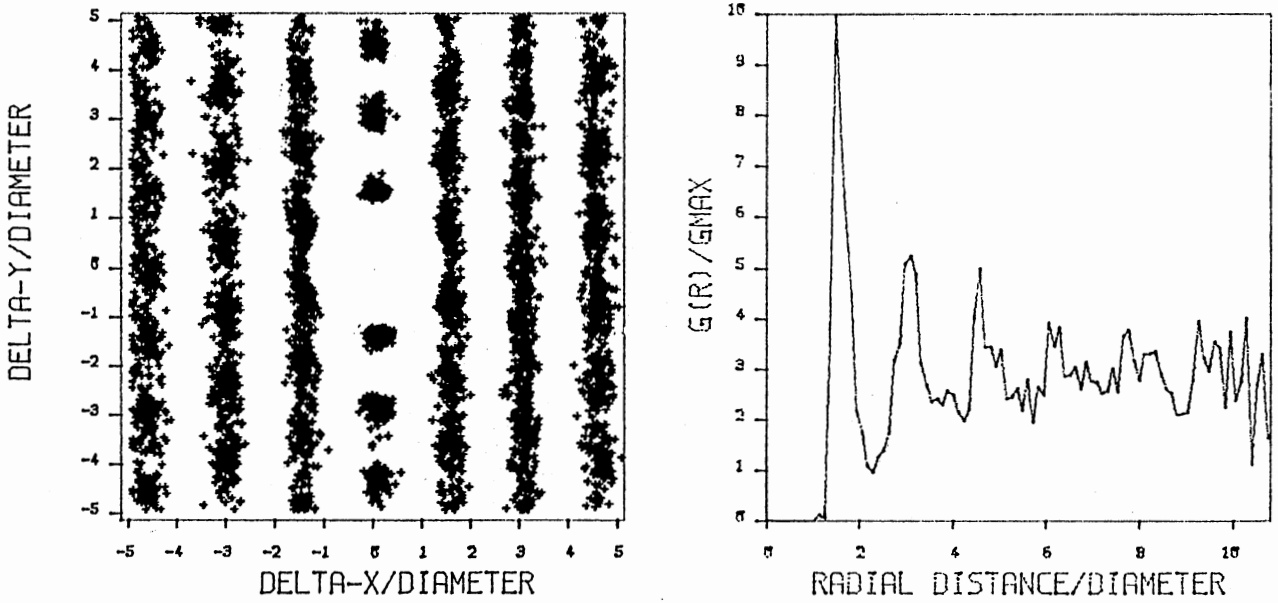

b) 2D Pair Correlation Function

a) 1D Pair Correlation Function

Figure 61. Pair Correlation Functions [a) g(r) and b) g($\underline{r}$)] for a Forced Monolayer at Incommensurate Fringe Period of 2.3um and Laser Power of 182mW.

For those input powers higher than 86mW, it is noted that the equilibrium phase ,single beam illumination, stays as a monolayered amorphous phase. Thus at these powers the analysis is considered as being carried on an amorphous single layer phase, but with the density of the equilibrium phase changing as the beams get crossed.

The arrangement of the microspheres as the beams are crossed at 111mW power is demonstrated by the correlation functions in Figure 60. The 1D function, g(r), shows a well defined peak at r=1.83um and a broader peak at r=3.45um. These peaks manifest the correlation between the charged spheres at these radii. This interdependence is more apparent with the 2D function, where it is observed that the correlation between the particles in the same fringe is strongest. There seems to be some correlation between adjacent fringes but is much less than that observed for lower input powers. This correlation decreases rapidly for distances greater than one fringe separation. The formed structure at this input power seems to be HCP with a lattice constant of 1.83um. As the input power is increased (>111mW), the particles become more localized in their fringes as is displayed by the 2D functions at 182mW (Figure 61). However, the correlation between adjacent rows at these powers is reduced, making the interdependence between the polyballs short ranged, as manifested by the string like distribution of the particles' positions. The loss of orientational correlation at these powers is not well understood.

The average density distribution of the 2D functions along the different fringe periods are given in Figures 62 to 64. These figures show how the correlation between adjacent wells starts developing as the applied field's strength is increased (Figure 62) and than starts

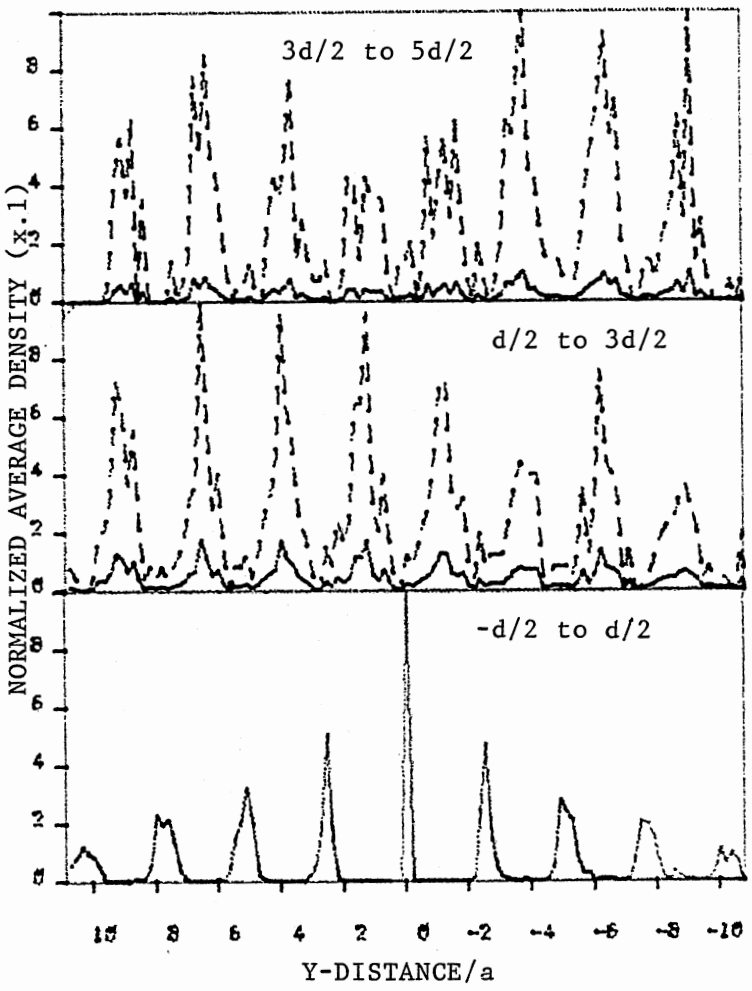

Figure 62. Normalized Average Density Distribution Along the Fringes of the 2D Correlation Function Shown in Figure 59b.

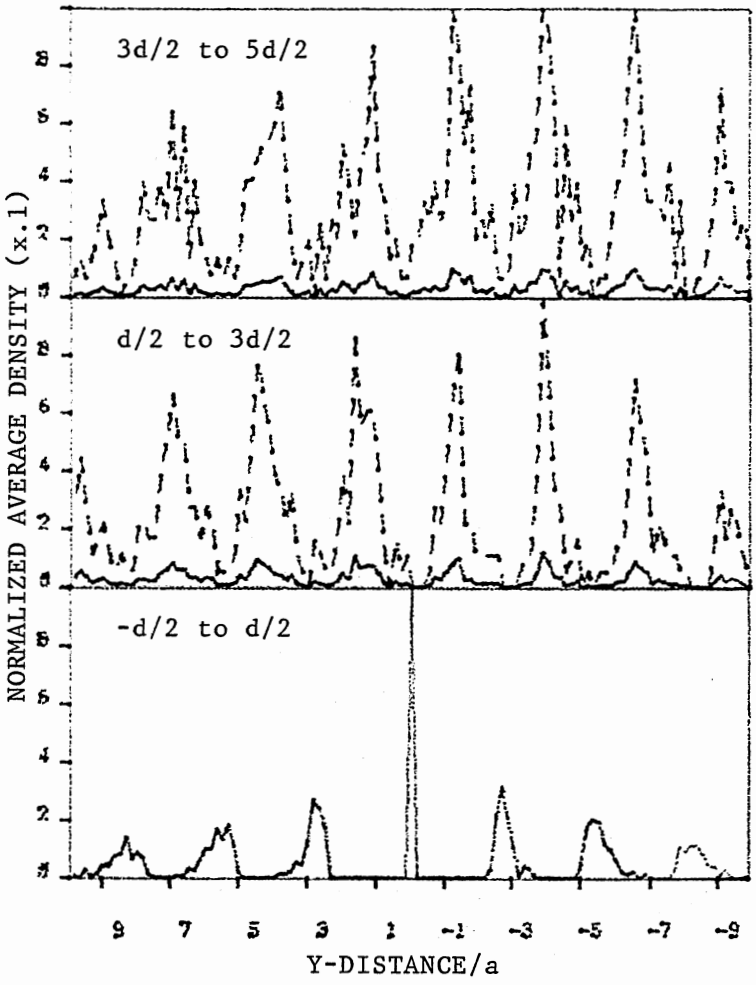

Figure 63. Normalized Average Density Distribution Along the Fringes of the 2D Pair Correlation Function Shown in Figure 60b.

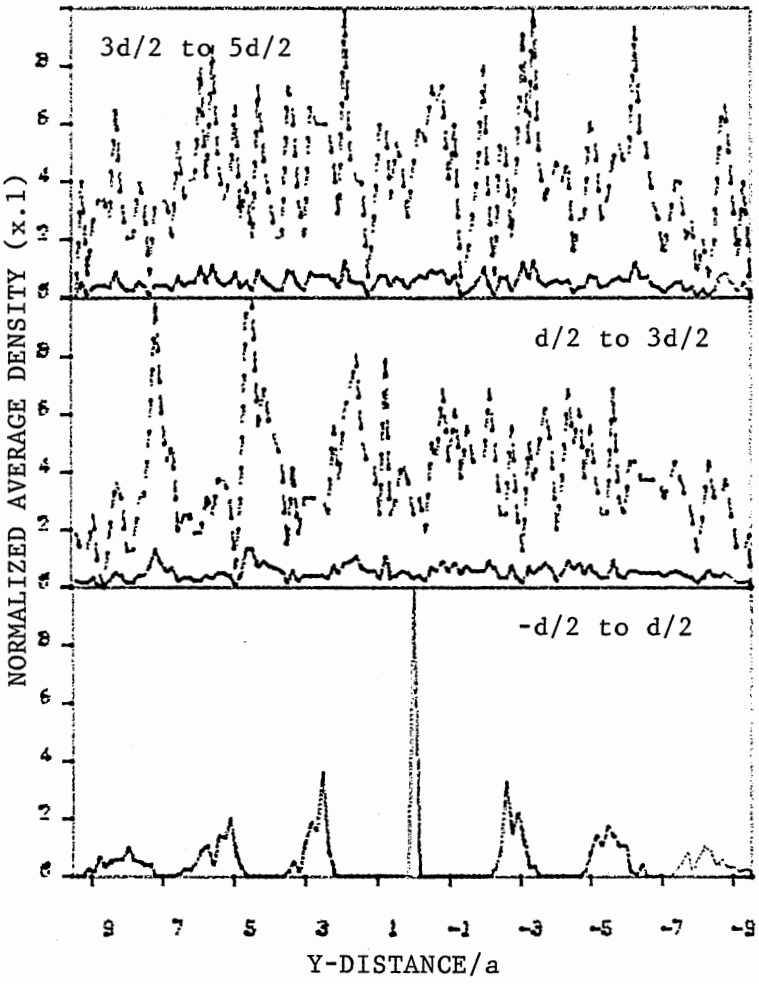

Figure 64. Normalized Average Density Distribution Along the Fringes of the 2D Pair Correlation Function Shown in Figure 61b.

decreasing at input powers larger than 135mW (Figure 64). Table VI is constructed from the data presented in the density distribution functions and is made to demonstrate how the microspheres get localized within the wells.

Increasing the fringe period to 3.34um (crossing angle of 8.38 degrees) caused the particles to line up in the fringes as shown in Figure 65a. In this case the light forces push the particles in the high intensity regions, but due to the large period of the fringe pattern and the Coulombic interaction between the microspheres some particles are forced to the low intensity regions. This kind of arrangement leads to loss of correlation between adjacent rows at weak radiation field's strength. The diffraction pattern produced from such structures is shown in Figure 65b, where the diffraction from the fundamental density modes (those directly excited by the crossed beams) is observed inside the Debye-Sherrer ring. The diffraction from the enslaved modes are not as well defined as in the commensurate structure case. The distribution of the microspheres positions for this fringe period and at input power of 86mW is shown in Figure 66a along with the density along the fringes (Figure 66b).

The real space analysis of a multilayered region of the sample at this crossing angle is demonstrated through the pair correlation functions shown in Figures 67 through 70. As the power was increased to 86mW the equilibrium state was transformed completely to a monolayered amorphous phase as seen by the correlation functions shown in Figure 67. The crossing of the beams in this case introduced some orientational order as can be seen by the 2D function in Figure 69b. The orientational order in this case is mainly along the fringes, even

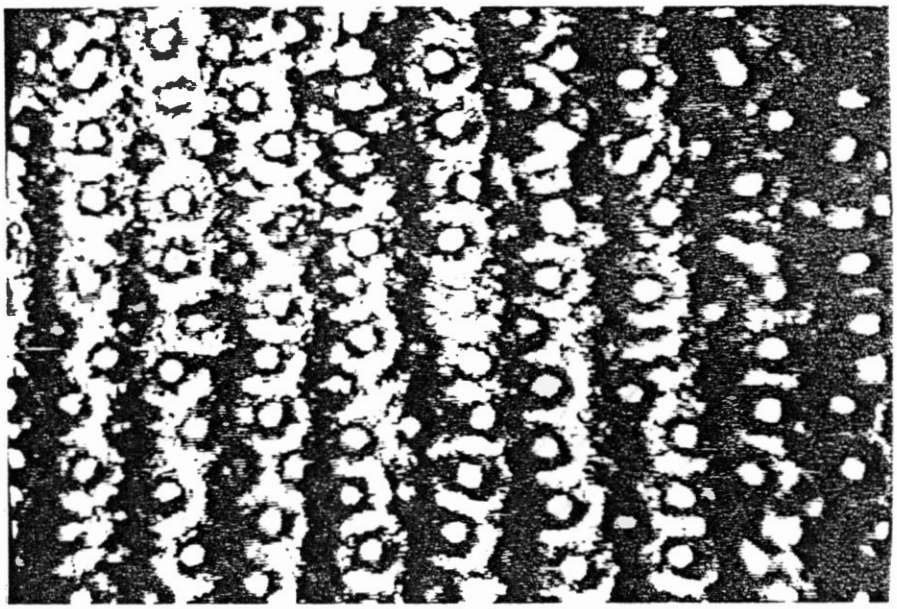

a) Particles Alinement Along the High Intensity Regions.

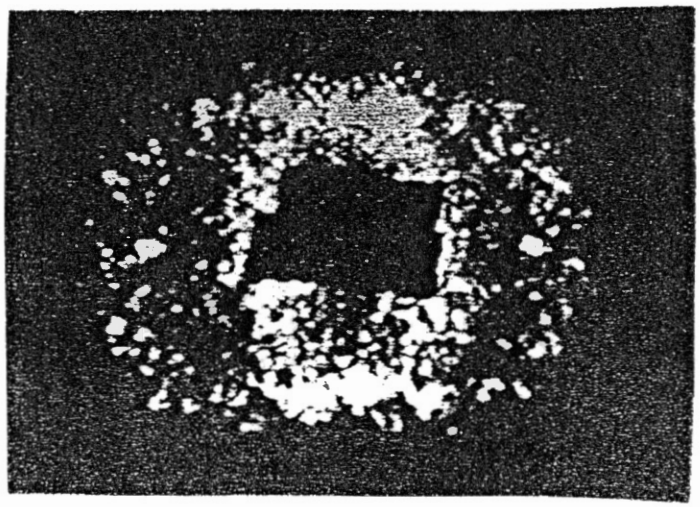

b) Self Scattering Pattern.

Figure 65. The Alinement of the Microspheres at Fringe Period of 3.34um (a) and the Produced Self Scattering Pattern at this Fringe Period and Laser Power of 111mW.

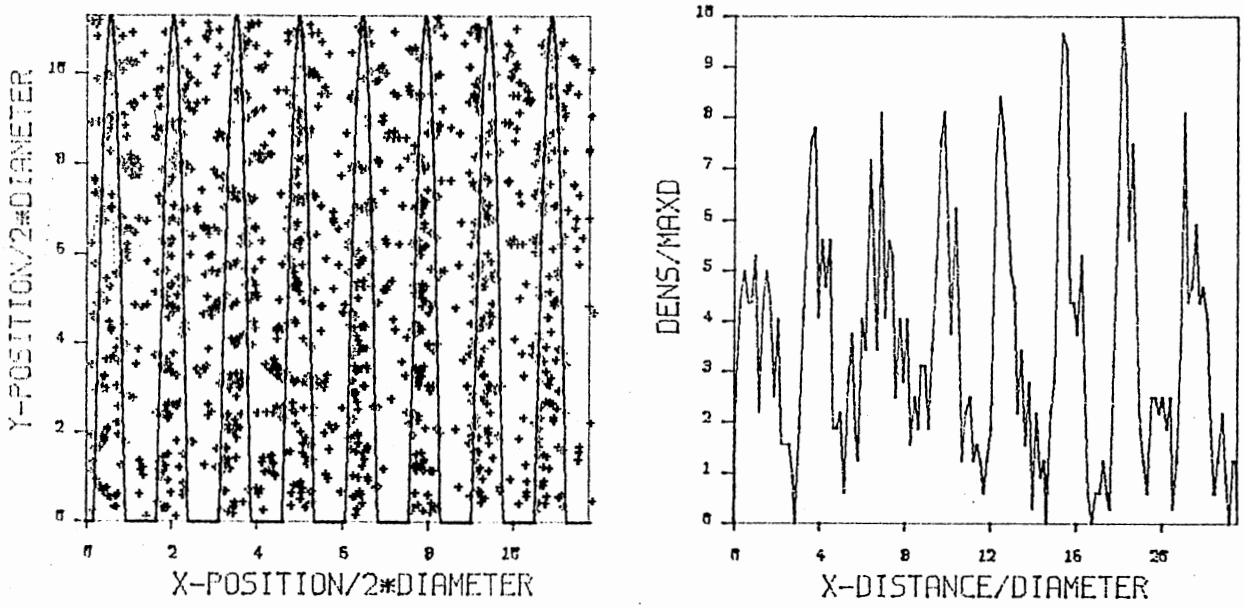

a) X-Y Position Files.

b) Density Distribution.

Figure 66. Position Files (a) and Denstiy Distribution for 20 Snap Shots of a Forced Monolayer at Fringe Period of 3.34um and Laser Power of 86mW. The Solid Curve in Part (a) Represents the Standing Sinusoidal Intensity Fringe Pattern.

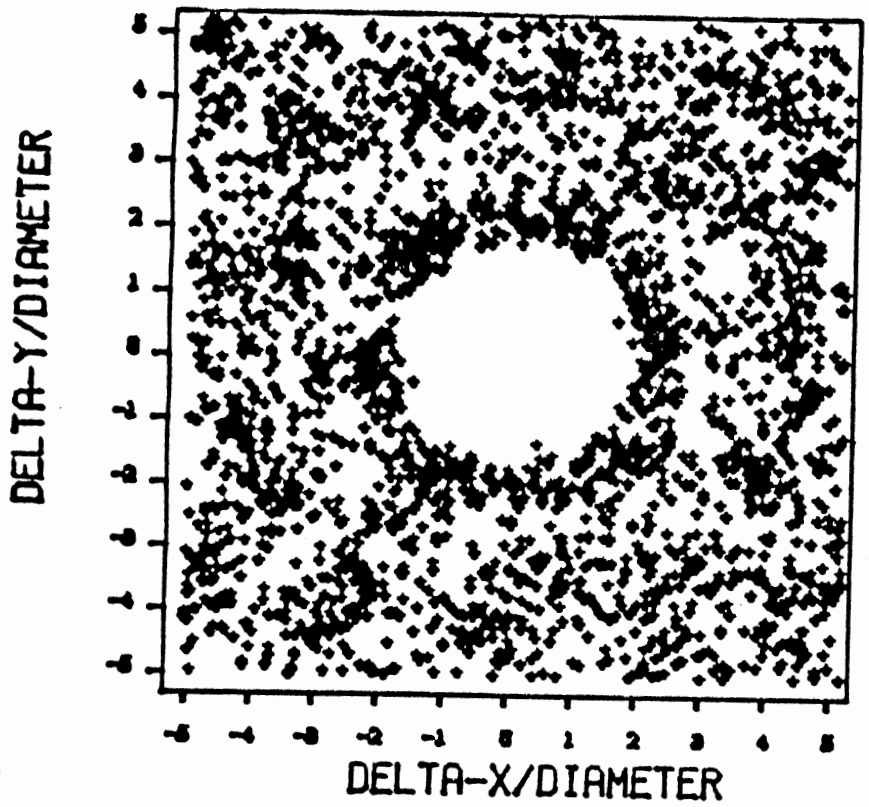

b) 2D Pair Correlation Function

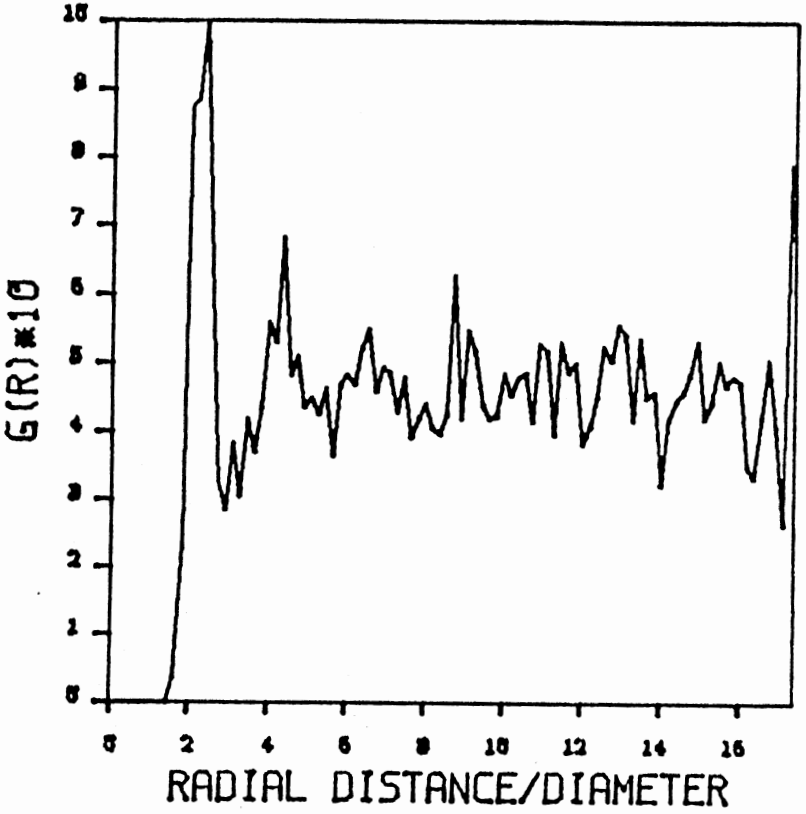

a) 1D Pair Correlation Function

Figure 67. Pair Correlation Functions for Forced Amorphous Monolayer Used for the Analysis at Fringe Period of 3.34um.

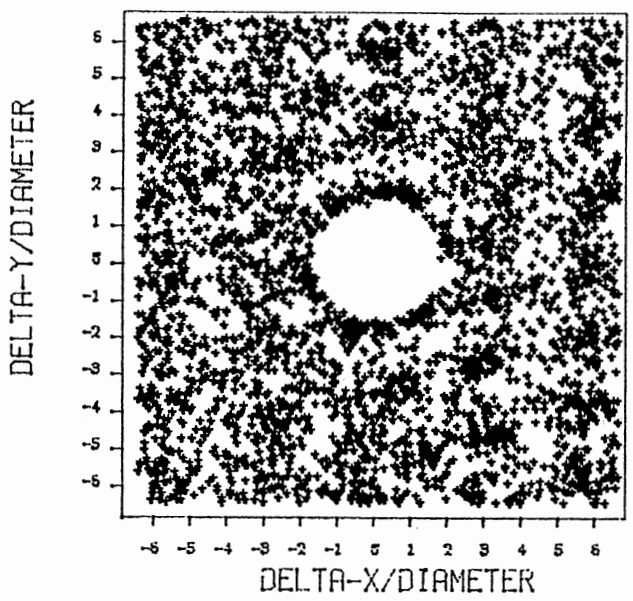

b) 2D Pair Correlation Function

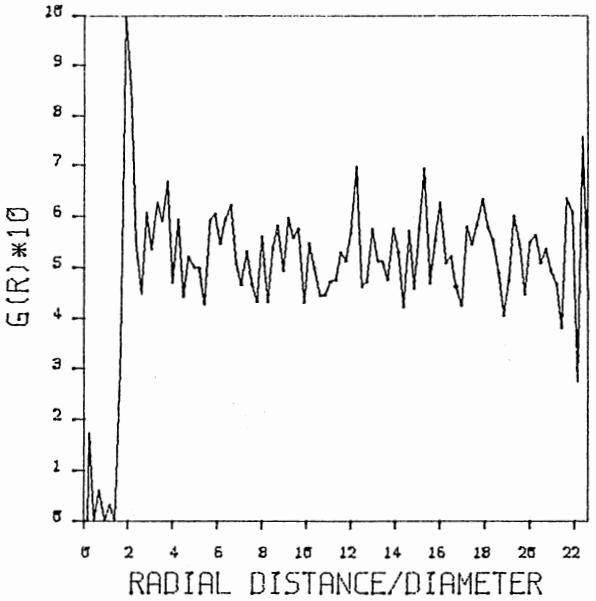

a) 1D Pair Correlation Function

Figure 68. Pair Correlation Functions [a) g(r) and b) g(r)] for a Forced Monolayer at Incommensurate Fringe Period of 3.34um and Laser Power of 86mW.

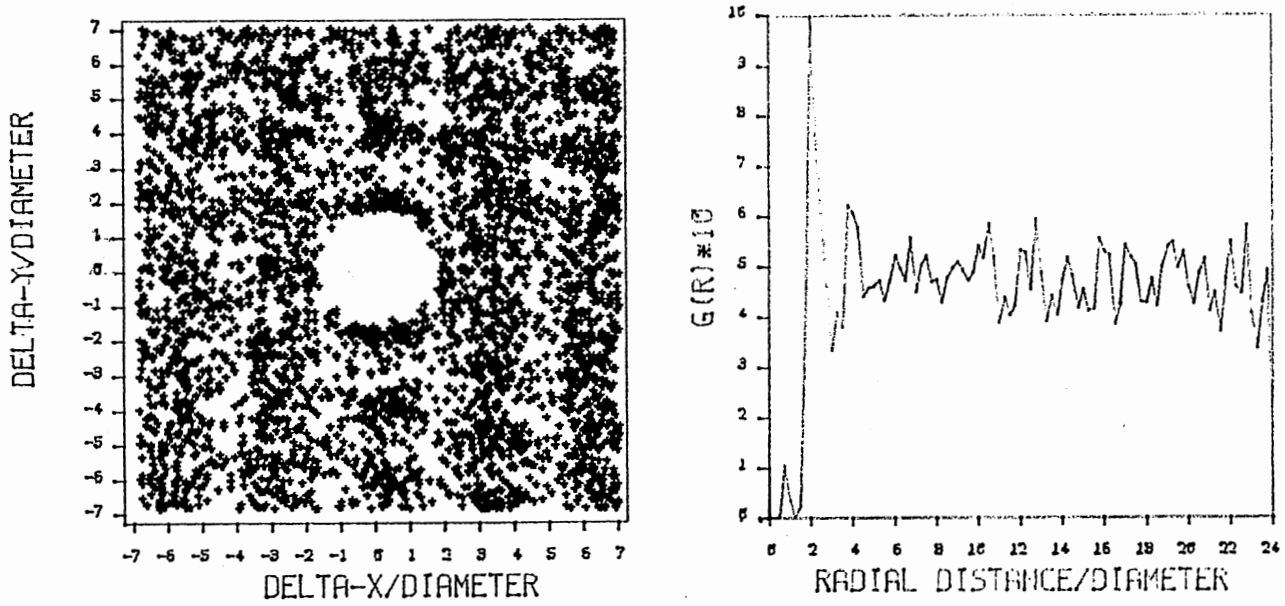

b) 2D Pair Correlation Function

a) 1D Pair Correlation Function

Figure 69. Pair Correlation Functions [a) g(r) and b) g(r)] for a Forced Monolayer at Incommensurate Fringe Period of 3.34um and Laser Power of 111mW.

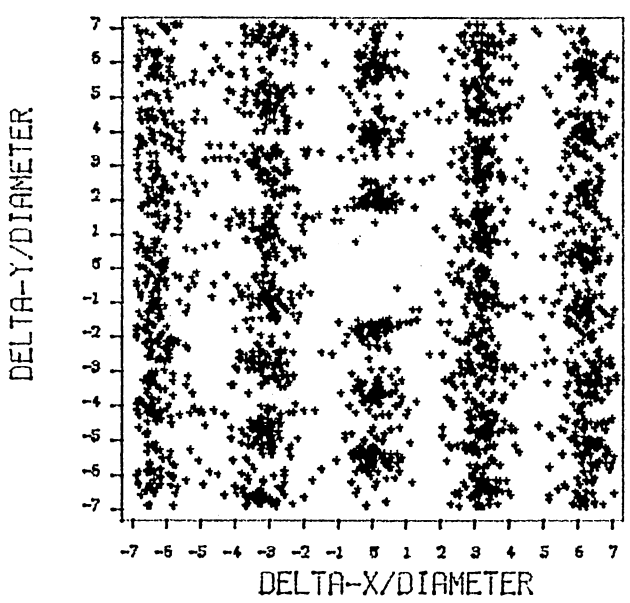

b) 2D Pair Correlation Function

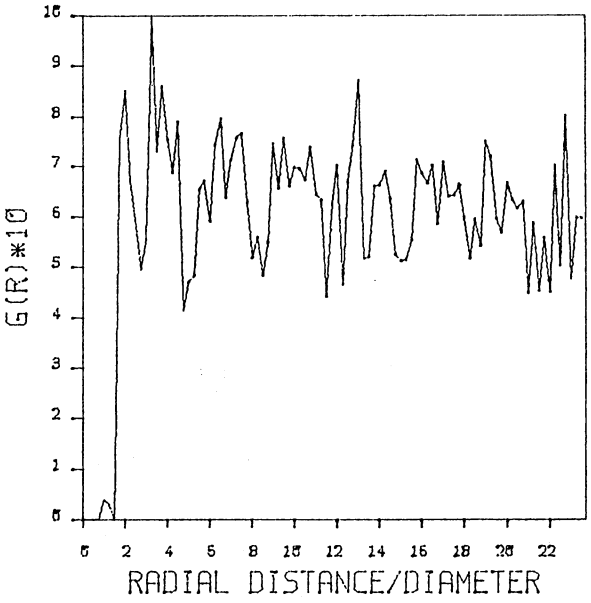

a) 1D Pair Correlation Function

Figure 70. Pair Correlation Functions [a) g(r) and b) g(r)] for a Forced Monolayer at Incommensurate Fringe Period of 3.34um and Laser Power of 182mW.

though it is not well defined due to the masking introduced by the 5% number of dumbbells present in this region. The crossed beam density at this input power increased by 10% from the equilibrium case (Table VII). The orientational order becomes more pronounced for the input powers higher than 86mW. At 111mW the 2D correlation function (Figure 69b) shows the existence of some interdependence between particles in adjacent wells. This correlation is made more pronounced for laser's power of 182mW demonstrated in Figures 70b. The density of the analyzed regions varied as a function of the radiation field exposure time and the laser's input power (Table VII). The density for at 65mW was .12 and then it changed to .143 at 182mW, a change of 40%. When one of the write beams, at any input power, was blocked it is observed that the density of the analyzed regions decreased by as much as 15% from the crossed beam situation.

The average density distribution of the 2D functions is shown in Figures 71 to 73. These Figures demonstrate that the induced order in the suspension is dependent on the lasers applied power. An analysis of the localization of the spheres along the fringes as a function of laser's input power is given in Table VI.

Scattered Intensity Study

The magnitude of the scattered intensity form the main density modes (modes directly excited by the crossing of the two laser beams) is studied as a function of input power in the static case. These modes correspond to the horizontal intensity maxima passing through the main beam positions shown in Figures 17 and 65. These are a product of particles' alignment in the high intensity regions of the

TABLE VII

ANALYSIS OF THE MULTILAYER REGIONS

		Commensurate d=1.85um				Incommensurate d=2.43um				d=3.34um			
P(mW)	a(um)	S	D	M	C	S	D	M	C	S	D	M	C
22	3.2					1.0	1.4	N	N				
42	2.9					1.2	1.5	N	N				
74	2.3	1.8	1.9	Y	N								
86	2.6	1.5	1.8	Y	N								
86	2.8					1.3	1.6	N	N				
86	2.9									1.2	1.3	Y	N
111	2.8					1.3	1.6	N	N				
111	1.9					1.2	1.4	N	N				
135	2.5	1.6	2.0	Y	N								
135	2.8					1.3	1.6	N	N				
135	2.8									1.3	1.23	Y	N
161	2.3	1.8	2.0	Y	Y								
161	2.7					1.4	1.6	Y	N				
161	2.8									1.3	1.4	Y	N
182	2.7					1.4	1.5	Y	Y				

S = Single Beam Illumination

D = Double Beam Illumination

M = Monolayer in the single beam illumination

C = String like behavior in the g(r) and density

d = Fringe period

a = average particle separation in the amorphous phase

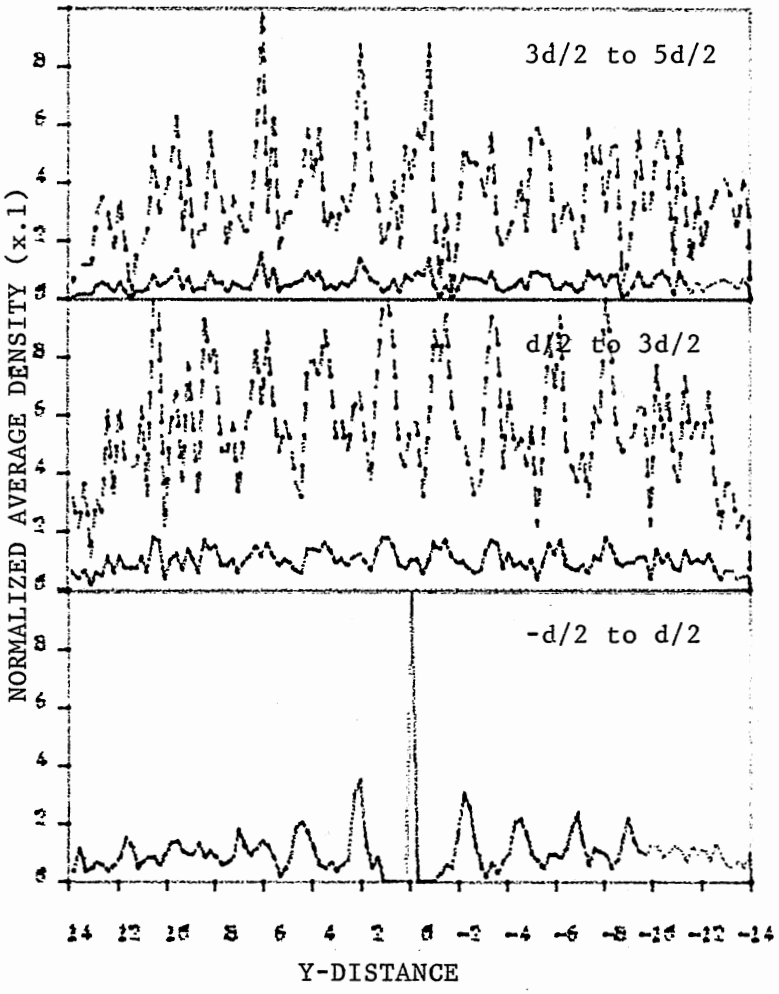

Figure 71. Normalized Average Density Distribution Along the Fringes of 2D Correlation Function Shown in Figure 68b.

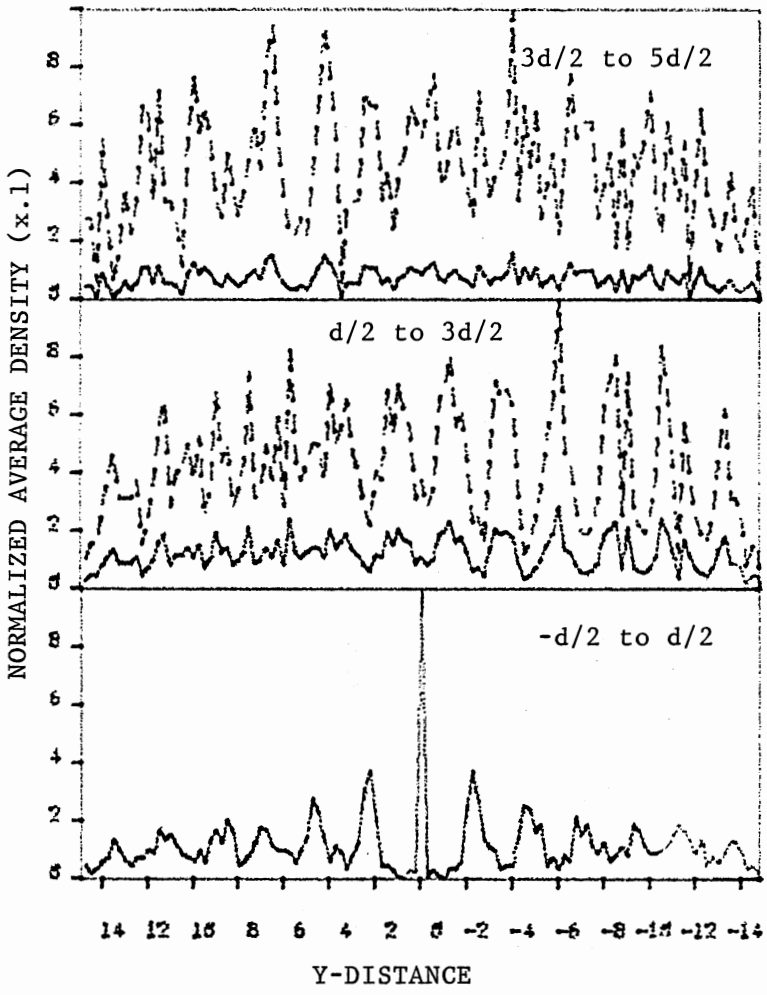

Figure 72. Normalized Average Density Distribution Along the Fringes of the 2D Pair Correlation Function Shown in Figure 69b.

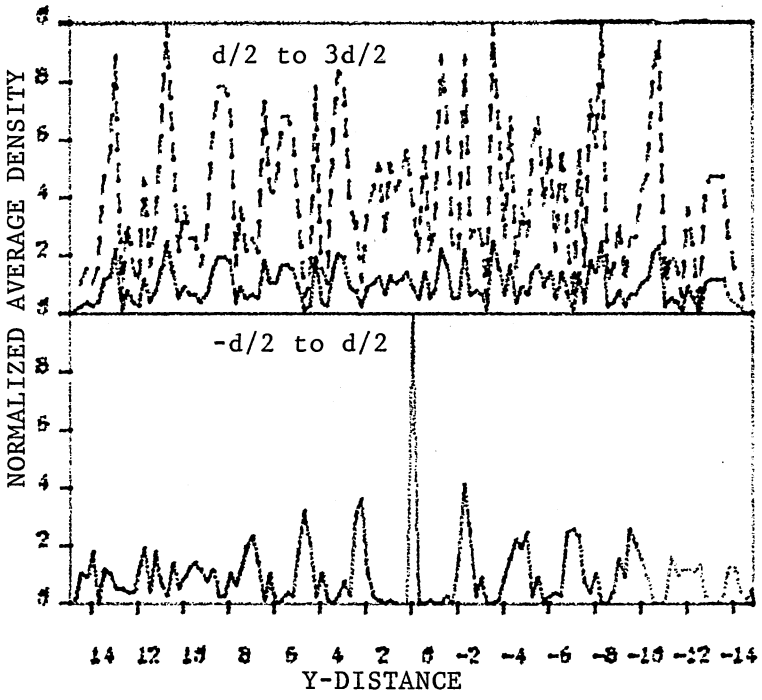

Figure 73. Normalized Average Density Distribution Along the Fringes of the 2D Correlation Function Shown in Figure 70b.

fringe pattern. The magnitude of these maxima is detected with a pin diode positioned on the diffracted intensities such that the area of this diode is totally covered by the light from these spots. The reason behind this is to reduce the effect of stray light and intensity fluctuations reaching the diode. The average intensity is found by using the same procedure described in reference (10). The pin diode's analog signal is fed to an A/D converter which digitizes the data and feeds it to the Apple IIe computer. The continuous reading and display of the data is done by using the weighted average

$$V_A = \sum_n W^n V(n) / \sum_n W^n \qquad (4\text{-}3)$$

$$= \sum_n W^n (1-W) v(n) \qquad (4\text{-}4)$$

V(n) = the nth data sample measured relative to the present time interval

V(0) = current data measurement

V(1) = Data measurement before V(0)

V(n) = Data measurement taken before V(n-1)

The weight factor W_n controls which data reading has the largest contribution in the averaging process. When this factor is unity equation (4-3) takes the form of the standard average. For this study W_n is chosen to be .95 in order to weight the most recent reading the most. The fluctuations in the signal are given by the equation

$$S=\{(1-W)[\sum_n W^n (D(n))^2 - (\sum_n W^n (D(n))^2 (1-W)]\} \qquad (4\text{-}6)$$

This running averaging gave minimized fluctuations and revealed any systematic drift in the signal. The intensity readings are displayed on a monitor and printed out after each 10 data points.

Plots of input powers versus the intensity of the first order maxima are displayed in Figures 74. These results are obtained by

probing the gratings with a He-Ne laser and subtracting the background obtained by blocking the main argon ion laser. The slopes of the least square linear fit line through the data points were found to 1.58 for the monolayer commensurate case (d=1.85um), and 1.59 for the multilayer noncommensurate case (d=3.34um). Thus it seems that there is a 1.585 power dependence between the lasers input power and the scattered intensity from the fundamental density modes. This result is in contradiction with Chowdhury's cubic power dependence (10), although when similar measurements were carried on noninteracting particles gave the same results as obtained by Chowdhury (10) meaning that our method was the same. When the error bars in the data were included the maximum slope obtained was 2.1.

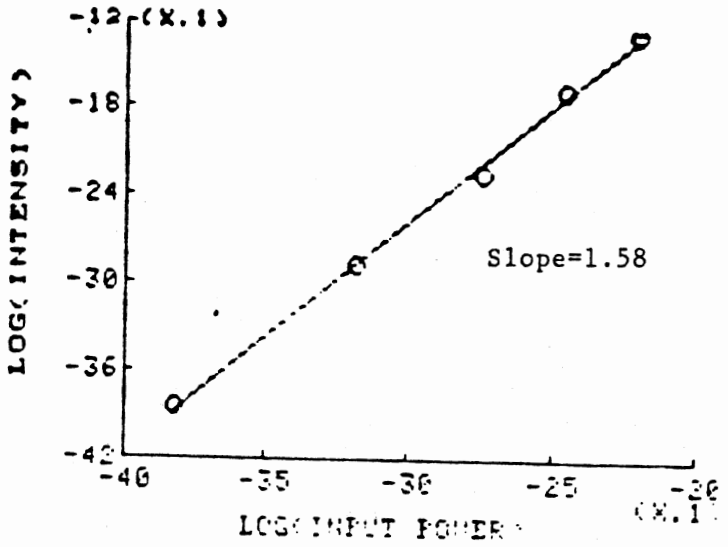

a) Fringe Period of 1.85um

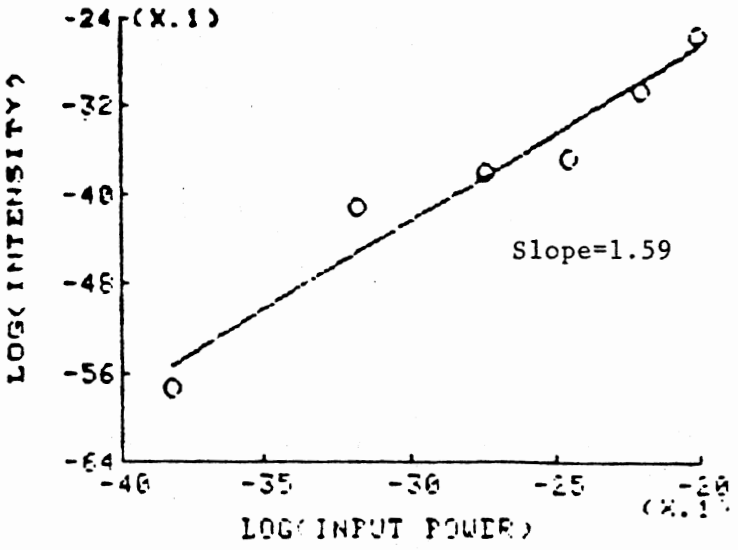

b) Fringe Period of 3.34um

Figure 74. Growth of the Main Density Mode for Interacting Multilayer (b) and Monolayer (a) as a Function of the Laser's Input Power.

CHAPTER V

MONTE CARLO SIMULATIONS

Introduction

Computer simulation "experiments" provide the opportunity for examining and following events at the level of individual particles, thus they have been used as a tool in characterizing the melting transition for a variety of model systems(21). Of these simulations the Monte Carlo (MC) and molecular dynamics (MD) describe accurately the liquid and solid phases and can be used to simulate multiple phase coexistence. The molecular dynamics method probes the microcanonical ensemble and furnishes dynamical information (21). The standard MD method uses a system of N particles in a cell, held at constant volume. The particles' positions and velocities are identified by a set of coordinate $\{X_i\}$ and $\{V_i\}$, which are found from Newton's equations of motion.

Alternatively, the Monte Carlo method provides thermodynamic averages computed in the canonical ensemble(21). The conventional constant NVT MC method was selected for this study, for its simplicity and its convenience in the computation of the spacial correlation functions. The aim behind this is to provide a model for the two-dimensional colloidal systems discussed in the previous chapter. This simulation serves as a means to test the effect of an externally applied sinusoidal field on the local order of 2D systems.

Model Potential and Parameters

The suspension of polystyrene spheres in water, causes the ionizable groups to dissociate and the microspheres surfaces to become uniformly charged with total charge Ze (24). This results in repulsion forces between the spheres which completely dominate the attractive Van der Waals force over the relevant range of particle separation (8). The repulsive interactions between particles in colloidal suspensions leads to a solid-liquid phase transition depending on the strength of interaction or density of the sample. As a result monodisperse suspensions of latex particles are perfect candidates for such studies.

To control the range and strength of the repulsive interaction many of the experimental parameter could be varied. For example, the charge Z on the spheres increases with surface area and varies with surface properties, thus one could use spheres of different diameters (29). There is also the possibility of varying the surface charge by using solvents with different dielectric constant (28). Experimentally, the above mentioned parameters are difficult to vary continuously over wide ranges. Changing the particle density and the excess ion concentration is the most convenient controllable experimental parameters. The salt concentration is measured in terms of the number of moles per liter of molecular acid HCl or salt added to the solution, e.g. n_{HCl}. This parameter will be used to control the interaction between paraticles.

To theoretically describe this model, the dynamics of only the polystyrene spheres is considered. The existence of many (at least Z) counterions per macroion and their rapid movement allows for the

replacement of their discreteness by a continuous density. This charge density of counterions ,d_c, obeys Boltzman's equation,

$$d_c(r) = q[e]n_q\exp(-Bq[e]V) \tag{5-1}$$

where q= 1, V is the total electrostatic potential, $B=1/k_BT$, 'e' is, the electronic charge and n_q is a normalization that fixes the overall ion density. Combining the above equation with Poisson's equation for a Coulomb potential, namely,

$$\text{div}[E(r)] = 4\pi/c\ [d_m + d_c] \tag{5-2}$$

$$E(r) = -\text{grad}[V(r)] \tag{5-3}$$

gives the Poisson-Boltzman's equation

$$V(r) = 4\pi/c\ \{d_m(r) + \sum_q q[e]n_q\exp(-bq[e]V)\} \tag{5-4}$$

where E(r) is the electric field at point 'r', 'c' is the solvent dielectric constant; d_m is the charge density on the polystyrene sphere.

This highly non-linear Boltzman-Poisson (BP) equation can be approximated by its linearized form, the Debye-Huckel (DH) equation when the electrostatic potential differences are much smaller than the thermal energy ($k_BTe>>0$). The solution of the resulting DH approximation for the potential on each sphere of radius R is the Yukawa potential or screened Coulomb interaction (24),

$$V(r) = z[e]e^{2kR}(1+kR)^{-2}e^{-kr}/cr \tag{5-5}$$

$$k^2 = 4\pi e^2/ck_BT\sum_q n_qq^2 \tag{5-6}$$

where n_q's are the mean densities of each species, K is the inverse Debye screening length associated with the small ions. The Bjerrum length (λ), which is the characteristic distance over which the Coulomb interaction for singly charged ions is comparable to the thermal energy is defined as:

$$\lambda = e^2/ck_BT \sim 7A \qquad (5\text{-}7)$$

In the case of a single point charge the DH solution is,

$$V(r) = z[e]\ e^{-kr}/r \qquad (5\text{-}8)$$

A comparison between equations (5-5) and (5-8) shows that the finite size of the spheres has the effect of increasing the prefactor of the interaction potential U_0 by $\exp(2kR)/(1+kR)^2$.

This potential has a shape that is continuously varying with the screening length (k). For small 'k' (k-->0) this potential is of the long range form (Coulomb potential). However, for large 'k' the short range effects dominate leading to a nearly hard sphere form. The change in k depends on the salt concentration, adding salt increases the screening rate and allows controlling the interparticle strength.

Wigner Seitz Unit Cell and Effective Charge

The DH treatment of PB equation is valid only for small potential gradients, in the more general case it has been shown that the interaction can still be described by the Yukawa potential with a normalized charged Z^* and salt concentration N^* (17).

Following the procedures outlined by Chaikin et al. (7, 17), the colloidal crystal is considered as a collection of cells surrounding each macroion. These cells are constructed by taking the smallest volume enclosed by planes which are the perpendicular bisectors to the nearest neighboring polystyrene spheres, or what is known as the Weigner Seitz cells (WS) (17). Figure 75 shows a polyhedron WS cell for such system. Such a unit cell contains all the information needed to calculate the effective charge on the spheres. Approximating the WS cell with a sphere of equal volume makes the calculations for the

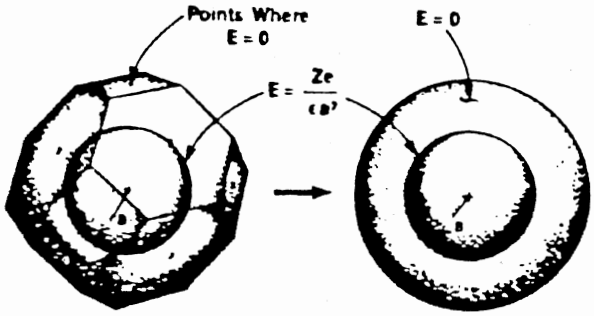

Source: S. Alexander, "Charge Renormalization, Osmotic Pressure, and Bulk Modulus Of Colloidal Crystals: Theory," Journal of Chemical Physics (1984).

Figure 75: Wigner Seitz Unit Cell For a BCC Crystal and the Spherical Wigner Seitz Cell Used In Charge Renormalization Calculations.

needed parameters easier with no loss of generality. The net charge inside this WS cell (charged sphere plus surrounding counter ions) is zero leading to a null surface electric field. Integrating the electric field from the cells surface inward the potential was found to be smaller than the thermal energy for some small distance (17). Thus DH is valid in for this region. Near the particles, the potential energy becomes dominant and the charge density varies far more rapidly than in the linearized approximation. However, since the counter ions are bound by more than k_BT, they may be considered as part of an effective sphere whith a reduced charge. This is analogous to replacing the nucleus and tightly bound core electrons of an atom by a single effective ionic charge. Through the above argument, Chaikin et al (17) justified the use of the Yukawa potential given in equation (5-8) with Z replaced by Z^* and with the screening length k^{*-1} given by the corresponding counterion concentration,

$$k^{*-2} = 4\pi Z^* e^2 d/ck_BT \qquad (5\text{-}9)$$

Note that in the above equation only zero salt concentration case is considered.

Using the general form for the potential that solves the DH in spherical coordinates,

$$V(r) = [Ae^{-kr} + Be^{kr}]/r + D \qquad (5\text{-}10)$$

the constants A,B and D are found by using the boundary condition of zero potential (equation 5-10) and electric field (equation (5-3), at the cell's surface and the PB density equal to the density found from equation (5-2) at the particle surface. The exact solution to the PB equation is calculated numerically by an iterative process where a charge density is chosen at the WS surface, this determines the total

charge inside a sphere an incremental radius smaller. Knowing the total charge Q(r) up to point r, the electric field the potential and the charge density are than calculated at the smaller radius (4). This iterative process is repeated until the solution converges.

In our experiments polystyrene spheres of 1.07um diameter size are used, these particles have a charge packing area of $239A^2$ per charge group or $4.184x10^{-3}$ charge groups/A^2. Multiplying this surface density by the sphere's surface area it is found that the actual charge groups per sphere is $1.5x10^6$. Using this data in the DH and BP algorithms Figures 76 and 77 were constructed. Figure 76 shows the effective charge z^* versus the actual charge Z for a macroion of radius a=764 in a WS cell of radius R=2500 (corresponding to our concentration) for a zero salt concentration. At low charge Z and Z^* are nearly equal. However, for an actual charge of $1.5x10^6$e, the effective charge shows saturation toward a value of 7800e. Using this effective charge value, the charge distribution of the DH solution is plotted and compared to the exact PB distribution (Figure 77). In this figure it is observed that the nonlinear terms in the PB equation bring considerably more protons in toward the charged sphere than would be expected form the DH treatment, this reduces the potential so that DH is appropriate far from the charged sphere, but with a reduced or renormalized effective charge. As a result of this analysis it is found that at zero salt concentration the effective charge is 7800e for the 1.07um diameter polystyrene spheres. The effect of added electrolytes was found to cause an increase in Z^* (17), but the change is small when s/Z^* is small, and is less than 10% for $s/Z^*=5$ (s is the total salt concentration).

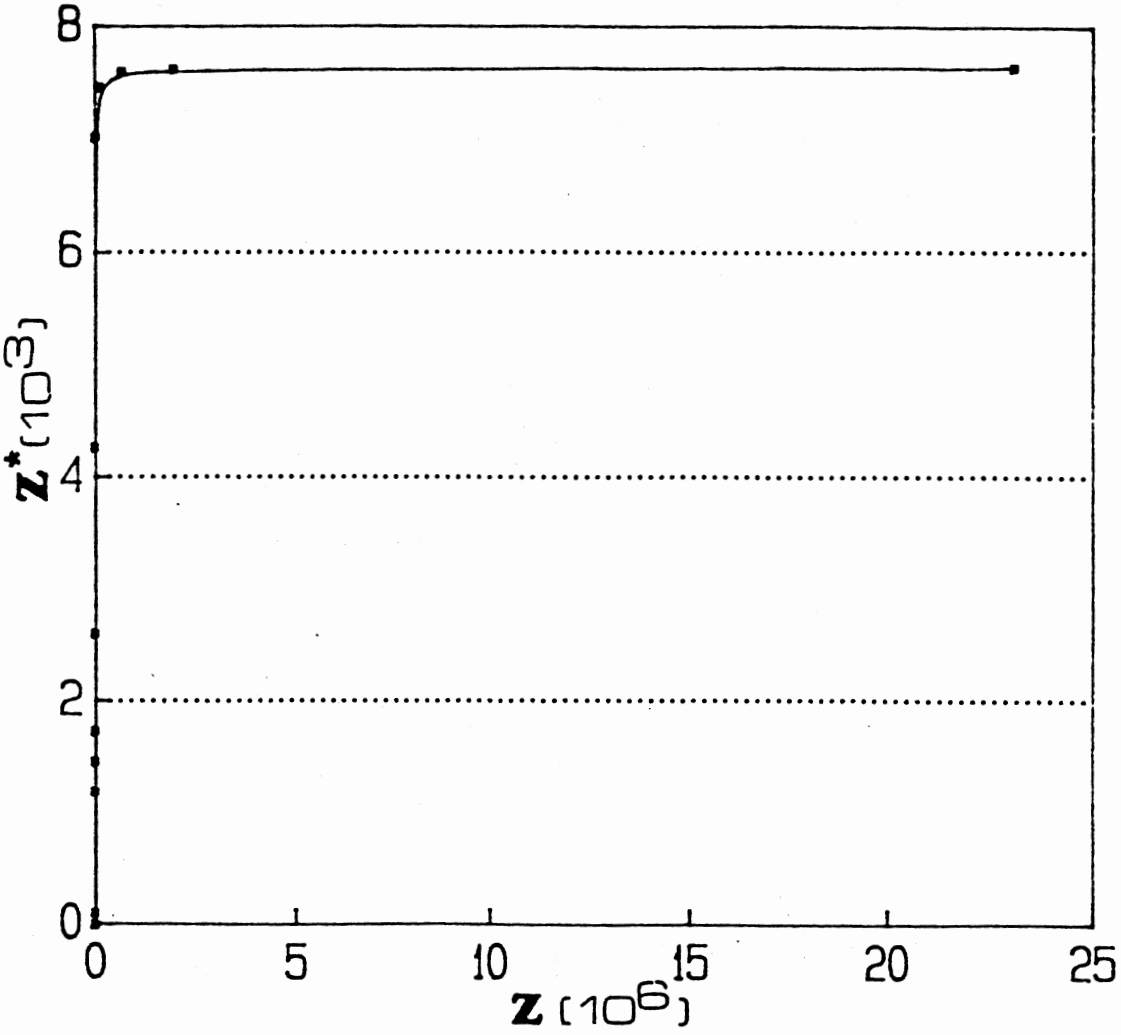

Figure 76. Effective Charge Vesus Actual Charge for the case of Zero Salt Concentration.

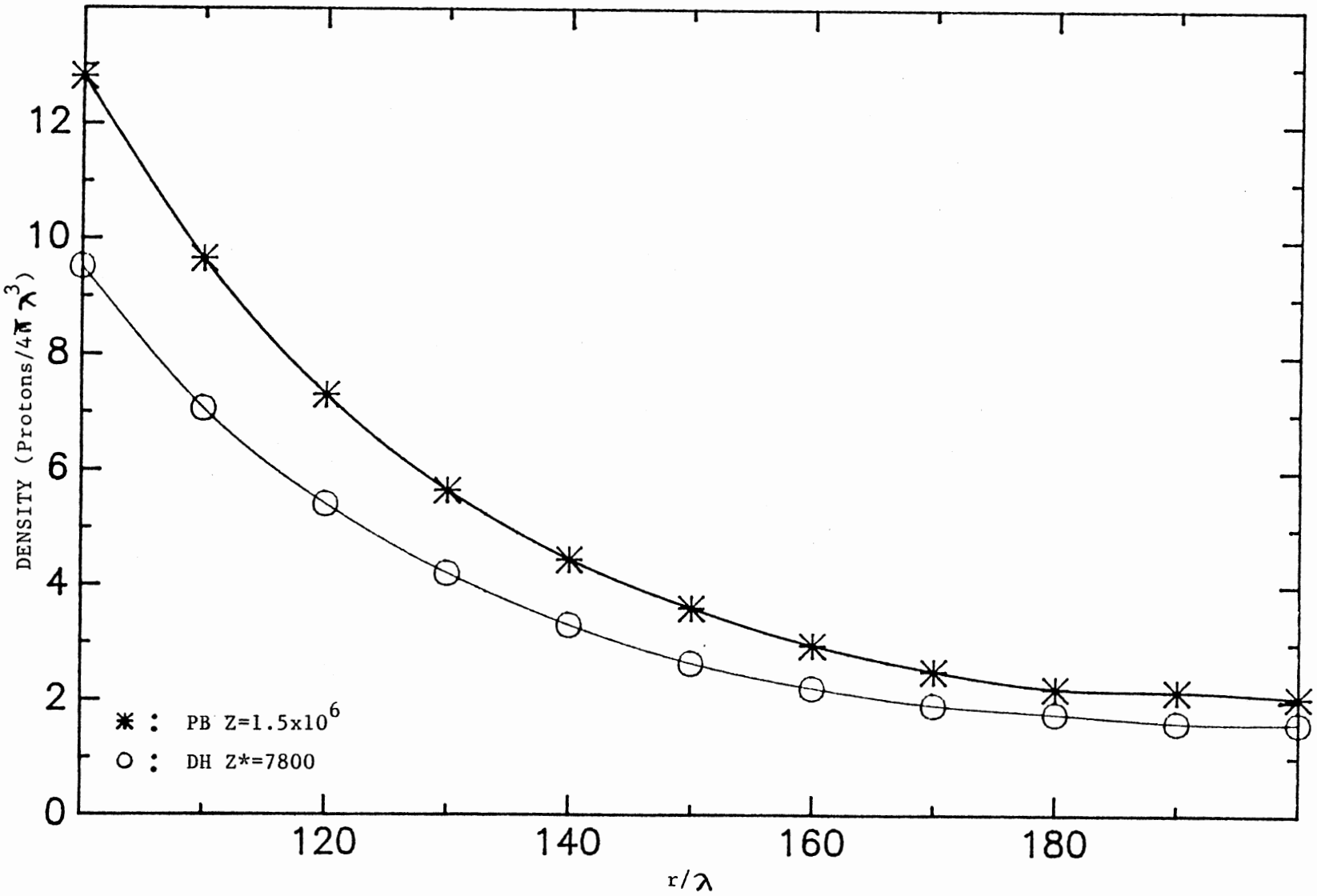

Figure 77. BP and DH Solutions for teh Charge Distribution in a Sphere.

Monte Carlo Algorithm

The standard Meropolis Monte Carlo method was used for this study. In this method a single particle is displaced at random, thus producing a new configuration, C, from the old configuration, C. The configuration change causes the energy of the system to change by $E_{C'}-E_C$, where E_C is the energy associated with configuration C and for particles interacting via the pairwise Yukawa potential this energy is given by:

$$\begin{aligned} E_C &= B \quad \exp(-kr_{ij})/r_{ij} \quad , r_{ij}<r_c \\ &= 0 \qquad\qquad\qquad\quad , r_{ij}>r_c \\ &= \infty \qquad\qquad\qquad\quad , r_{ij}<a \end{aligned} \tag{5-11}$$

$$B = ze^2/ca \tag{5-12}$$

r_c is a critical radius beyond which the pairwise energy has negligible effect on the total configuration energy. In this analysis a is the particle radius and r_c=7a. The energy difference, $E_{C'}-E_C$, governs the relative probability of configurations through the Boltzman distribution. This probability is built into the MC trajectory by a criterion for accepting and rejecting moves to new configurations (44). In particular, if $E_{C'}-E_C$ is negative or zero, the move is accepted. However, if this energy change is positive, a random number x between 0 and 1 is generated; and the move is accepted only if $x<\exp(-B(E_{C'}-E_C))$, $B=1/K_BT$, otherwise the move to a new configuration in the next step is rejected. That is if:

$$C(t)=C \tag{5-13}$$

then we will have,

$$C(t+1) = C' \quad \text{when} \quad E_{C'}-E_C<0 \tag{5-14}$$

and when $E_{C'}-E_C$ is greater than zero, we get

$$C(t+1) = C' \quad , \quad \exp(-B(E_{C'}-E_C))>X,$$
$$= C \quad , \quad \exp((-BE_{C'}-E_C))<X \qquad (5\text{-}15)$$

This procedure is repeated at least four million times moving particles at random, from 0 to a diameter's distance, for our systems to ensure equilibrium.

The systems used in MC analyses consisted of 100 particles constrained to two-dimensions in a rectangular boxs of fixed area (20.44a by 23.67a and 20aX20a). The advantage of using this small number of particles is in the computation time required for reaching the equilibrium state and other calculations. The MC density used in both boxes given above was chosen to be within the range of experimental densities discussed in the previous chapter, and similarly the number of particles used in the simulation is comparable to the average number of particles used in the experimental analysis. The difference between this simulation and the experiments is that the latter represents a grand canonical ensemble while the MC simulation represents a canonical ensemble. The disadvantage in the small number of particles used in the simulation is that the transition is not sharp due to the boundary problems, but this is the reason behind the use of two box dimensions. The different box sizes were observed to cause a distortion in the final structures.

The MC uses periodic boundary conditions, where a particle that is randomly moved outside the given box area is wrapped back to the other corner of the box. The effective charge used in the potential amplitude (equation (5-12)) calculation is taken as 8000e, as found from the Alexander (17) saturation analyis discussed in the previous section. The MC algorithm is shown in Appendix A.

Phase Transition Study

The aim behind this study is to find the phases that are similar to the equilibrium phases observed in Chapter IV for the interacting colloidal suspensions to serve as an overall check of our understanding.

The crystal-liquid phase transition is observed by changing the unitless inverse screening length, k*a, which is dependent on the number of ions present in the solution as described by equation (5-6). The values of k^*a used ranged from 10 to 1 for the 22aX22a box and 4 to 7 for the 20.44a by 23.67a box. Table VIII, shows the values of some of the parameters used in the simulation, such as the salt concentrations and the amplitudes corresponding to the given intensities.

In all the runs the equilibrium was monitored by observing the rejection rate, the specific heat, the 1-D and 2-D pair correlation functions to detect any phase transitions. It was observed that the disordered phases (liquid) reached equilibrium after 40000 MC steps. The ordered phases (crystalline) were in equilibrium at much lower MC steps ranging from 10000 to 30000.

To estimate the local order, the center particle in the box, labeled by O, was chosen as the coordinate origin. The number of particles surrounding O was counted within a pre-determined annulus of .1a width. That is to say the number of particles, n, within a ring (.1a thick) was found. The whole procedure is repeated for other annulae for 2000 MC steps, and for the results being averaged.

The translational (or 1-D) pair correlation function, g(r), is then given by:

TABLE VIII

PARAMETERS USED IN THE MC SIMULATION

Crossed Beams Intensity (mW)	Potential Amplitude Without Correction	Corrected Amplitude With d=1.85um	d=2.2um	d=3.3um
17	4.6	3.2	3.6	4.0
31	8.3	5.9	6.5	7.5
47	13.0	8.9	10.0	11.0
66	18.0	12.0	14.0	16.0
82	22.0	16.0	17.0	20.0
105	28.0	20.0	22.0	25.0
122	33.0	23.0	26.0	28.0

k^*a	n^* ($10^8/m^3$)
1	1.00
2	4.00
3	8.99
4	16.0
5	25.0
6	36.0
7	48.9
8	63.9
9	80.9
10	100.

k^* = inverse screening length (m)

a = particle's diameter

n^* = salt concentration

d = fringe period

$$g(r) = d(r)/d_0 = \langle n \rangle / [\pi d_0 (r_j^2 - r_i^2))] \qquad (5\text{-}16)$$

where <> represents the total averaging over 2000mc steps.

The orientational (or 2-D) pair correlation function is found by taking the center particle and its nearest neighbors, than using these as reference particles for constructing particle correlation function as described in Chapter IV. That is the distribution of particles that are at distance $\underline{r}$ from the reference particle as shown in Figure 83.

For both the 20aX20a and 20.44aX23.67a boxes, the high salt concentration values ($k^*a>4.5$) led to liquid structures as demonstrated by the particle positions, and the 1-D and 2-D pair correlation functions (Figures 78 to 80). In Figure 78 the (x,y) coordinates of the 100 particles are plotted for $k^*a=5$ and 7. These are distributed over the given area in a random way. It is clearly apparent that this system has no orientational nor translational order. The translational pair correlation functions (Figure 79), g(r), shows a maximum at r=2a and fluctuates around one at large r values indicating that at high r values the local density d(r) approachs the bulk density of the liquid. The 2-D correlation functions (Figure 80) demonstrate that the probability of locating a particle is largest at 2a, is independent of the direction of r and decreases to the average particle density at large $\underline{r}$ values.

As the salt concentration decreased ($k^*a=4$ and 3), the particles became localized around lattice points leading to crystalline phases (Figures 81 to 83). The observed crystalline structures for the 22a by 22a box had a distorted HCP lattice structure (Figures 83a and b), this is due to the effect of the box boundaries on the final order of

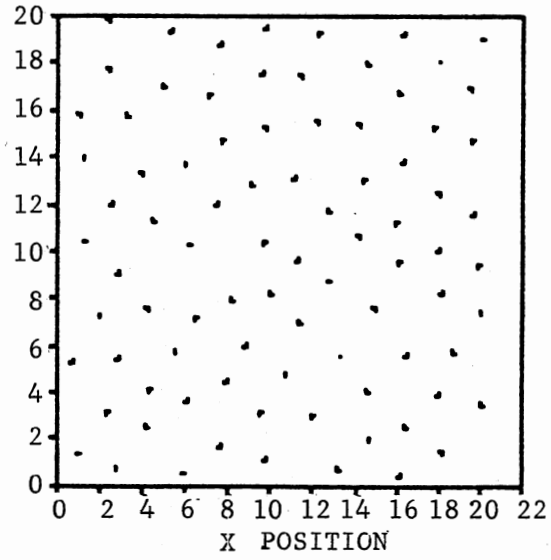

a) 22aX22a Box and k*a=5.

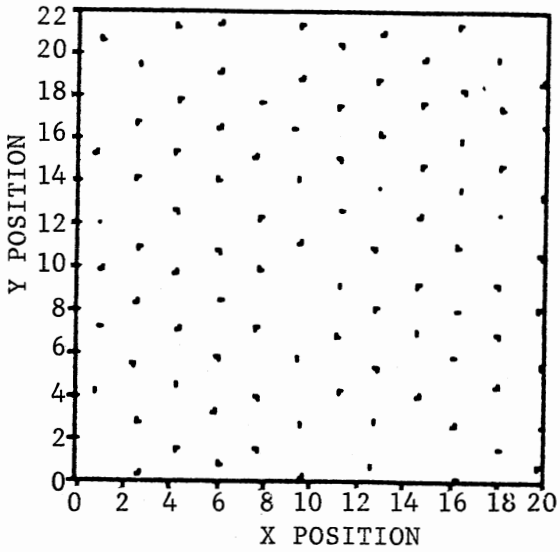

b) 20.44aX23.67a Box, k*a=5.

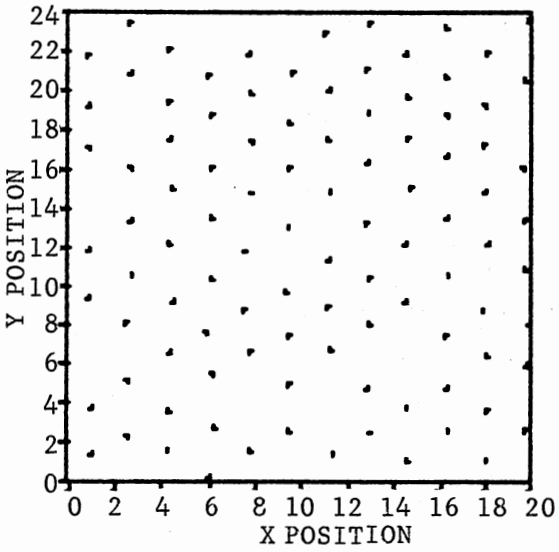

c) 22aX22a Box, k*a=7.

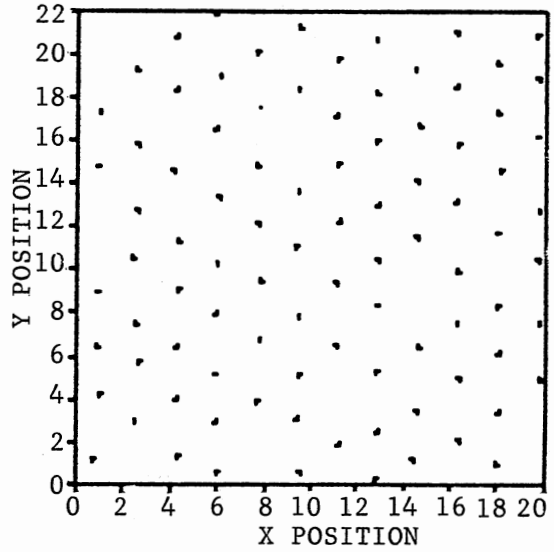

d) 20.44aX23.67a Box, k*a=7.

Figure 78. Position Files for the MC Simulation of 100 Interacting Particles in a 22aX22a and 20.44aX23.67a Box with the Potential's Inverse Screening Length k*a=5 (a and b) and 7 (c and d).

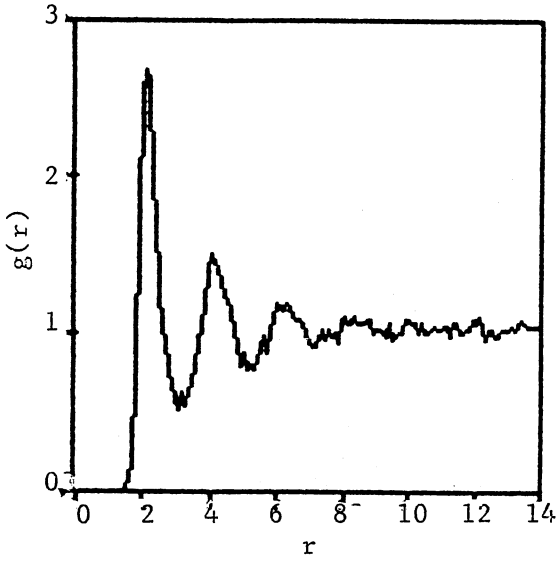

a) 22aX22a Box, k*a=5.

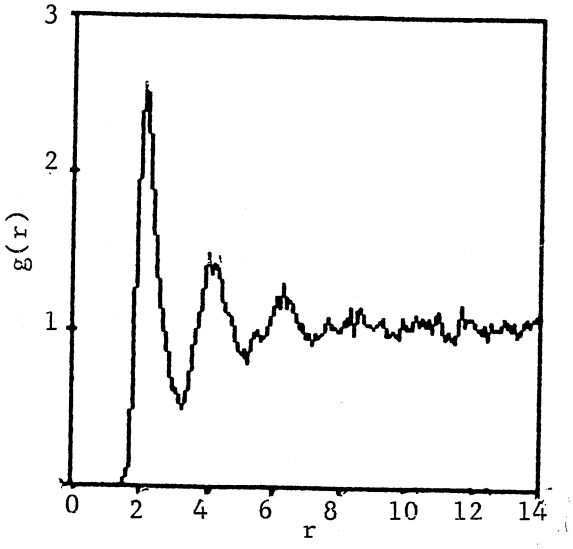

b) 20.44aX23.67a Box, k*a=5

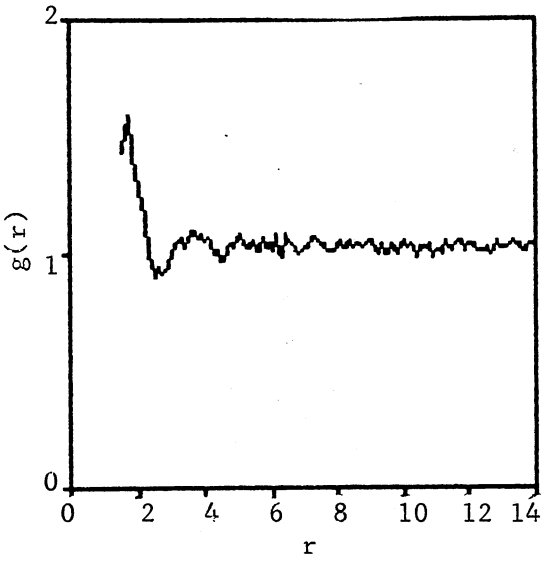

c) 22aX22a Box, k*a=7.

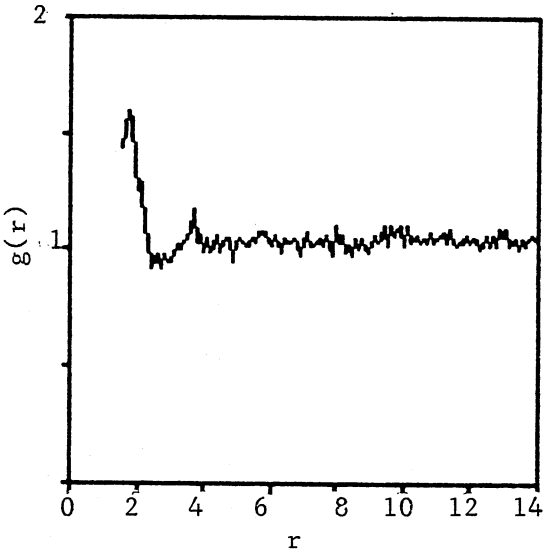

d) 20.44aX23.67a Box, k*a=7.

Figure 79. 1D Pair Correlation Functions (g(r)) for the MC Simulation of 100 Interacting Particles in a 22aX22a and 20.44aX23.67a Box with Inverse Screening Length k*a=5 and 7.

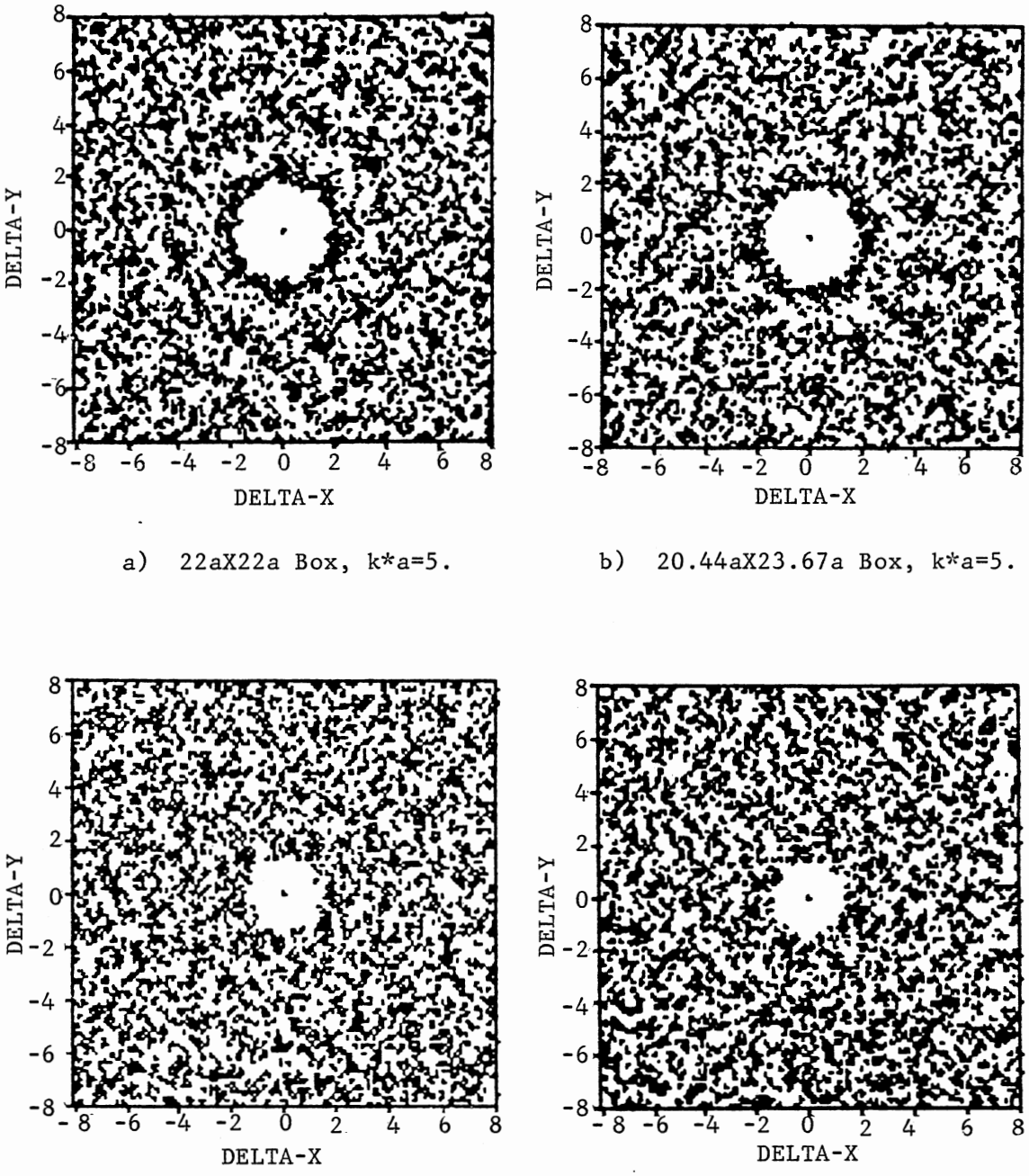

a) 22aX22a Box, k*a=5.

b) 20.44aX23.67a Box, k*a=5.

c) 22aX22a Box, k*a=7.

d) 20.44aX23.67a Box, k*a=7.

Figure 80. 2D Pair Correlation Functions (g(r)) for MC Simulation of 100 Interacting Particles in 22aX22a and 23.67aX20.44a Box with the Inverse Screening Length k*a=5 (a and b) and k*a=7 (c and d).

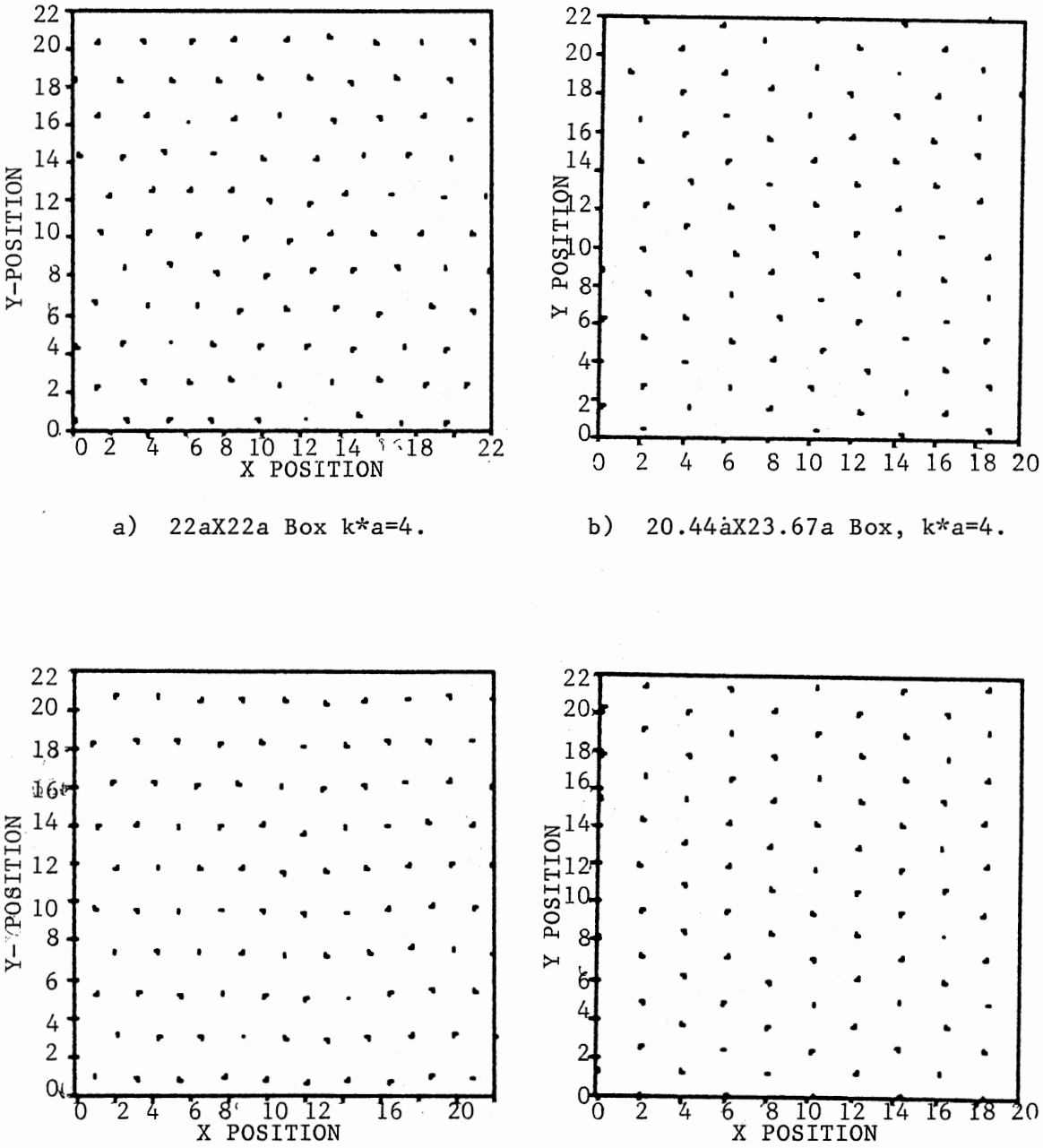

a) 22aX22a Box k*a=4.

b) 20.44aX23.67a Box, k*a=4.

c) 22aX22a Box, k*a=3.

d) 20.44aX23.67a Box, k*a=3.

Figure 81. Position Files for the MC Simulation of 100 Interacting Particles in a 22aX22a and 20.44aX23.67a Box with the Potential's Inverse Screening Length k*a=4 (a and b) and 3 (c and d).

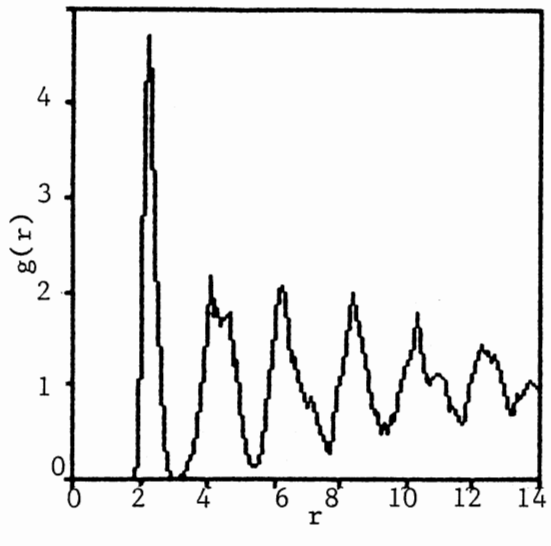

a) 22aX22a Box, k*a=4.

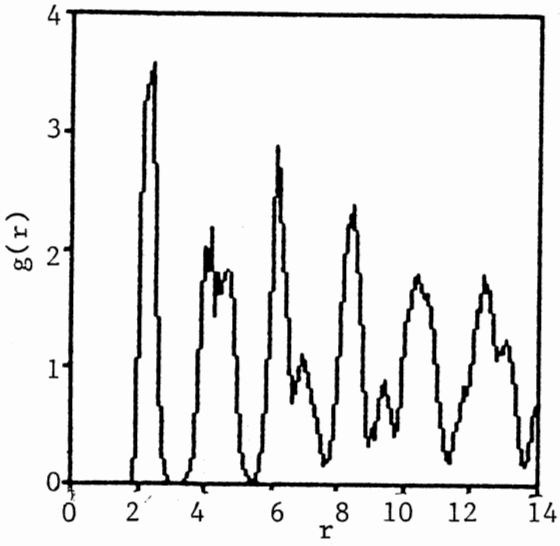

b) 20.44aX23.67a Box, k*a=4.

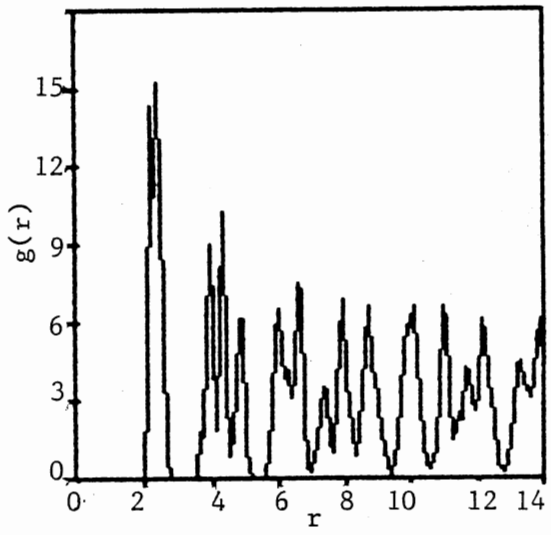

c) 22aX22a Box, k*a=3.

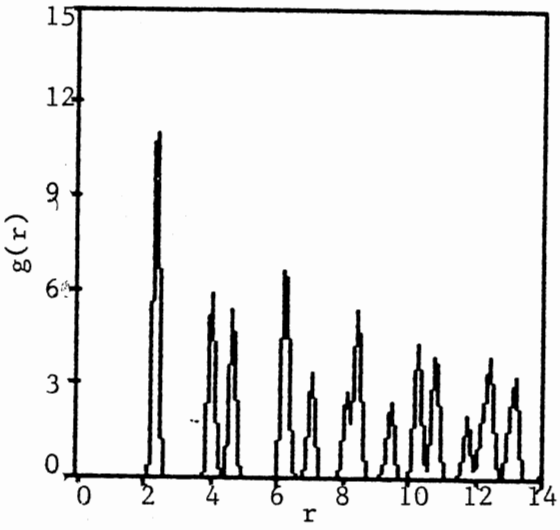

d) 20.44aX23.67a Box, k*a=3.

Figure 82. 1D Pair Correlation Functions for MC Simulation of 100 Interacting Particles in 22aX22a and 20.44aX23.67a Box with the Inverse Screeing Length k*a=3 and 4.

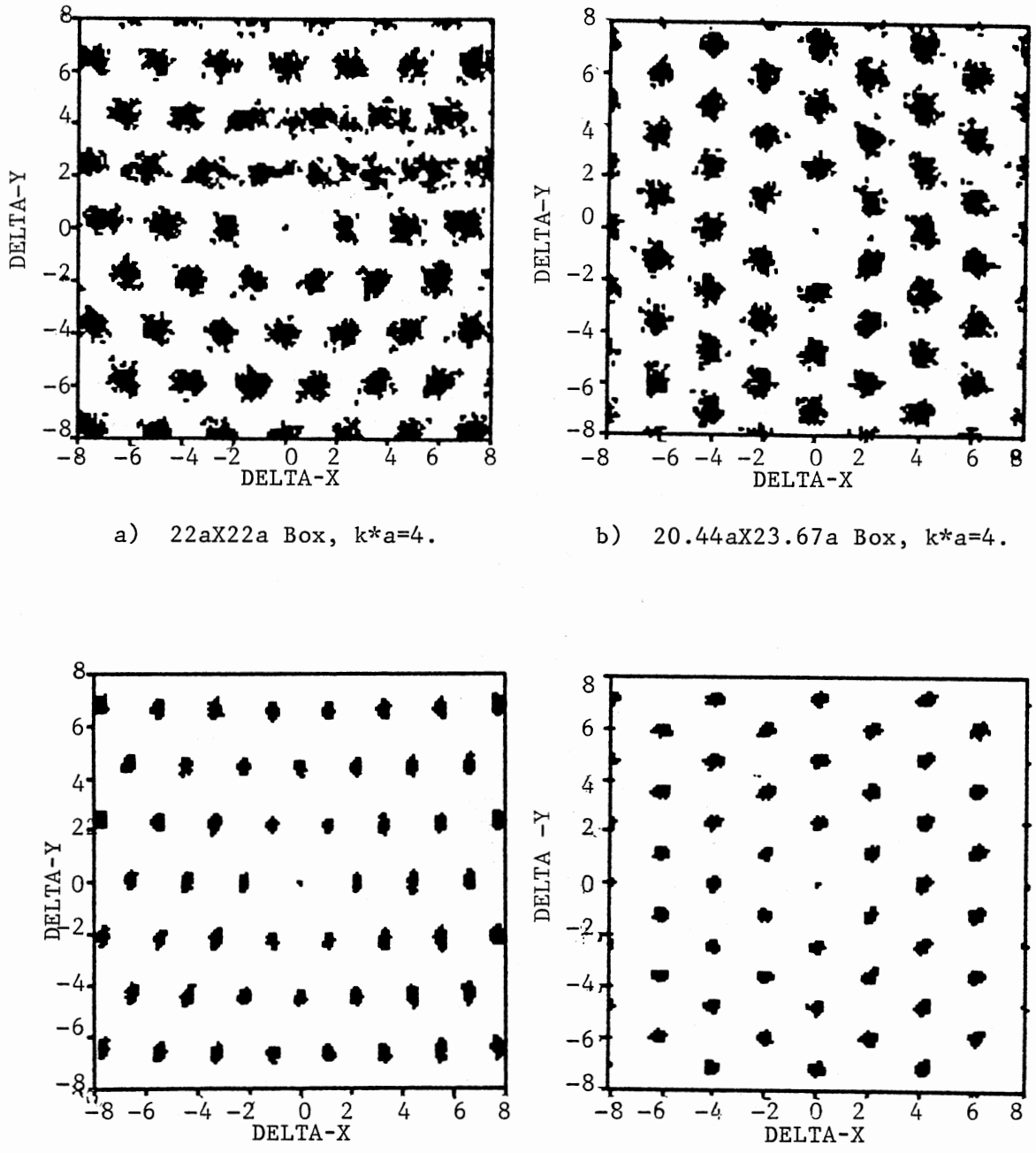

a) 22aX22a Box, k*a=4.

b) 20.44aX23.67a Box, k*a=4.

c) 22aX22a Box, k*a=3.

d) 20.44aX23.67a Box, k*a=3.

Figure 83. 2D Piar Correlation Function for the MC Simulation of 100 Particles in a 22aX22a and 20.44aX23.67a Box and with the Potential's Inverse Screening Length k*a=4 and 3.

the particles. These distorted structures are also rotated by 90 degrees from the undistorted HCP structures observed for the 20.44a by 23.67a box (Figures 83b and d). This shows the effect of the box size in the MC simulations on the observed structures. However, the transition was not affected by the box sizes.

This analysis shows that the phase transition from a disordered to an ordered phase occurs at values of k^*a between 5 and 4, as seen by the 1D pair correlation functions in Figures 79a and b and 82a and b, for a system of 100 particles interacting via a screened Coulomb potential in a 20aX20a or 20.44aX23.67a box.

Externally Applied Potential

The effect of the externally applied potential is introduced through the additional particle potential corresponding to the periodic radiation discussed in Chapter IV,

$$V(r) = A \cos(2 \quad x/d) \tag{5-17}$$

where d is the fringe period and A is given by equation (2-16). This constant (A) allows us to make the simulation comparable to real experimental values. The energy of the system when the external potential is applied is given as the sum of equations (5-20) and (5-25), which is written as,

$$E_{new} = E_C + V(r) \tag{5-18}$$

Both the depth (A) and the priod (d) of the potential wells presented in equation (5-17) are varied in the simulation. Using these parameters (A and d) the effect of the external potential on the equilibrium phases at different salt concentrations was analyzed.

The periods used in the 22aX22a box were 1.1a, 2.0a, 2.2a, and

4.4a. These specific periods were chosen due to their divisibility by the box's length and their closeness to the actual periods used in the experimental analysis. The particles in the 20aX23.67a box were exposed to the external potential at periods of 1.7a, 2.04a and 2.92a. These correspond to the periods used experimentally of 1.85um, 2.2um and 3.3um. The unitless potential's amplitude (A) was varied continuously for all periods used from a value of 1 to 30, and in some cases much higher amplitudes were considered, up to 100. A comparison of these amplitudes to the intensity of the crossed laser beams used in Chapter IV was given previously in Table VIII.

For the 20.44aX22.67a box, when the fluid phase shown in Figure 80b was exposed to the sinusoidal potential of period 1.7a (corresponding to commensurate period, d=b.cos(●) where b is the interparticle separation in the amorphous phase) the system started alining along the potential's minima at low amplitudes, A, (Figure 84). At amplitudes as low as 1 the particles thermal energy was still large enough compared to the external field that the particles are observed not to be well localized within the potential wells (Figures 84a). This effect is better seen through the average density distribution of the 2D correlation function (Figure 85) at this field amplitude (A=1). This distribution function is constructed in the same manner as described in Chapter IV. An analysis of the localization of the particles along the potential's minima at this amplitude and others is given in Table IX. As the amplitude increased the localization of the particles along the minima of the applied potential became more pronounced and so did the interdependence between particles in adjacent potential wells, as evidenced by the appearance of well defined

TABLE IX

ANALYSIS OF 2-D PAIR CORRELATION
FOR MC SIMULATION AT d=1.713

Amplitude/kT	Fringe Positions (d/2)		$Mean_x/a$	Std_x/a
1	-1	1	.016	.336
	1	3	1.72	.354
	3	5	3.44	.382
5	-1	1	.006	.157
	1	3	1.72	.182
	3	5	3.42	.173
10	-1	1	0	.108
	1	3	1.71	.120
	3	5	3.42	.120
30	-1	1	0	.060
	1	3	1.70	.067
	3	5	3.41	.068

$Mean_x$= mean x position of the particles in the given fringe period.

Std_x= standard deviation around the mean x-position of each fringe.

a = diameter of a single particle.

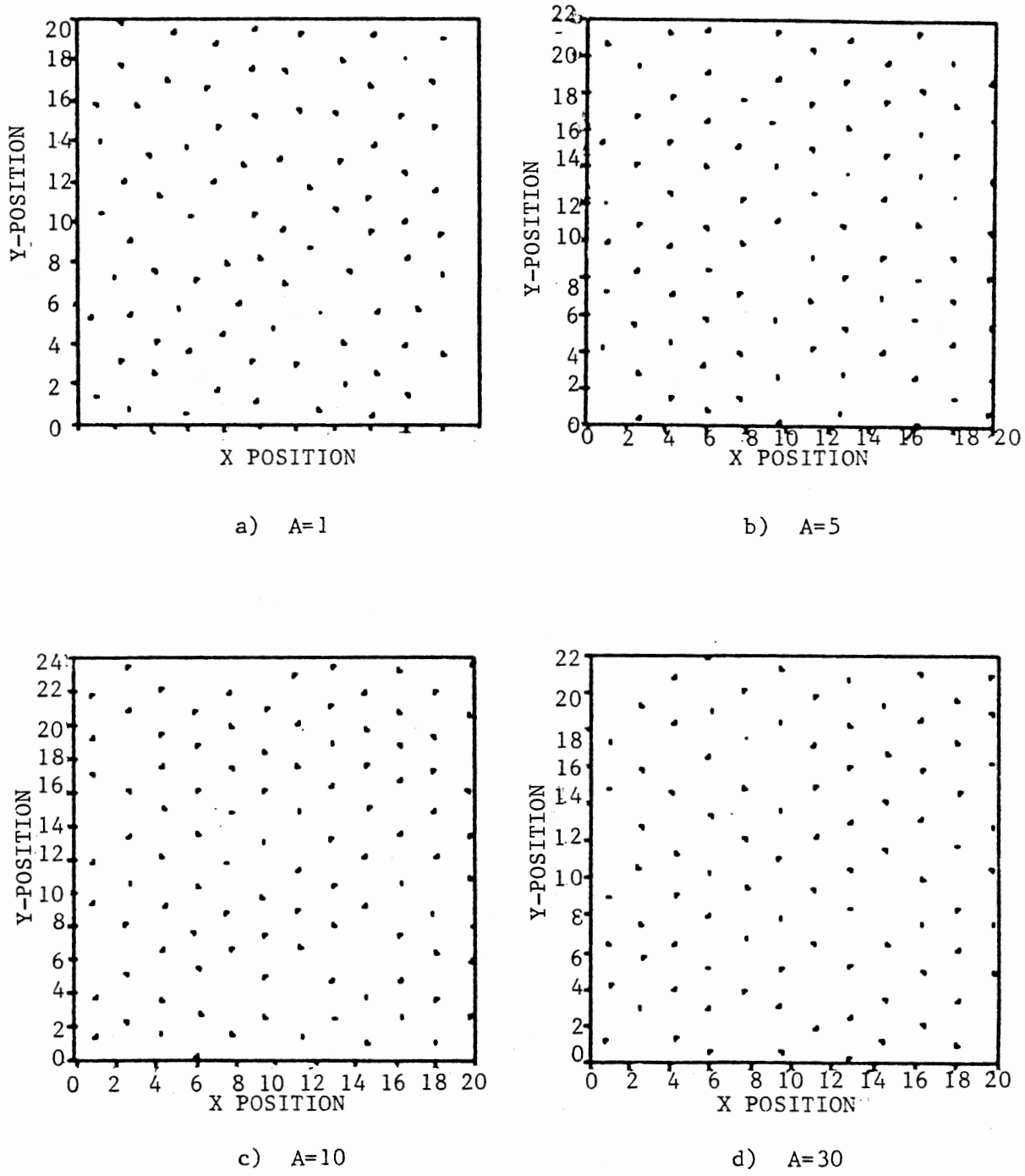

Figure 84. Position Files for MC Simulation of 100 Particles in a 20.44aX23.67a Box Interacting Via a Screened Coulomb Potential with an Inverse Screening Length k*a=5 and in the Presence of a Sinusoidal Potential with Period of 1.713a and Amplitudes A/k_BT= 1(a), 5(b), 10(c) and 30(d).

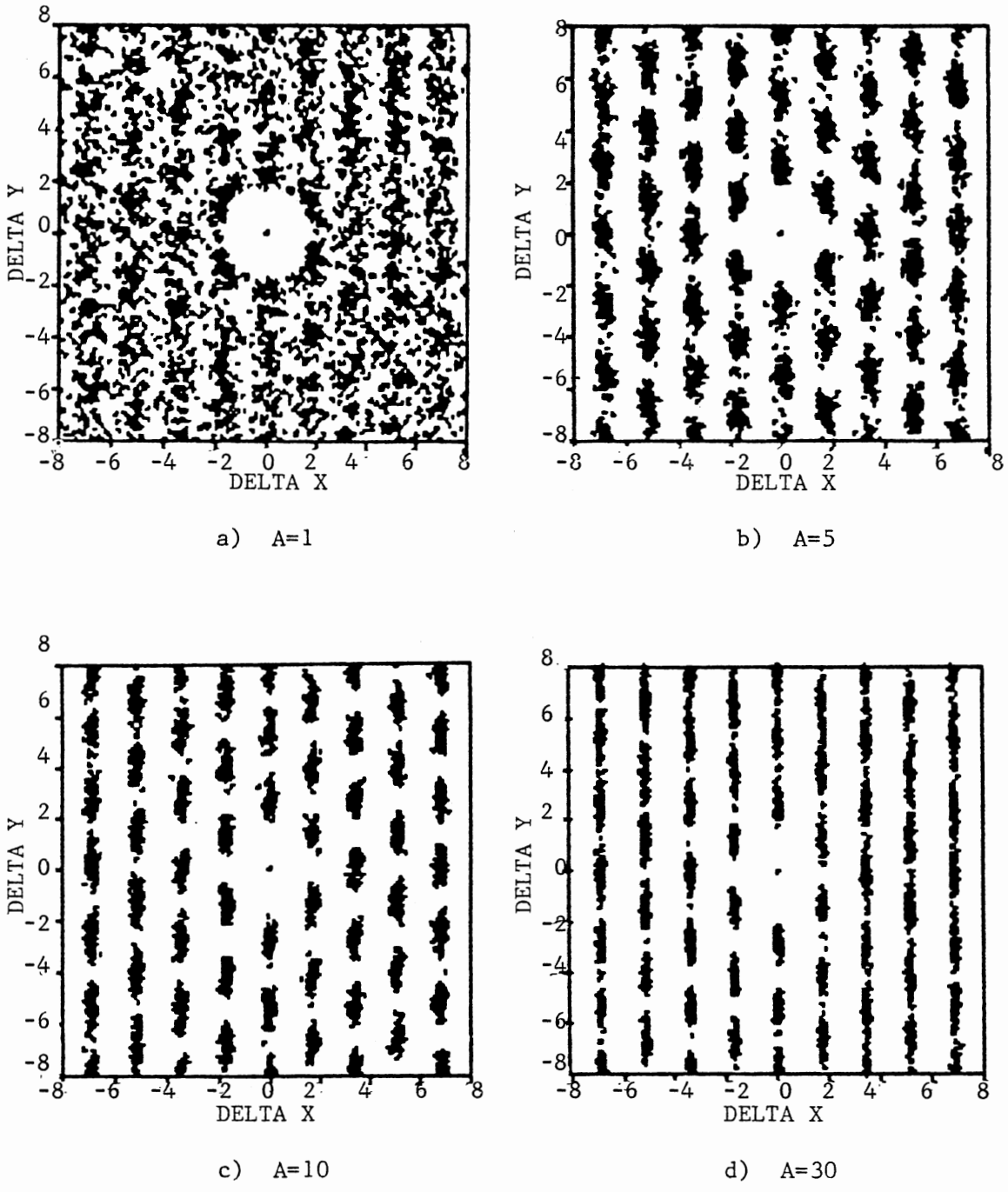

a) A=1

b) A=5

c) A=10

d) A=30

Figure 85. 2D Pair Correlation Functions for MC Simulation of 100 Particles in a 20.44aX23.67a Box, Interacting via a Screened Coulomb Potential (k*a=5) and in the Presence of a Sinusoidal Potential with Period d=1.713a and Amplitude A/k_BT= 1(a), 5(b), 10(c) and 30(d).

clusters around lattice points in the 2D correlation functions (Figure 84b, c and d). An analyis of these clusters is given through the average density distribution plots shown in Figures 86, 87 and 88 for the unitless amplitudes of 5, 10, and 30. To be noticed in this analysis is the string like behavior as the particles get more localized within the potential wells or as the field amplitude increases. This is believed to be due to restricting the particles' movement along the y-direction as the potential wells become deeper (increasing A) together with the effect of defects present in the periodic minima of the potential as seen in Figure 89.

As the potential period was increased to 2.02a the particle alinement in the potential wells started to develop at low amplitudes as evidenced from the 2D correlation functions given in Figure 90. This figure demonstrates the effect of the applied potential amplitude on the induced ordering of the amorphous equilibrium phase to a slightly distorted HCP lattice. The analysis of the 2D correlation function is given in Figures 91 to 94. These average density distribution plots show the evolution of the correlation between adjacent potential wells as the field strength is increased. The formation of well defined peaks for the different boxes (d/2 to 3d/2 and 3d/2 to 5d/2) show induced correlation between the adjacent wells as the field stength is increased. The analyis of the particles localization in the wells at this fringe period (d=2.02a) and the different amplitudes is given in Table X.

The effect of the external potential at fringe period of 2.92a on the local structure of the equilibrium phase (Figure 80b) is shown through the MC position files given in Figure 95. At low field

TABLE X

ANALYSIS OF 2-D PAIR CORRELATION
FOR MC SIMULATION AT d=2.02

Amplitude/kT	Fringe Positions (d/2)		$Mean_x/a$	Std_x/a
1	-1	1	.100	.336
	1	3	1.98	.329
	3	5	4.00	.354
5	-1	1	.070	.185
	1	3	1.97	.195
	3	5	3.97	.190
10	-1	1	0	.111
	1	3	2.00	.124
	3	5	4.00	.135
30	-1	1	0	.074
	1	3	2.00	.079
	3	5	4.00	.076

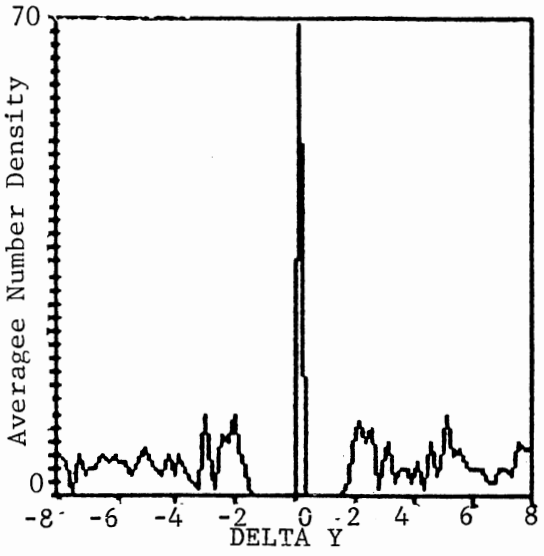

a) -d/2 to d/2

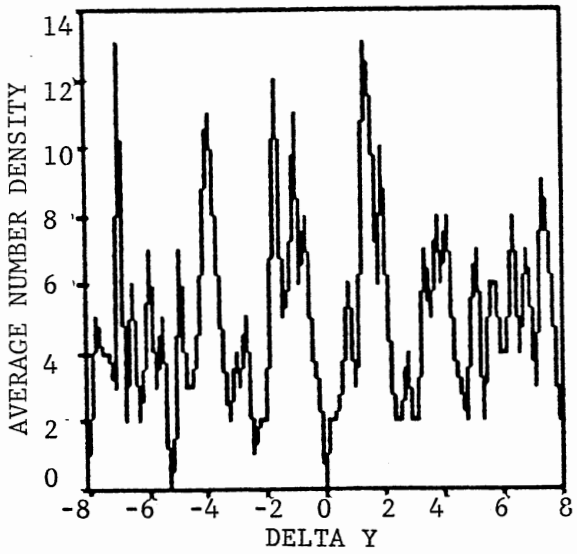

b) d/2 to 3d/2

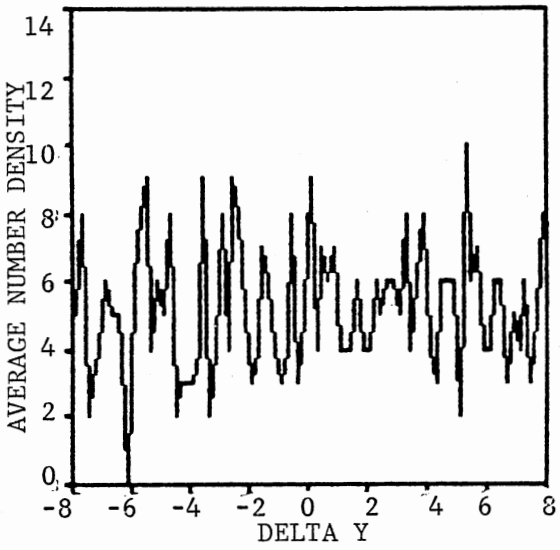

c) 3d/2 to 5d/2

Figure 86. Average Number Density Distribution along the Fringes of the 2D Pair Correlation Function Shown in Figure 85a.

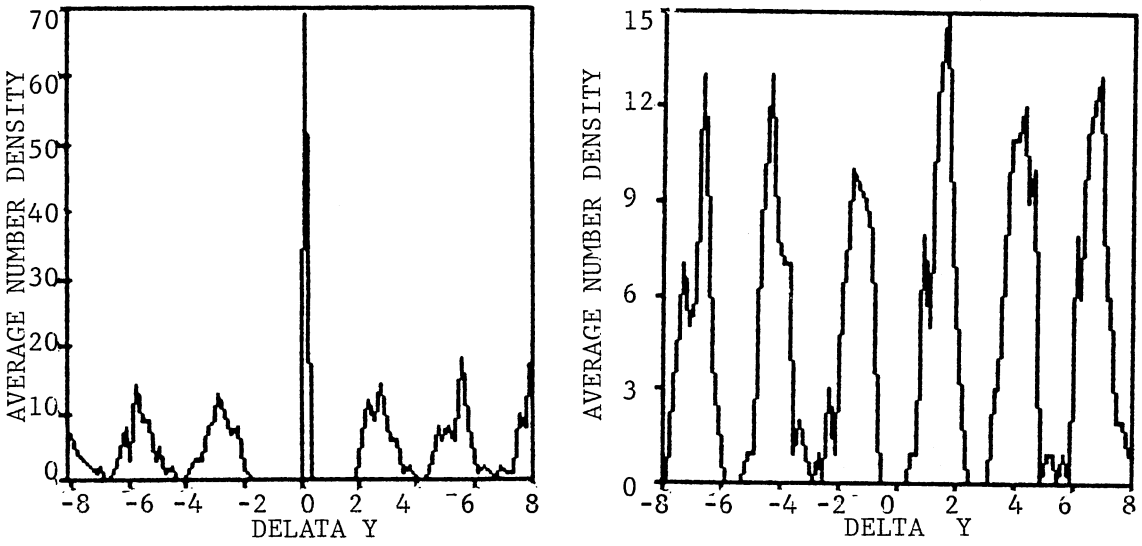

a) -d/2 to d/2

b) d/2 to 3d/2

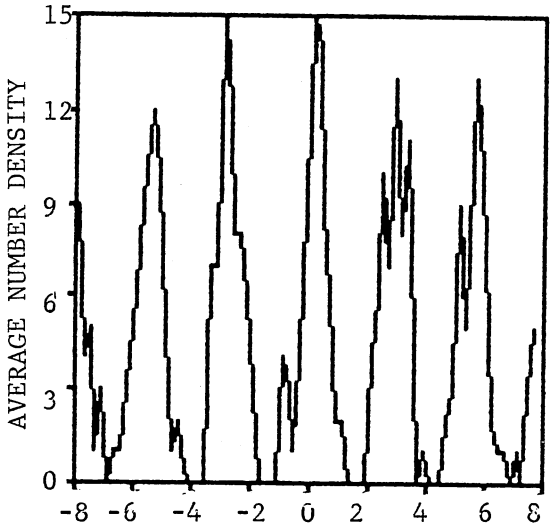

c) 3d/2 to 5d/2

Figure 87. Average Number Density Distribution along the Fringes of the 2D Pair Correlation Function Shown in Figure 85b.

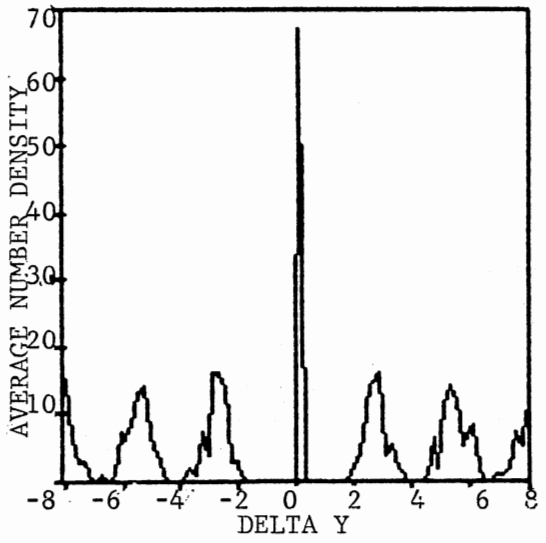

a) -d/2 to d/2

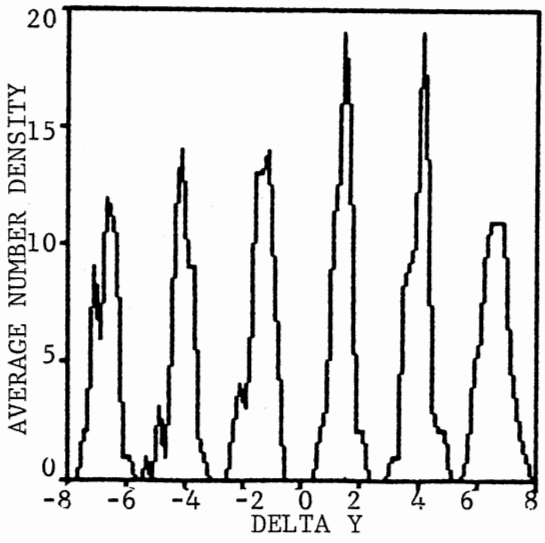

b) d/2 to 3d/2

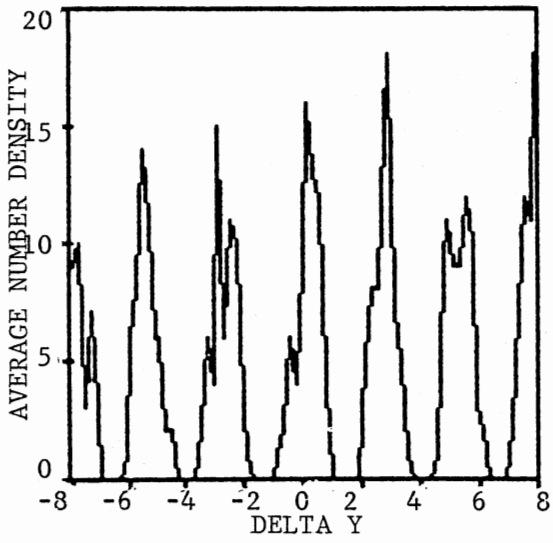

c) 3d/2 to 5d/2

Figure 88. Average Number Density Distribution along the Fringes of the 2D Piar Correlation Function Shown in Figure 85c.

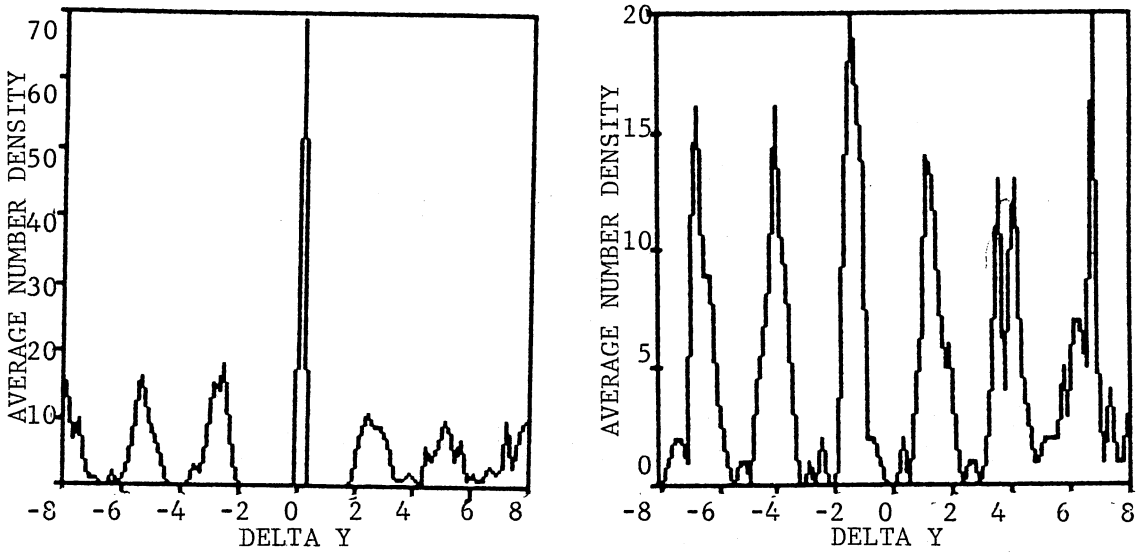

a) -d/2 to d/2

b) d/2 to 3d/2

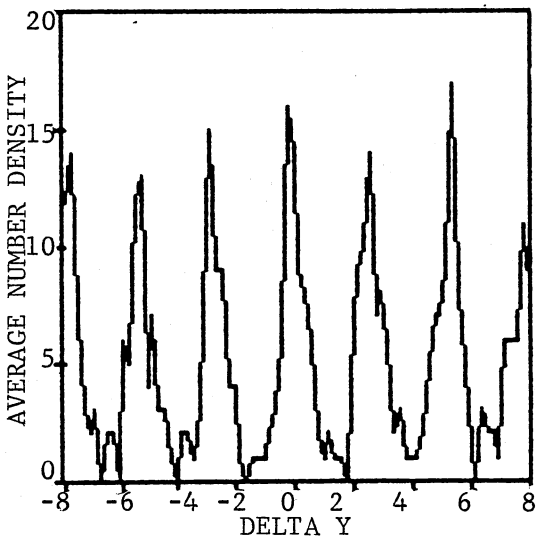

c) 3d/2 to 5d/2

Figure 89. Average Number Density Distribution along the Fringes of the 2D Pair Correlation Function Shown in Figure 85d.

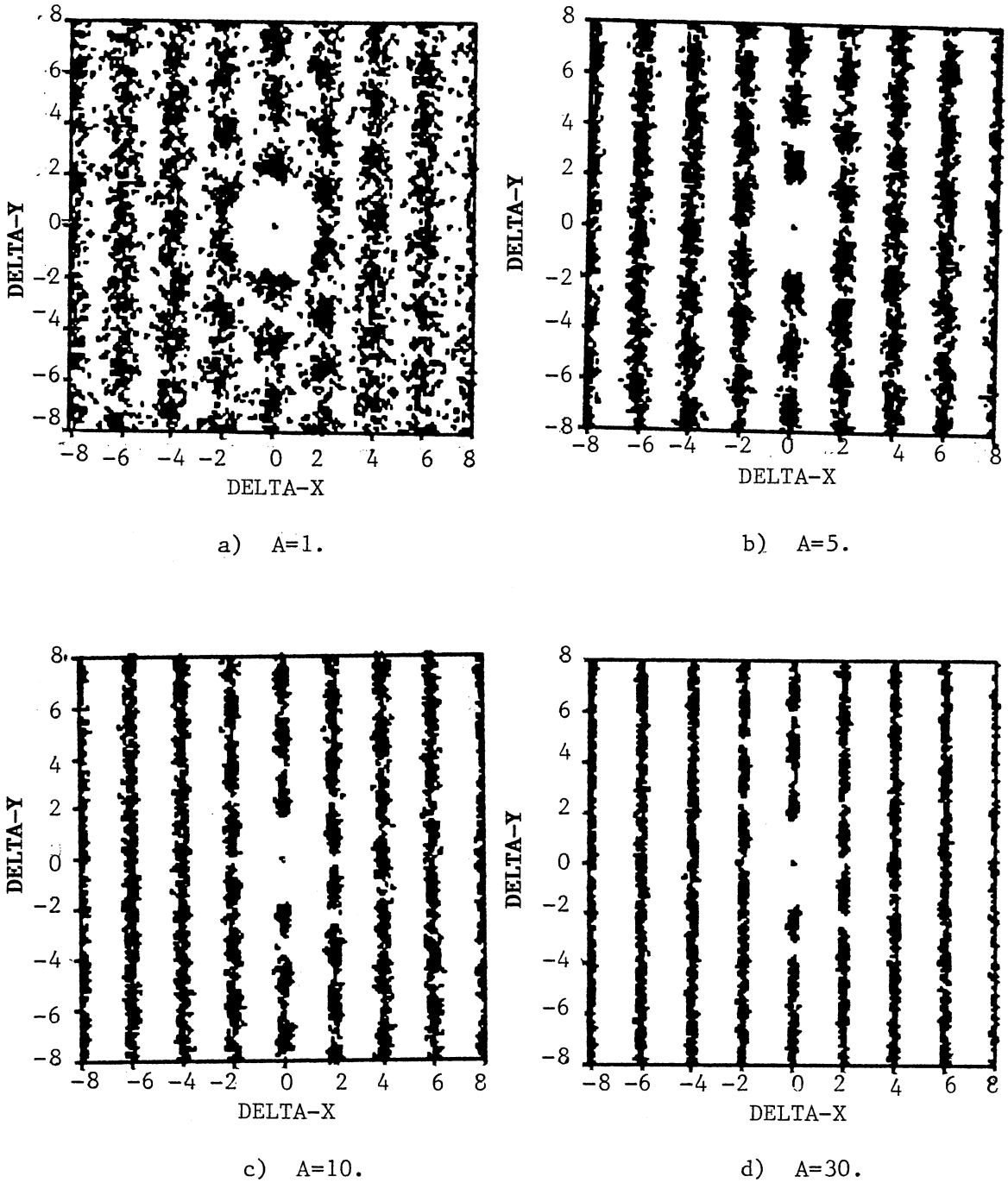

a) A=1.

b) A=5.

c) A=10.

d) A=30.

Figure 90. 2D Pair Correlation Functions for MC Simulation of 100 Particles in a 20.44aX23.67a Box, Interacting via a Screened Coulomb Potential (k*a=5) and in the Presence of a Sinusoidal Potential with Period d=2.02a and Aplitude A/k_BT= 1(a), 5(b), 10(c) and 30 (d).

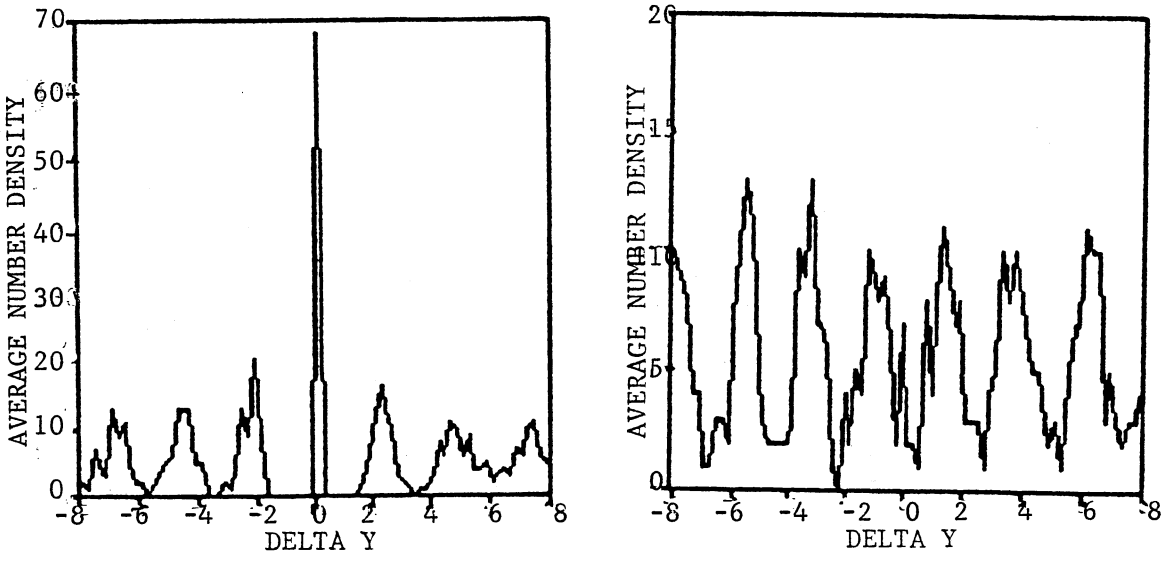

a) -d/2 to d/2

b) d/2 to 3d/2

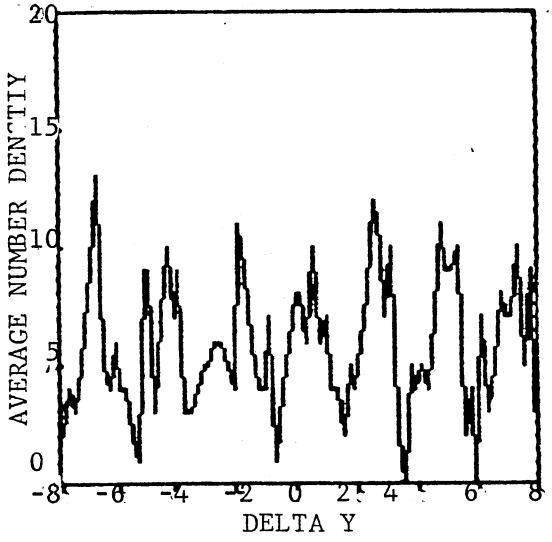

c) 3d/2 to 5d/2

Figure 91. Average Number Density Distribution along the Fringes of the 2D Pair Correlation Function Shown in Figure 90a.

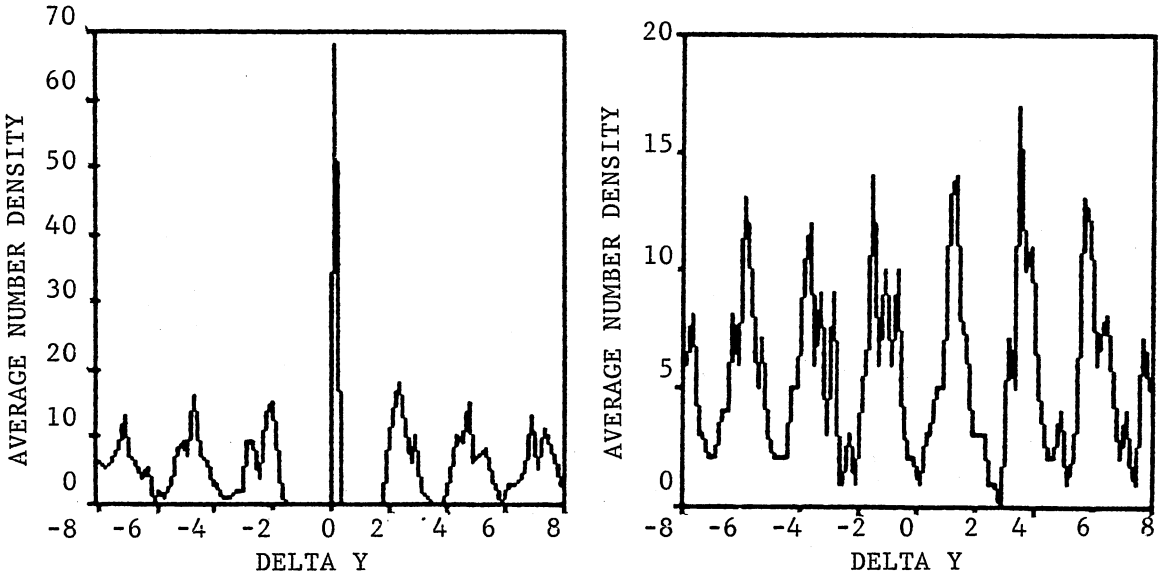

a) -d/2 to d/2

b) d/2 to3d/2

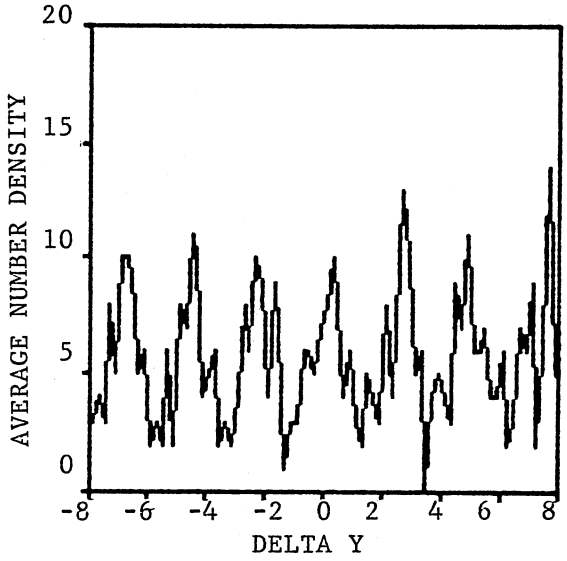

c) 3d/2 to 5d/2

Figure 92. Average Number Density Distribution along the Fringes of the 2D Pair Correlation Function Shown in Figure 90b.

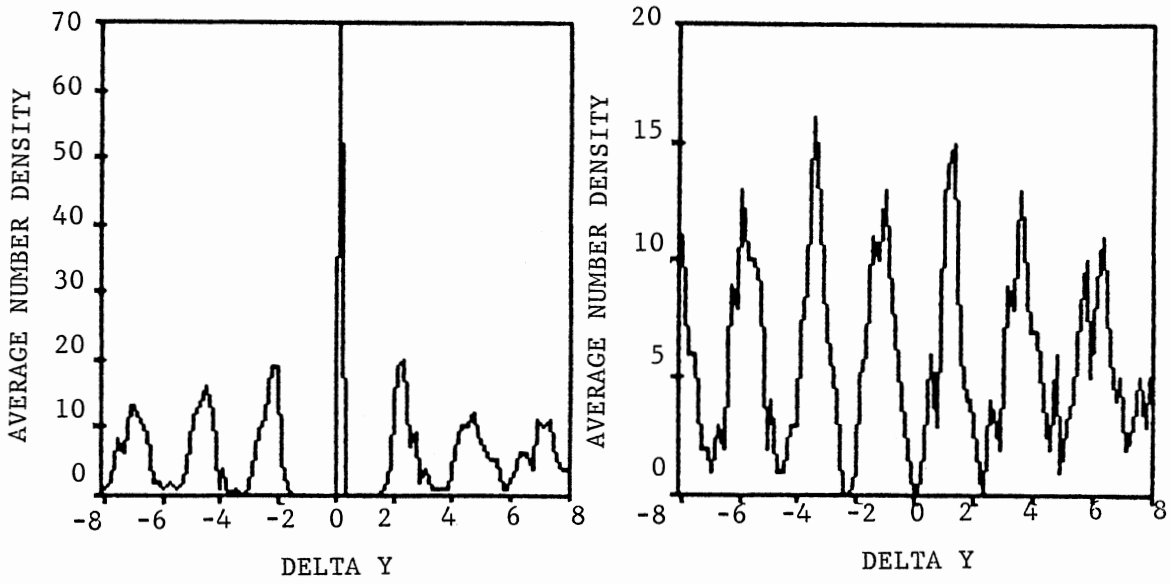

a) -d/2 to d/2

b) d/2 to 3d/2

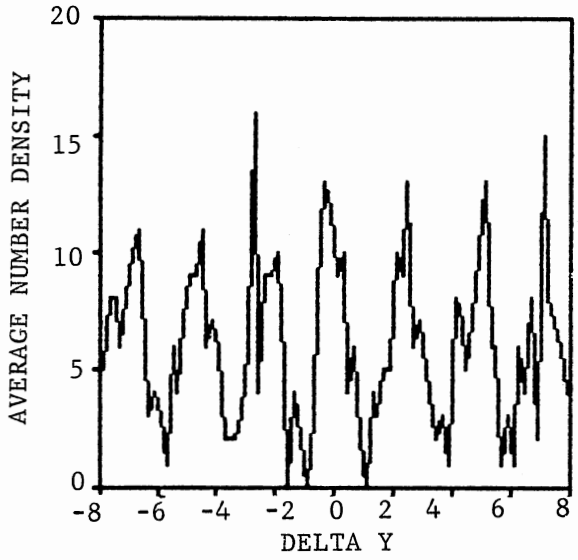

c) 3d/2 to 5d/2

Figure 93. Average Number Density Distribution along the Fringe of the 2D Pair Correlation Function Shown in Figure 90c.

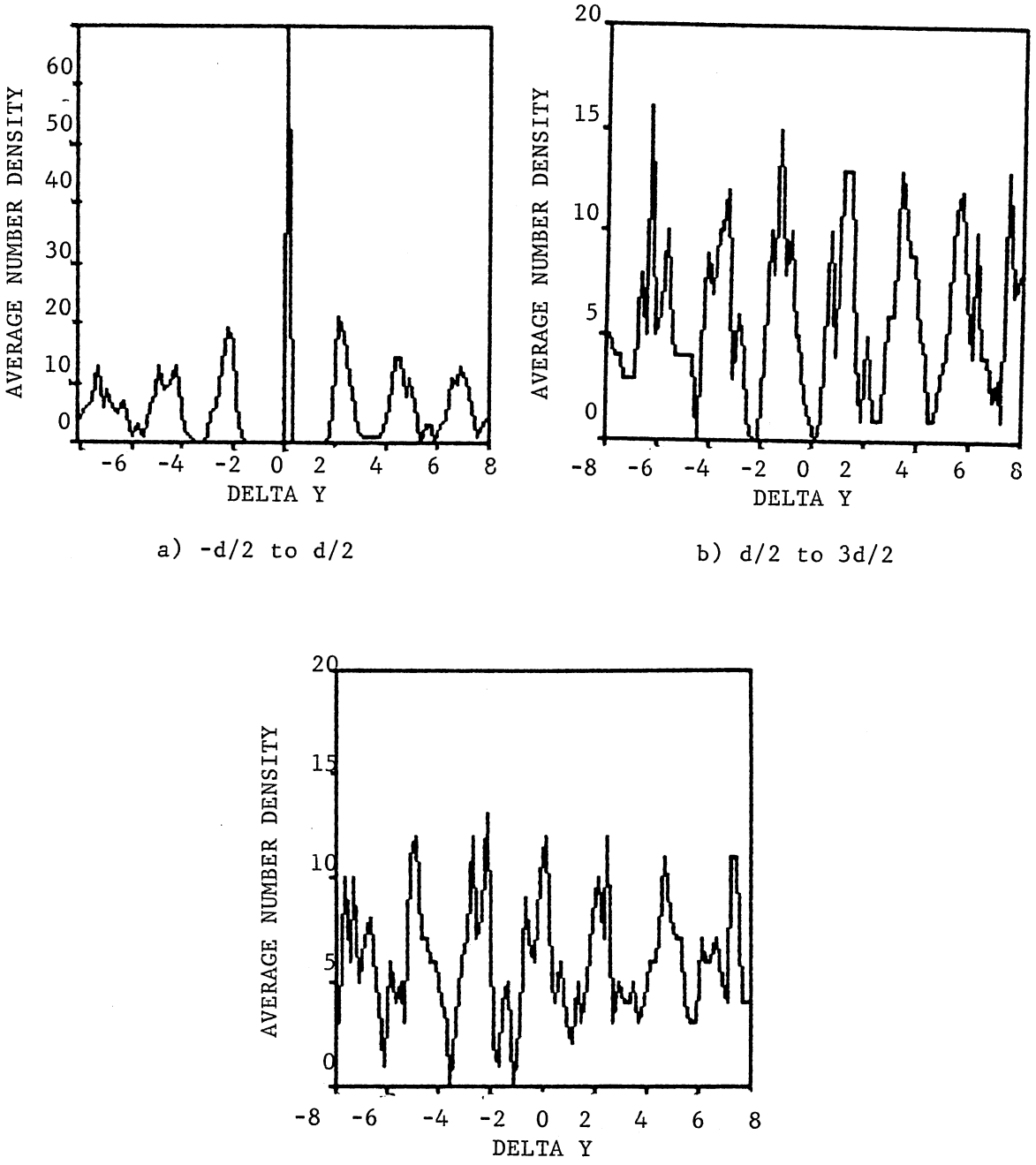

Figure 94. Average Number Density Distribution along the Fringes of the 2D Pair Correlation Function Shown in Figure 90d.

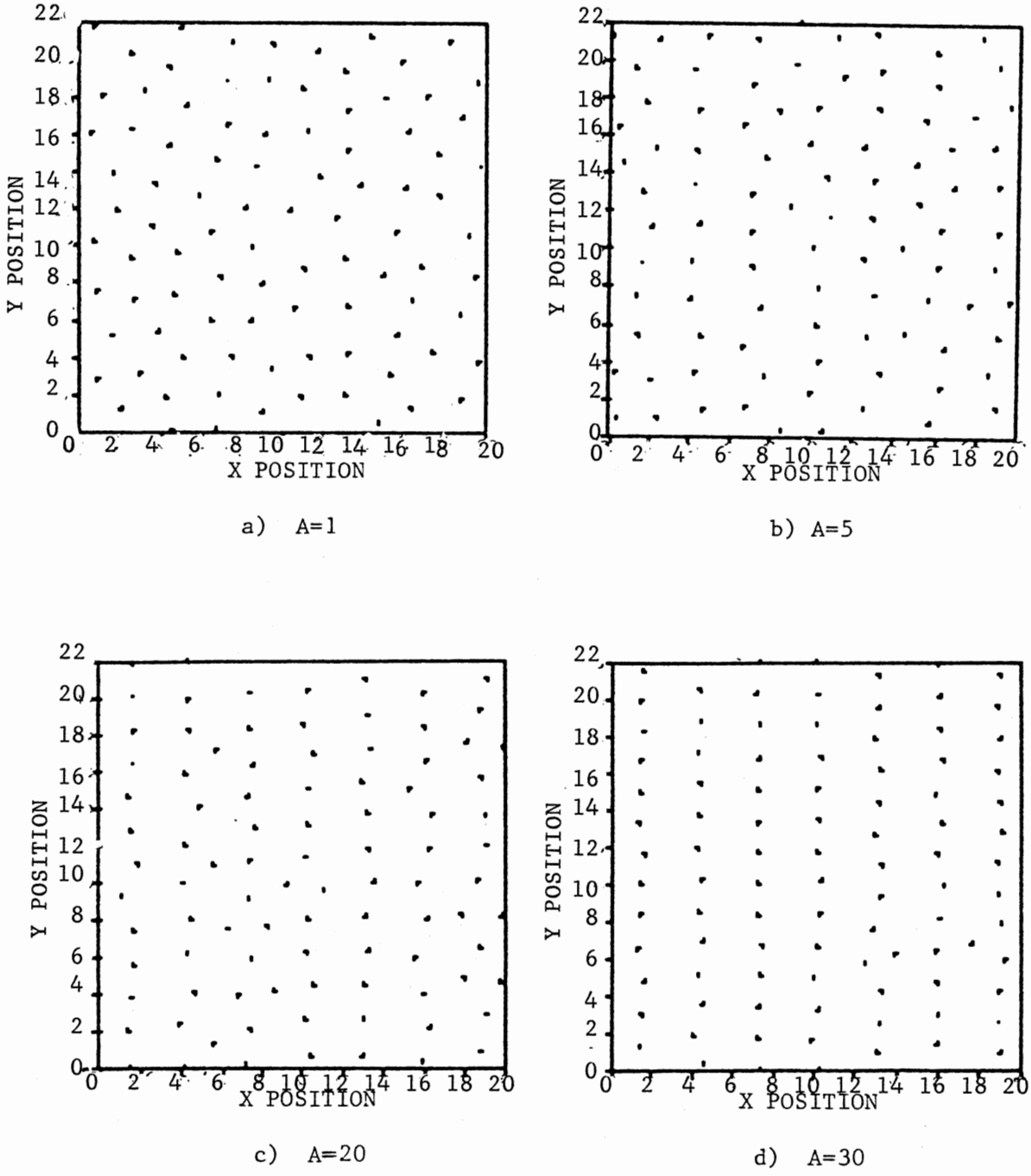

Figure 95. Position Files for MC Simulation of 100 Particles in a 20.44aX23.67a Box, Interacting via a Screened Coulomb Potential (k*a=5) and in the Presence of a Sinusoidal Potential (d=2.92um) with Unitless Amplitude of: a) 1, b) 5, c) 20 and d) 30.

amplitudes the interaction between the partiles causes them lign up in the low, as well as in the high, field regions. The effect of the applied potential amplitude on the localization of the particles along its minima is better seens through the 2D correlation functions (Figure 96). In Figure 96 we are also able to see the development of correlation between adjacent rows leading to a distorted HCP structure. The average density distribution for the 2D pair correlation functions at the given field amplitudes are shown in Figures 97 to 100. These show the development of interrow correlation as the external field's strength is increased. The localization of the particles whithin the wells as the amplitude of the applied potential is increased is demonstrated in Table XI through the decrease in the standard deviation around the mean x-position of the particles within a given well.

Similar analysis on the 22aX22a box were performed using equilibrium phases ranging from disordered (amorphous) to very ordered (crystalline) states. A general description of the forced ordering of these phases under the influence of the externally applied potential will be given in terms of the 2D pair correlation functions.

Starting with the fluid phase shown in Figure 80a ($k^*a=5$) and applying the external potential, with a period of 1.1a, which is less than commensurate, the induced ordering of the system is shown in Figure 101. It is observed that at low field value (A=1) the particles start moving to the potential's minima but the brownian motion is still large enough that considerable hopping from one minima to the next is also observed (Figure 101a). As the potential's amplitude is increased correlation between neighboring particles starts developing

TABLE XI

ANALYSIS OF 2-D PAIR CORRELATION
FOR MC SIMULATION AT d=2.92

Amplitude/kT	Fringe Positions (d/2)		$Mean_x/a$	Std_x/a
1	-1	1	.030	.810
	1	3	2.91	.862
	3	5	5.83	.836
5	-1	1	.051	.646
	1	3	2.95	.771
	3	5	5.88	.684
20	-1	1	.024	.275
	1	3	2.94	.323
	3	5	5.86	.295
30	-1	1	0	.245
	1	3	2.94	.321
	3	5	5.84	.317

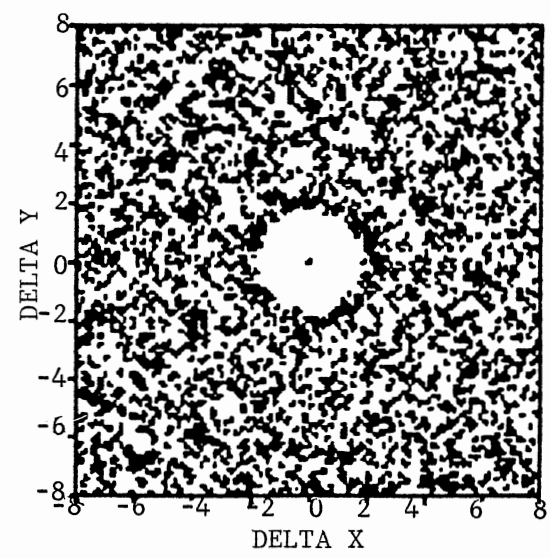

a) A=1

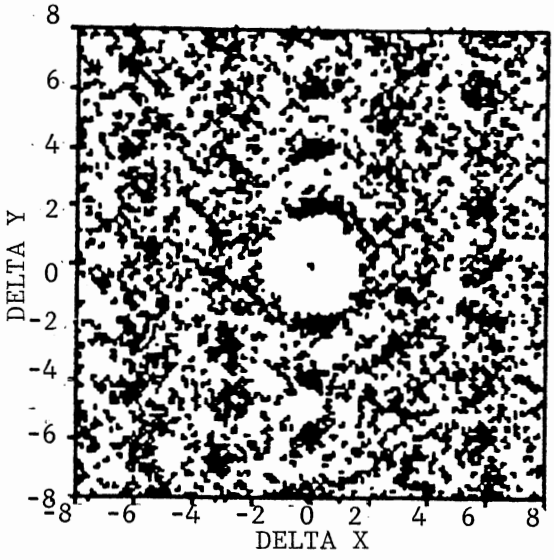

b) A=5

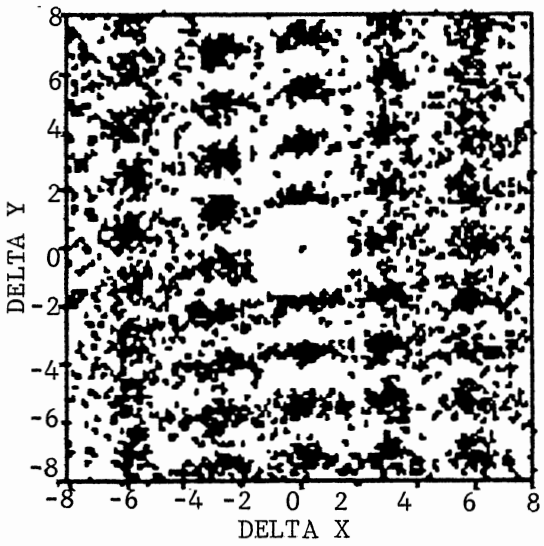

c) A=20

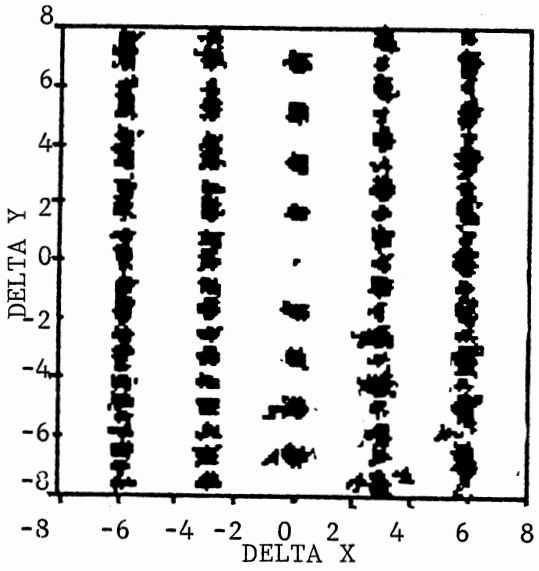

c) A=30

Figure 96. 2D Pair Correlation Functions for MC Simulation of 100 Particles in a 20.44aX23.67a Box, Interacting via a Screened Coulomb Potential (k*a=5) and in the Presence of a Sinusoidal Potential (d=2.92a) with Unitless Amplitude of: a) 1, b) 5, c) 20 and d) 30.

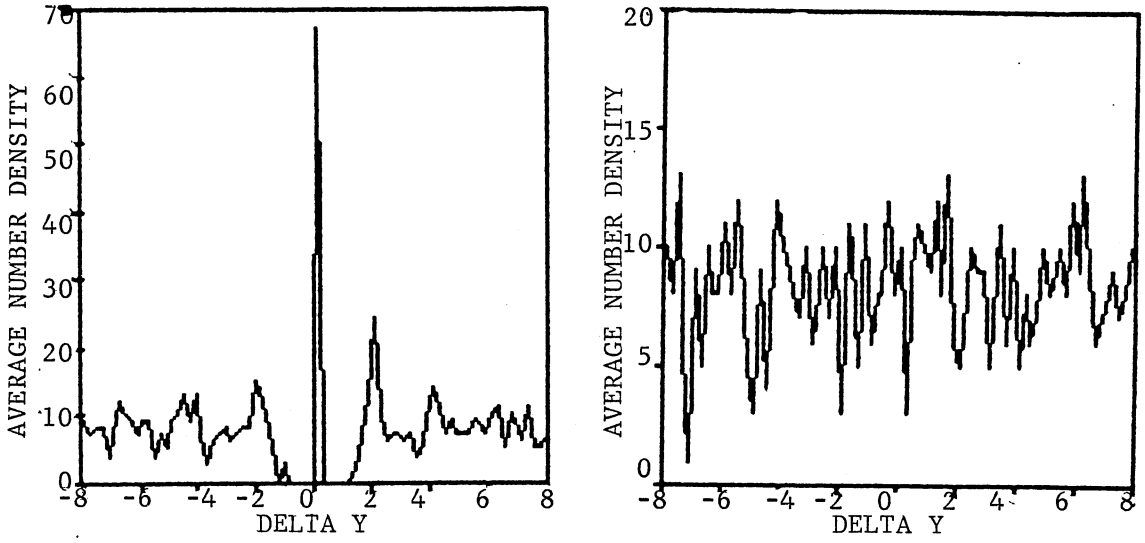

a) -d/2 to d/2

b) d/2 to 3d/2

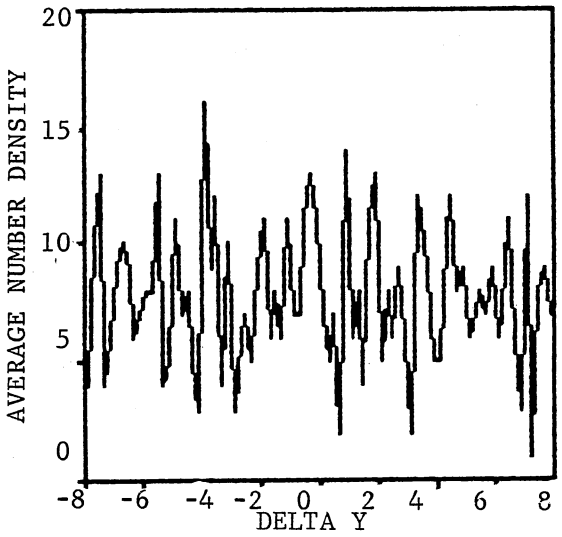

c) 3d/2 to 3d/2

Figure 97. Average Number Density Distribution along the Fringes of the 2D Piar Correlation Function Shown in Figure 96a.

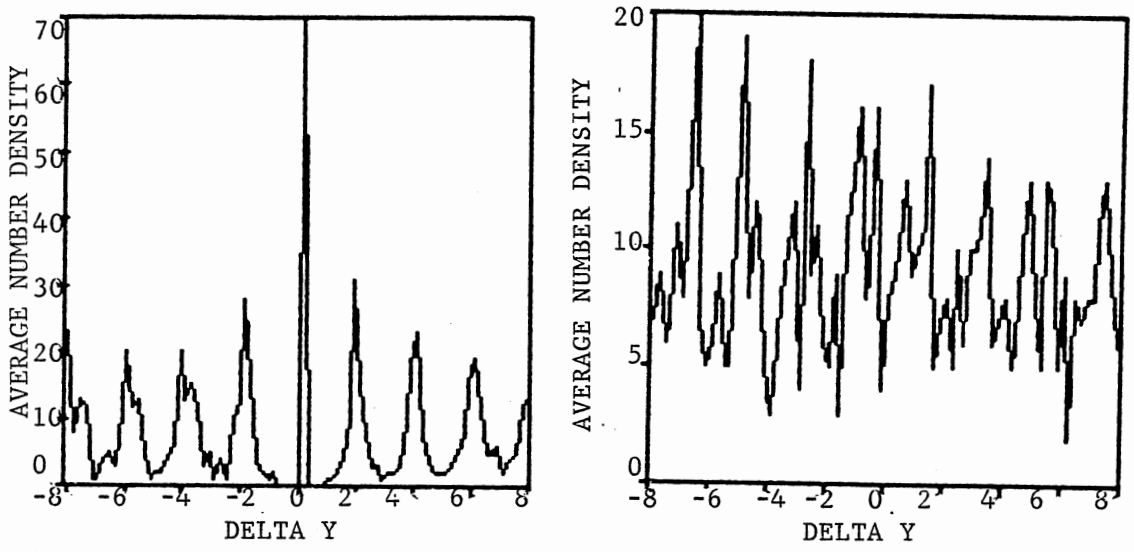

a) -d/2 to d/2

b) d/2 to 3d/2

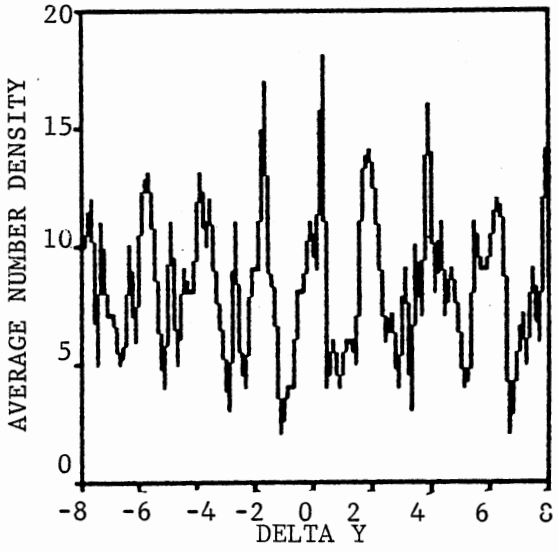

c) 3d/2 to 5d/2

Figure 98. Average Number Density Distribution along the Fringes of teh2D Piar Correlation Function Shown in Figure 96b.

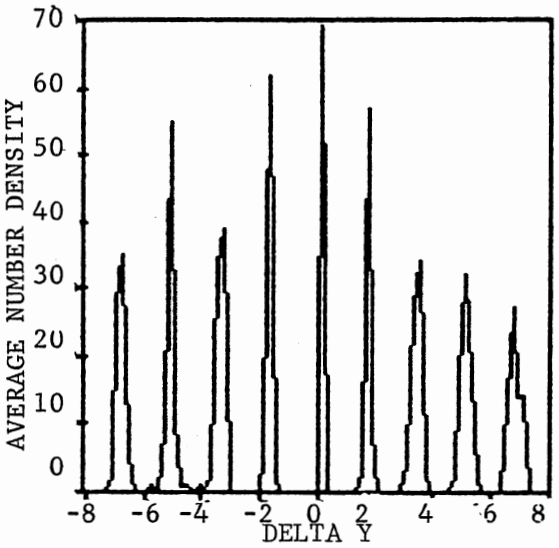

a) -d/2 to d/2.

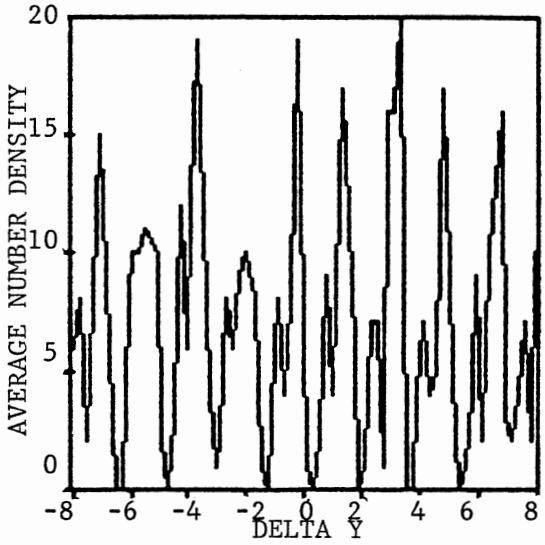

b) d/2 to 3d/2.

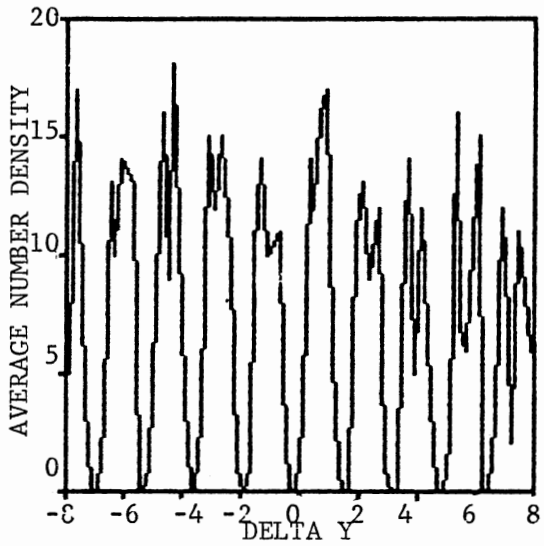

c) 3d/2 to 5d/2.

Figure 99, Average Number Density Distribution along the Fringes of the 2D Piar Correlation Function Shown in Figure 96c.

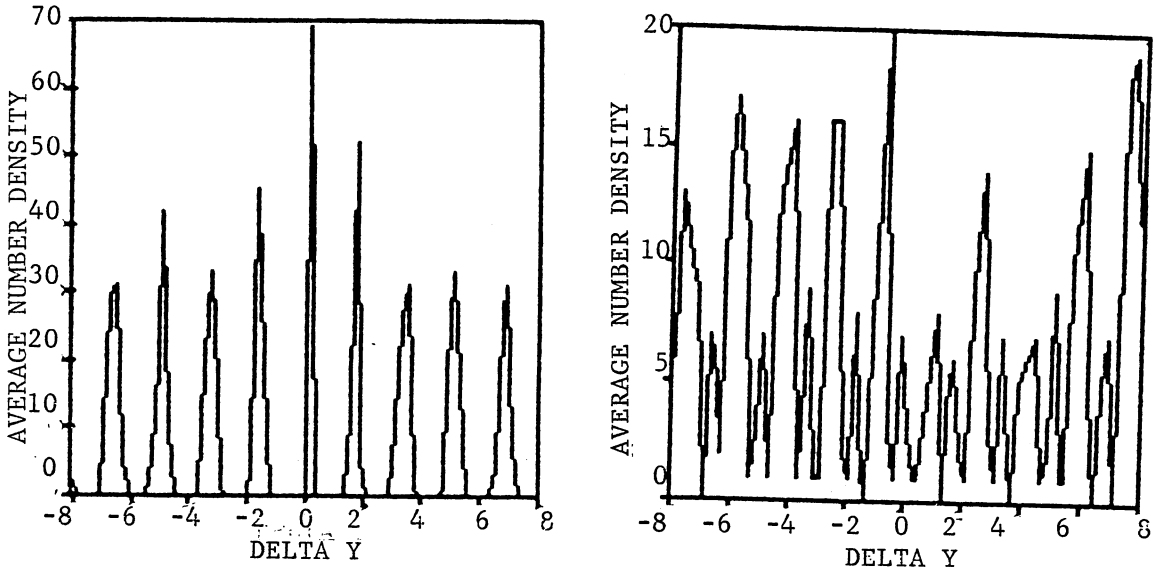

a) -d/2 to d/2.

b) d/2 to 3d/2.

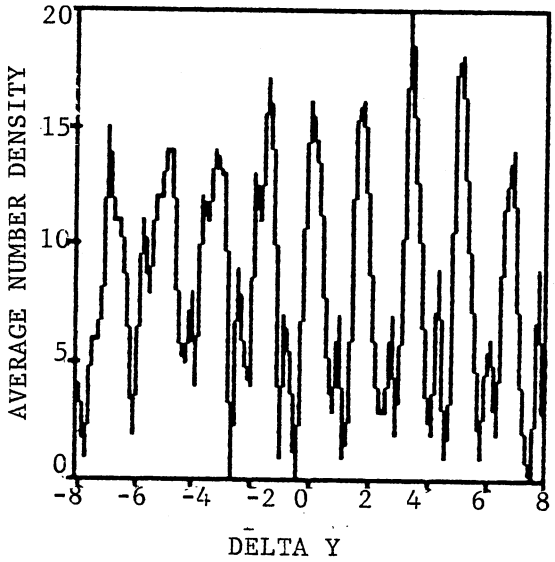

c) 3d/2 to 5d/2.

Figure 100. Average Number Density Distribution along the Fringes of the 2D Pair Correlation Function Shown in Figure 96d.

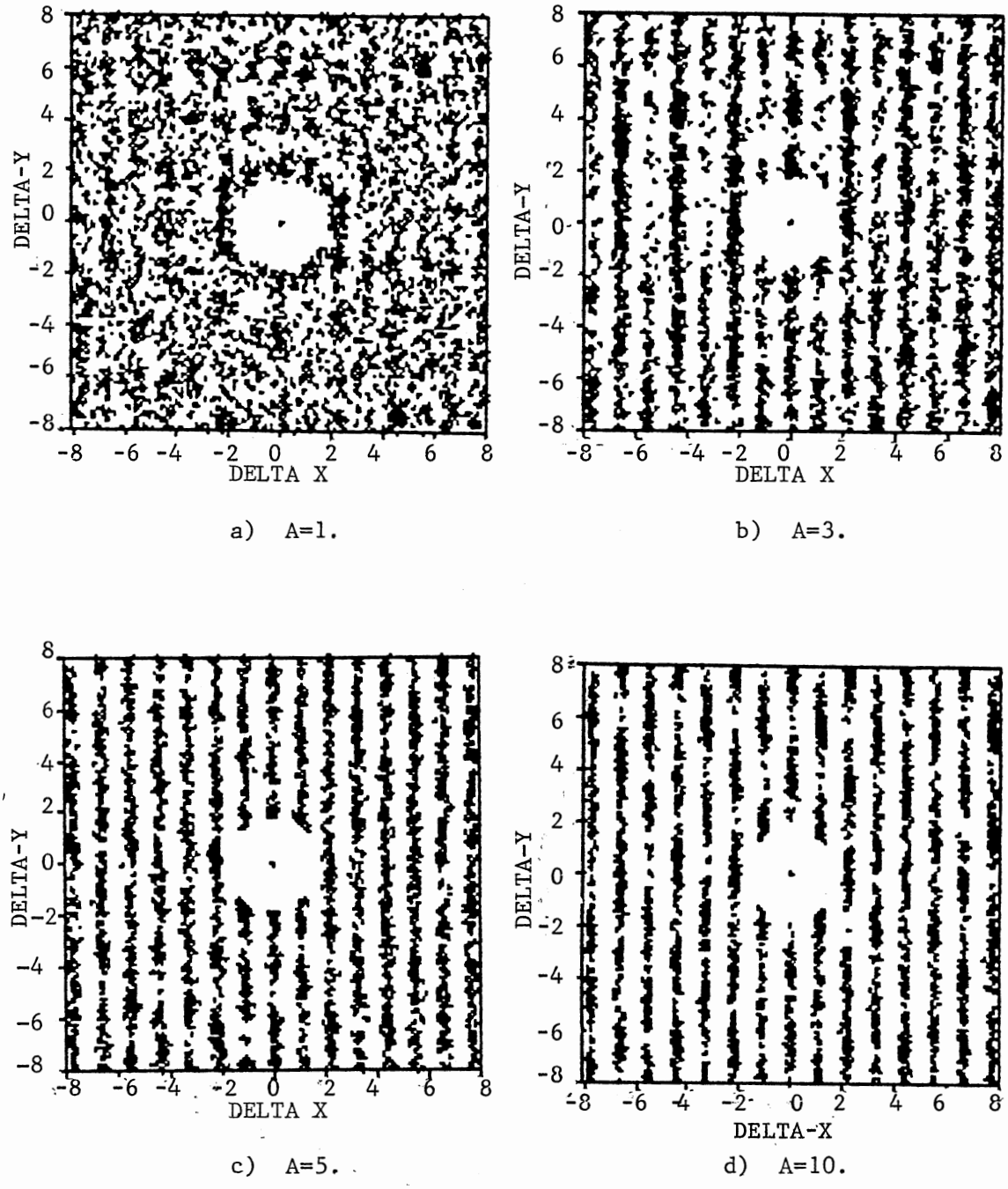

Figure 101. 2D Pair Correlation Functions for MC Simulation of 100 Particles in a 22aX22a Box, Interacting via a Screened Coulomb Potential (k*a=5) and in the Presence of a Sinusoidal Potential (d=1.1a) with Unitless Amplitude of: a) 1, b) 3, c) 5 and d)10.

and their localization within the minima of the external field becomes stronger (Figures 101a and b). The observed structure at this fringe period is not oriented the same way as the structures observed with periods greater than or equal to commensurate. This structure is rotated by 90 degrees in order for the system to be in its lowest energy state.

For the noncommensurate period of 2a, the external field breaks the fluid's symmetry in a continuous fashion as shown in Figure 102. This figure shows that an increase in the field's strength causes a localization of the particles in the potential wells. This leads to interrow correlation between the point particles, and structural arrangement between adjacent rows, as a result of the screened Coulomb interaction between the particles.

As the fringe period is made slightly larger (d=2.2a) the same restructering is observed as the A is increased (Figures 103). The alignment of the particles at the different potential wells gives a distorted HCP packing.

Starting with the crytalline phase shown in Figure 83a ($k^*a=4$), and applying the external potential with a period of 2.2a, the forced ordering of the particles as the field's amplitude is increased is shown in Figures 104. The reorientation of the equilibrium phase to a distorted HCP lattice at this fringe period occured at relatively low field's amplitude (A=2), Figure 104b. As the field's amplitude increased from a value of 5 to 10 (Figures 104c and d), the correlation between the adjacent rows starts get masked by the string like effect as observed earlier for the other systems.

At even lower salt concentration, $k^*a=3$, when the crystalline

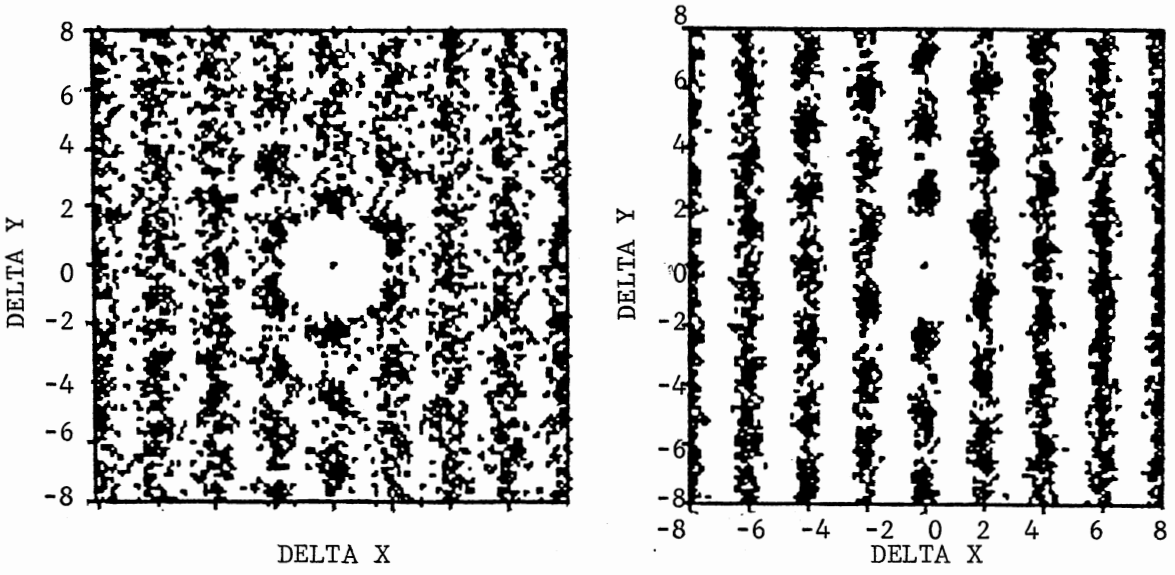

a) A=1.

b) A=3.

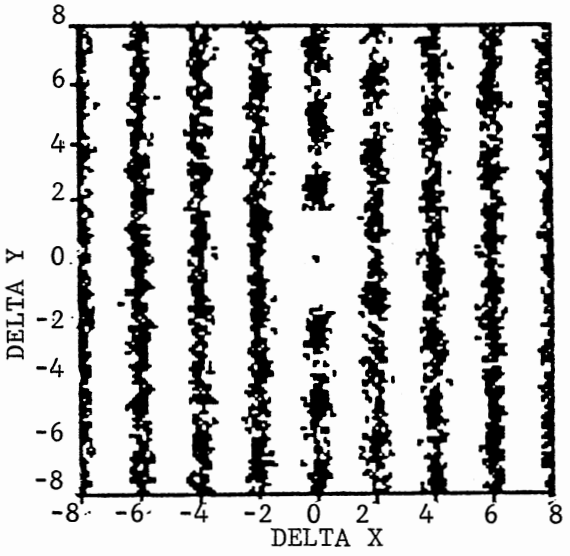

c) A=5.

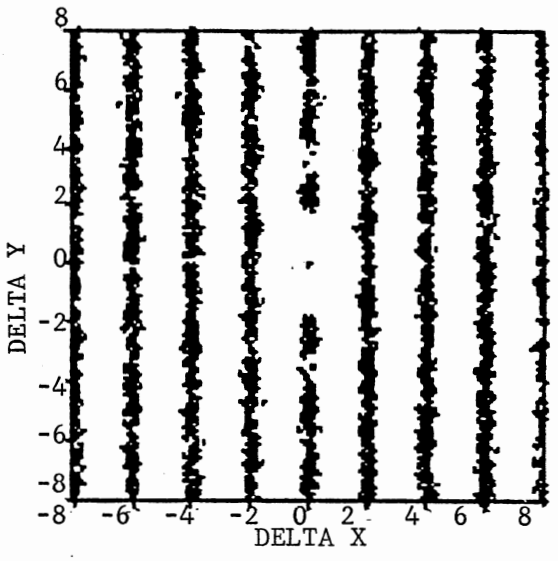

c) A=10.

Figure 102. 2D Pair Correlation Function for MC Simulation of 100 Particles in a 22aX22a Box, Interacting via a Screened Coulomb Potential (k*a=5) and in the Presence of a Simusoidal Potential (d=2.0um) with Unitless Amplitudes of: a) 1, b) 3, c) 5 and d) 10.

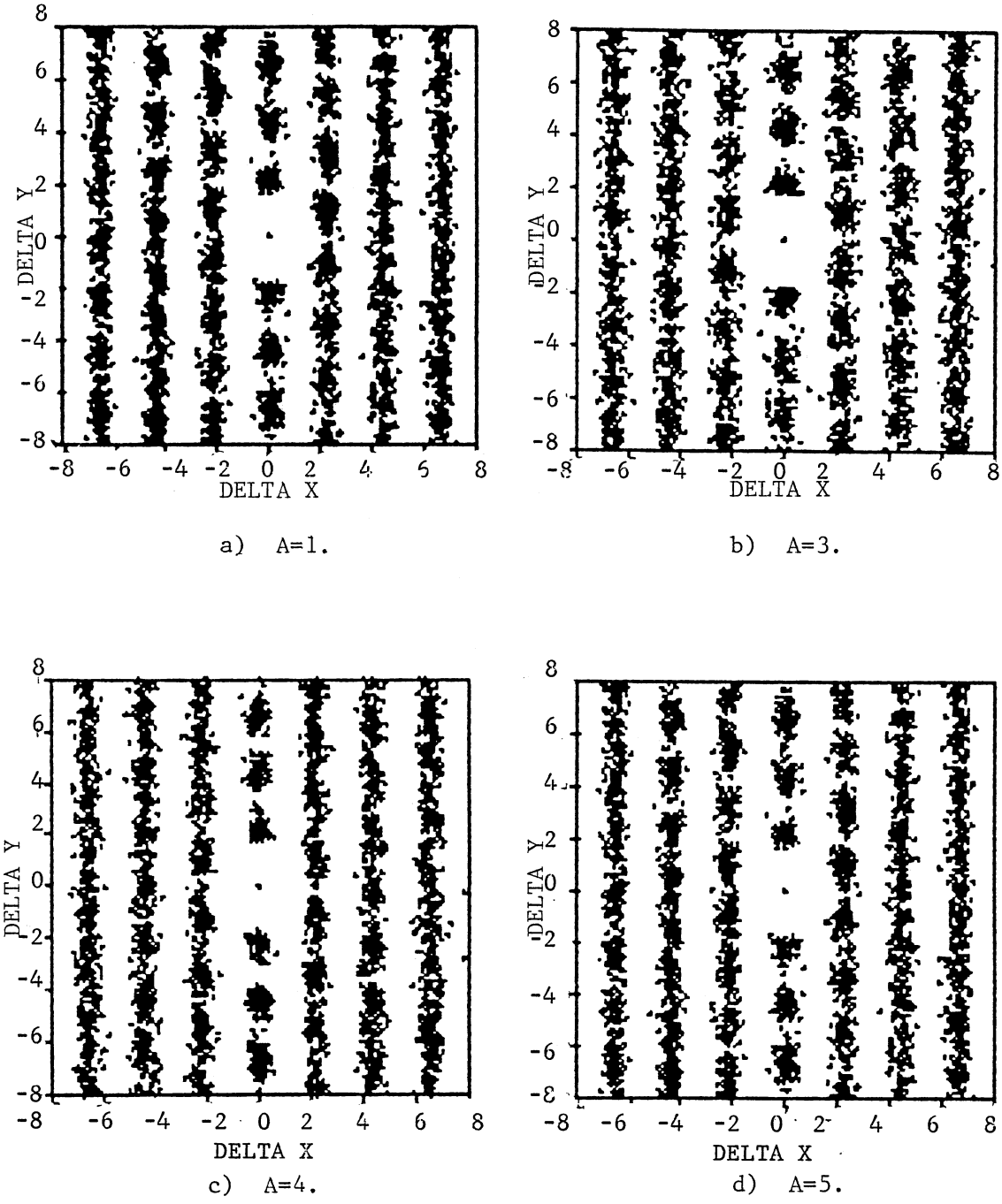

Figure 103. 2D Pair Correlation Function for MC Simulation of 100 Particles in 22aX22a Box, Interacting via a Screened Coulomb Potential (k*a=5) and in the Presence of a Sinusoidal Potential (d=2.2a) with Unitless Amplitudes of: a) 1, b) 3, c) 4 and d) 5.

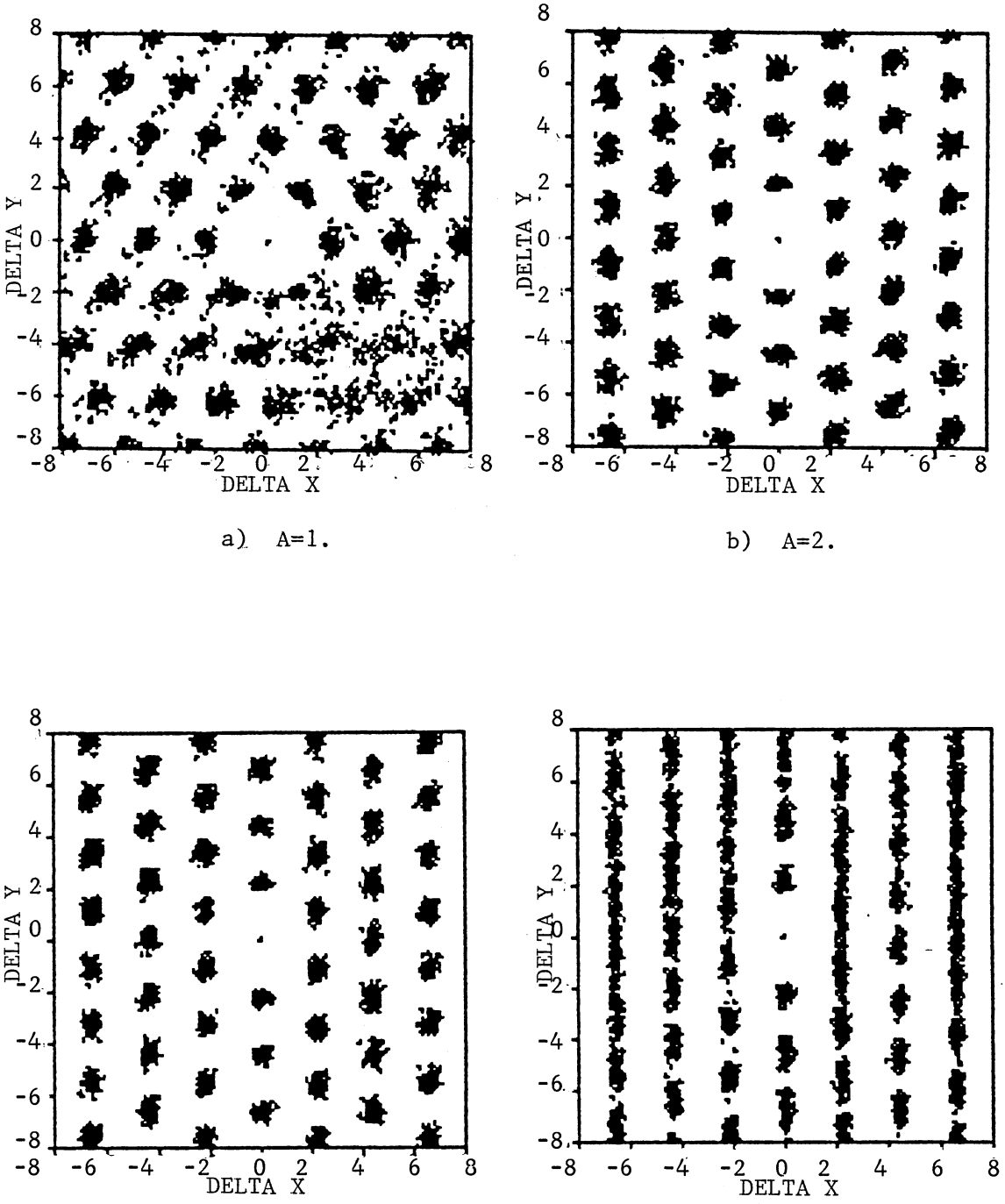

a) A=1.

b) A=2.

c) A=4.

d) A=10.

Figure 104. 2D Pair Correlation Functions for MC Simulation of 100 Particles in a 22aX22a Box, Interacting via a Screened Coulomb Potential (k*a=4) and in the Presence of a Sinusoidal Potential (d=2.2a) with Unitless Amplitudes of: a) 1, b) 2, c) 4 and d) 10.

equilibrium phase (Figure 83c) was subjected to the sinusoidally varying external potential with period of 2.0a, it is observed that at low amplitudes (A<8) the crystalline lattice did not change its order in the external field (Figures 105). However, at large enough amplitude the start up crystalline order was forced to form a new HCP lattice structure, as shown in Figure 105d.

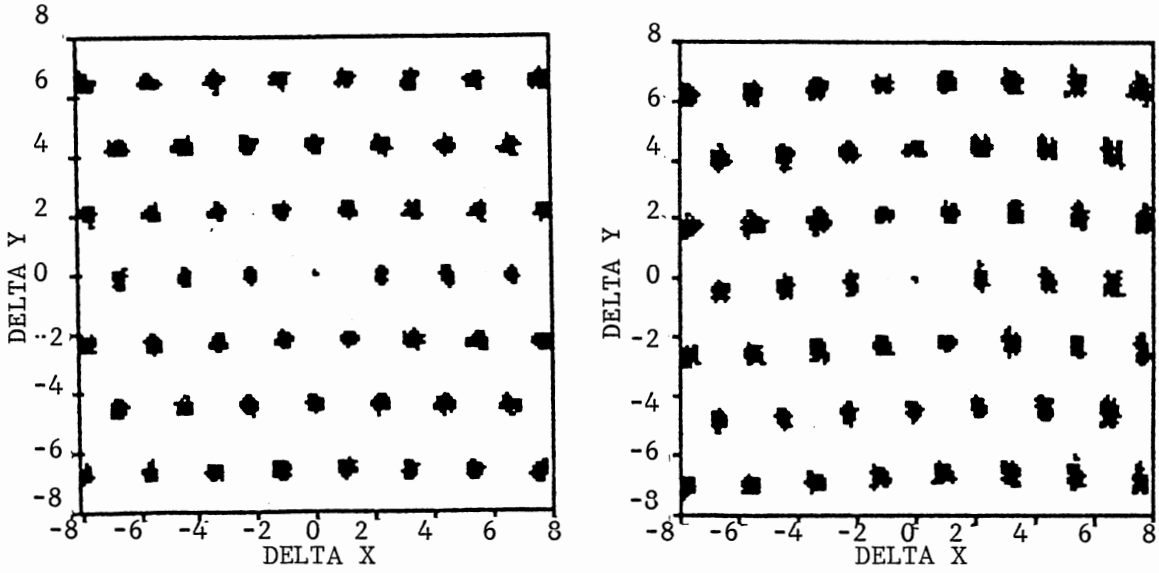

a) A=3. b) A=5.

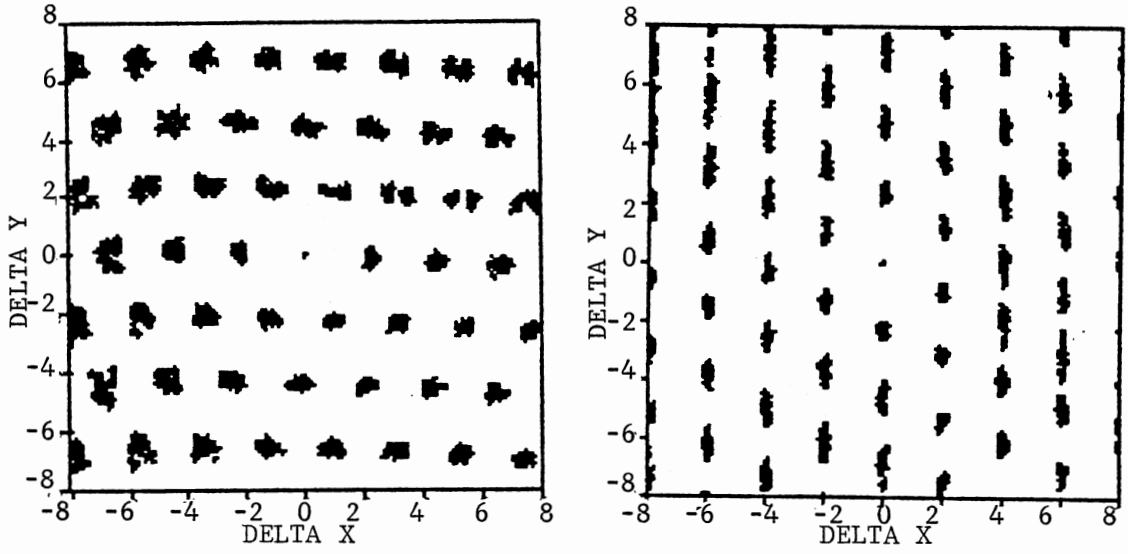

c) A=8. d) A=50

Figure 105. 2D Pair Correlation Function for MC Simulation of 100 Particles in a 22aX22a Box, Interacting via a Screened Coulomb Potential (k*a=3) and in the Presence of a Sinusoidal Potential (d=2.0a) with Unitless Amplitudes of: a) 3, b) 5, c) 8 and d) 50.

CHAPTER VI

COMPARISON OF MONTE-CARLO SIMULATIONS AND EXPERIMENTAL RESULTS

All the experimental samples used in this thesis work have experienced some structural transformation when exposed to periodic radiation field produced from the two wave mixing of 488nm Argon-Ion laser beams. The final ordering of the electrostatically interacting colloidal suspensions was observed to be time dependent on the radiation forces and the initial equilibrium phase.

The monolayer amorphous regions were analyzed experimentally at three crossing angles (15.1, 12.13 and 8.38 degrees), ranging from commensurate to very incommensurate fringe periods. The density of the equilibrium phases at these crossing angles and all input powers stayed within 3% from the constant value of $1.8 \times 10^{11}/m^2$. This same density was used in the Monte-Carlo simulation of 100 point particles interacting via a screened coulomb potential and bounded by a 20.44aX23.67a or a 22ax22a box with periodic boundary condition. The effect of the externally applied potential is incorporated in the simulation by adding to the Hamiltonian of the system a sinusoidally varying potential term. The amplitude of this potential was changed continuously from the lowest to the highest values used. In some cases the given amplitudes were applied directly to the equilibrium phase, The results obtained with this later procedure had more string like behavior at lower amplitudes than what is observed in the former

case. The periods used in the simulations were chosen to fit periodically within the given box's length, for both larger and smaller than commensurate periods. All MC simulations showed some kind of transformation at some given field amplitude.

To compare the experimental observations to MC simulations, the pair correlation functions for the two dimensional experimental equilibrium phases (Figures 19, 28 and 37) are compared with those found in the MC phase transition results (Figures 79, 80, 82 and 83). The 2D correlation functions show no orientational nor translational order. The experimental correlation functions are averaged over a small time period and fewer files than those used for The MC simulations. The observed peaks for the g(r) functions, shown in Figures 19a, 28a, 37a and 79b are compared in Table XII in terms of their height, FWHM, and position. The peak heights of g(r) and their prospective positions are shown in Figure 106. The similarities between the given data is well within the expected experimental errors. It is found that the phase obtained at normalized inverse screening length of $k^*a=5$ represents the experimental amorphous phases used in the two dimensional analysis. From this analysis we infer that an ion concentration of about $2.5 \times 10^9 m^{-3}$ is present in the experimental samples.

When the externally applied potential at commensurate fringe period (da=1.73 for the experimental case and da=1.713 for the MC simulation) was applied to the amorphous phases (Figure 19a and 79b), the induced order for both cases was the same. The amplitudes used in the simulation are not exactly equal to the equivalent experimental intensities (with and without the final size corrections), but they do

TABLE XII

ANALYSIS OF THE ONE DIMENSIONAL PAIR CORRELATION FUNCTIONS OF THE LIQUID PHASES USED IN THE MC SIMULATION AND THE 2D EXPERIMENTS.

Figure #	Peak Positions/a		Normalized Amplitudes		Peaks FWHM/a
	#1	#2	#1	#2	#1
19b	2.13	4.19	2.45	1.4	.72
28b	1.93	3.91	2.44	1.32	.50
37b	2.0	4.0	2.47	1.66	.56
79b	2.0	4.04	2.47	1.42	.66

#1 = first peak.

#2 = second peak.

a = particle diameter

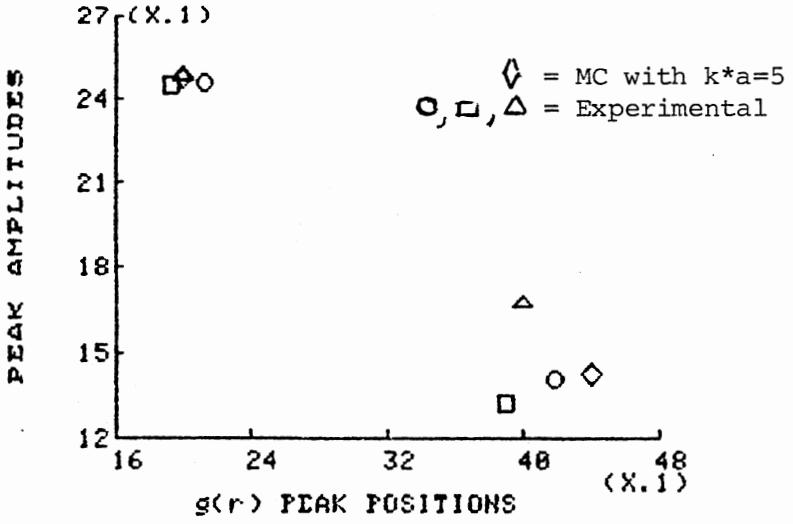

Figure 106. Comparison Between the 1D Pair Correlation Functions (g(r)) Obtained from the MC Simulation (k*a=5) and the Monolayer Experimental Amorphous Phases.

in general span the same range used experimentally. A comparison between the normalized peaks of the density distribution of the 2D correlation functions (Figures 24, 25, 26, 85, 86, 87 and 88) is demonstrated in Figure 107, where the plotted data is given in Table XIII. This analysis shows that at commensurate period both the simulation and the experiment formed a HCP structure with lattice constant of 2.21a and 2.4um (or in terms of unitless lattice constants 2.21 and 2.24) respectively. The formation of well defined peaks at the given positions, their heights and their FWHM are all within the same range although the percent difference in some cases was as high as 15% which well within the measurements error of 20%. Thus the MC simulation for the commensurate periods agrees well with the experimental results.

The experimental fringe period of 2.2um is compared to the MC simulation with the external potential's period of 2.02a (or da=2.04 and 2.02 respectively). The distorted HCP structures observed experimentally had lattice constants of 2.33um and 2.42um (or in terms of a sphere radius 2.18a and 2.26a), while the MC simulation's lattice constants were 2.1a and 2.25a. At the low field powers both the simulation and the experiment showed well defined peaks as demonstrated in the density distribution functions (Figures 34, 35, 36, and 91 to 94). However as the strength of the external potential increased the correlation between adjacent wells gets masked by the string like behavior for both cases. The comparison between the average density distribution functions for the simulation and the experiment is given in Table XIV. A plot the the peak heights versus their positions is given in Figure 108, this shows that the agreement

TABLE XIII

COMPARISON BETWEEN DENSITY DISTRIBUTION PLOTS
OBTAINED FROM MC SIMULATIONS (da=1.713)
AND 2D EXPERIMENT (da=1.73)

Box Size (d/2)	A/kT	P (mW)	Y-average/a #1	#2	#3	Normalized Peak Heights #1	#2	#3	Peak's FWHM/a #1	#2	#3
-1 to 1	1	-	4.1	5.0	-	.16	.15	-	-	-	-
-1 to 1	5		2.7	5.4	-	.18	.16	-	1.1	1.1	-
-1 to 1	10		2.7	5.2	-	.22	.19	-	.79	1.1	-
-1 to 1	30		2.6	5.1	-	.18	.16	-	1.0	1.0	-
-1 to 1		42	2.9	6.0	-	.21	.12	-	.81	1.0	-
-1 to 1		86	3.2	6.3	-	.20	.19	-	.75	.75	-
-1 to 1		111	3.1	6.1	-	.19	.16	-	.73	.85	-
1 to 3	1	-	1.4	3.8	-	.16	.11	-	1.3	1.2	-
1 to 3	5	-	1.5	4.2	6.6	.21	.17	.17	.75	1.1	1.2
1 to 3	10	-	1.4	4.0	6.5	.22	.20	.16	.75	.9	1.1
1 to 3	30	-	1.4	3.9	6.5	.23	.18	.12	.75	1.0	1.2
1 to 3		42	1.4	4.4	7.4	.22	.16	.12	.60	1.0	.85
1 to 3		86	1.6	4.8	7.8	.21	.19	.13	.81	1.0	.85
1 to 3		111	1.6	4.7	7.7	.23	.15	.14	.70	1.1	.90
3 to 5	5		.25	2.8	5.4	.22	.17	.16	.63	1.2	1.1
3 to 5	10		0	2.7	5.3	.20	.19	.18	.88	1.1	1.1
3 to 5	30		0	2.8	5.1	.22	.18	.18	.75	1.0	1.1
3 to 5		42	0	3.0	5.9	.14	.15	.12	1.1	1.1	1.0
3 to 5		86	0	3.2	6.2	.19	.18	.16	.88	.85	.80
		111	0	3.1	6.1	.21	.16	.15	.60	.95	1.0

A/kT = Normalized amplitude used in MC simulations

P = Single beam power used in the crossed beam experiments

a = particle diameter

#1 = first peak

#2 = second peak

#3 = third peak

TABLE XIV

COMPARISON BETWEEN DENSITY DISTRIBUTION PLOTS
OBTAINED FROM MC SIMULATIONS (d=2.02a)
AND 2D EXPERIMENT (d=2.14um)

Box Size (d/2)	A/kT	P (mW)	Y-average/a #1	#2	#3	Normalized Peak Heights #1	#2	#3	Peak's FWHM/a #1	#2	#3
-1 to 1	1		2.2	4.7	6.8	.23	.17	.15	.88	1.1	1.1
-1 to 1	5		2.4	4.8	7.1	.22	.16	.14	.75	1.1	1.1
-1 to 1	10		2.3	4.6	6.9	.28	.19	.16	.62	1.1	1.1
-1 to 1	30		2.2	4.4	6.9	.28	.19	.16	.62	1.0	1.1
-1 to 1		42	2.1	4.4	6.5	.38	.27	.18	.50	.75	1.0
-1 to 1		65	2.1	4.4	6.4	.23	.18	.14	.75	1.1	1.2
-1 to 1		165	2.3	4.4	6.6	.31	.23	.18	.58	.80	1.2
1 to 3	1	-	1.2	3.4	5.7	.13	.15	.16	1.2	1.2	1.0
1 to 3	5	-	1.2	3.5	5.7	.18	.16	.15	1.0	1.1	1.1
1 to 3	10	-	1.2	3.5	5.8	.17	.17	.15	.62	1.1	1.4
1 to 3	30	-	1.3	3.4	5.5	.19	.16	.15	1.0	1.2	1.4
1 to 3		42	1.1	3.2	5.3	.11	.11	.11	1.5	1.5	1.5
1 to 3		165	1.4	4.2	7.0	.19	.16	.14	.51	.88	1.1
3 to 5	5		.25	2.6	4.6	.12	.14	.12	1.4	1.0	1.2
3 to 5	10		0	2.4	5.5	.15	.15	.15	1.0	1.0	1.1
3 to 5	30		0	2.4	4.8	.15	.15	.15	1.0	.80	1.2
3 to 5		42	.25	2.1	4.3	.11	.11	.11	1.2	1.2	1.2
3 to 5		165	0	2.2	4.3	.12	.12	.12	1.0	1.1	1.1

A/kT = Normalized amplitude used in MC simulations

P = Single beam power used in the crossed beam experiments

a = particle diameter

#1 = first peak

#2 = second peak

#3 = third peak

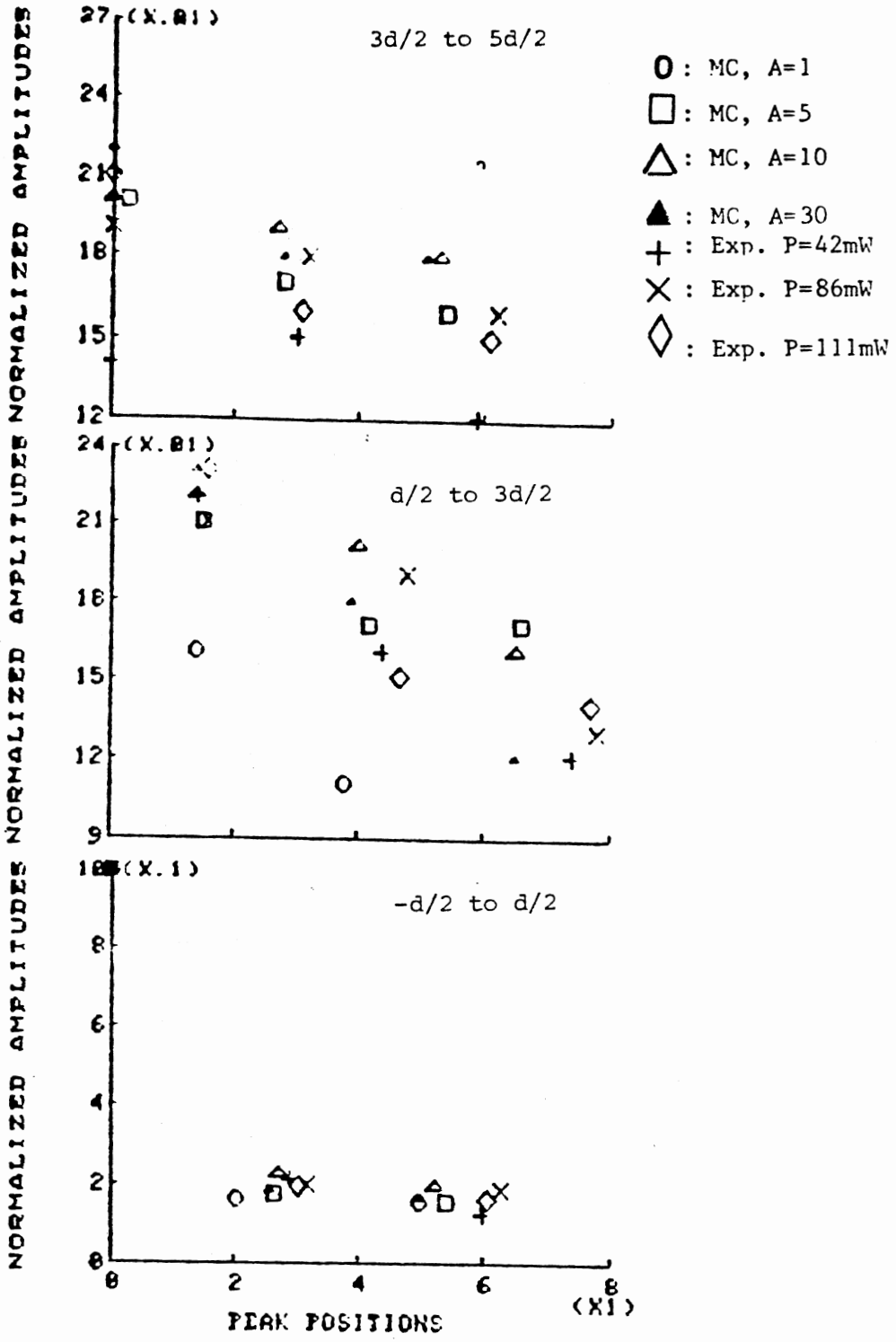

Figure 107. Peak Amplitudes Versus Positions of the Average Density Distribution Functions of the 2D Correlation Functions (d=1.71a and 1.87um).

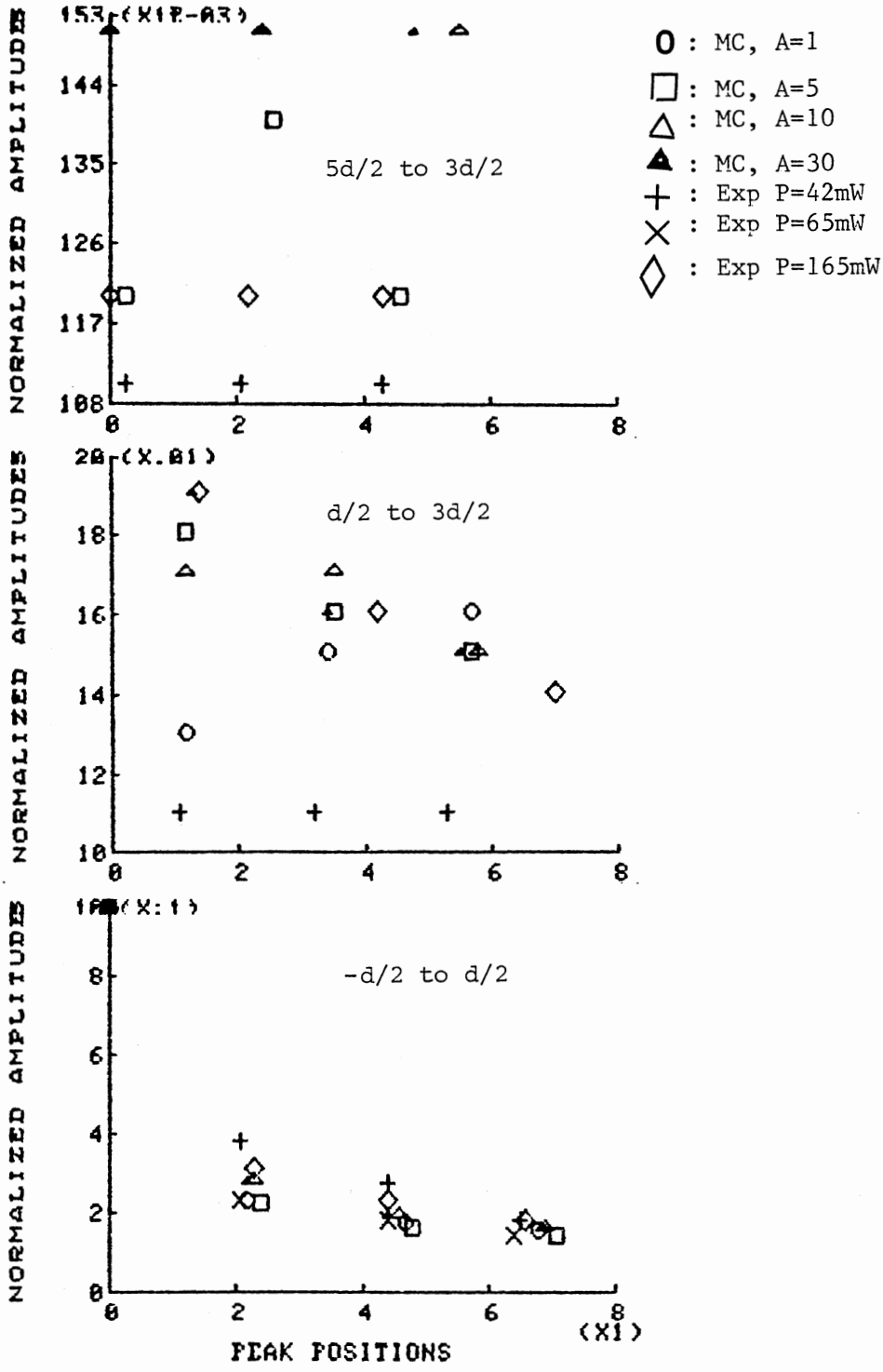

Figure 108. Density Distribution Functions Peaks Amplitudes Versus their Positions for Fringe Periods of 2.02a (MC Simulation) and 2.2um (Experimental).

between the simulation and the experiment at the given fringe periods is very good up to distances of 2d.

The experimental fringe period of 3.3um is compared to the MC simulation with potential's period of 2.92a (da=3.08 and 2.92). The 2D pair correlation functions (Figures 41 to 43 and 96) show that at low amplitudes of the externally applied potential the particles don't show any correlation, but as the field's amplitude is increased the particles are forced in the potential's minima. A comparison of the induced order at these fringe periods is given in Table XV where the amplitudes, positions and FWHM of the average density distribution functions (Figures 44 to 46 and 97 to 100) are presented. A plot of the normalized amplitudes of the observed peaks versus their prospective positions is given in Figure 109. Although the data in this figure does not show any systematic trends their appear to be a good agreement between the MC simulation results and the experimental observations.

In general we can conclude that the MC simulation gives a good theoretical prediction of the laser induced freezing of the charged colloidal suspensions.

TABLE XV

COMPARISON BETWEEN DENSITY DISTRIBUTION PLOTS
OBTAINED FROM MC SIMULATIONS (d=2.92a)
AND 2D EXPERIMENT (d=3.31um)

Box Size (d/2)	A/kT	P (mW)	Y-average/a #1	#2	#3	Normalized Peak Heights #1	#2	#3	Peak's FWHM/a #1	#2	#3
-1 to 1	1		2.0	4.2	-	.28	.20	-	.62	.75	-
-1 to 1	5		1.9	3.9	5.8	.42	.27	.24	.38	.69	.88
-1 to 1	20		1.8	3.3	5.1	.82	.56	.50	.38	.5	.75
-1 to 1	30		1.8	3.3	4.9	.70	.46	.53	.38	.46	.62
-1 to 1		42	2.1	4.3	-	.22	.14	-	1.0	1.3	-
-1 to 1		86	2.4	4.7	-	.19	.14	-	1.0	1.0	-
-1 to 1		165	2.1	4.3	-	.29	.19	-	.78	1.4	-
1 to 3	5	-	.75	1.2	2.8	.19	.19	.19	1.2	1.2	1.3
1 to 3	20	-	.50	1.2	2.0	.22	.22	.14	.85	.88	1.1
1 to 3		42	.48	1.7	4.0	.16	.13	.13	1.0	1.5	1.5
1 to 3		165	.50	1.9	2.9	.17	.17	.17	1.1	1.0	1.2
3 to 5	5		0	1.5	1.9	.19	.19	.19	.75	.75	1.0
3 to 5	20		.75	1.0	2.8	.23	.18	.16	.88	1.0	1.0
3 to 5		165	.38	1.9	2.5	.22	.16	.15	.88	1.1	1.4

A/kT = Normalized amplitude used in MC simulations

P = Single beam power used in the crossed beam experiments

a = particle diameter

#1 = first peak

#2 = second peak

#3 = third peak

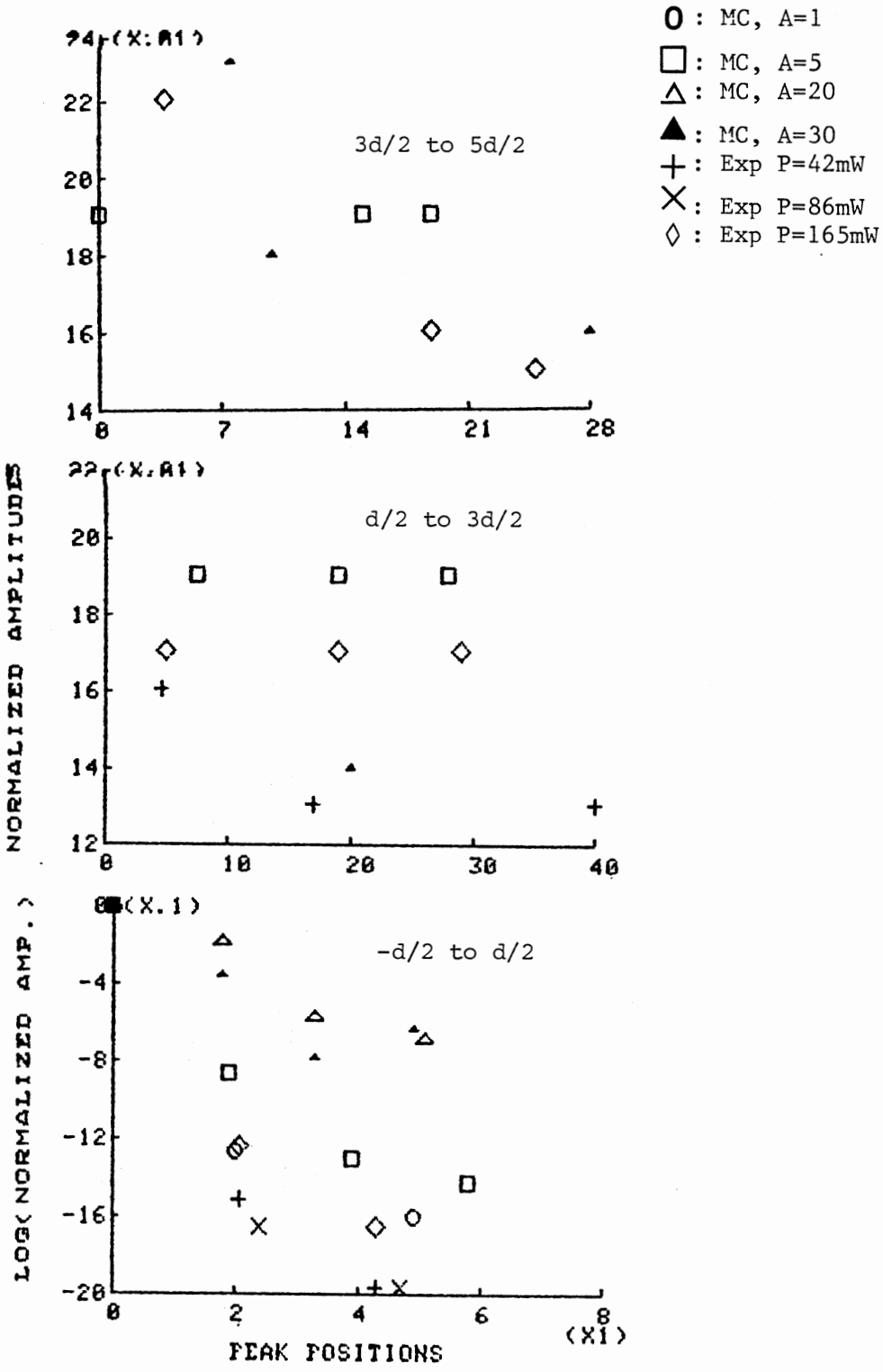

Figure 109. Density Distribution Functions Peaks' Amplitudes their Positions for Fringe Periods of 2.92a (MC Simulation) and 3.3um (Experimental)

CHAPTER VII

CONCLUSIONS AND FUTURE SUGGESTIONS

SUMMERY OF THE RESULTS

The main body of this thesis work has shown that the radiation forces created by the crossing of two mutually coherent laser beams can be used to induce order in highly charged colloidal suspensions. This forced order has been found to depend on the start up equilibrium phase, the radiation intensity, the time of exposure and the periods of the sinusoidal standing fringe pattern.

The monolayer amorphous equilibrium phase, with an average particle separation of the order of twice a sphere's diameter (2.0um), when exposed to the applied external field was observed to have the following behavior:

I. At commensurate crossing angles, the system organized in HCP structures where the localization of the system depended on the input powers.

II. As the crossing angle was made larger than commensurate, or as the fringe period was increased, the following observations were made:

1) For d=2.1um the structure observed at the lowest input powers had lattice constants of 2.3um and 2.44um. As the laser's power was increased, the localization along the high intensity regions became more pronounced and string like behavior of the particles' distribution started to develop. This string like behavior is believed to be

a result of the 5% number of dumbbells present in the analysis regions.

At high enough powers a heating of the analysis region resulted in convections which eventually led to string like behavior in the 2D correlation functions, and to density change of the system. Regions with such behavior were not analyzed in this work.

2) For d=3.3um the alignment of the microspheres in the high intensity regions was hindered by their coulombic interaction leading to minimal correlation between adjacent columns at moderate input powers (<100mW). At the higher powers (165mW) the localization along the intensity maxima became stronger and correlation between adjacent wells started to develop.

III. The induced order and localization of the particles seemed to be continuously dependent on the applied field's strength.

IV. Heat convection effects were observed to produce string like behavior in the 2D pair correlation functions and to cause a density change (drift) in the analyzed regions.

The amorphous multilayer regions used in this work were observed to go through the following transformations when exposed to the radiation forces:

I. As the input power was increased the longitudinal component of the radiation field forced the microspheres to end up in a monolayer regime. This forced monolayer developed at a faster rate when the radiation forces were caused by the crossing of two laser beams rather than by a single beam.

II. The system's density increased by as much as 25% when the beams were crossed. There was also a density drift observed at all

crossing angles.

III. At commensurate periods (d=1.85um) the mulilayer system organized in a HCP structure; and this structure persisted even when the forced monolayers started developing.

III. At the noncommensurate crossing angles it was found that:

1) For d=2.34um the multilyer region formed a distorted HCP structure where the localization of the spheres increased with input power up to 111mW. For input powers larger than 111mW a forced monolayer over the whole analysis area was observed, and the correlation between adjacent wells started to decrease as the power increased. This is believed to be a result of heat convection.

2) For d=3.34um an increase in the radiation field at the forced monolayer (>86mW) forced the spheres to get well localized within the intensity minima. At powers larger than 161mW the correlation between adjacent wells became more pronounced showing a distorted HCP lattice.

The Monte-Carlo simulations on the two dimensional Coulomb gas showed a phase transition from a fluid to a crystalline phase at normalized inverse screening length between 4 and 5. It was found that the MC liquid phase at k*a=5 was analogous to the observed experimental amorphous phases. Changing the dimensions of the box used in these simulations from 20.44aX23.67a to 22aX22a caused a distortion in the observed equilibrium phases.

When a sinusoidal varying potential was incorporated in the MC simulation and run for different equilibrium phases at different potential's periods the following were observed:

I. All the equilibrium phases showed some kind of transformation or rearrangement when exposed to the external potential. The final

ordering occurred at different amplitudes of the applied potential, depending on the start up equilibrium phase.

II. For the amorphous equilibrium phases (k*a=5), the external potential caused the localization of the spheres along its minima. This localization is a continuous function of the field's amplitude.

III. When the amorphous equilibrium phase (k*a=5) in the 20.44a by 23.67a box was exposed to the external potential at periods of 1.713a, 2.02a and 2.92a, the induced ordering results were consistent with the experimental findings at corresponding fringe periods of 1.85um, 2.14um and 3.3um. These results can be summarized as:

1) At the 1.713a periods the simulation resulted in an HCP structure with lattice constants that were comparable to those found experimentally. The positions, heights, and FWHM of the particles along the potential's minima were also consistent with the experimental observations at a fringe period of 1.85um.

2) The organization of the particles at a 2.02a MC fringe period was consistent with the experimental results at a 2.14um fringe period, where a distorted HCP lattice was observed.

3) The MC potential period of 2.92a was found to localize the interacting particles along the potential's minima at about the same external field's amplitudes as what was seen with the experiment at a fringe period of 3.3um. The final structuring of the MC system showed more peaks than observed experimentally. These peaks' positions and amplitudes were also slightly different (Table XV).

IV. The MC 22aX22a box was found to cause a distortion in the formed structures. The ordering of the liquid phase (k*a=5) in this box with external potential periods of 2.0a, 2.2a, and 4.4a showed the

same general behavior as the 20.44aX23.67a box except for the string like behavior that appeared at much less amplitudes than observed in the latter case.

Suggestions For Future Work

The work carried so far on the laser induced freezing of colloidal suspensions could be extended to study many interesting physical phenomena both experimentally and through an MC simulation. Among these are:

I. The nature of two-dimensional phase transition. By varying the crossing angles continuously and the laser's input powers, scattering results and real space analysis should provide enough data to construct translational as well as orientational correlation lengths which should provide information about the nature of the phase transition.

II. The response of three dimensional (Multilayered) systems to the external field.

III. The creation of a translating fringe pattern for the study of the drag near a plane wall.

BIBLIOGRAPHY

1) Murray, C. A., D. H. Van Winkle. "Experimental Observation of Two-Stage Melting In A Classical Two-Dimensional Screened Coulomb System." Physical Review Letters, Vol. 58, No. 12 (March 1987), pp. 1200-1203.

2) Hachisu, S., Y. Kobayashi, A. Kose. "Phase Separation in Monodisperse Latexes." Journal of Colloidal Interface Science, Vol. 42, No. 2 (Feb. 1973), pp. 342-348.

3) Van Megen, W., I. Snook. "Structure And Ordering In Dilute Dispersions Of Spherical Particles." The Journal Of Chemical Physics, Vol. 66, No.2 (15 January 1977), pp. 813-817.

4) Van Winkle, D. H., C. A. Murray. "Layering Transitions In Colloidal Crystals As Observed By Diffraction And Direct Lattice Imaging." Physical Review A, Vol. 34 (1986), pp. 562-565.

5) B. Tansu, P. Peiranski, and L. Stzelecki. "Thin Colloidal Crystals: A Series Of Structural Transitions." Journal De Physique, Vol. 44 (April 1983), pp.531-536.

6) Pansu, B., Pi. Pieranski, Pa. Pieranski. "Structures Of Thin Layers Of Hard Spheres: High Pressure Limit." Journal De Physique, Vol. 45 (Februaty, 1984), pp.331-339.

7) Alexander, S., P. M. Chaikin, P. Grant, G. J. Morales, P. Pincus. "Charge Renormaliztion, Osmostic Pressure, and Bulk Modulus Of Colloidal Crystals: Theory." Journal of Chemical Physics, Vol. 80, No. 11 (1 June 1984), pp. 5776-5779.

8) Pieranski . "Colloidal Crystals." Physical Review Letters, Vol. 45, No. 7 (18 Aug. 1980), pp. 569-572.

9) Chowdhury, A. H., F. Wood, K. Loudiyi, B.J. Ackerson. "External Field Induced Order in Suspensions." ORDERING AND ORGANIZATION IN IONIC SOLUTIONS. Ed. N. Ise and I. Sogami. Singapore: 1988, pp. 367-375.

10) Chowdhury, A. H. "Laser Induced Freezing." (Unpub. Ph.D. dissertation, Oklahoma State University, 1986.)

11) Chodhury, A. H., B. J. Ackerson, F. Wood. "Transverse Radiation Pressure Forces on Finite Sized Colloidal Particles." (To be Published.)

12) Chowdhury, A. H., B.J. Ackerson. "Laser Induced Freezing." Physical Review Letters, Vol. 55, No. 8 (19 August 1985), pp. 833-836

13) Sogami, I., N. Ise. "On The Electrostatic Interaction In Macoionic Solutions." Journal of Chemical Physics, Vol. 81, No. 12 (15 Dec. 1984), pp. 6320-6332.

14) Sogami,I. "Effective Potential Between Charged Spherical Particles In Dilute Suspension." Physics Letters, Vol. 96A, No. 4 (27 June 1983), pp. 199-203.

15) Overbeek,J. T. G. "On the Electrostatic Interaction in Macroionic Solutions and Suspensions." Journal of Chemical Physics, Vol 87, (1987)pp. 4406.

16) Ise, N., K. Ito, T. Okubo, S. Dosho, I. Sogami. "Ordered Structure in Dilute Suspensions of Highly Charged Polymer Lattices as Studied by Microscopy." American Chemical Society Journal, Vol. 107, pp. 8074-8077

17) Chaikin, P. M., J. M. Meglio, W. D. Dozier, H. M. Lindsay, D. A. Weitz. "Colloidal Crystals." Physics of Complex and Supermolecular Fluids. Ed. A. Safran and N. A. Clark. New York: New York, 1987, pp. 65-81.

18) Kosterlitz, J. M., D. J. Thouless. "Ordering, Metastability and Phase Transitions In Two-Dimensional Systems." Journal of Physics. C: Solid State Physics, Vol. 6 (1973), pp. 1181-1202.

19) Halperin, B. I., D. R. Nelson . "Theory of Tow-Dimensional Melting." Physical Review Letters, Vol.41, No. 2 (10 July 1978), pp. 121-124.

20) Young, A. P. "Melting and The Vector Coulomb Gas in Two Dimensions." Physical Review B, Vol. 19, No. 4 (15 Feb. 1979), pp. 1855- 1866.

21) Allen, M. P., D. Frenked, W. Gignac. "A Monte Carlo Simulation Study Of The Two-Dimensional Melting Mechanism." Journal of Chemical Physics, Vol 76, No. 6, pp. 4206-4222.

22) Cheng H., P. Dutta, D. E. Ellis, R. Kalia. "Molecualr Dynamics Study of a Two-Dimensional System with Screened Coulomb Interactions." Journal of Chemical Physics, Vol. 85, No. 4 (15 Aug. 1986), pp. 2232-2237

23) Tang,Y., A. J. Armstrong, R. C. Mockler, W. J. O'Sullivan. "Free Expansion Melting of a Colloidal Monolayer." Physical Review Letters, Vol. 62, No. 20 (15 May 1989), pp. 2401-2404

24) Robbins, M. O, K. Kremer, G. S. Grest. "Phase Diagram and Dynamics of Yukawa Systems." Journal of Chemical Physics, Vol. 88, No. 5, (1 March 1988), pp. 3286-3312.

25) Ackerson, B. J., N. A. Clark. "Sheared Colloidal Suspensions." Physica, Vol. 118A (1983), pp. 221-249.

26) Ackerson, B. J., N. A. Clark. "Shear Induced Partial Translational Ordering of a Colloidal Solid." Physical Review A, Vol. 30, No. 2 (Aug. 1984), pp. 906-918.

27) Ashkin, A. "Application of Laser Radiation Pressure." Science, Vol. 210, No. 4474 (5 December 1980), pp. 1081-1088

28) Ashkin, A., J.M. Dziedzic. "Optical Levitation by Radistion Pressure." Applied Physics Letters, Vol. 19, No. 8 (15 October 1971), pp. 283-285.

29) Ashkin, A., J.M. Dziedzic. "Stability of Optical Levitation by Radiation Pressure." Applied Physics Letters, Vol. 24, No. 12 (15 June 1974), pp. 586-588.

30) Ashkin, A. "Acceleration and Trapping of Particles by Radiation Pressure." Physical Review Letters, Vol. 24, No. 4 (25 January 1970), pp. 156-159.

31) Gordon, J.P. "Radiation Forces and Momenta in Dielectric Media." Physical Review A, Vol. 8, No. 1 (July 1973), pp. 14-21

32) Rogovin, D., S. Q. Sare. "Phase Conjugation in Liquid Suspensions of Microspheres." Physical Review A, Vol 31, No. 4 (1985), pp. 2375-2389.

33) Rogovin, D., R. McGraw, P. Yeh. "Harmonic Phase Conjugation in Liquid Suspensions of Microparticles via Higher-Order Gratings." Physical Review Letters, Vol. 55, No. 26 (23 December 1985), pp. 2864-2867

34) Smith, P.W., A. Ashkin, W.j. Tomlinson. "Four-Wave Mixing in an Artificial Kerr Medium." Optics Letter, Vol 6, No . 6 (June 1981), pp. 284-286

35) Leger, L., H. Hervet, F. Rondelez "Reptation in Entangled Polymer Solutions by Forced Raylegh Light Scattering." Macromolecules, Vol. 14, No. 6 (Nov.-Dec. 1981), pp. 1732-1738.

36) Hervet, H., W. Urbach, F. Rondelez "Mass Diffusion Measurements in Liquid Crystals by a Novel Optical Method." Journal of Chenical Physics, Vol. 68 (15 March 1978), pp. 2725-2729.

37) Dozier, B., H. M. Lindsay, P. M. Chaikin, H. Hervet, L. Leger. "Self Diffusion Constant and Viscosity of Charged Polystyrene Colloids." Liquid Crystals and Ordered Fluids, E. A. C. Griffin and J. F. Johnson. New York: Plenum Press,1984, pp. 987.

38) Rewo, L. "Enhancement and Detectionof Convesx Objects Using Regression Models." Computer Vision, Graphics, and Image Processing, Vol. 25 (1984), pp. 257-269.

39) Dyrdal, I. "Image Processing Algorithm for Automatic Detection and Position Assignment of Monodispersed Polystyrene Spheres from Microscope Images." Journal of Applied Physics, Vol. 60 (15 Sept. 1986), pp. 1913- 1915.

40) "Movement of Small Particles by bLight." American Scientist, Vol. 62, No.1, January-February 1974, pp. 92-98.

41) Ackerson, B. J., A. H. Chowdhury. "Cross-Correlation Intensity Fluctuation Spectroscopy and Laser Trapping Studies of Colloidal Suspensions." Kinam, Vol. 7, Serie A (1986), pp. 107-120.

42) Bak, P. "Commensurate Phases, Incommensurate Phases and the Devil's Staircase." Rep. Prog. Phys., Vol. 45 (1982), pp. 587-628.

43) Pieranski, P. "Two-Dimensional Interfacial Colloidal Crystal." Physical Review Letter, Vol. 45, No. 7 (18 Aug. 1980), pp. 569-572.

44) Chandler, David. Introduction to Modern Statistical Mechanics. New York: Oxford University Press, Inc., 1987.

APPENDIX

```
C
C************INTS****************
C  THIS SUBROUTINE IS THE MAIN SUBROUTINE FOR DETECTION
C  OF THE SPHERES.  THE EDGE INTENSITY AND THE MAXIMUN
C  INTENSITY AND THE CRITICAL RADIUS ARE VERY CRITICAL IN
C  PICKING UP THE SPHERES.
C
      SUBROUTINE INTS
      COMMON IXI(20),IYI(20),IXF(20),IYF(20)
      COMMON IR(20),MAX(20),LEA(20)
      COMMON /BLOCK1/ IX(1200),IY(1200)
      COMMON VERBOS
      INTEGER RPIXEL,ICOM
       IFRNGO=0
       NEND=0
      IP=0
      NEW=0
4     NIT=IGET('NO. FO ITTERATIONS=?')
      DO 999 ITT=1,NIT
      IPICT=IGET('1=IGNORE TAKING A PICTURE')
      IF(IPICT.EQ.1) GOTO 111
3     CALL ISUB
      CALL VSUB
2     IANS=IGET('1=TAKE A PICTURE ')
       IF (IANS.NE.1) GOTO 2
      NEW=0
      CALL TSUB
      CALL SSUB
      IANS=IGET('1=TAKE ANOTHER PICTURE ')
      IF (IANS.EQ.1) GOTO 3
111   IF(ITT.NE.1) GOTO 90
       CALL THRESH
       TYPE*,'LOOK FOR THE FOLLOWING THINGS:'
       TYPE*,'NO. OF REGIONS,MAX INTENSITIES, EDGE INTENS'
       TYPE*,'RADII OF SPHERES,SEPARATION BETWEEN SPHERES'
       TYPE*,'AND FRINGE SEPARATION'
       CALL ISUB
       CALL SSUB
       CALL CURS(50,50)
C  THIS PART WILL CHOOSE THE INITIAL POSITION OF THE CURSOR
      NSQ=IGET('NO. OF ANALYSIS AREAS=?')
      DO 22 NN=1,NSQ
30    TYPE*,'THE PARAMETER OF REGION:',NN
      WRITE(5,10)
10    FORMAT('INPUT:IXI,IXF,IYI,IYF,MAX.&MIN. INT., AND R')
      READ(5,25) I1,I2,J1,J2,M1,M2,IR(NN)
25    FORMAT(7I4)
      IF(I1.GT.I2.OR.I2.EQ.0.OR.I1.EQ.0) GOTO 30
      IF(J1.GT.J2.OR.J1.EQ.0.OR.J2.EQ.0) GOTO 30
      IF(M2.GT.M1.OR.M1.EQ.0.OR.M2.EQ.0) GOTO 30
      IF(IR(NN).EQ.0) GOTO 30
      IXI(NN)=I1
      IXF(NN)=I2
      IYI(NN)=J1
      IYF(NN)=J2
      MAX(NN)=M1
      LEA(NN)=M2
22    CONTINUE
      JFRNG=IGET('FRINGE SEPARATION=?')
      JFRNGD=JFRNG+JFRNG
      JFRNG1=JFRNG+10
      JFRNG2=JFRNG+5
      JFRN=INT(FLOAT(JFRNG)/3.)
      TYPE*,'INSERT AV-Y DIST BETWEEN PARTICLES'
      JRA=IGET('Y-DIST=?')
      YR1=JRA
```

```
        YR2=YR1/4.
        IYR1=INT(3*YR2)
        IYR2=INT(5*YR2)
        IYR3=IYR2+INT(YR2)
        TYPE*,' INPUT THE LONGEST RADIUS'
        KA=IGET('?')
C
C  STARTING THE PROCESS OF FINDING THE PROSTECTIC CENTER
C
        TYPE*,'***D=DOUBLE BEAM, S=SINGLE BEAM'
        ICOM=ICGET('D=2-BEAMS,S=1-BEAM:')
90      IF(ICOM.EQ.'S') GOTO 900
        DO 27 NN=1,NSQ
        RP=IR(NN)
        IRP=IR(NN)+INT(RP/2.)
        IP=NEW
        NEW1=NEW+1
        M2=LEA(NN)
C
C  INTENSITY SLICING BY COLUMNS.  FINDING THE CENTER OF EACH
C  HIGH INTENSITY SLICE.
C
        DO 21 J=IXI(NN),IXF(NN)
        IRAN=0
         DO 11 I=IYI(NN),IYF(NN)
        IV=RPIXEL(J,I)
        IF (IV.LT.MAX(NN)) GOTO 66
        IRAN=IRAN+1
        IV1=RPIXEL(J,I+1)
        IF (IV1.GE.MAX(NN)) GOTO 11
        IF(IRAN.LT.IR(NN)) GOTO 66
        I1=I-INT((IRAN)/2.)
        IP=IP+1
        IX(IP)=J
        IY(IP)=I1
66        IRAN=0
11      CONTINUE
21      CONTINUE
        TYPE *,'NUMBER OF DOTS=',IP
C  THIS SECTION WILL FIND THE CENTER OF EACH SPHERE
C  AS COMPARED TO THE MAX. RADIUS OF A SPHERE,RCRT.
        TYPE*,'COMPUTING EACH SPHERE-S CENTER'
        KOMPX=IR(NN)+IR(NN)
        DO 37 L=NEW1,IP-1
        IF(IY(L).EQ.0) GOTO 37
        FLAG=0.
        X=IX(L)
        Y=IY(L)
        COUT=1.
        K1=L+1
C
C  FINDING POSITION CLUSTERS THAT ARE WITHIN A DIAMETER SEPARATION
C
        DO 48 K=K1,IP
        IXD=IABS(IX(K)-IX(L))
        IF(IXD.GT.KOMPX) GOTO 48
        IYD=IABS(IY(K)-IY(L))
        IF(IYD.GT.IR(NN)) GOTO 48
        JUM=1
        IF(IX(L).LT.IX(K)) JUM=-1
        DO 42 KI=IX(K),IX(L),JUM
        IV1=RPIXEL(KI,IY(L))
        IF(IV1.LE.LEA(NN)) FLAG=1.
42      CONTINUE
        IF(FLAG.EQ.1.) GOTO 95
        COUT=COUT+1.
        X=X+FLOAT(IX(K))
```

```
        Y=Y+FLOAT(IY(K))
        IX(K)=0
        IY(K)=0
95      FLAG=0.
48      CONTINUE
        IF(COUT.LT.IR(NN)) GOTO 37
C
C  FINDING EACH CLUSTERS CENTER
C
        INX=INT(X/COUT)
        INY=INT(Y/COUT)
C
C  DETECTION OF AN EDGE IN THE X&Y DIRECTIONS FROM EACH CENTER
C
        IR1=INY-INT(RP/3.)
        IR2=INY-KOMPX
        IR3=INY+INT(RP/3.)
        IR4=INY+KOMPX
        ZZ=0.
        CALL EDGEY(IR2,IR1,INX,ZZ,M2)
        IF(ZZ.NE.1.) GOTO 37
        ZZ=0.
        CALL EDGEY(IR3,IR4,INX,ZZ,M2)
        IF(ZZ.NE.1.) GOTO 37
        ZZ=0.
        INXV=INX+KOMPX
        INXW=INX-KOMPX
        CALL EDGEX(INX,INXV,INY,ZZ,M2)
        IF(ZZ.NE.1.) GOTO 37
        ZZ=0.
        CALL EDGEX(INXW,INX,INY,ZZ,M2)
        IF(ZZ.NE.1.) GOTO 37
        ZZ=0.
        IF(INX.LE.0 .OR. INX.GT.512) GOTO 37
        IF(INY.LE.0 .OR. INY.GT.512) GOTO 37
C  ACCEPTING THE POSITIONS AS PROCPECTIVE CENTERS
C
        NEW=NEW+1
        IX(NEW)=INX
        IY(NEW)=INY
37      CONTINUE
        TYPE*,'NEW=',NEW
27      CONTINUE
        CALL ORDER(1,NEW,JFRNG)
        JN=NEW+80
        JYMA=IYF(NSQ)+50
        CALL WP(IX(1),IY(1),0)
         TYPE *,'1=CENTER NOT NOT OK'
         JANW=IGET('?')
         IF(JANW.EQ.0) GOTO 91
         IX0=IX(1)
         IY0=IY(1)
         CALL WP(IX0,IY0,255)
         CALL INSERT(0,NEW,IX0,IY0)
C   INTERACTIVE PART TO HELP THE COMPUTER IN ACCEPTING OR REJECTING
C  THE PROSPECTIVE POSITIONS AS PARTICLES' CENTERS.
C
91      DO 70 I=1,JN
        IF(I.GE.NEW) GOTO 70
        IF(I.NE.NEW) GOTO 72
        JYMA=IY(I)+IYR2
        IF(JYMA.LE.IYF(NSQ)) GOTO 97
        GOTO 70
72      CALL WP(IX(I+1),IY(I+1),0)
        IX0=IX(I)
        IXD=(IX(I+1)-IX(I))
        IABSX=IABS(IXD)
```

```
        IYD=IY(I+1)-IY(I)
C  CHECK IF PARTICLE IS WITHIN THE PRESENT FRINGE
C
        IF(IYD.GT.0.AND.IABSX.LT.JFRNG) GOTO 74
C  GET RIDE OF POSITIONS THAT MIGHT EXIST
        IF(IYD.LE.0 .AND. IABSX.LT.JFRNG) GOTO 81
C MOVE TO A NEW FRINGE POSITION
        IF(IXD.LT.0) GOTO 81
        IF(IYD.LT.0 .AND. IXD.LT.JFRNGD) GOTO 79
        IX0=IX(I+1)
        IY0=IY(I+1)
        CALL INSERT(I,NEW,IX0,IY0)
C61      IX0=IX(I)+JFRNG
C        IF(IX0.GT.IXF(NSQ)) GOTO 70
C        IY0=IYI(1)+10
C        CALL INSERT(I,NEW,IX0,IY0)
        GOTO 70
79      JYMA=IY(I)+IYR2
        JYMI=IY(I+1)-IYR3
        IX0=IX(I+1)
        IF(JYMA.GT.IYF(NSQ)) GOTO 51
        CALL WP(IX(I+1),IY(I+1),255)
97      IY0=IY(I)+JRA
        IX0=IX(I)
        GOTO 83
51      IF(JYMI.GE.IYI(1)) GOTO 82
        JCEN=IGET('1=CENTER IS NOT O.K.')
        IF(JCEN.NE.1) GOTO 70
87      TYPE*,'1=DELETE,2=INSERT,3=CONTINUE'
        JAW=IGET('?')
        GOTO(81,82,70),JAW
C  CALL SUBROUTINE TO DELETE A PIXEL
81      CALL WIPE(I,NEW)
        IF(I.GT.NEW) GOTO 70
        GOTO 72
C  SETTING PARAMETERS TO INSERT A POSITION
82      IYD=IY(I+1)-IYI(1)
      . GOTO 60
C  CHECKING WITHIN A COLUMN TO INSERT OR DELETE A POSITION
C
74      IF(IYD.LT.IYR1) GOTO 81
        IF(IYD.LT.IYR3) GOTO 12
60      LFL=0
        YD=IYD
        FRA=YD/YR1
        IF(FRA.LT.2.0) GOTO 84
        YR7=(FRA-1.)*YR1
        IY0=IY(I+1)-INT(YR7)
        CALL WP(IX(I+1),IY(I+1),255)
        GOTO 83
84      IY0=IY(I+1)-JRA
83      CALL WP(IX(I+1),IY(I+1),255)
        CALL INSERT(I,NEW,IX0,IY0)
        GOTO 70
12      CALL WP(IX(I+1),IY(I+1),0)
70      CONTINUE
        GOTO 310
900     CALL SINGLE(NSQ,NEW,KA)
310     TYPE*,'TYPE 1 TO DELETE A SPECIFIC POSITION'
        IDE=IGET(' ')
        IF (IDE.NE.1) GOTO 320
77      TYPE*,'WHAT IS THE PARTICLES NUMBER'
        I=IGET('COUNT BY COLUMNS?')
        IF(I.GT.NEW .OR. I.LT.0) GOTO 77
        CALL WP(IX(I),IY(I),255)
        NANS=IGET('0=YES THAT WAS IT')
        IF(NANS.NE.0) GOTO 76
```

```
        I=I-1
        CALL WIPE(I,NEW)
        GOTO 310
76      CALL WP(IX(I),IY(I),0)
        GOTO 77
320     TYPE*,'IF YOU WANT TO INSERT A SPHERE-S POSITION'
        TYPE*,'TYPE 1 TO GET TO CURSOR MODE'
        INEW=IGET(' ')
        IF(INEW.EQ.0) GOTO 190
        IX0=IGET('X-?')
        IY0=IGET('Y-?')
        CALL CURS(IX0,IY0)
        NEW=NEW+1
        IX(NEW)=IX0
        IY(NEW)=IY0
        TYPE*,'IX0 &IY0',IX0,IY0
        TYPE*,'NEW=',NEW
        CALL WP(IX0,IY0,0)
        GOTO 320
C  THIS SECTION SAVES A FILE OF THE X&Y POSITIONS
C
190     TYPE*,'DO YOU WANT TO SAVE X&Y POSITIONS'
        IANS=IGET('1=YES')
        IF(IANS.NE.1) GOTO 777
        CALL ORDER(1,NEW,KOMPX)
        TYPE*,'ENTER FILE/S NAME'
        TYPE*,' '
        CALL ASSIGN(2,,-2)
        WRITE(2,END=360,ERR=361) NEW
        WRITE(2,END=360,ERR=361)(IX(I),I=1,NEW)
        WRITE(2,END=360,ERR=361)(IY(I),I=1,NEW)
        CALL CLOSE(2)
360     TYPE*,'END OF FILE'
        GOTO 363
361     TYPE*,'ERROR IN WRITING THE FILE'
363     TYPE*,NEW,'IS THE NO. OF PTS. IN ABOVE FILE'
777     CONTINUE
999     CONTINUE
385     TYPE*,'DO YOU WANT TO CONTINUE:1=Y,0=N'
        IANS=IGET('  ')
        IF (IANS.EQ.1) GOTO 111
        RETURN
        END
C  THIS PROGRAM IS 'LOUDIY.FOR' DESIGNATED FOR LOUDIYI'S PROJECT
C
C
C
C
C LINK with IPBASD to provide a runnable source.
C
C ***************** MAIN PROGRAM *****************
C
        PROGRAM DETECT
        LOGICAL VERBOS
        COMMON VERBOS
        INTEGER ICOM
        VERBOS = .TRUE.
        TYPE *,''
        TYPE*,''
        TYPE*,'  WELCOME TO B.J. ACKERSONS COLLOIDAL PHYSICS LAB'
        TYPE*,'  PROGRAM EDITED AND WRITTEN BY KHALID LOUDIYI.'
        TYPE*,'  PHYSICS DEPARTMENT, OKLAHOMA STATE UNIVERSITY.'
        TYPE*,' '
        CALL HELP
        CALL SELGRP(1)
100     ICOM = ICGET('COMMAND:')
        CALL DISPAT(ICOM)
```

```
      GOTO 100
      END
C
C  ************ LOOK *********
C  TO VIEW THE PARTICLES POSITIONS
C
      SUBROUTINE LOOK
      COMMON /BLOCK1/ IX(1200),IY(1200)
      COMMON VERBOS
      INTEGER RPIXEL
      CALL ISUB
      CALL VSUB
      CALL TSUB
      CALL SSUB
      DO 10 I=1,510,50
      DO 20 J=1,480
      CALL WPIXEL(I,J,128)
20    CONTINUE
10    CONTINUE
      DO 30 I=1,480,50
      DO 40 J=1,510
      CALL WPIXEL(J,I,128)
40    CONTINUE
30    CONTINUE
90    TYPE*,' TYPE NAME OF FILE '
      TYPE*,' '
      CALL ASSIGN(2,,-2)
      READ(2,END=200,ERR=200) N
      READ(2,END=200,ERR=200) (IX(I),I=1,N)
      READ(2,END=200,ERR=200) (IY(I),I=1,N)
200   CALL CLOSE(2)
      DO 60 I=1,N
      CALL WP(IX(I),IY(I),0)
60    CONTINUE
       TYPE*,'0=ANOTHER FILE'
       IANS=IGET('?')
       IF(IANS.EQ.0) GOTO 90
      RETURN
      END
C  *********SINGLE****************
C  THIS SUBROUTINE IS THE MAIN SUBROUTINE FOR DETECTION
C  OF A PARTICLES IN THE SINGLE BEAM EXPERIMENT
      SUBROUTINE SINGLE(NSQ,NEW,KA)
      COMMON IXI(20),IYI(20),IXF(20),IYF(20)
      COMMON IR(20),MAX(20),LEA(20)
      COMMON /BLOCK1/ IX(1200),IY(1200)
      COMMON VERBOS
      INTEGER RPIXEL
      NEW=0
90    DO 27 NN=1,NSQ   !STARTING A NEW ANALYSIS REGION
      IRP=IR(NN)+INT(RP/2.)
      IP=NEW
      NEW1=NEW+1
      DO 21 J=IYI(NN),IYF(NN)  !LOOKING AT DIFFERENT ROWS
      K3=IXI(NN)
       DO 11 I=IXI(NN),IXF(NN)  !SLICING THE INTENSITIES IN THE ROW
      IF(I.LT.K3) GOTO 11
      IV=RPIXEL(I,J)
      IF (IV.GT.LEA(NN)) GOTO 11
C  CHECKING FOR THE FIRST EDGE OF A SPHERE
C
      IFLAG=0
      K1=I+3
      IF(K1.GT.IXF(NN)) GOTO 11
      DO 30 K=I+1,K1
      IV=RPIXEL(K,J)
      IF(IV.LE.LEA(NN)) GOTO 30
```

```
        IFLAG=1
        K3=K+1
30      CONTINUE
        IF(IFLAG.EQ.1) GOTO 11
C  CHECK FOR AN EGDE IN THE Y-DIRECTION
C
        KY1=J+4
        DO 35 K=J+1,KY1
        IV=RPIXEL(I+1,K)
        IF(IV.LE.LEA(NN)) GOTO 35
        IFLAG=1
        KY3=K
35      CONTINUE
        IF(IFLAG.EQ.1) GOTO 11
        K2=K1+KA  ! STARTING TO CHECK FOR HIGH INTENSITIES
        IF(K2.GT.IXF(NN)) K2=IXF(NN)
        NEDG=0
        IFL=0
        IRAN=0
        DO 40 K=K1+1,K2
        IF(IFL.EQ.1 .OR.NEDG.GT.2) GOTO 40
        IV=RPIXEL(K,J)
        IF(IV.GT.LEA(NN)) GOTO 45
        IF(IRAN.LT.IR(NN)) GOTO 50
        DO 60 MC=K+1,K+3  ! CHECKING FOR SECOND EDGE
        IV2=RPIXEL(MC,J)
        IF(IV2.GT.LEA(NN)) IFL=1
60      CONTINUE
        IF(IFL.NE.1) NEDG=3
        K3=K  ! SETTING THE STARTING POSITION
        GOTO 40
C
C
C COUNTING THE RANGE OF THOSE PIXELS WITH HIGH INTENSITIES
C
45      IF(IV.GE.MAX(NN)) IRAN=IRAN+1
        GOTO 40
50      IF(IRAN.EQ.0) GOTO 40
        IFL=1
        IRAN=0
        K3=K
40      CONTINUE
        IF(NEDG.NE.3) GOTO 80
C
C
C  COUTING THOSE POSITION THAT WILL BE CONSIDERED FOR THE DETECTION
C
        IP=IP+1
        RAN=FLOAT(IRAN)
        IX(IP)=K3-3-INT(RAN/2.)
        IY(IP)=J
80      RAN=0.
11      CONTINUE
21      CONTINUE
        TYPE *,'NUMBER OF DOTS=',IP
C  THIS SECTION WILL FIND THE CENTER OF EACH SPHERE
C  AS COMPARED TO THE MAX. RADIUS OF A SPHERE,RCRT.
        TYPE*,'COMPUTING EACH SPHERE-S CENTER'
        CALL ORDER(NEW1,IP,IR(NN))
        KOMPX=IR(NN)+IR(NN)
        KOMPY=KOMPX+KOMPX
        DO 37 L=NEW1,IP-1
        IF(IX(L).EQ.0) GOTO 37
        X=FLOAT(IX(L))
        Y=FLOAT(IY(L))
        COUT=1.
        K1=L+1
```

```
      DO 48 K=K1,IP
      IF(IY(K).EQ.0) GOTO 48
      IXD=IABS(IX(K)-IX(L))
      IF(IXD.GT.IR(NN)) GOTO 48
      IYD=IABS(IY(K)-IY(L))
      IF(IYD.GT.KOMPY) GOTO 48
      FLAG=0.
      X3=FLOAT(IX(K))
      Y3=FLOAT(IY(K))
      IYA=INT((Y+Y3)/2.)
      IXA=INT((X+X3)/2.)
      JUM=1
      IF(IX(L).LT.IX(K)) JUM=-1
      DO 42 KI=IX(K),IX(L),JUM
      IV1=RPIXEL(KI,IYA)
      IF(IV1.LE.LEA(NN)) FLAG=1.
42    CONTINUE
      IF(FLAG.EQ.1.) GOTO 48
      JUM=1
      IF(IY(L).LT.IY(K)) JUM=-1
      DO 93 KI=IY(K),IY(L),JUM
      IF(FLAG.EQ.1.) GOTO 93
      IV=RPIXEL(IXA,KI)
      IF(IV.LE.LEA(NN)) FLAG=1.
93    CONTINUE
      IF(FLAG.EQ.1.) GOTO 48
      COUT=COUT+1.
      X=X+X3
      Y=Y+Y3
      IX(K)=0
      IY(K)=0
48    CONTINUE
      NEW=NEW+1
      IX(NEW)=INT(X/COUT)
      IY(NEW)=INT(Y/COUT)
37    CONTINUE
      TYPE*,'NEW=',NEW
27    CONTINUE
      NP=0
      CALL ORDER(1,NEW,KOMPX)
      NN=NEW
      DO 70 I=1,NN-1
      IF(I.EQ.NEW) GOTO 100
      IF(I.GT.NEW .OR. IX(I).EQ.0) GOTO 70
      DO 73 JI=I+1,NN
      IF(JI.GT.NEW .OR. IX(JI).EQ.0) GOTO 73
      ID=IABS(IX(JI)-IX(I))
      JD=IABS(IY(JI)-IY(I))
      IF(JD.GT.KOMPY .OR. ID.GT.KOMPX) GOTO 73
      YD=FLOAT(IY(JI)+IY(I))
      XD=FLOAT(IX(JI)+IX(I))
      IX(I)=INT(XD/2.)
      IY(I)=INT(YD/2.)
      IX(JI)=0
      IY(JI)=0
73    CONTINUE
100   TYPE*,IX(I),IY(I)
      CALL WP(IX(I),IY(I),0)
      TYPE*,'0=THIS POSITION IS O.K.'
      IANS=IGET('?')
      IF(IANS.NE.0) GOTO 170
      NP=NP+1
      IX(NP)=IX(I)
      IY(NP)=IY(I)
      GOTO 70
170   CALL WP(IX(I),IY(I),255)
      IX(I)=0
```

```
        IY(I)=0
70      CONTINUE
        NEW=NP
        TYPE*,'NEW=',NEW
        RETURN
        END
C
C****************WIPE*****************
C  THIS SUBROUTINE IS TO DELETE THE SEPECIFIC X-Y POSITIONS FROM
C  AN X&Y ARRAYS.
C
        SUBROUTINE WIPE(I,NEW)
        COMMON VERBOS
        COMMON/BLOCK1/IX(1200),IY(1200)
        TYPE*,'DELETING PIXELS:',IX(I+1),IY(I+1)
        CALL WP(IX(I+1),IY(I+1),255)
        NEW=NEW-1
        DO 76 J=I+1,NEW
        IX(J)=IX(J+1)
        IY(J)=IY(J+1)
76      CONTINUE
        TYPE*,'NEW=',NEW
        IX(NEW+1)=0
        IY(NEW+1)=0
        RETURN
        END
C
C ******************INSERT**********************
C
C  THIS SUBROUTINE IS FOR INSERTING A POSITION IN THE X&Y POSITION
C  ARRAYS.  THAT IS A NEW CENTER.
C
        SUBROUTINE INSERT(I,NEW,IX0,IY0)
        COMMON VERBOS
        COMMONN/BLOCK1/IX(1200),IY(1200)
        TYPE *,'INSERT A NEW POSITION AT:'
        CALL CURS(IX0,IY0)
        NEW=NEW+1
        DO 77 J=NEW,I+2,-1
        IX(J)=IX(J-1)
        IY(J)=IY(J-1)
77      CONTINUE
        IX(I+1)=IX0
        IY(I+1)=IY0
        CALL WP(IX0,IY0,0)
        TYPE*,'YOU HAVE ADDED PIXEL:',IX0,IY0
        TYPE*,'NEW=',NEW
        RETURN
        END
C
C  *************EDGEX************************
C
C  DETECTING AN EDGE IN THE X-DIRECTION FROM THE PARTICLE'S CENTER
C
         SUBROUTINE EDGEX(INX,INXV,INY,ZZ,LEA)
         COMMON VERBOS
        INTEGER RPIXEL
        DO 642 JX=INX,INXV
        IF(ZZ.EQ.1.) GO TO 642
        NOOR=RPIXEL(JX,INY)
        IF(NOOR.LE.LEA) ZZ=1.
642     CONTINUE
        RETURN
         END
C
C  **************EDGEY*****************************
C
```

```
C
C  DETECTING AN EDGE IN THE Y-DIRECTION FROM THE CENTER
C
        SUBROUTINE EDGEY(IR2,IR1,INX,ZZ,LEA)
        COMMON VERBOS
        INTEGER RPIXEL
        DO 641 JE=IR2,IR1
        IF(ZZ.EQ.1.) GO TO 641
        NOOR=RPIXEL(INX,JE)
        IF(NOOR.LE.LEA) ZZ=1.
641     CONTINUE
        RETURN
        END
C
C*********DISPLAY A CROSS***********
C
        SUBROUTINE WP(IX0,IY0,IN)
        COMMON VERBOS
        CALL WPIXEL(IX0,IY0,IN)
        CALL WPIXEL(IX0+1,IY0,IN)
        CALL WPIXEL(IX0-1,IY0,IN)
        CALL WPIXEL(IX0,IY0+1,IN)
        CALL WPIXEL(IX0,IY0-1,IN)
        RETURN
        END
C
C
C ***************** DISPATCH *****************
C
        SUBROUTINE DISPAT(ICHAR)
        INTEGER ICHAR
C
C "Case" statment to select function:
C
        IF(ICHAR.LT."40) GOTO 1000      !Ignore characters below octal 40
        IF(ICHAR.LT."77) CALL VOID      !Unrecognized character
        IF(ICHAR.EQ.'A') CALL LOOK       !VIEW POSITIONS
        IF(ICHAR.EQ.'B') CALL VOID      !Blank and unblank
        IF(ICHAR.EQ.'C') CALL CSUB      !Clear screen
        IF(ICHAR.EQ.'D') CALL CURS(X,Y)      !MOVE TARGET
        IF(ICHAR.EQ.'E') CALL GRID      !Exit
        IF(ICHAR.EQ.'F') CALL VOID      !Frame Buffer Group select
        IF(ICHAR.EQ.'G') CALL VOID      !Guard pixel planes or values
        IF(ICHAR.EQ.'H') CALL HELP      !Help routine
        IF(ICHAR.EQ.'I') CALL ISUB      !Initilization
        IF(ICHAR.EQ.'J') CALL TVVIEW    !LOAD PICTURE FORM DISKETTE
        IF(ICHAR.EQ.'L') CALL VOID      !Look Up tables
        IF(ICHAR.EQ.'M') CALL VOID      !Mode select
        IF(ICHAR.EQ.'P') CALL VOID      !Pixel Read & Write
        IF(ICHAR.EQ.'R') CALL RSUB
        IF(ICHAR.EQ.'S') CALL SSUB      !Sync select
        IF(ICHAR.EQ.'T') CALL TSUB      !Take a picture
        IF(ICHAR.EQ.'U') CALL INTS
        IF(ICHAR.EQ.'V') CALL VSUB      !View Image
        IF(ICHAR.EQ.'W') CALL VOID      !Draw wedges
        IF(ICHAR.EQ.'X') CALL THRESH    !THRESHOLD VALUE
        IF(ICHAR.EQ.'Y') CALL TRAF      !TANSFER FUNCTION
        IF(ICHAR.EQ.'Z') CALL ZSUB      !Zoom
        IF(ICHAR.EQ.'?') CALL HELP
1000    RETURN
        END
C
C ***************** HELP *****************
C
        SUBROUTINE HELP
        TYPE *,'Commands are a single capital letter as follows:'
        TYPE*,'A:CALCULATE AVERAGE OF ALREADY SAVED FILES'
```

```
        TYPE*,'C:CLEAR SCREEN TO A VALUE OF 255 INTENSITY'
        TYPE*,'E:GRID'
        TYPE*,'K:DESTORTION CORRECTION'
        TYPE*,'S:SYNC. SOURCE SELECT'
        TYPE*,'I:INITIALIZE HARDWARE'
        TYPE*,'R:ROAM (PAN AND SCREEN ROLL)'
        TYPE*,'T:TAKE A PICTURE'
        TYPE*,'V:VIEW INPUT'
        TYPE*,'Z:ZOOM'
        TYPE*,'D:MOVE TARGET'
        TYPE*,'J:LOAD PICTURE FROM DISKETTE'
        TYPE*,'K:READ OR WRITE DATA (RECTANGULAR FORMAT)'
        TYPE*,'N:READ OR WRITE DATA (POLAR FORMAT)'
        TYPE*,'?:HELP'
        TYPE*,'O:FIND THE CENTER OF THE PARTICLES IN SINGLE BEAM'
        TYPE*,'Q:PLOT INTENSITY'
        TYPE*,'Y:SELECT TRANSFER FUNCTION'
        TYPE*,'X:SELECT THRESHOLD VALUE FOR THE INTENSITIES'
        TYPE*,'U:SELECTS WINDOW AND PLOTS INTENSITY INSIDE IT'
        RETURN
        END
C***************GRID******************
C
C THIS SUBROUTINE IS TO DRAW A GRID
C
        SUBROUTINE GRID
        COMMON VERBOS
        DO 10 I=50,510,50
        DO 20 J=20,510
20      CALL WPIXEL(J,I,255)
        DO 25 K=20,510
25      CALL WPIXEL(I,K,255)
10      CONTINUE
        RETURN
        END
C
C ***************** VOID: Unrecognized command ****************
C
        SUBROUTINE VOID
        COMMON VERBOS
        IF (VERBOS) TYPE *,'Unrecognized Command.  Use ? for Help'
        RETURN
        END
C*****************THRESHOLD*****************
C
C  THIS SUBROUTINE WILL ASK FOR A THRESHOLD VALUE FOR THE INTENSITIES.
C   ALL PIXELS WITH A GREY LEVEL GREATER THAN THE THRESHOLD VALUE ARE
C   SET TO 255
C WHILE THE REST OF THE PIXELS ARE SET TO ZEROGREY LEVEL.
C
        SUBROUTINE THRESH
        COMMON VERBOS
30       CALL SELLUT(2,0)
        TYPE*,'THE THRESHOLD INTENSITY=?'
        MAX=IGET(' ')
        DO 10 I=1,MAX
10      CALL SETLUT(I,0)
        DO 20 J=MAX,255
20      CALL SETLUT(J,255)
        TYPE*,'0=CONTINUE THREHOLDING'
        IT=IGET('0=CONTINUE')
        IF(IT.EQ.0) GOTO 30
        RETURN
        END
C **************ORDERING*************
C  THIS SUBROUTINE WILL ORDER THE PARTICLES IN COLUMNS
C
```

```
      SUBROUTINE ORDER(IPI,IPF,JFRNG)
      COMMON VERBOS
      COMMON/BLOCK1/IX(1200),IY(1200)
C  THIS PART WILL ORDER THE PARTICLES IN COLUMNS.
      DO 33 I=IPI,IPF-1
      J1=I+1
      DO 39 J=J1,IPF
      IF(IX(J).GT.IX(I)) GOTO 39
      IA=IX(J)
      IB=IX(I)
      IC=IY(I)
      ID=IY(J)
      IX(I)=IA
      IX(J)=IB
      IY(I)=ID
      IY(J)=IC
39    CONTINUE
      M1=IX(I)+JFRNG
      DO 62 J=J1,IPF
      IF(IX(J).GT.M1 .OR. IY(J).GT.IY(I))GOTO 62
      IA=IX(J)
      IB=IX(I)
      IC=IY(I)
      ID=IY(J)
      IX(I)=IA
      IX(J)=IB
      IY(I)=ID
      IY(J)=IC
62    CONTINUE
33    CONTINUE
      RETURN
      END
C
C
C*********TRAF***************
C THIS IS A SUBROUTINE FOR INTENSITY EQUALIZATION
C
      SUBROUTINE TRAF
      COMMON VERBOS
      INTEGER RPIXEL
      TYPE*,'TRANSFER FUNCTION'
      TYPE*,'SELECT IA2>IA1'
      IA1=IGET('ENTER IA1')
      IA2=IGET('ENTER IA2')
      DO 10 I=20,500
      DO 20 J=20,500
      IA=RPIXEL(I,J)
      IF (IA.LT.IA1) GO TO 30
      IF (IA.GT.IA2) GO TO 40
      FA1=IA1
      FA2=IA2
      FV=(255./(FA2-FA1))*(IA-FA1)
      IV=INT(FV)
      CALL WPIXEL(I,J,IV)
      GOTO 20
30    CALL WPIXEL(I,J,0)
      GO TO 20
40    CALL WPIXEL(I,J,255)
20    CONTINUE
10    CONTINUE
      RETURN
      END
C
C ********** TVVIEW **********
      SUBROUTINE TVVIEW
      DIMENSION IZ(512)
      COMMON VERBOS
```

```
      INTEGER RPIXEL
      INTEGER X,Y,XI,XF,YI,YF
      XI=IGET('XI=?')
      XF=IGET('XF=?')
      YI=IGET('YI=?')
      YF=IGET('YF=?')
      CALL ASSIGN (2,,-2)
      DO 25 Y=YI,YF
      READ (2,END=500,ERR=500)(IZ(X),X=XI,XF)
      DO 10 X=XI,XF
      IZ(X)=INT(ABS(FLOAT(RPIXEL(X,Y)-IZ(X))))
      CALL WPIXEL(X,Y,IZ(X))
10    CONTINUE
25    CONTINUE
500   TYPE *,'END OF FILE'
      CALL CLOSE(2)
      RETURN
      END
C
C ***************** CSUB: CLEAR SCREEN *****************
C
      SUBROUTINE CSUB
      COMMON VERBOS
      INTEGER INTENS
      IF (VERBOS) TYPE *,'**** Clear Screen ****'
      INTENS =130
      CALL CLEAR(INTENS)
      RETURN
      END
C
C************CURSOR MOVEMENT************
C
C   THIS SUBROUTINE MOVES THE CURSOR TO A DESIRED POSITION
C
      SUBROUTINE CURS(IX0,IY0)
      COMMON VERBOS
      INTEGER X1,Y1,RPIXEL
      INC=1
      X1=IX0
      Y1=IY0
      IKEY=3
 50   IV=RPIXEL(X1,Y1)
      IV1=RPIXEL(X1,Y1-1)
      IV2=RPIXEL(X1+1,Y1)
      IV3=RPIXEL(X1-1,Y1)
      IV4=RPIXEL(X1,Y1+1)
      IREM=IKEY
      IZ=0
      IF (IV .LE. 128 ) IZ=255
      CALL WP(X1,Y1,IZ)
      IKEY=IGET('?')
      IF(IKEY .EQ.0) IKEY=IREM
      TYPE *,X1,Y1,IV
      CALL WPIXEL(X1,Y1,IV)
      CALL WPIXEL(X1,Y1-1,IV1)
      CALL WPIXEL(X1+1,Y1,IV2)
      CALL WPIXEL(X1-1,Y1,IV3)
      CALL WPIXEL(X1,Y1+1,IV4)
      IF(IKEY .EQ. 1 ) X1=X1+INC
      IF(IKEY .EQ. 2 ) X1=X1-INC
      IF(IKEY .EQ. 3 ) Y1=Y1+INC
      IF(IKEY .EQ. 4 ) Y1=Y1-INC
      IF(IKEY .EQ. 5) GOTO 260
      IF(IKEY.EQ.6) GOTO 10
      IF(IKEY.EQ.12) INC=10
      IF(IKEY .EQ. 11) INC=1
      IF(IKEY .EQ. 9 ) GO TO 250
```

```
        GO TO 50
260     X1=IGET('X=?')
        Y1=IGET('Y=')
        IKEY=3
        GOTO 50
10      IXF=X1+30
        IYF=Y1+30
        DO 12 I=X1,IXF
        DO 14 J=Y1,IYF
        IV=RPIXEL(I,J)
        IZ=0
        IF(IV.LE.128) IZ=255
        CALL WPIXEL(I,J,IZ)
        TYPE*,I,J,IV
        CALL WPIXEL(I,J,IV)
14      CONTINUE
12      CONTINUE
        X1=IXF
        Y1=IYF
        GOTO 50
250     IX0=X1
        IY0=Y1
        RETURN
        END
C
C ***************** ISUB: INITILIZE ****************
C
        SUBROUTINE ISUB
        COMMON VERBOS
        INTEGER WHICH
        IF (VERBOS) TYPE *,'**** Initilize Hardware Registers ****'
        WHICH='E'
        IF (WHICH.EQ.'A') CALL APINIT
        IF (WHICH.EQ.'F') CALL FBINIT
        IF (WHICH.EQ.'L') CALL LUINIT
        IF (WHICH.EQ.'E') GOTO 100
        RETURN
100     CALL APINIT
        CALL FBINIT
        CALL LUINIT
        RETURN
        END
C
C ***************** RSUB: ROAM ****************
C
        SUBROUTINE RSUB
        COMMON VERBOS
        INTEGER X,Y
        IF (VERBOS) TYPE *,'**** Roam (Pan and Scroll) ****'
        X = IGET('Pan Value=')
        Y = IGET('Scroll Value=')
        CALL PAN(X)
        CALL SCROLL(Y)
        RETURN
        END
C
C ***************** SSUB: SYNC ****************
C
        SUBROUTINE SSUB
        COMMON VERBOS
        INTEGER SOURCE
        IF (VERBOS) TYPE *,'**** Select Sync Source ****'
        SOURCE='C'
        IF (SOURCE.EQ.'P') SOURCE = 0
        IF (SOURCE.EQ.'C') SOURCE = 1
        CALL SYNC(SOURCE)
        RETURN
```

```
        END
C
C ***************** TSUB: TAKE A PICTURE ****************
C
        SUBROUTINE TSUB
        COMMON VERBOS
        IF (VERBOS) TYPE *,'**** Take A Picture ****'
        CALL SNAP
        RETURN
        END
C
C ***************** VSUB: VIEW *****************
C
        SUBROUTINE VSUB
        COMMON VERBOS
        IF (VERBOS) TYPE *,'**** View Input Image ****'
        CALL VIEW
        RETURN
        END
C ***************** ZSUB: ZOOM *****************
C
        SUBROUTINE ZSUB
        COMMON VERBOS
        INTEGER X,Y
        IF (VERBOS) TYPE *,'**** Zoom in X and Y'
        X = ICGET('Zoom X -- Y(es or N(o:')
        IF (X.EQ.'Y') X=1
        IF (X.EQ.'N') X=0
        Y = ICGET('Zoom Y -- Y(es or N(o:')
        IF (Y.EQ.'Y') Y=1
        IF (Y.EQ.'N') Y=0
        CALL ZOOM(X,Y)
        RETURN
        END
C
C ***************** USEFUL ROUTINES ****************
C
C FUNCTION ICGET('String') = Prints string and waits for a single
C character.  No line feed at the end of the string.  Character is
C automatically capitalized if proper bit is set in JSW
C (normal condition).
C
        FUNCTION ICGET(STR)
        LOGICAL*1 STR(1)
        INTEGER ANS
        WRITE (7,10,END=2,ERR=3) (STR(I),I=1,LEN(STR))
        READ(5,1) ANS
1       FORMAT(A1)
        ICGET = ANS
        RETURN

2       TYPE *,'? ICGET: END OF FILE ERROR'
        GOTO 5
3       TYPE *,'? ICGET: HARDWARE ERROR'
5       ICGET = 0
        RETURN

10      FORMAT ('$',200A1)
        END

C FUNCTION IGET('String') = Prints string and waits for a single
C integer.  No line feed at the end of the string.
C
        FUNCTION IGET(STR)
        LOGICAL*1 STR(1)
        INTEGER ANS
        WRITE (7,10,END=2,ERR=3) (STR(I),I=1,LEN(STR))
```

```
        READ(5,1) ANS
1       FORMAT(I5)
        IGET = ANS
        RETURN

2       TYPE *,'? IGET: END OF FILE ERROR'
        GOTO 5
3       TYPE *,'? IGET: HARDWARE ERROR'
5       IGET = 0
        RETURN

10      FORMAT ('$',200A1)
        END

C
C FUNCTION IOGET('String') = Prints string and waits for a single
C Octal integer.  No line feed at the end of the string.
C
        FUNCTION IOGET(STR)
        LOGICAL*1 STR(1)
        INTEGER ANS
        WRITE (7,10,END=2,ERR=3) (STR(I),I=1,LEN(STR))
        READ(5,1) ANS
1       FORMAT(O7)
        IOGET = ANS
        RETURN

2       TYPE *,'? IOGET: END OF FILE ERROR'
        GOTO 5
3       TYPE *,'? IOGET: HARDWARE ERROR'
5       IOGET = 0
        RETURN

10      FORMAT ('$',200A1)
        END
```

```
TYPE ANAL3.FOR
C
C ************************XDENS SUBROUTINE*******************
C  THIS SUBROUTINE IS FOR FINDING THE DENSITY OF THE PARTICLES
C  ALONG THE FRINGES DIRECTION
C
        SUBROUTINE XDENS(MX1,MXX1,MY1,MYY1,IFRNS,DIA)
        COMMON KK,NUMB,N,IX(300),IY(300),RP(520),PHI(520)
        DIMENSION AVX(100),STDF(100),AREA(50),DENS(50)
        FRNS=IFRNS
        TYPE*,'1-PLOT SIN(2*PI*X/PERIOD + TETA)'
        READ(5,33) IANS
33      FORMAT(I4)
        TYPE*,' 1-PRINT STATISTICAL ANALYSIS, CHANGE OUTPUT DEVICE'
        READ(5,190) JANS
190     FORMAT(I4)
        ARS=1.07/5.
        DX=FLOAT(MXX1-MX1)/FRNS
        DY=FLOAT(MYY1-MY1)/FRNS
        ABOX=DX*DY
        FAREA=FRNS*DY/FRNS
        JUMPX1=INT(DIA/5.)
        PI=4.*ATAN(1.)
        DO 50 I=1,520
        RP(I)=0.
        PHI(I)=0.
50      CONTINUE
        DO 52 I=1,100
        AVX(I)=0.
        STDF(I)=0.
52      CONTINUE
C
C  READ DATA AND FIND THE NUMBER OF PARTICLES AT EACH X-POSITION.
C
        NUMF=0
        DO 200 KK=2,NUMB+1
        CALL RDATA
        DO 20 J=1,N
        NUM=IX(J)
        IF(NUM.LE.MXX1 .AND. NUM.GE.MX1) THEN
        IF(IY(J).LE.MYY1.AND.IY(J).GE.MY1) THEN
        RP(NUM)=RP(NUM)+1.
        NUMF=NUMF+1
         ENDIF
          ENDIF
20      CONTINUE
200     CONTINUE
        TBD=(FLOAT(NUMF))/(ABOX*(FLOAT(NUMB)))
C
C  FINDING THE FOURIER COEFFICIENTS
        XD=FLOAT(MXX1-MX1)
        DIV=XD/FRNS
        MULT=INT(DIV)
        ARG=2.*PI/FRNS
        IFINAL=INT(FRNS*FLOAT(MULT))
        A1=0.
        B1=0.
        DO 300 I=MX1,IFINAL
        W=FLOAT(I)
        A=COS(ARG*W)
        B=SIN(ARG*W)
        A1=A1+A*RP(I)
        B1=B1+B*RP(I)
300     CONTINUE
        IF(A1.EQ.0.) THEN
        TETA=PI/2.
         ELSE
```

```
        TETA=ATAN(B1/A1)
         ENDIF
        TYPE*,'A1,B1,TETA=',A1,B1,TETA
        IF(IANS.EQ.1) THEN
C
C  PLOT SIN(2*PI*X/L + TETA)
C
        LENGTH =700
        IXO=300
        IYO=350
        IXI=0
        IYI=0
        WRITE(6,350) IXO,IYO
350     FORMAT(' HAU ',I4,',',I4,' O')
        XS=700./XD
        DO 310 I=MX1,MXX1
        X=FLOAT(I)
        Y=SIN((ARG*X)+TETA)
        IF(Y.LT.0.) Y=0.
        SX=XS*(FLOAT(I-MX1))
        NX=INT(SX)
        NY=INT(700.*Y)
        WRITE(6,320) NX,NY
320     FORMAT(' D ',I4,',',I4)
310     CONTINUE
        WRITE(6,330)
330     FORMAT(' U H ')
        ENDIF
C
C  FINDING THE DENSITY AND THE STATISTICS OF EACH FRINGE
C
        KC=0
        RPTM=0.
        DO 80 J=MX1,MXX1,IFRNS
        AX=0.
        AREAT=0.
        RPTT=0.
        JRPF=J+IFRNS-1
        IF(JRPF.GT.MXX1) JRPF=MXX1
        DO 85 K=J,JRPF,JUMPX1
        RPT=0.
        KF=K+JUMPX1-1
        IF(KF.GT.JRPF) KF=JRPF
        DO 210 I=K,KF
        RPT=RPT+RP(I)
        AX=(FLOAT(I))*RP(I)+AX
210     CONTINUE
        PHI(KF)=RPT
        RPTT=RPTT+RPT
        IF(RPT.GT.RPTM) THEN
        RPTM=RPT
          ENDIF
85      CONTINUE
        IF(RPTT.NE.0.) THEN
        STD=0.
        KC=KC+1
        AVX(KC)=AX/RPTT
        AREA(KC)=RPTT*ARS
        DENS(KC)=RPTT/FAREA
        DO 120 K=J,JRPF
        STD=STD+((K-AVX(KC))**2.)*RP(K)
120     CONTINUE
        STD=STD/RPTT
        STDF(KC)=SQRT(STD)
        ENDIF
80      CONTINUE
        IF(JANS.EQ.1) THEN
```

```
      WRITE(6,730) TBD
730   FORMAT(' DENSITY OF PARTICLES IN GIVEN AREA:',F12.6)
      WRITE(6,733)
733   FORMAT('  MX1, MXX1, MY1, MYY1, IFRNS, IDIA')
      WRITE(6,737) MX1,MXX1,MY1,MYY1,IFRNS,DIA
737   FORMAT(5(3X,I4),3X,F12.6)
      WRITE(6,720)
720   FORMAT('  FRINGE NO.,MEAN POS., STDV, AREA AND DENSITY')
      DO 70 I=1,KC
      WRITE(6,77) I,AVX(I),STDF(I),AREA(I),DENS(I)
77    FORMAT(3X,I4,4(3X,E12.6))
70    CONTINUE
        ELSE
C
C  SETTING THE PARAMETERS FOR THE PLOTTING AREA
C
      LENGTH=700
      JUMP=4
      IXO=1200
      IYO=350
      IXI=0
      IYI=0
      CALL BOX(IXO,IYO,LENGTH,IXI,IYI)
C
C  SETTING THE PARAMETERS FOR SCALING AND LABELING THE
C  X-AXIS.
C
      I1=0
      I2=INT(XD/FRNS)
      XS=FRNS*700./XD
      CALL XAXIS(IXI,IYI,I1,I2,JUMP,XS)
      WRITE(6,65)
65    FORMAT(' 122,-100 U S12 X-DISTANCE/PERIOD_')
C
C  SETTING THE PARAMETERS FOR LABELING AND SCALING THE
C  Y-AXIS
C
      YS=70
      JUMP=1
      I2=10
      CALL YAXIS(IXI,IYI,I1,I2,JUMP,YS)
      WRITE(6,60)
60    FORMAT(' -80,260 U S42 DENS/MAXD_')
      SCX=700./XD
      WRITE(6,68)
68    FORMAT(' U 0,0 ')
C
C  PLOTTING THE DENSITY OF THE PARTICLES PER FRINGE PERIOD
C
      WRITE(6,170)
170   FORMAT(' U 0,0 D ')
      XS=700./XD
      YS=700./RPTM
      DO 140 J=MX1,MXX1,IFRNS
      JRPF=J+IFRNS-1
      IF(JRPF.GT.MXX1) JRPF=MXX1
      DO 130 K=J,JRPF,JUMPX1
      KF=K+JUMPX1-1
      IF(KF.GT.JRPF) KF=JRPF
      NY=INT(YS*PHI(KF))
      NX=INT(XS*(FLOAT(KF-MX1)))
      WRITE(6,160) NX,NY
160   FORMAT(X,I4,',',I4)
130   CONTINUE
140   CONTINUE
      WRITE(6,180)
180   FORMAT(' U H ')
```

```
        ENDIF
        RETURN
        END
C
C  ********************************************************
C  ********************************************************
C  THIS PROGRAM IS FOR PLOTING THE PAIR CORRELATION FUNCTION G(R)
C  USING THE HOUSTON INSTRUMENT DIGITAL PLOTTER.  NOTE THAT THE
C  PLOTER BAUD RATE IS 9600.
C
        PROGRAM ANAL3
        COMMON KK,NUMB,N,IX(300),IY(300),RP(520),PHI(520)
        COMMON/BLOCK2/MAXR1,NNEIG(2,6),DIV(520),COR(5,2),PN(520)
901     DO 10 I=1,520
        RP(I)=0.
        DENSITY=0.
10      CONTINUE
999     KK=0
        CALL RDATA
        TYPE *,' DIAMETER,MINX,MAXX,MINY,MAXY'
        READ(5,50) IDIA,MX1,MXX1,MY1,MYY1
50      FORMAT(5(I4))
        DIA=FLOAT(IDIA)
        XM=(FLOAT(MXX1-MX1))/2.
        YM=(FLOAT(MYY1-MY1))/2.
        IXM=INT(XM)+MX1
        IYM=INT(YM)+MY1
        MIN1=INT(XM/2.)
        MINY=6
C
C  INPUT THE ANALYSIS TO BE PERFORMED
C
        TYPE*,' 0=G(R) VRS. R PLOT'
        TYPE*,' 1= DELTA-X VRS. DELTA-Y PLOT'
        TYPE*,' 2=CCIFS PLOTS'
        TYPE*,' 3=PARTICLE DENSITY IN Y-DIRECTION'
        TYPE*,' 5=X-Y POSITIONS RELATIVE TO FRINGE POS.'
        TYPE*,' 6=PARTICLE DENSITY IN X-DIRECTION'
        READ(5,15) JAWAB
15      FORMAT(I3)
        WRITE(6,11)
11      FORMAT(' ;:I OD 100 HAU')
        IF(JAWAB.EQ.0) THEN
        TYPE*,' INPUT THE ANULUS WIDTH:'
        READ(5,83) JR
83      FORMAT(I3)
        ENDIF
        IF(JAWAB.EQ.1) THEN
        IYM=INT(.8*(FLOAT(IYM)))
        CALL ONE(MIN1,DIA,IXM,IYM)
          ENDIF
        IF(JAWAB.EQ.2) THEN
        CALL TWO
          ENDIF
        IF(JAWAB.EQ.3 .OR. JAWAB.EQ.4) THEN
        CALL JAW34(JAWAB,DIA,MIN3,MAX3,MIN4,MAX4)
          ENDIF
        IF(JAWAB.EQ.5) THEN
        CALL FIVE(MX1,MXX1,MY1,MYY1,DIA)
          ENDIF
        IF(JAWAB.EQ.6) THEN
        TYPE*,'INPUT FRINGE PERIOD'
        READ(5,20) IFR
20      FORMAT(I4)
        FRNS=FLOAT(IFR)
        CALL XDENS(MX1,MXX1,MY1,MYY1,IFR,DIA)
        GOTO 900
```

```
        ENDIF
C  PROCESSING THE DATA FILES
C
        DO 130 KK=2,NUMB+1
        CALL RDATA
        DO 81 I=1,N
        YPOS=IY(I)
        IY(I)=INT(0.8*YPOS)
81      CONTINUE
        IF(JAWAB.EQ.0) THEN
         CALL PAIRC(DENSITY,DIA,JR,IXM,IYM)
        IF(KK.EQ.NUMB+1)THEN
        DENSITY=DENSITY/(FLOAT(NUMB+1))
        CALL ZERO(JR,DIA,DENSITY)
           ENDIF
           ENDIF
        IF(JAWAB.EQ.1) CALL ORIENT(MIN1,IXM,IYM,DIA)
        IF(JAWAB.EQ.2) THEN
        CALL CCIFS
         ENDIF
        IF(JAWAB.EQ.3) THEN
         CALL XDENS(MX1,MXX1,MY1,MYY1,DIA)
        IF(KK.EQ.NUMB+1) THEN
        CALL DENSC(MIN3,MAX3,DIA)
           ENDIF
        ENDIF
        IF(JAWAB.EQ.4) THEN
          CALL YDENS(MIN4,MAX4,DIA)
        IF(KK.EQ.NUMB+1) THEN
        CALL DENSC(MIN4,MAX4,DIA)
          ENDIF
        ENDIF
        IF(JAWAB.EQ.5) THEN
        CALL POSP(MX1,MXX1,MY1,MYY1,DIA)
          ENDIF
130     CONTINUE
        WRITE(6,92)
92      FORMAT(3H UH)
900     CONTINUE
        GOTO 901
        END
C
C
C ***************** MIDPOS SUBROUTINE ***************
C
C FIND THE CLOSEST PARTICLE IN A FILE THAT IS CLOSEST TO
C A GIVEN POSITION
C
        SUBROUTINE MIDPOS(IXM,IYM,MX,MY)
        COMMON KK,NUMB,N,IX(300),IY(300),RP(520),PHI(520)
        X1=FLOAT(IXM)
        Y1=(FLOAT(IYM))
        C=25000
        DO 90 I=1,N
        X=FLOAT(IX(I))
        Y=FLOAT(IY(I))
        R=(X-X1)**2.+(Y-Y1)**2.
        IF(R.LT.C) THEN
        C=R
        MX=IX(I)
        MY=IY(I)
         ENDIF
90      CONTINUE
        RETURN
        END
C ****************** MAMI SUBROUTINE ****************
C
```

```
C  FINDING THE MINIMUM AND MAXIMUM X&Y POSITIONS FOR ALL
C  THE DATA FILES CONTAINED IN A CONPLETE FILE
C
       SUBROUTINE MAMI(MX1,MXX1,MY1,MYY1)
       COMMON KK,NUMB,N,IX(300),IY(300),RP(520),PHI(520)
       DO 100 KK=2,NUMB+1
       CALL RDATA
       CALL LLMM(MINX,MAXX,MINY,MAXY)
       IF(MINX.LT.0 .OR. MAXX.GT.512) GOTO 100
       IF(MINY.LT.0 .OR. MAXY.GT.480) GOTO 100
       IF(MINX.LT.MX1) MX1=MINX
       IF(MAXX.GT.MXX1) MXX1=MAXX
       IF(MINY.LT.MY1) MY1=MINY
       IF(MAXY.GT.MYY1) MYY1=MAXY
 100    CONTINUE
       RETURN
       END
       END
C
C  ***************** DENSC SUBROUTINE **********************
C THIS SUBROUTINE IS FOR PLOTING THE THE DENSITY OF THE PARTICLES
C ALONG AND PERPENDICULAR TO THE POTENTIAL'S PERIODICITY DIRECTION
C
       SUBROUTINE DENSC(MIN3,MAX3,DIA)
       COMMON KK,NUMB,N,IX(300),IY(300),RP(520),PHI(520)
        RM=0.
        SX=700.*DIA/FLOAT(MAX3-MIN3)
        DO 12 I=MIN3,MAX3,4
        IF(RP(I).GT.RM) RM=RP(I)
12      CONTINUE
        SY=700./RM
        WRITE(6,33)
33      FORMAT(' U 0,0 D')
        DO 25 I=MIN3,MAX3,4
        IS=INT(SX*(FLOAT(I-MIN3))/DIA)
        JY=INT(RP(I)*SY)
        WRITE(6,30) IS,JY
30      FORMAT(X,I4,',',I4)
25      CONTINUE
       RETURN
       END
C
C  ***************** ZERO SUBROUTINE ************************
C  THIS SUBROUTINE IS FOR SETTING AND PLOTTING THE DATA FOR\
C  THE TRANSLATIONAL PAIR CORRELATION FUNCTION
C
       SUBROUTINE ZERO(JR,DIA,DENSITY)
       COMMON KK,NUMB,N,IX(300),IY(300),RP(520),PHI(520)
       COMMON/BLOCK2/MAXR1,NNEIG(2,6),DIV(520),COR(5,2),PN(520)
       IXO=1200
       IYO=350
       LENGTH=700
       LH=0
C  DRAWING A BOX AROUND THE PLOTTING AREA
      CALL BOX(IXO,IYO,LENGTH,LH,LH)
C  THIS PART WILL PLOT G(R) VRS. R, SCALING BOTH AXIS FOR
C  MAXIMUM POSITION. G(R) IS DEFINED AS THE NUMBER OF PARTICLES
C  WITHIN AN ANULUS OF WIDTH DR AT A DISTANCE R FROM THE CENTER
C  PARTICLE DEVIDED BY THE CIRCUMFERENCE TIMES DELTA R (DR).
C
        MAXR=MAXR1
        PMAX=0.
        JS=INT(FLOAT(JR)/2.)
        IXI=0
        IYI=0
        XS=DIA*700./FLOAT(MAXR)
        I1=0
```

```
         I2=FLOAT(MAXR)/DIA
         JUMP=2
         YS=70.
C LABELING THE X-AXIS
         CALL XAXIS(IXI,IYI,I1,I2,JUMP,XS)
        WRITE(6,23)
23      FORMAT(' 62,-100 U S12 RADIAL DISTANCE/DIAMETER_')
C LABELING THE Y-AXIS
         JUMP=1
         I2=10
         CALL YAXIS(IXI,IYI,I1,I2,JUMP,YS)
         WRITE(6,27)
27       FORMAT(' -80,260 U S42 G(R)/GMAX_')
        DO 70 I=JR,MAXR,JR
        IF(DIV(I).EQ.0.) GOTO 70
        PN(I)=PN(I)/(DIV(I)*DENSITY)
        IF(PN(I).GT.PMAX) PMAX=PN(I)
70      CONTINUE
        SCY=700./PMAX
        TYPE*,'DENS,PMAX,SCY:',DENSITY,PMAX,SCY
        XNU=FLOAT(MAXR)
        SCX=700./XNU
        X=FLOAT(JR)
        I1=INT(SCX*(X-1.))
        WRITE(6,66) I1
66      FORMAT('U 0,0 D ',I4,',0')
        DO 40 I=JR,MAXR,JR
        X=I
        I1=INT(SCX*X)
        NY=INT(PN(I)*SCY)
        WRITE(6,90) I1,NY
90      FORMAT(' ',I4,',',I4)
40      CONTINUE
        RETURN
        END
C
C ****************** RDATA SUBROUTINE ************************
C THIS SUBROUTINE IS FOR OPENING FILES AND READING DATA
C
        SUBROUTINE RDATA
        COMMON KK,NUMB,N,IX(300),IY(300),RP(520),PHI(520)
        CHARACTER*7 D(100),FICH
        IF(KK.EQ.0) THEN
        TYPE*,'INPUT NUMBER OF FILE'
        TYPE*,', IF NUMB=0 FILE NAMES ARE SAVED'
        READ(5,100) NUMB
100     FORMAT(I3)
        IF(NUMB.NE.0) THEN
        DO 110 I=2,NUMB+1
        WRITE(5,120) I
120     FORMAT('   FILE NAME',I3)
        READ(5,125) D(I)
125     FORMAT(A7)
        WRITE(5,122) D(I)
122     FORMAT(3X,A7)
110     CONTINUE
       FICH=D(2)
         ELSE
        TYPE*,'INPUT THE NAME OF THE FILENAMES'
        READ(5,101) FICH
101     FORMAT(A7)
        WRITE(6,10) FICH        :
10      FORMAT(5X,'DATA ANALYSIS FOR FILE:  ',A7)
        CALL ASSIGN(2,FICH,0)
        READ(2,END=510,ERR=510) D(1)
        DECODE(6,160,D(1)) NUMB
160     FORMAT(I3)
```

```
        READ(2,END=510,ERR=510) (D(I),I=2,NUMB+1)
510     CLOSE(2)
        END IF
           ELSE
        CALL ASSIGN(2,D(KK),0)
        READ(2,END=500,ERR=500) N
        TYPE*,'***PROCESSING FILE:  ',D(KK),N
        READ(2,END=500,ERR=500) (IX(I),I=1,N)
        READ(2,END=500,ERR=500) (IY(I),I=1,N)
500     CALL CLOSE(2)
             ENDIF
        RETURN
        END
C
C ****************** ONE SUBROUTINE*********************************
C
C THIS SUBROUINE IS FOR PLOTTING THE AXIS FOR THE ORIENTATIONAL
C CORRELATION FUNCTION
C
        SUBROUTINE ONE(MIN1,DIA,IXM,IYM)
        COMMON KK,NUMB,N,IX(300),IY(300),RP(520),PHI(520)
        IXO=300
        IYO=350
        LENGTH=700
        LH=INT(FLOAT(LENGTH)/2.)
        IXI=-LH
        IYI=-LH
C DRAWING A BOX AROUND THE PLOTTING AREA
        CALL BOX(IXO,IYO,LENGTH,LH,LH)
C  LABELING THE X-AXIS
        XS=(DIA*FLOAT(LH))/FLOAT(MIN1)
        I2=INT(FLOAT(MIN1)/DIA)
        I1=-I2
        YS=XS
        JUMP=1
        CALL XAXIS(IXI,IYI,I1,I2,JUMP,XS)
        JH=192-LH
         JD=IYI-100
        WRITE(6,203) JH,JD
203     FORMAT(X,I4,',',I4,' U S12 DELTA-X/DIAMETER_')
C LABELING THE Y-AXIS
        CALL YAXIS(IXI,IYI,I1,I2,JUMP,YS)
        JH=IXI-130
        JD=192-LH
        WRITE(6,109) JH,JD
109     FORMAT(XI4,',',I4,' U S42 DELTA-Y/DIAMETER_')
        RETURN
        END
C
C ****************** TWO SUBROUTINE ********************
C  THIS SUBROUTINE IS FOR SETTING THE PLOTTING PARAMETERS
C  WHEN JAWAB=2.
C
         SUBROUTINE TWO
C
C  DRAW EDGES AROUND THE PLOTTING AREA
        IXO=400
        IYO=800
        LENGTH=700
        LH=INT(FLOAT(LENGTH)/2.)
        IXI=-LH
        IYI=-LH
        JUMP=100
C DRAWING A BOX AROUND THE PLOTTING AREA
        CALL BOX(IXO,IYO,LENGTH,LH,LH)
        WRITE(6,10)
10      FORMAT(' -100,-400 D S12 DELTA-X_')
```

```
C  LABELING THE X-AXIS
        CALL XAXIS(IXI,IYI,I1,I2,JUMP,XS)
C LABELING THE Y-AXIS
        CALL YAXIS(IXI,IYI,I1,I2,JUMP,YS)
        WRITE(6,20)
20      FORMAT(' -200,-400 U S12  R*COS(ANN)_')
        WRITE(6,30)
30      FORMAT(' -420,200 U S42 R*SIN(ANN)_ U')
         RETURN
         END
C
C  ****************JAW34 SUBROUTINE ****************
C
C  THIS SUBROUTINE IS FOR THE DENSITY MODES ANALYSIS
C  WHEN JAWAB=3 OR 4.
C
        SUBROUTINE JAW34(JAWAB,DIA,MIN3,MAX3,MIN4,MAX4)
        COMMON KK,NUMB,N,IX(300),IY(300),RP(520),PHI(520)
        MIN3=400
        MAX3=0
        MIN4=400
        MAX4=0
        DO 70 KK=2,NUMB+1
        CALL RDATA
        CALL LLMM(MINX,MAXX,MINY,MAXY)
        IF(MINX.LT.MIN3) MIN3=MINX
        IF(MINY.LT.MIN4) MIN4=MINY
        IF(MAXX.GT.MAX3) MAX3=MAXX
        IF(MAXY.GT.MAX4) MAX4=MAXY
70      CONTINUE
        IXI=0
        IYI=0
        LENGTH=700
        IF(JAWAB.EQ.3) THEN
        JUMP=5
        IXO=300
        IYO=350
        P1=(FLOAT(MAX3-MIN3))/DIA
        I1=0
          ELSE
        IXO=1200
        IYO=350
        JUMP=5
         I1=0
         P1=(FLOAT(MAX4-MIN4))/DIA
           ENDIF
         LH=0
C DRAWING A BOX AROUND THE PLOTTING AREA
        CALL BOX(IXO,IYO,LENGTH,LH,LH)
        XS=700./(P1)
         I2=INT(P1)
C  DRAWING THE XAXIS
        CALL XAXIS(IXI,IYI,I1,I2,JUMP,XS)
        JUMP=2
        I2=10
        YS=70.
C DRAWING AND LABELING THE YAXIS
        CALL YAXIS(IXI,IYI,I1,I2,JUMP,YS)
        WRITE(6,10)
10      FORMAT(' -80,134 U S42 NORMALIZED DENSITY_')
        RETURN
          END
C
C **************** FIVE SUBROUTINE ***************************
C
C THIS SUBROUTINE IS FOR SETTING THE PLOTTING AREA AND
C PARAMETERS TO BE USED IN THE X-Y POSITION PLOT OF THE
```

```
C DATA FILE
C
        SUBROUTINE FIVE(MX1,MXX1,MY1,MYY1,DIA)
        COMMON KK,NUMB,N,IX(300),IY(300),RP(520),PHI(520)
        IXO=300
        IYO=350
        LENGTH=700
        LH=INT(FLOAT(LENGTH)/2.)
C        DO 100 KK=2,NUMB+1
C        CALL RDATA
C        CALL LLMM(MINX,MAXX,MINY,MAXY)
C        IF(MINX.LT.0 .OR. MAXX.GT.512) GOTO 100
C        IF(MINY.LT.0 .OR. MAXY.GT.480) GOTO 100
C        IF(MINX.LT.MX1) MX1=MINX
C        IF(MAXX.GT.MXX1) MXX1=MAXX
C        IF(MINY.LT.MY1) MY1=MINY
C        IF(MAXY.GT.MYY1) MYY1=MAXY
C 100     CONTINUE
        IXI=0
        IYI=0
        MY1=INT(.8*(FLOAT(MY1)))
        MYY1=INT(.8*(FLOAT(MYY1)))
        CALL BOX(IXO,IYO,LENGTH,IXI,IYI)
        XS=2.*DIA*700./(FLOAT(MXX1-MX1))
        JUMP=2
        I1=0
        I2=INT((FLOAT(MXX1-MX1))/(2.*DIA))
        CALL XAXIS(IXI,IYI,I1,I2,JUMP,XS)
        WRITE(6,30)
30      FORMAT(' 120,-100 U S12 X-POSITION/2*DIAMETER_')
        I2=INT((FLOAT(MYY1-MY1))/(DIA*2.))
        YS=2.*DIA*700./(FLOAT(MYY1-MY1))
        CALL YAXIS(IXI,IYI,I1,I2,JUMP,YS)
        WRITE(6,50)
50      FORMAT(' -80,120 U S42 Y-POSITION/2*DIAMETER_')
        RETURN
        END
C
C ******************** BOX SUBROUTINE ******************************
C
C THIS SUBROUTINE PLOTS A BOX AROUND THE PLOTTING AREA
C
        SUBROUTINE BOX(IXO,IYO,LENGTH,IXI,IYI)
        WRITE(6,10) IXO,IYO
10      FORMAT(' HAU ',I4,',',I4,' OD')
        WRITE(6,20) LENGTH,LENGTH,LENGTH,LENGTH
20      FORMAT(' 0,',I4,X,I4,',',I4,X,I4,',0 0,0 U')
        WRITE(6,40) IXI,IYI
40      FORMAT(X,I4,',',I4,' O')
        RETURN
        END
C  ***************** XAXIS SUBROUTINE ******************************
C
C  THIS SUBROUTINE IS FOR LABELING THE XAXIS
C
        SUBROUTINE XAXIS(IXI,IYI,I1,I2,JUMP,XS)
        L1=IYI-10
        L2=IYI-50
        DO 202 I=I1,I2,JUMP
        ISX=INT((FLOAT(I))*XS)
        WRITE(6,200) ISX,IYI,ISX,L1
200     FORMAT(' U ',I4,',',I4,' D ',I4,',',I4,' U')
         IS=ISX-40
         WRITE(6,30) IS,L2,I
30       FORMAT(X,I4,','I4,' S11 ',I4,'_')
202     CONTINUE
        RETURN
```

```
10      CONTINUE
        RETURN
        END
C
C ********************CCIFS PLOTING SUBROUTINE************************
C  THIS SUBROUTINE IS FOR THE CCIFS PLOTS.  THIS IS DONE BY TAKING
C  THE CENTER PARTICLE, FINDING ITS NEAREST NEIGHBORS, FINDING THE
C  ANGLE BETWEEN THE NNEIG. AND CENTER PARTICLE, THEN TRANSLATE AND
C  ROTATE THE REST OF THE PARTICLE WITH THE GIVEN ANGLE.
C
        SUBROUTINE CCIFS(ICOUNT)
        COMMON KK,NUMB,N,IX(300),IY(300),RP(520),PHI(520)
        DIMENSION NNEIG(2,7)
        PI=4.0*ATAN(1.0)
        PIH=PI/2.
        X=FLOAT(IX(1))
        Y=FLOAT(IY(1))
        C=(X-256.)**2.+(Y-192.)**2.
        X1=256.
        Y1=192.
        DO 90 I=1,N
        X=FLOAT(IX(I))
        Y=FLOAT(IY(I))
        R=(X-X1)**2.+(Y-Y1)**2.
        IF(R.LT.C) THEN
        C=R
        MX=IX(I)
        MY=IY(I)
         END IF
90      CONTINUE
        DO 25 I=1,N
        X=FLOAT(IX(I)-MX)
        Y=FLOAT(IY(I)-MY)
        RP(I)=SQRT(X*X+Y*Y)
        IF(X.EQ.0.) THEN
        PHI(I)=PIH
          ELSE
        PHI(I)=ATAN2(Y,X)
          ENDIF
25      CONTINUE
        CALL ORDER(N)
        SX=300./256.
        SY=300./192.
        DTETA=PIH-PHI(2)
        DO 30 J=1,N
        X=RP(J)*COS(PHI(J)+DTETA)
        Y=RP(J)*SIN(PHI(J)+DTETA)
        IX(J)=INT(X*SX)
        IY(J)=INT(Y*SY)
30      CONTINUE
        CALL ORDER2(N)
         DO 60 I=1,N
        IF(IX(I).LT.-300 .OR. IX(I).GT.300) GOTO 60
        IF(IY(I).LT.-300 .OR. IY(I).GT.300) GOTO 60
        WRITE(6,50) IX(I),IY(I)
50      FORMAT(' ',I4,',',I4,' S11 +_ U')
60       CONTINUE
        RETURN
        END
C *************** PAIRC ***********************
C  ANALYSIS FOR THE TRANSLATIONAL PAIR CORRELATION FUNCTION
C
        SUBROUTINE PAIRC(DENSITY,DIA,JR,IXM,IYM)
        COMMON KK,NUMB,N,IX(300),IY(300),RP(300),PHI(300)
        COMMON/BLOCK2/MAXR1,NNEIG(2,6),DIV(520),COR(5,2),PN(520)
        CALL LLMM(MINX,MAXX,MINY,MAXY)
        XMIN=FLOAT(MINX)
```

```
        END
C
C ********************** YAXIS SUBROUTINE ************
C
C  THIS SUBROUTINE LABELS THE Y-AXIS
C
        SUBROUTINE YAXIS(IXI,IYI,I1,I2,JUMP,YS)
        L1=IXI-15
        L2=IXI-80
        DO 106 I=I1,I2,JUMP
        IYS=YS*(FLOAT(I))
        WRITE(6,107) L1,IYS,IXI,IYS
107     FORMAT(' U ',I4,',',I4,' D ',I4,',',I4,' U')
        WRITE(6,108) L2,IYS,I
108     FORMAT(X,I4,',',I4,' S11 ',I4,'_')
106     CONTINUE
        RETURN
        END
C
C ******************** YDENS SUBROUTINE ************************
C THIS SUBROUTINE IS FOR FINDING THE DENSITY
C IN THE DIRECTION OF THE FRINGE PATTERN PERIODICITY
C
        SUBROUTINE YDENS(MIN4,MAX4,DIA)
        COMMON KK,NUMB,N,IX(300),IY(300),RP(520),PHI(520)
        JUMP=4
        DO 10 I=MIN4,MAX4,JUMP
        INCX=I+JUMP
        NUM=0
        DO 20 J=1,N
        IF(IY(J).LT.I.OR.IY(J).GT.INCX) GOTO 20
        NUM=NUM+1
20      CONTINUE
        RP(I)=FLOAT(NUM)+RP(I)
10      CONTINUE
        RETURN
        END
C
C ***************** LLMM SUBROUTINE *************************
C THIS SUBROUTINE IS FOR FINDING THE MINIMUM X&Y VALUES AND THE
C MAXIMUM X&Y VALUES IS EACH DATA FILNDING THE PARTICLES' DENSITYE
        SUBROUTINE LLMM(MINX,MAXX,MINY,MAXY)
        COMMON KK,NUMB,N,IX(300),IY(300),RP(520),PHI(520)
        MINX=IX(1)
        MINY=IY(1)
        MAXX=IX(N)
        MAXY=IY(N)
        IF(MINX.LT.0.OR.MINY.LT.0) THEN
        TYPE *,'*** PROBLEMS IX1,IY1: **',MINX,MINY
          ELSE
        IF(MAXX.GT.512.OR.MAXY.GT.512) THEN
        TYPE *,,'***PROBLEMSIX(N),IY(N) ***',MAXX,MAXY
           ENDIF
            ENDIF
        DO 10 I=1,N-1
        IF(IX(I+1).GT.512 .OR. IX(I+1).LT.0) THEN
        TYPE*,'***POSITION PROBLEMS:***',I+1,IX(I+1),IY(I+1)
          ELSE
        IF(IY(I+1).GT.480. .OR.IY(I+1).LT.0) THEN
        TYPE*,'***POSITION PROBLEMS:***',I+1,IX(I+1),IY(I+1)
          ELSE
        IF(IX(I+1).GT.MAXX) MAXX=IX(I+1)
        IF(IY(I+1).GT.MAXY) MAXY=IY(I+1)
        IF(IX(I+1).LT.MINY) MINX=IX(I+1)
        IF(IY(I+1).LT.MINY) MINY=IY(I+1)
          ENDIF
            ENDIF
```

```
        XMAX=FLOAT(MAXX)
        YMIN=FLOAT(MINY)
        YMAX=FLOAT(MAXY)
        AREAB=(XMAX-XMIN)*(YMAX-YMIN)
        DENSITY=DENSITY+N/AREAB
        X=FLOAT(IX(1))
        Y=FLOAT(IY(1))
        XMIDL=FLOAT(IXM)
        YMIDL=FLOAT(IYM)
        C=(X-XMIDL)**2.+(Y-YMIDL)**2.
        LN=1
        IF(KK.EQ.2) THEN
        IRC=520
        MAXR1=512
        DR=JR
        JS=INT(DR/2.)
        DO 80 I=1,IRC
        DIV(I)=0.
        PN(I)=0.
        RP(I)=0.
        PHI(I)=0.
80      CONTINUE
        MAXR1=0
C THIS PART WILL INPUT THE CORNERS
        COR(1,1)=XMIN
        COR(1,2)=YMIN
        COR(2,1)=XMAX
        COR(2,2)=YMIN
        COR(3,1)=XMIN
        COR(3,2)=YMAX
        COR(4,1)=XMAX
        COR(4,2)=YMAX
        COR(5,1)=XMIDL
        COR(5,2)=YMIDL
        PI=4.*ATAN(1.0)
C
          ENDIF
C  THIS PART WILL FIND THE CLESEST PARTICLE WITH TO THE POSITION
C  MX, MY.
C
170     DO 175 IC=1,5
        IF(LN.GT.7) GOTO 175
        X1=COR(IC,1)
        Y1=COR(IC,2)
        DO 10 I=1,N
        X=FLOAT(IX(I))
        Y=FLOAT(IY(I))
        R=(X-X1)**2.+(Y-Y1)**2.
        IF(R.LT.C) THEN
        C=R
        MX=IX(I)
        MY=IY(I)
         END IF
10      CONTINUE
C  THIS PART WILL FIND THE LARGEST CIRCLE WITH CENTER AT THE
C  MX,MY THAT WILL BE ENCLOSED IN THE RECTANGULAR AREA
C
        IF(IC.NE.5) THEN
        X=MX
        Y=MY
        C=XMAX**2.+YMAX**2.
C
C  FINDING EACH CORNERS' MAXIMUM ANALYSIS RADIUS AND ENCLOSED ANGLE
C
        GOTO (191,192,192,191),IC
191     R4=SQRT((XMAX-X)**2.+(Y-YMIN)**2.)
        R5=SQRT((XMIN-X)**2.+(YMAX-Y)**2.)
```

```
        GOTO 195
192     R4=SQRT((XMIN-X)**2.+(YMIN-Y)**2.)
        R5=SQRT((XMAX-X)**2.+(YMAX-Y)**2.)
195     MAXR=INT(R4)
        IF(R5.LT.R4) MAXR=INT(R5)
        A=(R4*R4+R5*R5-C)/(R4*R5*2.)
        TETA=ACOS(A)
         ELSE
C
C  MAXIMUM CIRLE ENCLOSED BY THE CENTER PARTICLE
C
        LN=LN+1
        MIX=MX
        MIY=MY
        TETA=2.*PI
        IF(MX.GT.IXM) MIX=MAXX-MX
        IF(MY.GT.IYM) MIY=MAXY-MY
        MAXR=MIX
        IF(MIX.GT.MIY) MAXR=MIY
         END IF
190     RPMAX=0.
        PMAX=0.
C  THIS PART WILL FIND THE CHANGE IN X&Y-POSITIONS BETWEEN THE
C  EACH PARTICLE AND THE CENTER ONE.
        DO 20 I=1,N
        X=FLOAT(IX(I)-MX)
        Y=FLOAT(IY(I)-MY)
        RP(I)=SQRT(X*X+Y*Y)
20      CONTINUE
        CALL ORDER(N)
        IF(LN.EQ.2) THEN
C
C  NEAREST NEIGHBORS TO THE CENTER PARTICLE(NNEIG(I,J))
C
        DO 240 I=2,7
        NNEIG(1,I-1)=IX(I)
        NNEIG(2,I-1)=IY(I)
240     CONTINUE
         END IF
C  THIS PART WILL COUNT THE NUMBER OF PARTICLE THAT ARE AT A DISTANCE
C  R-DR/2. AND R+DR/2.   R IS THE DISTANCE FROM THE CENTER PARTICLE.
C
        X0=MX
        Y0=MY
        DO 30 J=JR,MAXR,JR
        A8=0.
        RADI=J
        R1=RADI-DR/2.
        R2=RADI+DR/2.
        DRAD=R2*R2-R1*R1
        DIV(J)=DIV(J)+1.
        DO 70 I=2,N
        IF(IC.GT.4) GOTO 260
        X=IX(I)
        Y=IY(I)
        GO TO (310,320,330,340),IC
310     IF(X.GE.X0.AND.Y.GE.Y0) GOTO 260
        IF(Y.LT.Y0) THEN
        C=((X-XMIN)**2.+(YMAX-Y)**2.)
        R7=R5
         ELSE IF(X.LT.X0) THEN
        C=((XMAX-X)**2.+(Y-YMIN)**2.)
        R7=R4
        END IF
        GOTO 420
320     IF(X.LE.X0.AND.Y.GE.Y0) GOTO 260
        IF(Y.LT.Y0) THEN
```

```
        R7=R5
        C=(XMAX-X)**2.+(YMAX-Y)**2.
        ELSE
        R7=R4
        C=(X-XMIN)**2.+(Y-YMIN)**2.
        END IF
        GOTO 420
330     IF(X.GE.X0.AND.Y.LE.Y0) GOTO 260
        IF(Y.GT.Y0) THEN
        R7=R4
        C=(X-XMIN)**2.+(Y-YMIN)**2.
        ELSE
        R7=R5
        C=(XMAX-X)**2.+(YMAX-Y)**2.
        END IF
        GOTO 420
340     IF(X.LE.X0.AND.Y.LE.Y0) GOTO 260
        IF(Y.GT.Y0) THEN
        R7=R4
        C=(XMAX-X)**2.+(Y-YMIN)**2.
        ELSE
        R7=R5
        C=(X-XMIN)**2.+(YMAX-Y)**2.
        END IF
420     A=(R7*R7+RP(I)*RP(I)-C)/(R7*RP(I)*2.)
        IF(A.GT.1. .OR. A.LT.-1.) THEN
        TYPE*,'ARGUMENT=',A
         END IF
        TETA1=ACOS(A)
        IF(TETA1.GT.TETA) GOTO 70
260     IF(RP(I).LE.R2 .AND. RP(I).GE.R1) A8=A8+1.
70      CONTINUE
C  CALCULATING THE AREA OF EACH RING
C
        ARCL=DRAD*TETA/2.
        PN(J)=PN(J)+A8/ARCL
30      CONTINUE
      . IF(MAXR.GT.MAXR1) MAXR1=MAXR
        IF(LN.LE.7 .AND. LN.GT.1) THEN
        MX=NNEIG(1,LN-1)
        MY=NNEIG(2,LN-1)
        MIX=MX
        MIY=MY
        TETA=2.*PI
        IF(MX.GT.IXM) MIX=MAXX-MX
        IF(MY.GT.IYM) MIY=MAXY-MY
        MAXR=MIX
        IF(MIX.GT.MIY) MAXR=MIY
        LN=LN+1
        GOTO 190
         END IF
175     CONTINUE
        RETURN
        END
C
C  ************************SUBROUTINE ORDER2*****************
C  THIS SUBROUTINE WILL ORDER THE PARTICLES ACCORDING TO THEIR
C  X AND Y POSITIONS IN ORDER TO MAKE THE PLOTTING LESS TIME CONSUMING
C
        SUBROUTINE ORDER2
        COMMON KK,NUMB,N,IX(300),IY(300),RP(520),PHI(520)
        DO 210 I=1,N
        DO 220 J=I+1,N
        IF(IX(J).LT.IX(I)) THEN
        JX1=IX(I)
        JX2=IX(J)
        JY1=IY(I)
```

```
//U12604A JOB (12604,499-82-3198),'KHALID',
// TIME=(600,00),CLASS=4,MSGCLASS=X,NOTIFY=U12604A,MSGLEVEL=(1,1)
/*PASSWORD ????
/*JOBPARM FORMS=9001,ROOM=K
// EXEC FORTVCLG,PARM.FORT='LANGLVL(77),OPT(3),MAP,XREF',FVREGN=2500K,
// REGION.GO=8840K
//FORT.SYSIN DD *
C
C ******************************************************
C
C   THIS PROGRAM IS A MONTE CARLO SIMULATION OF THE LASER FREEZING
C   OF COLLOIDAL PARTICLES IT FINDS THE 2D PAIR CORRELATION FUNCTION
C
C   WRITTEN BY KHALID LOUDIYI
C
C ******************************************************
C
C *** REMEMBER TO CHECK THE FOLLOWINGS BEFORE SUBMITTING ANY JOB
C
C   MAKE SURE THE DATA FILE NAME IS RIGHT
C   FOR INITIAL RUN SET IBIT=1 AND KSTART=1
C   FOR THE SECOND RUN IBIT=1 AND KSTART=0
C   FOR THE THIRD RUN IBIT=0 AND KSTART=0
C
C  IF IBIT=1 SET NMAX=20,IREP=50
C  IF IBIT=0 SET NMAX=20,IREP=20
C  IF KSTART = 1 THEN START FROM LATTICE (NEW DATA FILE)
C  IF KSTART = 0 THEN START FROM PREVIOUS CONFIGURATION (DATA FILE
C  MUST ALREADY HAVE THE LATTICE POSITIONS STORED)
C
C  REMEMBER TO CHANGE THE VALUE OF IRAN, IN ORDER TO START AT
C  DIFFERENT POINTS OF THE RANDOM NUMBER GENERATOR.
C
C ******************************************************
C
C
C
C  SETTING THE PARAMETERS FOR THE POTENTIAL CALCULATION
C
C  ZEFF=EFFECTIVE CHARGE, SIZEX=LENGTH OF THE BOX
C  SIZEY=WIDTH OF THE BOX, DEPTH=SEPARATION BETWEEN GLASS PLATES
C  AREA=AREA OF THE BOX, BOLTZ=BOLTZMAN CONSTANT, TEMPER=TEMPERATURE
C  ROI=MACROIONS' DENSITY, DIELC=BACKGROUND DIELECTRIC CONSTANT
C  CHARGE=ELEMENTARY CHARGE IN CGS., AMP=STRENGTH OF THE INTERACTION
C  ALPHA=SCREENING LENGTH MULTIPLIED BY INTERPARTICLE SPACING
C  PARTS=CHARACTERISTIC INTERPARTICLE SPACING
C  NLOOP=NUMBER OF WELLS IN THE BOX WITH THE CROSS BEAMS ON
C  NPART=NUMBER OF PARTICLES IN THE MONTE CARLO SIMULATION
C  PNSQRT=SQUARE-ROOT OF NUMBER OF PARTICLES.
C
      IMPLICIT REAL*8(A-H,O-Z)
      COMMON CP(2,100),ENERG(101,100)
      COMMON SIZEX,SIZEY,ENEW,SY,SX,ALFA
      COMMON INUM,IFLAG,IFLAG1,NPART,NPARTH
      DIMENSION DEVI(100),AI1(300)
      DIMENSION DN(2,300),AMSQ(2),DD(9),ANR(3,300)
      PARAMETER(NMAX=10,PERIOD=2.200)
      PARAMETER(IREP=1,IRAN=7,DPOTEN=2.,CBOUN=7.)
      PARAMETER(IBIT=1,KSTART=0)
C
C
     NPART=100
     SIZEX=22.
```

```
      SIZEZ=22.
      ZEFF=8000.
      DELTAR=.1
      DELRH=DELTAR/2.
      NPARTH=NPART+1
      PARTN=FLOAT(NPART)/10.
      PNSQRT=SQRT(FLOAT(NPART))
      NPC=INT(PNSQRT)
      JPOS=INT(PARTN)
      NPARTS=NPART*NPART
      JUMP=1
      PI=4.0*ATAN(1.0)
      PRD=SIZEX/PNSQRT
      HPRD=PRD/2.
      APD=PERIOD/2.
      AREA=SIZEX*SIZEY
      NLOOP=INT(SIZEX/PERIOD)+1
      DIAMET=1.07
      RADIUS=DIAMET/2.
      ROI=FLOAT(NPART)/(AREA*SIZEZ)
      BOLTZ=1.381E-16
      DIELC=80.0
      CHARGE=4.8029E-10
      TEMPER=300.0
      PARTS=2.0
      AMP=(ZEFF*CHARGE)**2./(DIELC*DIAMET*1.E-4)
      AMP=AMP/(BOLTZ*TEMPER)
      ALFA=7.0
C     AMP=20000.
C     ALFA=3.
C
C  CHANGE IRAN TO START WITH DIFFERENT RANDOM NUMBERS
C  EACH RUN
C
      DO 10 I = 1,IRAN
      XYZ = RANF(0)
10    CONTINUE
      SX=SIZEX-CBOUN
      SY=SIZEY-CBOUN
      IF (KSTART .EQ. 1) THEN
      ICOR=0
C
C  SETTING THE STARTING LATTICE CONFIGURATION
C
      DO 12 I = 1,NPC
      Y=PRD*FLOAT(I-1)
      X1=.5*FLOAT(I)
      IX1=2*INT(X1)
      IF(IX1 .EQ. I) THEN
      HPRDX=HPRD/2.
      ELSE
      HPRDX=PRD*HPRD/2.
      ENDIF
      DO 14 J = 1,NPC
      X = PRD*FLOAT(J-1)
      ICOR =ICOR+ 1
      XPOSI=.5 - 1.*RANF(0)
      YPOSI=.5 - 1.*RANF(0)
      CP(1,ICOR)=HPRDX+X+XPOSI
      CP(2,ICOR)=HPRD+Y+YPOSI
14    CONTINUE
12    CONTINUE
        ELSE
C
C   READ DATA FROM THE DISK
```

```
C STARTING FROM PREVIOUS CONFIGURATION
C
      REWIND 15
      DO 18 I =1,NPART
      READ(15,102) CP(1,I),CP(2,I),DEVI(I)
102   FORMAT(10X,F12.7,10X,F12.7,10X,F12.7)
18    CONTINUE
      REWIND 15
        ENDIF
C
C   PRINT THE INITIAL STATE DATA
C
        PRINT 100
100     FORMAT(10X,'INITIAL STATE')
        DO 16 I=1,NPART
        PRINT 101, CP(1,I),CP(2,I),DEVI(I)
101     FORMAT(3(5X,F12.6))
16      CONTINUE
C
C  INITILIZE
C
      ICOUNT=0
      STOTA=0.
      ATOTS=0.
      DO 105 I=1,NPART
      DO 107 J=1,NPART
      ENERG(I,J)=0.0
107   CONTINUE
105   CONTINUE
      IF(IBIT.EQ.1) GOTO 63
C     DO 62 I = 1,300
C     AIO=.1*FLOAT(I)
C     AI1(I)=AIO-DELRH
C     DN(1,I)=0.0
C     DN(2,I)=0.0
C62    CONTINUE
C      AMSQ(1) = 0.0
C      AMSQ(2) = 0.0
63    CONTINUE
C
C   MAIN MONTE CARLO'S LOOPS
C
      DO 30 LMON=1,NMAX
      ICOUNT=ICOUNT+1
      DO 25 KMON=1,100
      IREJT=0
      STOTAL=0.
      DO 40 I = 1,NPART
      INUM = I
C
C  SAVE THE COORDINATE AND ENERGY
C
      CPS1=CP(1,I)
      CPS2=CP(2,I)
C
C  CALCULATE THE ENERGY BEFORE MOVE
C
      IFLAG1=1
      ENEW=0.
      CALL ENERGY
      ENEW=AMP*ENEW
C     ENERG(I,I)=ENEW
      ENERG(I,I)=ENEW+(DPOTEN*(1.0+DCOS(2.*PI*CP(1,I)/PERIOD)))
C
C  RANDOM MOVEMENT OF THE PARTICLE, WITH EQUAL PROBABILITY
```

```
      CPTX=CP(1,I)
      CPTY=CP(2,I)
      FLIP=RANF(0)
      CP(1,I) = CP(1,I)+APD*(1.0-2.0*RANF(0))
      CP(2,I) = CP(2,I)+APD*(1.0-2.0*RANF(0))
      IF (FLIP .LE. 0.33) THEN
      CP(2,I)=CPTY
      ELSE
      IF (FLIP .GT. 0.33 .AND. FLIP .LE. 0.66) THEN
      CP(1,I)=CPTX
      ENDIF
      ENDIF
C
C   CHECK YOUR PERIODIC BOUNDARY CONDITION
C
      IF(CP(1,I).GT.SIZEX)CP(1,I)=CP(1,I)-SIZEX
      IF(CP(1,I).LT.0.)CP(1,I)=CP(1,I)+SIZEX
      IF(CP(2,I).GT.SIZEY)CP(2,I)=CP(2,I)-SIZEY
      IF(CP(2,I).LT.0.)CP(2,I)=CP(2,I)+SIZEY
C
C    CALCULATE THE ENERGY AND ACCEPT OR REJECT
C
      IFLAG=0
      IFLAG1=0
      ENEW=0.
      CALL ENERGY
      ENEW=AMP*ENEW
      IF (IFLAG .EQ. 1) GO TO 1010
C     ESAV=ENEW
      ESAV=ENEW+(DPOTEN*(1.0+DCOS(2.*PI*CP(1,I)/PERIOD)))
      DEL=ENERG(I,I)-ESAV
      IF(DEL .GE. 0.) GO TO 1000
      IF(DEL .LE. -10.0) GO TO 1010
      DELTA=DEXP(DEL)
      TEST=RANF(0)
      IF (DELTA .GT. TEST) GO TO 1000
C
C   REJECT THIS STEP
C
1010  IREJT=IREJT+1
      CP(1,I)=CPS1
      CP(2,I)=CPS2
C     DO 70 IREE=1,NPART
C     ENERG(I,IREE)=ENERG(NPARTH,IREE)
C70    CONTINUE
      GO TO 40
C
C   ACCEPT THE MOVE
C
1000  ENERG(I,I)=ESAV
40    CONTINUE
      IF (IBIT .EQ. 1) GO TO 25
C
C   INITIALIZE THE MATIX COUNTING THE NUMBER OF PARTICLES
C   WITHIN AN ANULLUS
C
      DO 78 I = 1,250
      DN(1,I)=0.0
78    CONTINUE
      ES = 0.0
      EC = 0.0
C
502   CONTINUE
C
C   FIND THE SUM OF ALL PAIRS' POTENTIALS AFTER ONE MC STEP
```

```
C
      DO 50 J = 1,NPART
      STOTAL=STOTAL+ENERG(J,J)
C
      IF (IBIT .EQ. 1) GO TO 50
C CALCULATING THE COMPONENTS FOR MEASUREMENTS OF THE SCATTERED
C INTENSITY (EXP(I(K.R))), WHERE K IS IN THE X DIRECTION.
C
      EC=EC+DCOS(2.*PI*CP(1,J)/PERIOD)
      ES=ES+DSIN(2.*PI*CP(1,J)/PERIOD)
C
C SETTING PERIODIC BOUDARIES FOR THE PAIR CORRELATION FUNCTION
C
      XP=CP(1,J)+SIZEX
      XN=CP(1,J)-SIZEX
      YP=CP(2,J)+SIZEY
      YN=CP(2,J)-SIZEY
C
C   SETTING PARAMETERS FOR FINDING IF PARTICLES ARE WITHIN
C   A CERTAIN ANULLUS.
C
      IFIXT=1
      RX1=CP(1,IFIXT)-CP(1,J)
      RX1=DABS(RX1)
      RY1=CP(2,IFIXT)-CP(2,J)
      RY1=DABS(RY1)
      RXP1=CP(1,IFIXT)-XP
      RXP1=DABS(RXP1)
      RXN1=CP(1,IFIXT)-XN
      RXN1=DABS(RXN1)
      RYP1=CP(2,IFIXT)-YP
      RYP1=DABS(RYP1)
      RYN1=CP(2,IFIXT)-YN
      RYN1=DABS(RYN1)
      DD(1)=DSQRT((RX1**2)+(RY1**2))
      DD(2)=DSQRT((RX1**2)+(RYP1**2))
      DD(3)=DSQRT((RX1**2)+(RYN1**2))
      DD(4)=DSQRT((RXP1**2)+(RY1**2))
      DD(5)=DSQRT((RXP1**2)+(RYP1**2))
      DD(6)=DSQRT((RXP1**2)+(RYN1**2))
      DD(7)=DSQRT((RXN1**2)+(RY1**2))
      DD(8)=DSQRT((RXN1**2)+(RYP1**2))
      DD(9)=DSQRT((RXN1**2)+(RYN1**2))
C
C   COUTING THE NUMBER OF PARTICLES THAT ARE WITHIN
C   AN ANNULUS OF RADIUS DELTAR FOR THE FIRST PARTICLE
C   IN THE BOX.
C
      DO 65 I=1,250,JUMP
      IF (I .GT. 15) THEN
      DO 66 K=1,9
      IF (DD(K).LE.AI1(I+1).AND.DD(K).GE.AI1(I)) THEN
      DN(1,I)=DN(1,I)+1.0
      ENDIF
66    CONTINUE
        ENDIF
65    CONTINUE
50    CONTINUE
C
C   SUN OF THE TOTAL ENERGY CALCULATED FROM ALL THE MC STEPS
C   AND OF THE SQUARE ENERGY.
C
      STOTA=STOTA+STOTAL
      ATOTS=ATOTS+(STOTAL**2)
      IF (IBIT .EQ. 1) GO TO 25
```

```
C  SCATTERED INTENSITY AND INTENSITY FLUCTUATIONS CALCULATIONS.
C
      AMSQ(1)=AMSQ(1)+(EC**2+ES**2)/NPARTS
      AMSQ(2)=AMSQ(2)+(((EC**2+ES**2)/NPARTS)**2)
C
C  TOTAL NUMBER OF PARTICLES WITHIN A CERTAIN REGION
C
      DO 72 I = 1,250
      DN(2,I)=DN(2,I)+DN(1,I)
72    CONTINUE
C
25    CONTINUE
      IF (ICOUNT .EQ. IREP) THEN
C
C  OUTPUT THE RESULTS
C
C     PRINT 104, LMON,IREJT,DPOTEN
C104   FORMAT(5X,'AFTER 100 X',I4,' MC STEPS, REJECT = ',I3,5X,
C    /'U = ',F6.3)
C     TN=100.*FLOAT(LMON)
C
C  SPECIFIC HEAT CALCULATIONS
C
C     SHEAT=((ATOTS/TN) - ((STOTA/TN)**2))/(FLOAT(NPART))
C     PRINT 106, SHEAT
C106   FORMAT(5X,'SP.HEAT = ',E16.6)
C501   CONTINUE
      ICOUNT=0
C
C  THIS PART FINDS THE MIDDLE PARTICLE WITHIN THE BOX
C
      COMPAR=2000.
      DO 52 I = 1,NPART
      DX=CP(1,I)-11.
      DY=CP(2,I)-11.
      IF(DX.GT.COMPAR .OR. DY.GT.COMPAR) GOTO 52
      RDM=DX*DX + DY*DY
      IF(RDM.LE.COMPAR) THEN
      COMPAR=RDM
      ICOMP=I
      ENDIF
52    CONTINUE
C  FINDING THE DISTANCE BETWEEN THE MIDDLE PARTICLE AND THE
C  REST OF THE PATICLES
C
      DO 58 I=1,NPART
      DX=CP(1,I)-CP(1,ICOMP)
      DY=CP(2,I)-CP(2,ICOMP)
      AI1(I)=DX*DX + DY*DY
58    CONTINUE
      DO 54 I=1,NPART
      DO 57 II=I+1,NPART
      IF(AI1(II).GT.AI1(I)) GOTO 57
      C1=CP(1,I)
      C2=CP(1,II)
      C3=CP(2,I)
      C4=CP(2,II)
      C5=AI1(I)
      C6=AI1(II)
      CP(1,I)=C2
      CP(1,II)=C1
      CP(2,I)=C4
      CP(2,II)=C3
      AI1(I)=C6
      AI1(II)=C5
57    CONTINUE
```

```
54     CONTINUE
C  FINDING DX AND DY AND THE ANGLE BETWEEN EVERY PARTICLE
C AND THE CENTER PARTICLE AND ITS ITS SIX NEAREST NEIGHBORS
C
       DO 53 II=1,7
       DO 59 I=1,NPART
       DELX=CP(1,I)-CP(1,II)
       DELY=CP(2,I)-CP(2,II)
       IF(ABS(DELX).GT.8. .OR. ABS(DELY).GT.8.) GOTO 59
       IF(DELX.EQ.O.) THEN
       IF(DELY.EQ.O.) THEN
       ANG=O.
         ELSE
       ANG=PI/2.
         ENDIF
         ELSE
       ANG=ATAN2(DELY,DELX)
         ENDIF
       WRITE(15,108) DELX,DELY,ANG
108    FORMAT(3(10X,F12.7))
59     CONTINUE
53     CONTINUE
C      DO 81 I=1,NPART
C      PRINT 109, CP(1,I),CP(2,I)
C109    FORMAT(2(5X,F12.7))
C81     CONTINUE
       IF (IBIT .EQ. 1) GO TO 503
C
C  SCATTERED INTENSITY AND INTENSITY FLUCTIONS
C
       SQINTN=AMSQ(1)/TN
       FINTEN=(AMSQ(2)/TN)-(SQINTN**2)
       PRINT 112, SQINTN,FINTEN
112    FORMAT(5X,'SCAT. INT. = ',E16.6,' FLUC. INT. = ',E16.6)
C
C
C  PAIR CORRELATION CALCULATIONS, USING THREE DIFFERENT WAYS.
C
       DO 76 I = 1,250
       IF (I .GT. 15) THEN
       AI4=AI1(I+1)*AI1(I+1)-AI1(I)*AI1(I)
       ANR(1,I)=DN(2,I)/(TN*PI*2.*AI1(I)*DELTAR)
       ANR(2,I)=DN(2,I)*AREA/(TN*PI*AI4*FLOAT(NPART))
       ANR(3,I)=AI1(I)*DELTAR*DN(2,I)*2./(TN*AI4)
C       PRINT 114, AI1(I),ANR(1,I),ANR(2,I),ANR(3,I)
C114    FORMAT(' R=',2X,E12.6,3(5X,E12.6))
       WRITE(15,230) AI1(I),ANR(1,I),ANR(2,I),ANR(3,I)
230    FORMAT(2X,F6.2,3(2X,E10.4))
         ENDIF
76     CONTINUE
503    CONTINUE
       ENDIF
30     CONTINUE
         STOP
         END
C
C ********************************************************
C  SUBROUTINE TO CALCULATE ENERGY=AMPLITUDE*(EXP(-ALFA*DIS))/DIS
C
C ********************************************************
C
       SUBROUTINE ENERGY
       IMPLICIT REAL*8(A-H,O-Z)
       COMMON CP(2,100),ENERG(101,100)
       COMMON SIZEX,SIZEY,ENEW,SY,SX,ALFA
       COMMON INUM,IFLAG,IFLAG1,NPART,NPARTH
```

```
C  IGNORE THE SAME PARTICLE
      IF (J .EQ. INUM) GO TO 60
      DX=DABS(CP(1,INUM)-CP(1,J))
      DY=DABS(CP(2,INUM)-CP(2,J))
C
C FINDING DISTANCES WITH PARTICLES AT THE EDGE OF THE BOX
C
      IF (DX .GE. SX) THEN
      DX=DABS(DX-SIZEX)
      ENDIF
      IF (DY .GE. SY) THEN
      DY=DABS(DY-SIZEY)
      ENDIF
C
C  INTRODUCING A CUTOFF FOR ENERGY CALCULATION AFTER
C  A CERTAIN DISTANCE (RANGE OF INTERACTION)
C
      IF(DX.GT.7. .OR. DY.GT.7.) GOTO 60
C CALCULATING ENERGY BEFORE A MOVE
C
      DIS=(DX*DX)+(DY*DY)
      IF(IFLAG1.EQ.1) GOTO 75
C     IF(IC.NE.1) THEN
C     ENEW=ENEW+ENERG(J,INUM)
C     ENERG(INUM,J)=ENERG(J,INUN)
C     ENERG(NPARTH,J)=ENERG(INUM,J)
C      ELSE
C     DIS=(DX*DX)+(DY*DY)
C     IF (DIS .LE. 49.0) THEN
C    DIS=DSQRT(DIS)
C     ENG1=ALFA*DIS
C     ENG=(DEXP(-ENG1))/DIS
C     ENEW=ENEW+ENG
C     ENERG(NPARTH,J)=ENERG(INUM,J)
C     ENERG(INUM,J)=ENG
C      ELSE
C     ENERG(INUM,J)=0.
C     ENERG(NPARTH,J)=0.
C      ENDIF
C        ENDIF
C        ELSE
C  CALCULATING ENERGIES AFTER A MOVE
      IF(DIS.LE.1.) THEN
      IFLAG=1
      RETURN
       ENDIF
75    IF (DIS .LE. 49.0) THEN
      DIS=DSQRT(DIS)
      ENG1=ALFA*DIS
      ENG=(DEXP(-ENG1))/DIS
      ENEW=ENEW+ENG
C     ENERG(INUM,J)=ENG
C       ELSE
C     ENERG(INUM,J)=0.
C       ENDIF
        ENDIF
60    CONTINUE
      RETURN
      END
//GO.FT15F001  DD DSNAME=U12604A.SPT52E.DATA,UNIT=STORAGE,
// DISP=(MOD,KEEP),SPACE=(TRK,(50,20)),
// DCB=(LRECL=255,BLKSIZE=6080,RECFM=VB)
//GO.SYSIN DD *
//
```

VITA

Khalid Loudiyi

Candidate for the Degree of

Doctor of Philosophy

Thesis: REAL SPACE ANALYSIS OF LASER INDUCED FREEZING

Major Field: Physics

Biographical:

Personal Data: Born in Kenitra, Morocco, January 5, 1956.

Education: Graduated from Kenitra American High School, Kenitra, Morocco, in June, 1975; received the Bachelor of Science degree in Engineering Physics (Electronics) and Mathematics from Southwest Missouri State University, Springfield, Missouri, in May, 1980; received Master of Science degree from Oklahoma State University in May, 1983; completed requirements for the Doctor of Philosophy degree at Oklahoma State University in December, 1989.

Professional Experience: Teaching Assistant, Southwest Missouri State University, 1979-1980; Teaching Assistant, Department of Physics, Okalhoma State University, August, 1980, to May, 1981; Research Assistant, Department of Physics, Oklahoma State University, June, 1981, to August, 1989; Supervisor of Teaching Assistants, Oklahoma State University, August 1985, to December, 1988; Lecturer, Oklahoma State University, January, 1989, to May 1989; Visiting Assistant Professor, Oklahoma State University, August, 1989, to present.